was maintained at 37°C, pH 7.4, and had an osmolality of 290–293 mmol kg^{-1} water as measured by a freezing point-based osmometer (model 3320; Advanced Instruments, Norwood, MA, USA).

Measurement of epithelial electrical parameters

Three electrical parameters, i.e., potential difference (PD), short-circuit current (Isc), and transepithelial resistance (TER), were determined according to the method of Charoenphandhu et al. [6]. In brief, a pair of Ag/AgCl electrodes connected to agar bridges was placed near each surface of the mounted tissue for PD measurement. The other ends of the PD-sensing electrodes were connected to the EVC-4000 pre-amplifier (World Precision Instruments, Sarasota, FL, USA) and finally to a PowerLab 4/30 operated with the software Chart 5.2.2 for Mac OS X (ADInstruments, Colorado Springs, CO, USA). Another pair of Ag/AgCl electrodes was placed at the end of each hemichamber to supply external current, which was also measured by a PowerLab 4/30 connected in series to the EVC-4000 current-generating unit. TER and conductance (G; G=1/TER) were calculated by Ohm's equation. Fluid resistance was automatically subtracted by the EVC-4000 system. In some experiments, Isc was continuously applied to nullify PD, i.e., the experiments were performed under short-circuit condition. Unless otherwise specified, the experiments were normally performed under open-circuit condition since the absence of PD did not significantly affect calcium flux (Supplemental Figure S1). In other words, the voltage-dependent calcium transport in the cecum could be considered negligible, similar to that observed in the duodenum [6].

Measurement of calcium flux

Transepithelial calcium flux was determined by the method of Charoenphandhu et al. [6]. In brief, after 20-min incubation, Ussing chamber was filled on one side with $^{45}CaCl_2$-containing bathing solution (specific activity of 500 mCi/mol; Amersham). Unidirectional flux ($J_{H\rightarrow C}$) from the hot side (H) to the cold side (C) was calculated with Eqs. 1 and 2.

$$J_{H\rightarrow C} = R_{H\rightarrow C}/(S_H \times A) \quad (1)$$

$$S_H = C_H/C_T \quad (2)$$

where $R_{H\rightarrow C}$ was the rate of tracer appearance in the cold side (counts per minute per hour), S_H was the specific activity in the hot side (counts per minute per nanomole) and did not vary with time (a constant value), A was the surface area of the tissue (0.69 cm^2), C_H was the radioactivity in the hot side (counts per minute), and C_T was the total calcium in the hot side (nanomole). Radioactivity of ^{45}Ca in counts per minute was analyzed by liquid scintillation spectrophotometry (model Tri-Carb 3100; Packard Instruments, Meriden, CT, USA). Total calcium concentration in the hot side was determined by atomic absorption spectrophotometry (model SpectrAA-300; Varian Techtron, Springvale, Australia).

Calcium fluxes in the absence of transepithelial calcium gradient, i.e., bathing solution in both hemichambers containing equal calcium concentration, represented the active calcium transport [6]. The calcium gradient-dependent paracellular passive fluxes were measured by determining the calcium fluxes in the presence of varying apical calcium concentrations [48], i.e., 1.25, 2.5, 5, 10, and 20 mmol/L (n=4 per each concentration).

Unless otherwise specified, the measured calcium fluxes represented calcium transport in mucosa-to-serosa direction. The serosa-to-mucosa calcium flux in the cecum was relatively small and had no significant influence on the net calcium transport (Supplemental Figure S2). In addition, PRL did not enhance calcium transport in serosa-to-mucosa direction (Supplemental Figure S2).

Determination of the epithelial permeability and Na^+/Cl^- selectivity

Permeability of sodium (P_{Na}) and chloride (P_{Cl}) which are indicative of the epithelial charge selectivity were measured by the dilution potential technique [21, 26]. The mounted cecum was equilibrated for 20 min in bathing solution containing 145 mmol/L NaCl before the apical solution was replaced with 72.5 mmol/L NaCl-containing solution. Osmolality of the solution was maintained by an equivalent amount of mannitol. Changes in the electrical parameters before and after fluid replacement were continuously recorded by PowerLab 4/30 until stable. The ion permeability ratio (P_{Na}/P_{Cl}) was calculated from the dilution potential (V_δ) using the modified Goldman–Hodgkin–Katz equation (Eq. 3).

$$\rho = (\phi - e^{\nu})/(\phi e^{\nu} - 1) \quad (3)$$

where ρ=P_{Na}/P_{Cl}; ϕ=C_b/C_a; ν=FV_δ/RT; P_{Na} was the absolute permeability of sodium; P_{Cl} was the absolute permeability of chloride; C_a was the mucosal NaCl concentration; C_b was the serosal NaCl concentration; and R, T, and F had their conventional meanings.

Thereafter, P_{Na} and P_{Cl} were calculated from the conductance (G) and P_{Na}/P_{Cl} using Kimizuka–Koketsu equations [31], as follows:

$$P_{Na} = \frac{GRT}{C_a F^2} \times \frac{\rho}{1+\rho} \quad (4)$$

$$P_{Cl} = P_{Na}/\rho \quad (5)$$

The paracellular calcium permeability (P_{Ca}) was calculated from Eq. 6 [48].

$$P_{Ca} = J_{Ca}/\Delta C \quad (6)$$

where J_{Ca} was the paracellular passive calcium flux and ΔC was the difference between the apical and basolateral calcium concentrations.

Experimental protocol

To demonstrate the effects of PRL on calcium transport, electrical parameters, and epithelial permeability, the mounted cecal tissue was directly exposed on the serosal side to 200, 400, 600, 800, or 1,000 ng/mL PRL (catalog no. L6520; Sigma) during the 80-min experiment. In some experiments, the most efficient dose of PRL (i.e., 800 ng/mL) plus RNA polymerase II inhibitor (50 μmol/L 5,6-dichloro-1-β-D-ribofuranosylbenzimidazole (DRB); Calbiochem, San Diego, CA, USA), protein synthesis inhibitor (70 μmol/L cycloheximide (CCH); Sigma), Janus kinase (JAK) 2 inhibitor (50 μmol/L AG490; Calbiochem), PI3K inhibitors (75 μmol/L LY294002 or 200 nmol/L wortmannin; Tocris Bioscience, Bristol, UK), pan-specific PKC inhibitor (1 μmol/L GF109203X; A.G. Scientific, San Diego, CA, USA), selective ROCK inhibitor (1 μmol/L Y27632; Calbiochem), or myristoylated protein kinase A inhibitor 14–22 amide (10 μmol/L PKAI 14–22; Calbiochem) were added to the serosal solution to identify possible PRL signaling pathways. Wortmannin was more potent but less specific than LY294002 [18, 23]. PKAI 14–22 was first dissolved in distilled water, while other inhibitors were dissolved in DMSO (Sigma). Concentration of dimethyl sulfoxide (DMSO) in the bathing solution was 0.3% vol/vol, which did not affect the viability of cells [6]. To verify that PRL was able to stimulate the transcellular calcium transport, the cecal tissue was directly exposed to inhibitors of apical calcium uptake (50 μmol/L ruthenium red; Sigma) or calmodulin-dependent PMCA (100 μmol/L trifluoperazine; TFP; Sigma). Polyclonal antibody against PRLR (1 μg/mL; catalog no. sc-30225; Santa Cruz) was directly

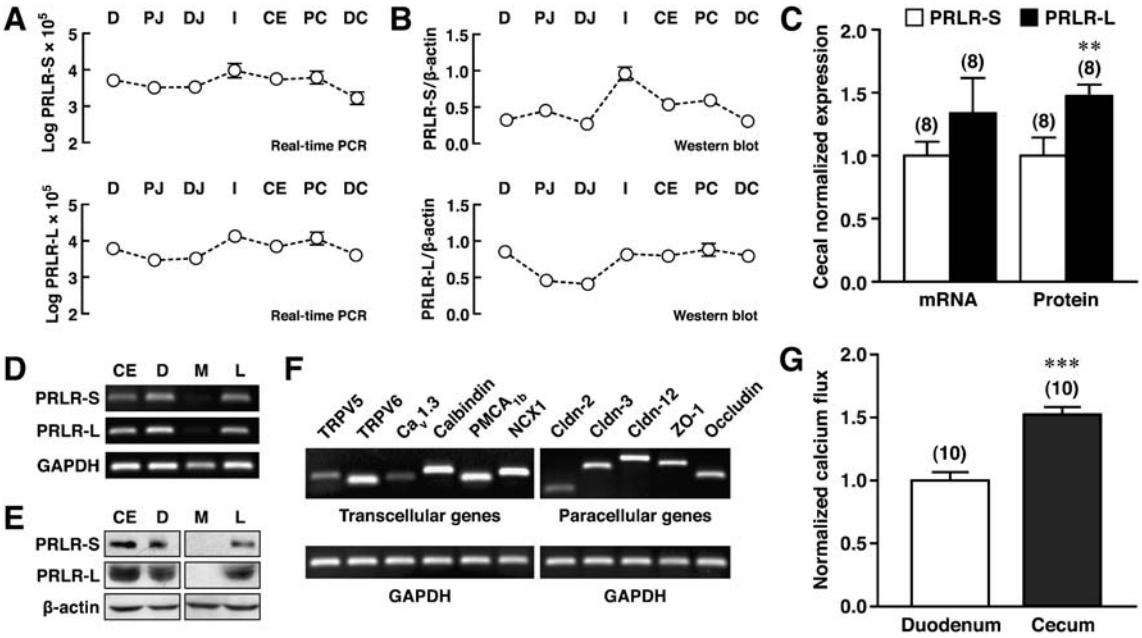

Fig. 1 **a**, **b** Expression of short (-S) and long (-L) isoforms of PRLRs in the duodenum (*D*), proximal (*PJ*) and distal jejunum (*DJ*), ileum (*I*), cecum (*CE*), and proximal (*PC*) and distal colon (*DC*) as demonstrated by qRT-PCR (**a**; $n=8$ per segment) and Western blot analysis (**b**; $n=8$ per segment). qRT-PCR data expressed as log means ± SE were normalized by GAPDH expression, while PRLR protein expression was normalized by β-actin expression. **c** Normalized expression of PRLR-S and PRLR-L in the cecum of female rats. PRLR-L expression appears as fold difference from PRLR-S expression, while setting PRLR-S expression as 1. $^{**}p<0.01$ PRLR-S expression vs. PRLR-L expression. **d** Representative electrophoretic bands of PRLR-S and PRLR-L mRNAs in duodenum (*D*) and cecum (*CE*). Gastrocnemius muscle (*M*) and liver (*L*) were used as negative and positive controls, respectively. **e** Representative bands of PRLR-S and PRLR-L proteins in duodenum (*D*) and cecum (*CE*). Gastrocnemius muscle (*M*) and liver (*L*) were negative and positive controls, respectively. **f** Electrophoretic bands of genes related to the transcellular and paracellular calcium transport in the cecum ($n=10$). GAPDH was used as a housekeeping gene. **g** Normalized transepithelial calcium fluxes in the duodenum and cecum as determined by Ussing chamber technique. Calcium concentration on both sides was 1.25 mmol/L. $^{***}p<0.001$ cecal flux vs. duodenal flux. *Numbers in parentheses* (**c** and **g**) represent the number of experimental animals

added in bathing solution to confirm that PRLR mediated PRL actions.

Statistical analysis

Results are expressed as means ± standard error (SE). Two sets of data were compared by using the unpaired Student's *t* test. Multiple comparisons were performed by one-way analysis of variance with Dunnett's multiple comparison test. Linear regression was used to demonstrate the relationships between mucosal calcium and paracellular calcium flux, and mucosal calcium and TER. The level of significance for all statistical tests was $p<0.05$. All data were analyzed by GraphPad Prism 4.0 for Mac OS X (GraphPad Software, San Diego, CA, USA).

Results

Cecal epithelial cells expressed PRLRs and essential calcium transporters

As shown in Fig. 1a, b, both short (-S) and long (-L) isoforms of PRLR mRNAs and proteins were expressed in the duodenum, proximal and distal jejunum, ileum, cecum, and proximal and distal colon of rats. In the cecum (Fig. 1c–e), PRLR-L was more abundant than PRLR-S. Although calcium absorption has been demonstrated in cecum [28], the expression of calcium transport genes has not been completely investigated in cecal epithelial cells. Therefore, we used PCR to show that cecal cells strongly expressed all essential genes required for the transcellular calcium transport, i.e., TRPV5, TRPV6, $Ca_v1.3$, calbindin-D_{9k}, $PMCA_{1b}$, and NCX1, and for the paracellular calcium transport, i.e., claudin-2, claudin-3, claudin-12, ZO-1, and occludin (Fig. 1f). Thus, the results suggested that the cecal epithelium of female rats could absorb calcium via both transcellular and paracellular pathways. Calcium transport in the cecum may be of importance since the cecal calcium flux was ~1.5-fold higher than that in the duodenum even in the absence of calcium concentration gradient (Fig. 1g).

PRL stimulated the cecal calcium transport in a biphasic dose–response manner

Dose–response study demonstrated that high physiological concentrations of PRL of 600 and 800 ng/mL, which were comparable to the levels observed during suckling in lactating rats [1], markedly enhanced the transcellular calcium transport by ~1.5- and ~2-fold, respectively, while 200 and 400 ng/mL PRL were without effects (Fig. 2a). Interestingly, the pathological concentration of 1,000 ng/mL, as seen in prolactinomas, only slightly increased calcium transport in the cecum (Fig. 2a). Since such PRL effect was not observed in the presence of apical calcium uptake inhibitor (50 μmol/L ruthenium red) or basolateral calcium extrusion inhibitor (100 μmol/L trifluoperazine), the PRL-stimulated calcium transport in this experiment was confirmed to occur via the transcellular pathway (Fig. 2b). The fact that the PRL-enhanced cecal calcium transport occurred rapidly within 60 min after exposure and was not abolished by inhibitors of gene transcription (50 μmol/L DRB) or protein biosynthesis (70 μmol/L cycloheximide; Fig. 2b), suggesting that the stimulatory actions of PRL was exerted via the nongenomic signaling pathways. Direct exposure to DRB and cycloheximide alone did not affect the basal rate of the transcellular

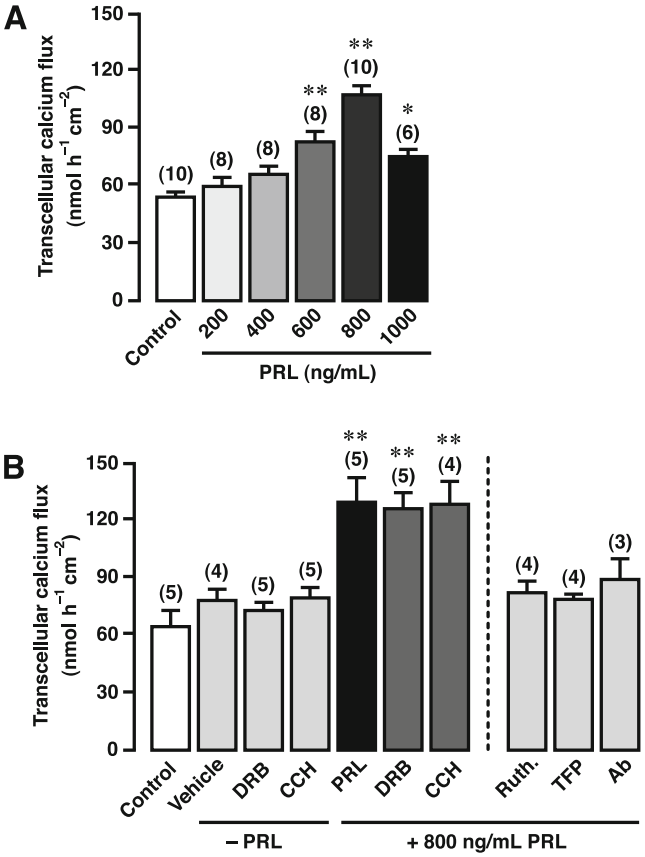

Fig. 2 **a** Dose-dependent effect of PRL on the transcellular calcium transport in the cecum. **b** Transcellular calcium transport in the cecum directly exposed to inhibitors of RNA polymerase II (50 μmol/L DRB), protein synthesis (70 μmol/L CCH), apical calcium uptake (50 μmol/L ruthenium red (*Ruth.*); apical side), basolateral calcium extrusion (100 μmol/L trifluoperazine (*TFP*); basolateral side), or 1 μg/mL PRLR antibody (*Ab*; basolateral side) with (+*PRL*) and without (−*PRL*) 800 ng/mL PRL (maximal effective concentration). DMSO was a vehicle for preparation of DRB and CCH. *Numbers in parentheses* represent the number of animals. *$p<0.05$, **$p<0.01$ compared with its respective control group

Table 2 Effects of PRL on epithelial electrical parameters

Condition	Number	Electrical parameters		
		PD (mV)	Isc (μAcm^{-2})	TER (Ω cm^2)
Control	7	5.43±0.67	55.23±4.15	102.90±11.53
PRL				
200 ng/mL	5	3.67±0.39	52.20±5.50	71.90±3.39
400 ng/mL	4	4.22±0.69	55.21±6.29	79.02±11.04
600 ng/mL	4	3.97±0.72	57.37±8.06	68.23±5.93*
800 ng/mL	8	4.26±0.18	59.52±1.22	69.41±3.27*
1,000 ng/mL	5	4.02±0.56	58.84±9.52	69.91±2.65*

Values are means ± SE. Cecum was directly exposed to 200, 400, 600, 800, or 1,000 ng/mL PRL. Mounted tissue was bathed on both sides with 1.25 mmol/L calcium-containing solution. The mucosal side was negative with respect to the serosal side. The experiments were performed under open-circuit condition interrupted by measuring the short-circuit current

*$p<0.05$ compared with the control group

calcium transport (Fig. 2b). PRL-stimulated calcium transport was absent when the cecum was continuously exposed to 1 μg/mL PRLR antibody, indicating that PRLR mediated PRL actions in this intestinal segment (Fig. 2b). Moreover, the decrease in TER by 600, 800, and 1,000 ng/mL PRL (Table 2) suggested the PRL-induced increase in paracellular permeability. Since 800 ng/mL was the maximal effective concentration of PRL for stimulation of calcium transport, this concentration was used in the subsequent experiments.

The PRL-enhanced transcellular calcium transport in cecum was mediated by PI3K, PKC, and ROCK signaling pathways

Previous investigations showed that PRL signaling in mammary epithelium was mediated by JAK2, whereas that in the duodenum and Caco-2 monolayer was mediated by PI3K, PKC, and ROCK [25, 48]. Moreover, an increase in intestinal calcium absorption via the transcellular route was also reported to be protein kinase A (PKA)-dependent [9, 30]. Herein, we found that the PRL-enhanced transcellular calcium transport in cecum was completely abolished by inhibitors of PI3K (75 μmol/L LY294002 and 200 nmol/L wortmannin), PKC (1 μmol/L GF109203X), and ROCK (1 μmol/L Y27632), but not inhibitors of JAK2 (50 μmol/L AG490) and PKA (10 μmol/L PKAI 14–22; Fig. 3). Exposure to inhibitors alone did not affect the calcium flux. The data, therefore, indicated that PRL exerted its stimulatory actions on the cecal calcium transport via the PI3K, PKC, and ROCK signaling pathways.

PRL increased the paracellular calcium transport and calcium permeability in cecum via PI3K and ROCK pathways

Paracellular calcium transport and calcium permeability were evaluated in the presence of the transepithelial calcium gradient. Under normal conditions (Fig. 4a–d), the paracellular cecal calcium transport increased linearly with the mucosal calcium concentration ($r^2=0.86$). After exposure to PRL (Fig. 4a–d), the paracellular calcium

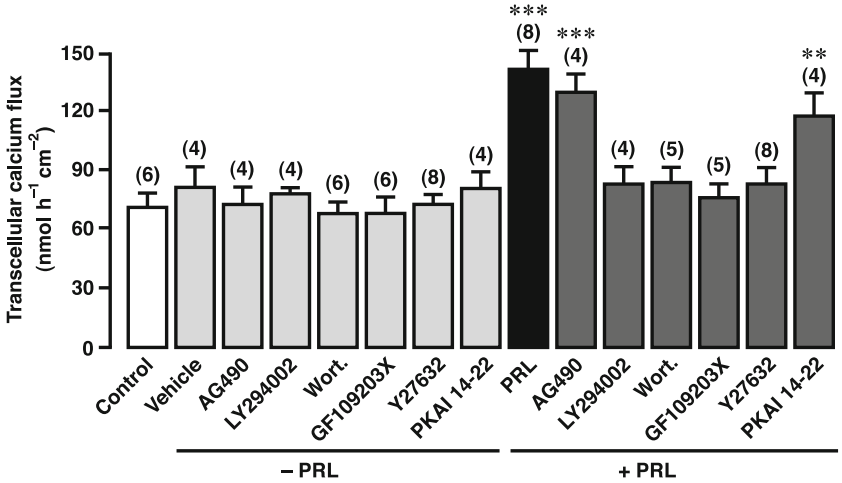

Fig. 3 Transcellular calcium transport in the cecum exposed to JAK2 inhibitor (50 μmol/L AG490), PI3K inhibitors (75 μmol/L LY294002 and 200 nmol/L wortmannin), PKC inhibitor (1 μmol/L GF109203X), ROCK inhibitor (1 μmol/L Y27632), or myristoylated PKA inhibitor 14–22 amide (10 μmol/L PKAI 14–22) with (+*PRL*) and without (−*PRL*) 800 ng/mL PRL. PKAI 14–22 was dissolved in water, whereas other inhibitors were dissolved in DMSO (vehicle). All experiments were performed under open-circuit condition. *Numbers in parentheses* represent the number of animals. **$p<0.01$, ***$p<0.001$ compared with the control group

fluxes were markedly enhanced, and the correlation between mucosal calcium concentrations and calcium fluxes still showed linearity (r^2=0.93). The slopes of the regression lines were significantly increased by 2.4-fold, i.e., from the control value of 63.06±5.95 to 152.62± 9.67 cm h^{-1} (p<0.001). PRL also increased calcium permeability of the cecal epithelium as demonstrated in Fig. 4e–h. The PRL-induced increases in the paracellular calcium transport and calcium permeability in the cecum were totally abolished by inhibitors of PI3K (Fig. 4a, e) and ROCK (Fig. 4c, g), but not by PKC inhibitor (Fig. 4b, f) or JAK2 inhibitor (Fig. 4d, h).

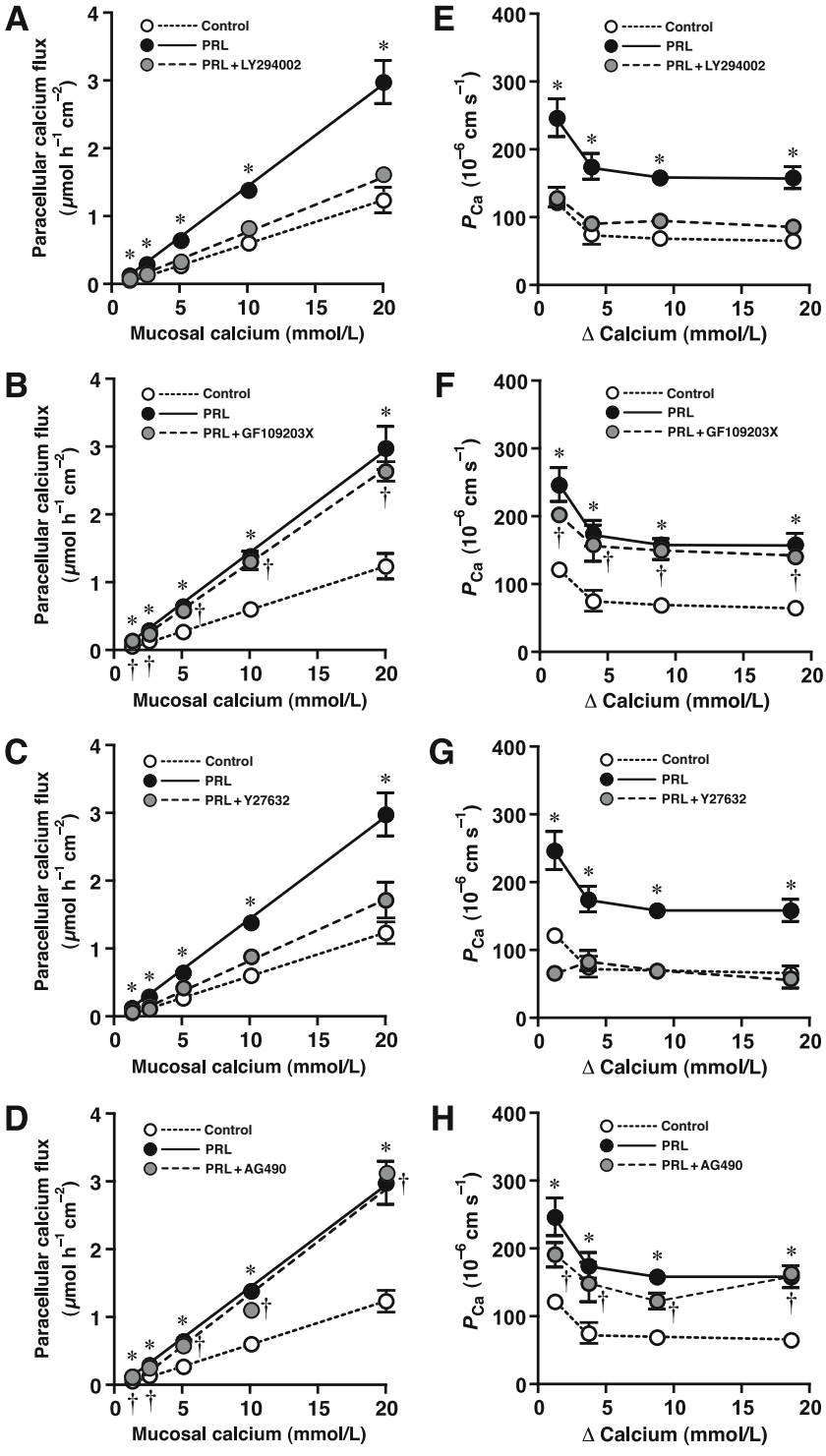

Fig. 4 **a**–**d** Paracellular calcium transport and **e**–**h** calcium permeability (P_{Ca}) in the cecum directly exposed to 800 ng/mL PRL in the presence and absence of PI3K inhibitor (75 μmol/L LY294002), PKC inhibitor (1 μmol/L GF109203X), ROCK inhibitor (1 μmol/L Y27632), or JAK2 inhibitor (50 μmol/L AG490). The mucosal side was bathed with solution containing various calcium concentrations, i.e., 1.25, 2.5, 5, 10, or 20 mmol/L (n=4 per each concentration; total 120 setups used), whereas the serosal solution had calcium concentration of 1.25 mmol/L. The same values of the control and PRL-treated groups are presented in **a**–**d** and **e**–**h** with those of the inhibitor-treated groups for clear comparisons. All experiments were performed under open-circuit condition. *p<0.001 PRL vs. control. †p<0.001 PRL+inhibitor vs. control

As seen in Fig. 5, TER values of normal cecal epithelia were linearly increased with mucosal calcium concentration (r^2=0.99) as a result of the calcium-induced conductance block of the paracellular pores, similar to that reported previously [47]. Hence, Isc but not PD was gradually decreased when mucosal calcium concentration was increased (data not shown). In 800 ng/mL PRL-treated cecal epithelia, although the relationship between mucosal calcium and TER still showed linearity (r^2=0.99), PRL markedly reduced TER, and the slopes were reduced from the control value of 119.59±3.03 to 71.01±1.77 kΩ cm^2 L mmol^{-1} (p<0.001). Such PRL effects on TER were abolished by PI3K inhibitor (Fig. 5a) and ROCK inhibitor (Fig. 5c), but not by PKC inhibitor (Fig. 5b) or JAK2 inhibitor (Fig. 5d). Inhibitors alone and vehicle (DMSO) had no effect on TER (data not shown).

PRL altered Na^+/Cl^--selective property of the cecal epithelium

Since the paracellular calcium transport and epithelial calcium permeability could be increased by altering the charge-selective property of cecal epithelium, we determined the absolute permeability to sodium (P_{Na}) and chloride (P_{Cl}) as well as the P_{Na}/P_{Cl} ratio, all of which are indicative of the paracellular charge selectivity [21, 47]. Under normal conditions (Fig. 6), the cecal epithelium exhibited a cation selectivity with P_{Na} being greater than P_{Cl} (p<0.001), and P_{Na}/P_{Cl} was ~2.0. After exposure to 800 ng/mL PRL, P_{Na} was markedly increased by ~2.6-fold (Fig. 6a) without any change in P_{Cl} (Fig. 6b), thereby raising P_{Na}/P_{Cl} (Fig. 6c). The increases in P_{Na} and P_{Na}/P_{Cl}, similar to the increase in paracellular calcium transport, were diminished by PI3K and ROCK inhibitors, but not by PKC inhibitor (Fig. 6a, c). Inhibitors alone were without effects. The results, therefore, suggested that PRL enhanced the paracellular cecal calcium transport by increasing the epithelial cation selectivity through PI3K and ROCK pathways.

Discussion

In the present study, we demonstrated, for the first time, that PRL stimulated the transcellular and paracellular calcium transport in rat cecum. The presence of PRLRs in cecal epithelial cells and the ability of PRLR antibody to block PRL-stimulated calcium transport confirmed direct action of PRL on this intestinal segment. It was evident that the PRL-enhanced transcellular cecal calcium transport was dependent on PI3K, PKC, and ROCK, while the enhanced paracellular calcium transport required PI3K and ROCK, but not PKC. Such PRL signalings were nongenomic, since they were observed within 60 min after PRL exposure, and were not abolished by inhibitors of gene transcription (DRB) or protein biosynthesis (cycloheximide).

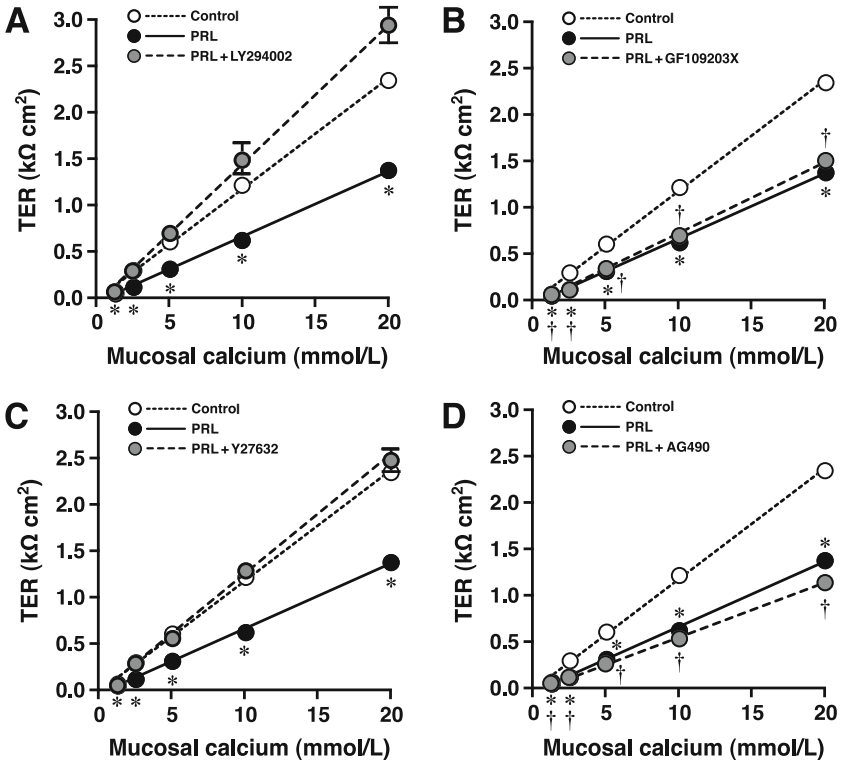

Fig. 5 Effect of 800 ng/mL PRL on the relationship between mucosal calcium concentration and transepithelial resistance (*TER*) of cecal epithelium (n=4 per each concentration) incubated with **a** PI3K inhibitor (75 μmol/L LY294002), **b** PKC inhibitor (1 μmol/L GF109203X), **c** ROCK inhibitor (1 μmol/L Y27632), or **d** JAK2 inhibitor (50 μmol/L AG490). The same control and PRL data are presented in **a**–**d** with those of the inhibitor-treated groups for clear comparisons. *p<0.001 PRL vs. control. $^{\dagger}p$<0.001 PRL+inhibitor vs. control

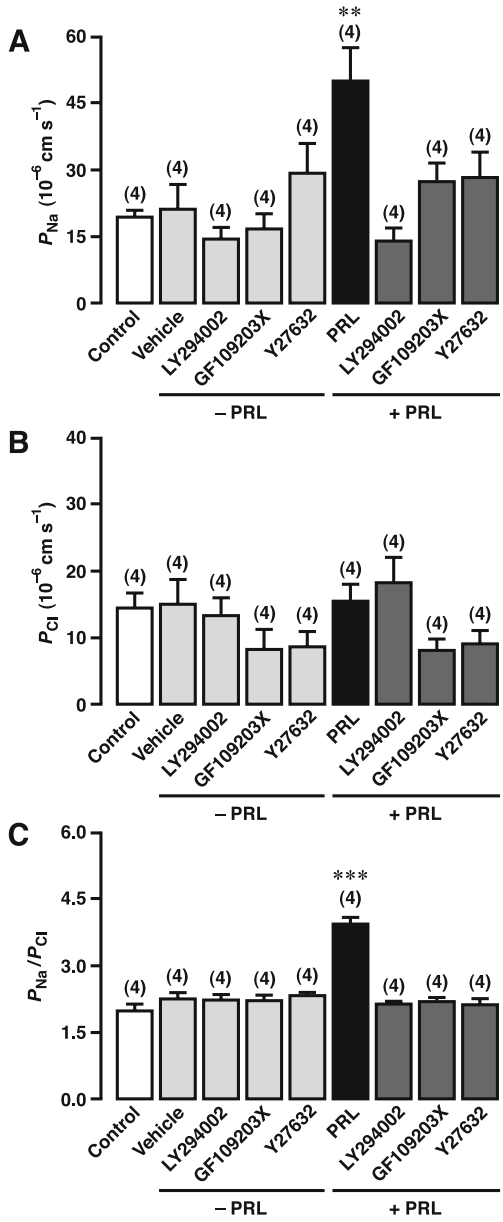

Fig. 6 **a** P_{Na}, **b** P_{Cl}, and **c** P_{Na}/P_{Cl} of the cecal epithelia exposed to PI3K inhibitor (75 μmol/L LY294002), PKC inhibitor (1 μmol/L GF109203X), or ROCK inhibitor (1 μmol/L Y27632) with (+*PRL*) and without (−*PRL*) 800 ng/mL PRL. DMSO was used as vehicle for inhibitor preparation. *Numbers in parentheses* represent the number of animals. $^{**}p<0.01$, $^{***}p<0.001$ compared with the control group

Although most recent investigations have focused on calcium transport in the small intestine, the proximal large intestine, particularly the cecum, is a highly efficient site for calcium absorption [39]. Karbach and Feldmeier reported that the rat cecum, as compared to other intestinal segments, had the highest rate of calcium absorption [28]. The present calcium flux study confirmed that the cecal calcium transport was greater than that in the duodenum by ~1.5-fold. Besides, the cecum which strongly expresses transcellular calcium transporters (Fig. 1f) is another site with sizable transcellular calcium absorption [28]. In some mammals, e.g., mole rats, the transcellular active calcium transport exclusively occurs in the proximal large intestine [41].

Physiological significance of the cecum in an overall calcium absorption was questionable because calcium may be present in the cecal lumen as a water-insoluble complex with indigestible luminal content [12]. Cecectomy also did not affect the fractional calcium absorption in 1,25 $(OH)_2D_3$-repleted rats [4]. However, other studies showed that microbial fermentation in the cecum could liberate calcium from the indigestible fibers [10, 51]. Moreover, short-chain fatty acid as well as small organic acids, e.g., propionic acid, succinic acid, and lactic acid, produced during fermentation decreased the luminal pH, which in turn released calcium from the complexes [10, 36, 38]. Cecal calcium absorption becomes salient when hindgut fermentors, such as humans and rats, ingest naturally occurring resistant starch (e.g., oatmeal and pearl barley), a fermentable carbohydrate that benefits healthy individuals as well as diabetic patients [44, 51].

The aforementioned evidence also collectively suggests that the cecum has a high capacity to supply additional calcium to the body when needed, for examples, in pregnancy and lactation [42]. Coincidentally, PRL is a hormone with markedly elevated levels during these periods, and we have previously shown that it was an important hormone to enhance calcium absorption, especially in the duodenum and proximal jejunum [5]. However, PRL was without effect on calcium transport in the distal large intestine although it could regulate water absorption and inhibit the calcium-dependent Cl^- and K^+ secretion in the colon [34, 43]. In the present study, the cecum, which expressed essential genes for the transcellular and paracellular calcium transport, responded to PRL by increasing calcium fluxes via both transcellular and paracellular pathways, similar to that seen in the duodenum [25]. Calcium fluxes observed in the 800 ng/mL PRL-treated cecum was greater than that in the duodenum exposed to the same PRL concentration by 2-fold, i.e., ~120 nmol h^{-1} cm^{-2} in the cecum compared to ~60 nmol h^{-1} cm^{-2} reported in the duodenum [25]. In the presence of ~5–20 mmol/L transepithelial calcium gradient, this PRL concentration markedly increased the amount of calcium transported by cecal epithelium from a nanomole range to micromole range. These information collectively strengthened the physiological significance of the cecal calcium absorption during hyperprolactinemic states, such as in lactating animals.

Nevertheless, nothing was known pertaining the detailed mechanisms by which PRL enhanced cecal calcium transport. The PRL-stimulated transcellular calcium absorption in the duodenum was explained by increases in the brush-border calcium uptake and PMCA activity [7]. In the

cecum, the PRL effect was also abolished by inhibitors of apical calcium uptake (ruthenium red) or basolateral calcium extrusion (trifluoperazine). Regarding the cecal paracellular calcium transport, the PRL-induced increase in calcium movement through the paracellular space was explained by a decrease in TER (Fig. 5) as well as an increase in the epithelial cation selectivity, as indicated by the increased P_{Na} and P_{Na}/P_{Cl} (Fig. 6), similar to that observed in Caco-2 monolayer [48]. The P_{Na}/P_{Cl} value of the control groups, which increased from the mobility ratio of Na^+ and Cl^- of ~0.6 in free solution to ~2.0 [17], also suggested that, under normal conditions, the cecal epithelium naturally prefers paracellular movement of cations more than anions. Generally, tight junction proteins of the claudin family undergo polymerization to form charge-selective paracellular pores [15]. Thus, the epithelial charge selectivity is determined by the fixed negative or positive charges on the extracellular loops of claudins which impede the movement of ions with the opposite charge [50]. Claudin-2, claudin-3, and claudin-12, which are also expressed in cecal epithelial cells, have been suggested to regulate the paracellular calcium transport [14, 35]. Our recent preliminary study in Caco-2 monolayer showed that an increase in cation selectivity observed after the PRL-induced claudin phosphorylation could increase the paracellular calcium movement (Nakkrasae et al. 2009, unpublished observation). However, further experiment is required to demonstrate that the PRL-induced increases in paracellular cecal calcium transport and cation selectivity are directly mediated by claudin phosphorylation.

PRL signaling pathways in the intestinal epithelial cells have been studied in the duodenum and Caco-2 intestinal-like cells [25, 48], while that in the cecum was unknown. Since cecal epithelial cells predominantly expressed PRLR-L, it was likely that PRL exerted its functions through PRLR-L, similar to that reported in Caco-2 cells [48]. In contrast, as PRLR-S lacks the cytoplasmic tails required to activate the intracellular downstream pathways, PRLR-S may act as the dominant-negative molecules to silence or reduce PRL actions [2]. Interestingly, the typical biphasic response to PRL was also demonstrated in the cecum, i.e., in contrast to the lower effective doses (600 and 800 ng/mL), 1,000 ng/mL PRL only slightly increased calcium transport. This phenomenon has been explained by inability of PRLRs to form functional dimers. At extremely high PRL concentrations, most available PRLRs were occupied as nonfunctional 1:1 complexes instead of 1:2 functional complexes needed to induce signal transduction [13, 22].

The principal PRL signaling pathways found in the cecum, i.e., PI3K, PKC, and ROCK, were consistent with those reported in duodenal epithelial cells and Caco-2 monolayer [25, 48]. Although JAK2 usually mediates PRL signals in several tissues, e.g., mammary epithelium [24], and several factors, e.g., $1,25(OH)_2D_3$, could increase calcium uptake through PKA [30], the PRL effects herein appeared to be independent of both JAK2 and PKA. Generally, PI3K is the most upstream enzyme of several kinase targets, including PKC and ROCK known to modulate the transepithelial calcium transport and paracellular permeability [19, 27, 37, 46]. In the cecum, PKC was likely to be more important in the transcellular calcium transport than the paracellular transport, presumably by its ability to augment the basolateral calcium efflux [30]. In contrast, ROCK was essential for both transport mechanisms. It was noteworthy that activation of ROCK is commonly required to increase paracellular permeability or decrease TER in several epithelia, e.g., brain endothelium, renal proximal tubule, and human colonic epithelial monolayer [27, 45, 46]. Hence, PRL might use this common pathway to decrease TER, and increase cation selectivity and paracellular calcium permeability, thereby enhancing the paracellular calcium transport.

Finally, it could be concluded that the rat cecum was a target tissue of PRL, in which it directly stimulated the transcellular and paracellular calcium transport via the non-genomic signaling pathways. The downstream pathways for PRL signaling involved PI3K, ROCK, and PKC, the last of which mainly mediated the signal for the PRL-enhanced transcellular calcium transport. The present investigation, therefore, elaborated possible physiological roles of PRL in the cecum and provided more complete understanding of the effects of PRL on calcium homeostasis. Since the rate of cecal calcium absorption is subjected to effects of certain dietary components, e.g., resistant carbohydrates, we speculate that such nutraceuticals could be useful for enhancement of calcium absorption during lactation, when the plasma PRL surge is in the range of ~650–800 ng/mL [1].

Acknowledgments This work was supported by the Thailand Research Fund (RSA5180001 to N. Charoenphandhu) and the Mahidol University Postdoctoral Fellowship Program (to L.-i. Nakkrasae).

Conflict of interest The authors have no conflict of interest.

References

1. Arbogast LA, Voogt JL (1998) Endogenous opioid peptides contribute to suckling-induced prolactin release by suppressing tyrosine hydroxylase activity and messenger ribonucleic acid levels in tuberoinfundibular dopaminergic neurons. Endocrinology 139:2857–2862
2. Berlanga JJ, Garcia-Ruiz JP, Perrot-Applanat M, Kelly PA, Edery M (1997) The short form of the prolactin (PRL) receptor silences PRL induction of the β-casein gene promoter. Mol Endocrinol 11:1449–1457
3. Boass A, Lovdal JA, Toverud SU (1992) Pregnancy- and lactation-induced changes in active intestinal calcium transport in rats. Am J Physiol Gastrointest Liver Physiol 263:G127–G134

4. Brommage R, Binacua C, Carrie AL (1995) The cecum does not participate in the stimulation of intestinal calcium absorption by calcitriol. J Steroid Biochem Mol Biol 54:71–73
5. Charoenphandhu N, Krishnamra N (2007) Prolactin is an important regulator of intestinal calcium transport. Can J Physiol Pharmacol 85:569–581
6. Charoenphandhu N, Limlomwongse L, Krishnamra N (2001) Prolactin directly stimulates transcellular active calcium transport in the duodenum of female rats. Can J Physiol Pharmacol 79:430–438
7. Charoenphandhu N, Limlomwongse L, Krishnamra N (2006) Prolactin directly enhanced Na^+/K^+- and Ca^{2+}-ATPase activities in the duodenum of female rats. Can J Physiol Pharmacol 84:555–563
8. Charoenphandhu N, Wongdee K, Teerapornpuntakit J, Thongchote K, Krishnamra N (2008) Transcriptome responses of duodenal epithelial cells to prolactin in pituitary-grafted rats. Mol Cell Endocrinol 296:41–52
9. de Boland AR, Norman A (1990) Evidence for involvement of protein kinase C and cyclic adenosine 3′, 5′ monophosphate-dependent protein kinase in the 1, 25-dihydroxyvitamin D_3-mediated rapid stimulation of intestinal calcium transport, (transcaltachia). Endocrinology 127:39–45
10. Duflos C, Bellaton C, Pansu D, Bronner F (1995) Calcium solubility, intestinal sojourn time and paracellular permeability codetermine passive calcium absorption in rats. J Nutr 125:2348–2355
11. Favus MJ (1985) Factors that influence absorption and secretion of calcium in the small intestine and colon. Am J Physiol 248: G147–G157
12. Favus MJ, Pak C (2001) Evidence for absorption of ionic calcium and soluble calcium complexes by the duodenum and cecum in the rat. Am J Ther 8:425–431
13. Fuh G, Colosi P, Wood WI, Wells JA (1993) Mechanism-based design of prolactin receptor antagonists. J Biol Chem 268:5376–5381
14. Fujita H, Sugimoto K, Inatomi S, Maeda T, Osanai M, Uchiyama Y, Yamamoto Y, Wada T, Kojima T, Yokozaki H, Yamashita T, Kato S, Sawada N, Chiba H (2008) Tight junction proteins claudin-2 and -12 are critical for vitamin D-dependent Ca^{2+} absorption between enterocytes. Mol Biol Cell 19:1912–1921
15. Furuse M, Tsukita S (2006) Claudins in occluding junctions of humans and flies. Trends Cell Biol 16:181–188
16. Garcia J, Carabano R, Perez-Alba L, de Blas JC (2000) Effect of fiber source on cecal fermentation and nitrogen recycled through cecotrophy in rabbits. J Anim Sci 78:638–646
17. Greger R (1996) Epithelial transport. In: Greger R, Windhorst U (eds) Comprehensive human physiology: from cellular mechanisms to integration. Springer, Berlin, pp 1217–1232
18. Hawkins PT, Anderson KE, Davidson K, Stephens LR (2006) Signalling through class I PI3Ks in mammalian cells. Biochem Soc Trans 34:647–662
19. Hirsch E, Costa C, Ciraolo E (2007) Phosphoinositide 3-kinases as a common platform for multi-hormone signaling. J Endocrinol 194:243–256
20. Hoenderop JG, Nilius B, Bindels RJ (2005) Calcium absorption across epithelia. Physiol Rev 85:373–422
21. Hou J, Paul DL, Goodenough DA (2005) Paracellin-1 and the modulation of ion selectivity of tight junctions. J Cell Sci 118:5109–5118
22. Ilondo MM, Damholt AB, Cunningham BA, Wells JA, de Meyts P, Shymko RM (1994) Receptor dimerization determines the effects of growth hormone in primary rat adipocytes and cultured human IM-9 lymphocytes. Endocrinology 134:2397–2403
23. Imaizumi MO, Sakurai T, Nakamura S, Nakanishi S, Matsuda Y, Muramatsu S, Nonomura Y, Kumakura K (1992) Inhibition of Ca^{2+}-dependent catecholamine release by myosin light chain kinase inhibitor, wortmannin, in adrenal chromaffin cells. Biochem Biophys Res Commun 185:1016–1021
24. Jahn GA, Daniel N, Jolivet G, Belair L, Bole-Feysot C, Kelly PA, Djiane J (1997) In vivo study of prolactin (PRL) intracellular signalling during lactogenesis in the rat: JAK/STAT pathway is activated by PRL in the mammary gland but not in the liver. Biol Reprod 57:894–900
25. Jantarajit W, Thongon N, Pandaranandaka J, Teerapornpuntakit J, Krishnamra N, Charoenphandhu N (2007) Prolactin-stimulated transepithelial calcium transport in duodenum and Caco-2 monolayer are mediated by the phosphoinositide 3-kinase pathway. Am J Physiol Endocrinol Metab 293:E372–E384
26. Kahle KT, Macgregor GG, Wilson FH, Van Hoek AN, Brown D, Ardito T, Kashgarian M, Giebisch G, Hebert SC, Boulpaep EL, Lifton RP (2004) Paracellular Cl^- permeability is regulated by WNK4 kinase: insight into normal physiology and hypertension. Proc Natl Acad Sci USA 101:14877–14882
27. Kapus A, Szászi K (2006) Coupling between apical and paracellular transport processes. Biochem Cell Biol 84:870–880
28. Karbach U, Feldmeier H (1993) The cecum is the site with the highest calcium absorption in rat intestine. Dig Dis Sci 38:1815–1824
29. Khanal RC, Nemere I (2008) Regulation of intestinal calcium transport. Annu Rev Nutr 28:179–196
30. Khanal RC, Nemere I (2008) Endocrine regulation of calcium transport in epithelia. Clin Exp Pharmacol Physiol 35:1277–1287
31. Kimizuka H, Koketsu K (1964) Ion transport through cell membrane. J Theor Biol 6:290–305
32. Kornberg A, Daft FS, Sebrell WH (1944) Mechanism of production of vitamin K deficiency in rats by sulfonamides. J Biol Chem 155:193–200
33. Krause LJ, Forsberg CW, O'Connor DL (1996) Feeding human milk to rats increases *Bifidobacterium* in the cecum and colon which correlates with enhanced folate status. J Nutr 126:1505–1511
34. Krishnamra N, Ousingsawat J, Limlomwongse L (2001) Study of acute pharmacologic effects of prolactin on calcium and water transport in the rat colon by an in vivo perfusion technique. Can J Physiol Pharmacol 79:415–421
35. Kutuzova GD, DeLuca HF (2004) Gene expression profiles in rat intestine identify pathways for 1, 25-dihydroxyvitamin D_3 stimulated calcium absorption and clarify its immunomodulatory properties. Arch Biochem Biophys 432:152–166
36. Levrat MA, Remesy C, Demigne C (1991) High propionic acid fermentations and mineral accumulation in the cecum of rats adapted to different levels of inulin. J Nutr 121:1730–1737
37. Little D, Dean RA, Young KM, McKane SA, Martin LD, Jones SL, Blikslager AT (2003) PI3K signaling is required for prostaglandin-induced mucosal recovery in ischemia-injured porcine ileum. Am J Physiol Gastrointest Liver Physiol 284: G46–G56
38. Mineo H, Amano M, Minaminida K, Chiji H, Shigematsu N, Tomita F, Hara H (2006) Two-week feeding of difructose anhydride III enhances calcium absorptive activity with epithelial cell proliferation in isolated rat cecal mucosa. Nutrition 22:312–320
39. Nellans HN, Goldsmith RS (1981) Transepithelial calcium transport by rat cecum: high-efficiency absorptive site. Am J Physiol 240:G424–G431
40. Nellans HN, Goldsmith RS (1983) Mucosal calcium uptake by rat cecum: identity with transcellular calcium absorption. Am J Physiol 244:G618–G622
41. Pitcher T, Buffenstein R (1995) Intestinal calcium transport in mole-rats (*Cryptomys damarensis* and *Heterocephalus glaber*) is independent of both genomic and non-genomic vitamin D mediation. Exp Physiol 80:597–608
42. Prentice A (2000) Calcium in pregnancy and lactation. Annu Rev Nutr 20:249–272

43. Puntheeranurak S, Schreiber R, Spitzner M, Ousingsawat J, Krishnamra N, Kunzelmann K (2007) Control of ion transport in mouse proximal and distal colon by prolactin. Cell Physiol Biochem 19:77–88
44. Robertson MD, Bickerton AS, Dennis AL, Vidal H, Frayn KN (2005) Insulin-sensitizing effects of dietary resistant starch and effects on skeletal muscle and adipose tissue metabolism. Am J Clin Nutr 82:559–567
45. Samarin SN, Ivanov AI, Flatau G, Parkos CA, Nusrat A (2007) Rho/Rho-associated kinase-II signaling mediates disassembly of epithelial apical junctions. Mol Biol Cell 18:3429–3439
46. Stamatovic SM, Dimitrijevic OB, Keep RF, Andjelkovic AV (2006) Protein kinase Cα-RhoA cross-talk in CCL2-induced alterations in brain endothelial permeability. J Biol Chem 281:8379–8388
47. Tang VW, Goodenough DA (2003) Paracellular ion channel at the tight junction. Biophys J 84:1660–1673
48. Thongon N, Nakkrasae LI, Thongbunchoo J, Krishnamra N, Charoenphandhu N (2008) Prolactin stimulates transepithelial calcium transport and modulates paracellular permselectivity in Caco-2 monolayer: mediation by PKC and ROCK pathways. Am J Physiol Cell Physiol 294:C1158–C1168
49. Thongon N, Nakkrasae LI, Thongbunchoo J, Krishnamra N, Charoenphandhu N (2009) Enhancement of calcium transport in Caco-2 monolayer through PKC_{ζ}-dependent $Ca_v1.3$-mediated transcellular and rectifying paracellular pathways by prolactin. Am J Physiol Cell Physiol (in press). doi: 10.1152/ajpcell.00053.2009
50. Van Itallie CM, Anderson JM (2006) Claudins and epithelial paracellular transport. Annu Rev Physiol 68:403–429
51. Younes H, Demigne C, Remesy C (1996) Acidic fermentation in the caecum increases absorption of calcium and magnesium in the large intestine of the rat. Br J Nutr 75:301–314

Enhancement of calcium transport in Caco-2 monolayer through PKC ζ-dependent Ca_V 1.3-mediated transcellular and rectifying paracellular pathways by prolactin

Narongrit Thongon, La-iad Nakkrasae, Jirawan Thongbunchoo, Nateetip Krishnamra and Narattaphol Charoenphandhu

Am J Physiol Cell Physiol 296:C1373-C1382, 2009. First published 1 April 2009;
doi:10.1152/ajpcell.00053.2009

Am J Physiol Cell Physiol 296: C1373–C1382, 2009.
First published April 1, 2009; doi:10.1152/ajpcell.00053.2009.

Enhancement of calcium transport in Caco-2 monolayer through PKC$_\zeta$-dependent Ca$_v$1.3-mediated transcellular and rectifying paracellular pathways by prolactin

Narongrit Thongon,[1,2,3] La-iad Nakkrasae,[1] Jirawan Thongbunchoo,[1] Nateetip Krishnamra,[1,2] and Narattaphol Charoenphandhu[1,2]

[1]*Consortium for Calcium and Bone Research (COCAB) and* [2]*Department of Physiology, Faculty of Science, Mahidol University, Bangkok, Thailand; and* [3]*Department of Medical Science, Faculty of Science, Burapha University, Chonburi, Thailand*

Submitted 28 January 2009; accepted in final form 29 March 2009

Thongon N, Nakkrasae L, Thongbunchoo J, Krishnamra N, Charoenphandhu N. Enhancement of calcium transport in Caco-2 monolayer through PKC$_\zeta$-dependent Ca$_v$1.3-mediated transcellular and rectifying paracellular pathways by prolactin. *Am J Physiol Cell Physiol* 296: C1373–C1382, 2009. First published April 1, 2009; doi:10.1152/ajpcell.00053.2009.—Previous investigations suggested that prolactin (PRL) stimulated the intestinal calcium absorption through phosphoinositide 3-kinase (PI3K), protein kinase C (PKC), and RhoA-associated coiled-coil forming kinase (ROCK) signaling pathways. However, little was known regarding its detailed mechanisms for the stimulation of transcellular and voltage-dependent paracellular calcium transport. By using Ussing chamber technique, we found that the PRL-induced increase in the transcellular calcium flux and decrease in transepithelial resistance of intestinal-like Caco-2 monolayer were not abolished by inhibitors of gene transcription and protein biosynthesis. The PRL-stimulated transcellular calcium transport was completely inhibited by the L-type calcium channel blockers (nifedipine and verapamil) and plasma membrane Ca^{2+}-ATPase (PMCA) inhibitor (trifluoperazine) as well as small interfering RNA targeting voltage-dependent L-type calcium channel Ca$_v$1.3, but not TRPV6 or calbindin-D$_{9k}$. As demonstrated by ^{45}Ca uptake study, PI3K and PKC, but not ROCK, were essential for the PRL-enhanced apical calcium entry. In addition, PRL was unable to enhance the transcellular calcium transport after PKC$_\zeta$ knockdown or exposure to inhibitors of PKC$_\zeta$, but not of PKC$_\alpha$, PKC$_\beta$, PKC$_\varepsilon$, PKC$_\mu$, or protein kinase A. Voltage-clamping experiments further showed that PRL markedly stimulated the voltage-dependent calcium transport and removed the paracellular rectification. Such PRL effects on paracellular transport were completely abolished by inhibitors of PI3K (LY-294002) and ROCK (Y-27632). It could be concluded that the PRL-stimulated transcellular calcium transport in Caco-2 monolayer was mediated by Ca$_v$1.3 and PMCA, presumably through PI3K and PKC$_\zeta$ pathways, while the enhanced voltage-dependent calcium transport occurred through PI3K and ROCK pathways.

calcium uptake; protein kinase C; rectification; small interfering RNA; voltage-dependent calcium transport

PROLACTIN (PRL) IS A CRUCIAL calcium-regulating hormone in pregnant and lactating animals since it increases intestinal calcium absorption, renal calcium reabsorption, and bone turnover ultimately to supply more calcium for fetal growth and milk production (4, 5). In vivo studies in rats suggested that PRL could stimulate transcellular and paracellular calcium absorption in several intestinal segments, particularly in the duodenum and proximal jejunum in which PRL receptors (PRLR) are strongly expressed (20, 25, 26). Although direct stimulatory actions of PRL on intestinal calcium transport has been demonstrated, little is currently known regarding the detailed mechanisms of PRL in intestinal epithelial cells.

Under normal conditions, calcium predominantly traverses the intestinal epithelium via the paracellular pathway, especially after a calcium-enriched meal that favors the calcium gradient-dependent paracellular calcium transport, whereas the transcellular calcium transport becomes more significant during high calcium demand, such as pregnancy and lactation (5, 23). A number of calcium transport proteins are essential for the transcellular calcium transfer, namely, transient receptor potential vanilloid family calcium channel (TRPV)-6 and voltage-dependent L-type calcium channel Ca$_v$1.3 for the apical calcium entry, calcium-binding protein (CaBP) calbindin-D$_{9k}$ for cytoplasmic translocation, and plasma membrane Ca^{2+}-ATPase (PMCA) isoform 1b and Na^+/Ca^{2+} exchanger (NCX)-1 for basolateral extrusion (18, 34, 35). It was apparent that, under the influence of various hormones and physiological conditions, different transport proteins may be recruited to augment calcium absorption. For example, L-type calcium channels were responsible for the enhanced transcellular calcium transport in response to parathyroid hormone-related peptide and luminal glucose (34, 51), while TRPV6 was required for the 1,25$(OH)_2D_3$- and 17β-estradiol-stimulated calcium absorption (23, 46). Regarding the PRL-stimulated calcium transport, it was not known which transporter proteins were involved.

The paracellular calcium transport driven by an electrochemical gradient (i.e., calcium gradient and voltage difference), on the other hand, is regulated by several tight junctions proteins, e.g., claudin-2 and -12, which polymerize to form an array of channel-like paracellular pores (15, 43, 47). Thus, the paracellular channels appeared to exhibit charge and size selectivity, voltage response, and rectification similar to those found in typical ion channels (12, 30, 41, 43). Physiological significance of the voltage-dependent calcium transport in the small intestine is controversial, but it may be of greater importance when the transepithelial potential difference (PD) is increased by some nutrients, such as glucose, short-chain fatty acid, phenylalanine, cysteine, and proline (14, 40, 48). Recently, PRL has been shown to modify some properties of the paracellular channel, i.e., charge selectivity and calcium permeability, which led to an enhancement of the calcium gradient-dependent paracellular calcium transport (45). The effects of PRL on other paracellular properties, such as response to

Address for reprint requests and other correspondence: N. Charoenphandhu, Dept. of Physiology, Faculty of Science, Mahidol Univ., Rama VI Road, Bangkok 10400, Thailand (e-mail: naratt@narattsys.com).

voltage change and rectification, or the voltage-dependent calcium transport remained unknown. However, they could not be demonstrated in the presence of calcium gradient because high calcium concentration occluded the paracellular pores (known as the paracellular conductance block), which in turn altered the transepithelial resistance (TER) (43, 45). Such paracellular properties should be validated by a voltage-clamp study in an absence of calcium gradient.

In addition to the calcium transport mechanism, the signaling pathways of PRL were also elusive. In the rat duodenum and intestinal epithelium-like Caco-2 monolayer, phosphoinositide 3-kinase (PI3K) was required for PRL signaling (20, 45). Further investigations in Caco-2 cells suggested that the PRL-stimulated transcellular and gradient-dependent paracellular calcium transport relied on protein kinase C (PKC) and RhoA-associated coiled-coil forming kinase (ROCK) (45), but which PKC isozyme was involved was not known.

Therefore, the objectives of the present study were *1*) to identify the transcellular transporters and PKC isozyme that were essential for the PRL-stimulated transcellular calcium transport, *2*) to investigate the paracellular properties altered by PRL, and *3*) to demonstrate the effects of PRL on the voltage-dependent calcium transport as well as the responsible signaling pathways. The human colorectal adenocarcinoma Caco-2 cells were used in this study because they have functional similarities to the small intestinal cells, including the presence of brush border, expression of sucrase-isomaltase, and expression of the transcellular calcium transporters and charge-selective paracellular proteins, e.g., TRPV6, PMCA, claudin-1, -2, -3, and -5 (32, 37, 38, 50, 52). Caco-2 monolayer was also a standard model for calcium absorption study and was responsive to PRL (20, 45).

MATERIALS AND METHODS

Cell culture. Caco-2 intestinal cells [no. HTB-37, American Type Culture Collection (ATCC)] were grown in Dulbecco's modified Eagle's medium (Sigma, St. Louis, MO) supplemented with 15% fetal bovine serum (Gibco, Grand Island, NY), 1% L-glutamine (Gibco), 1% nonessential amino acid (Sigma), 100 U/ml penicillin/streptomycin (Sigma), and 0.25 μl/ml amphotericin B (Sigma). Cells were propagated in 75-cm^2 T flask (Corning, NY) under a humidified atmosphere containing 5% CO_2 at 37°C and were subcultured as described in the ATCC protocol. Confluent Caco-2 monolayers were prepared by seeding cells (5.0×10^5 cells/cm^2) on polyester Snapwell with 12-mm diameter and 0.4-μm pore size (Corning). Culture medium was changed daily after 48 h of seeding. On *day 14* after seeding, the Snapwell was mounted in a modified Ussing chamber with an exposed surface area of 1.13 cm^2 to measure the electrical parameters and calcium fluxes, as previously described (45). The monolayer was equilibrated for 20 min in the chamber before the 60-min experiment was performed.

Small interfering RNA transfection. Small interfering RNA (siRNA) oligonucleotides targeted for human TRPV6 (5′-GGGAAACACAGUGUUACAC-3′ and 5′-GTGUAACACUGUGUUUCCC-3′), $Ca_v1.3$ (5′-GAGCACCUUUGACAAUUUC-3′ and 5′-AAGAAAUUGUCAAAGGTGCUC-3′), calbindin-D_{9k} (5′-GAUGAUCUCUUUCAAGAAC-3′ and 5′-GUUCUUGAAAGAGAUCAUC-3′), and PKC_ζ (5′-GACGACAAGAACGAGGACG-3′ and 5′-CUGCUGUUCUUGCUCCUGCAA-3′) were designed by siRNA Target Designer (version 1.51; Promega, Madison, WI), and synthesized by T7 RiboMax Express RNAi System (Promega) according to the manufacturer's instruction. Scramble siRNA that had no homology to any other genes was used as a negative control. As previously described (45), Caco-2 cells were first plated on Snapwell at 5.0×10^5 cells/cm^2. At *day 12* after seeding, in vitro transfection was performed with 10 μg/ml polyethyleneimine and 1 μmol/ml siRNA molecules. At *day 14* (i.e., 48 h after transfection), transepithelial calcium flux was determined. Efficiency of siRNA was evaluated by quantitative real-time PCR (qRT-PCR). The knockdown protocol was approved by the Institutional Biosafety Committee (IBC) of Mahidol University.

mRNA isolation, quantitative real-time PCR, and sequencing. By using TRIzol reagent (Invitrogen, Carlsbad, CA), total RNA was prepared from Caco-2 cells, as previously described (45). One microgram of total RNA was reverse-transcribed with iScript kit (Bio-Rad, Hercules, CA). Glyceraldehyde-3-phosphate dehydrogenase (GAPDH), a housekeeping gene, served as a control gene to check the consistency of the reverse transcription. Sense and antisense primers used for qRT-PCR are presented in Table 1. The amplification reaction using real-time PCR (model MiniOpticon; Bio-Rad) was performed with iQ SYBR Green SuperMix (Bio-Rad). Relative expression of studied genes over GAPDH was calculated from the threshold cycle (C_t) values by using $2^{\Delta C_t}$ method. After qRT-PCR, the PCR products were also visualized on a 1.5% agarose gel stained with 1.0 μg/ml ethidium bromide. Thereafter, all PCR products were extracted by the HiYield Gel/PCR DNA Extraction kit (Real Biotech, Taipei, Taiwan) and were sequenced by the ABI Prism 3100 Genetic Analyzer (Applied Biosystems, Foster City, CA).

Bathing solution. The bathing solution for Ussing chamber experiments contained (in mmol/l) 118 NaCl, 4.7 KCl, 1.1 $MgCl_2$, 1.25 $CaCl_2$, 23 $NaHCO_3$, 12 D-glucose, and 2 mannitol (all purchased from Sigma). The solution, continuously gassed with humidified 5% CO_2 in 95% O_2, was maintained at 37°C, pH 7.4, and had an osmolality of 290–293 mmol/kg water as measured by a freezing point-based osmometer (model 3320; Advanced Instruments, Norwood, MA).

Table 1. *Homo sapiens oligonucleotide sequences used in the quantitative real-time PCR experiments*

Name	Accession No.	Primer (forward/reverse)	Product Length, bp
TRPV6	AF365928	5′-TCTGACTGCGTGTTCTCAC-3′ 5′-ACATTCCTTGGCGTTCAT-3′	144
$Ca_v1.3$	EU363339	5′-TGATCCAAGTGGAGCAGTCA-3′ 5′-GTGTGAAAGTCCGGTAGGAGA-3′	113
Calbindin-D_{9k}	L13220	5′-TCTCCTGAGGAACTGAAGAGG-3′ 5′-GGGAATTCAGCCTGAATCAA-3′	106
PKC_ζ	NM_002744	5′-TAATCAGAGTCATCGGGCG-3′ 5′-TCTGTCTGTACCCAGTCAA-3′	138
GAPDH	NM_002046	5′-CTGGTAAAGTGGATATTGTTG-3′ 5′-GAGGCTGTTGTCATACTTCTC-3′	359

TRPV6, transient receptor potential vanilloid family Ca^{2+} channel 6; $Ca_v1.3$, voltage-dependent L-type Ca^{2+} channel 1.3; PKC_ζ, ζ-isozyme of protein kinase C; GAPDH, glyceraldehyde-3-phosphate dehydrogenase.

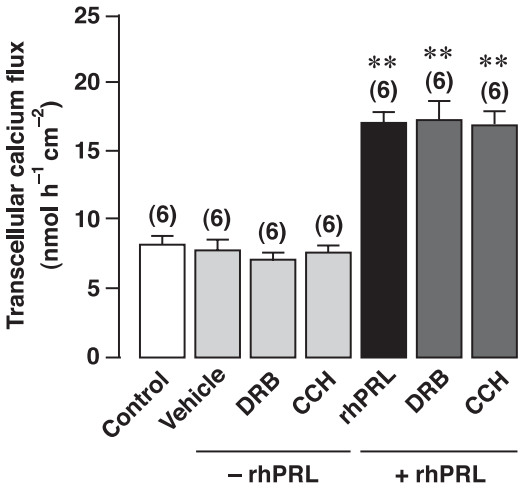

Fig. 1. Transcellular calcium transport in Caco-2 monolayers directly exposed to RNA polymerase II inhibitor [50 μmol/l 5,6-dichloro-1-β-D-ribobenzimidazole (DRB); inhibitor of gene transcription] or protein synthesis inhibitor (70 μmol/l cycloheximide; CCH) in the presence (+rhPRL) and absence (−rhPRL) of 600 ng/ml recombinant human prolactin (rhPRL). DMSO was used as vehicle for inhibitor preparation. Numbers in parentheses represent the number of independent Snapwells. $^{**}P < 0.01$ compared with the control group.

Distilled water used in the present work had a resistance >18.3 MΩ·cm and free-ionized calcium <2.5 nmol/l.

Measurement of electrical parameters. Electrical parameters, i.e., potential (voltage) difference (PD), short-circuit current (I_{sc}), and TER, were determined as described previously (7, 20). In brief, a pair of Ag/AgCl electrodes connected to agar bridges (3.0 mol/l KCl per 4 g% agar) was located near each surface of the mounted Snapwell for measurement of PD. The other ends of the PD-sensing electrodes were connected to a preamplifier (model EVC-4000; World Precision Instruments, Sarasota, FL). Another pair of Ag/AgCl electrodes connected in series to the EVC-4000 current-generating unit was placed at the end of each hemichamber to supply I_{sc} or external current for voltage clamping. TER was calculated from Ohm's equation. Fluid resistance was automatically subtracted by the EVC-4000 system.

Calcium flux measurement. Calcium fluxes were determined by modified method of Charoenphandhu et al. (7). After a 20-min incubation in Ussing chamber, the bathing solution was changed to a fresh one. The solution on one side contained ^{45}Ca (initial specific activity of 5 mCi/ml, final specific activity of ~450–500 mCi/mol; Amersham, Buckinghamshire, UK). Samples were collected from the chamber to calculate the unidirectional flux ($J_{H\rightarrow C}$) from the hot side (H) to the cold side (C), as follows:

$$J_{H\rightarrow C} = R_{H\rightarrow C}/(S_H \times A)$$

$$S_H = C_{45_{Ca}}/C_T$$

where $R_{H\rightarrow C}$ was the rate of tracer appearance in the cold side (cpm/h), S_H was the specific activity in the hot side (cpm/nmol), A was the surface area of Snapwell (cm^2), $C_{45_{Ca}}$ was a mean radioactivity in the hot side (cpm), and C_T was the total calcium in the hot side (nmol).

Radioactivity of ^{45}Ca in counts per minute (cpm) was analyzed by liquid scintillation spectrophotometer (model Tri-Carb 3100; Packard, Meriden, CT). Total calcium concentration in the hot side was determined by atomic absorption spectrophotometry (model SpectrAA-300; Varian Techtron, Springvale, Victoria, Australia). In the absence of transepithelial calcium gradient, i.e., bathing solution in both hemichambers contained equal calcium concentration of 1.25 mmol/l, the measured calcium fluxes represented the transcellular active calcium transport (45).

As for the experimental protocol, Caco-2 monolayer was directly incubated on the basolateral side for 60 min with 600 ng/ml recombinant human PRL (rhPRL) (purity >97%; catalog no. 682-PL; R&D Systems, Minneapolis, MN), which is the maximal effective concentration reported by Jantarajit et al. (20). In some experiments, the monolayers were also exposed to PKC activator [100 nmol/l phorbol-12-myristate-13-acetate (PMA), Calbiochem, San Diego, CA], or inhibitors for RNA polymerase II [50 μmol/l 5,6-dichloro-1-β-D-ribobenzimidazole (DRB), Calbiochem], protein biosynthesis (70 μmol/l cycloheximide, Sigma), L-type calcium channel (1, 5, or 10 μmol/l nifedipine, or 100 nmol/l verapamil; Sigma), calmodulin-dependent PMCA (100 μmol/l trifluoperazine, Sigma), $PKC_{\alpha/\beta}$ (5 μmol/l Gö-6976, Calbiochem), PKC_ζ (40 μmol/l myristoylated PKC_ζ pseudosubstrate peptide; Calbiochem), PKC_θ (30 μmol/l myristoylated PKC_θ pseudosubstrate peptide; Calbiochem), PKC_ε (4 μmol/l PKC_ε translocation inhibitor peptide; Calbiochem), or PKA (10 μmol/l myristoylated PKA inhibitor 14–22 amide; Calbiochem).

Voltage clamping. Calcium fluxes in clamped preparations represented the voltage-dependent calcium transport through the paracellular route (22). Transepithelial potential differences across the con-

Table 2. *Epithelial electrical parameters of Caco-2 monolayers*

Condition	n	Electrical Parameter		
		PD, mV	I_{sc}, μA/cm^2	TER, Ω·cm^2
Control	15	1.01±0.12	2.73±0.70	376.67±37.56
Vehicle	10	0.94±0.32	2.60±0.84	386.67±35.83
600 ng/ml rhPRL	15	0.88±0.19	3.47±0.92	253.22±28.01*
Inhibitors				
50 μmol/l DRB	12	1.03±0.28	2.50±0.67	418.75±82.28
70 μmol/l CCH	13	1.03±0.23	2.62±0.51	396.15±55.76
10 μmol/l Nifedipine	14	1.17±0.33	3.00±0.88	395.48±48.35
100 nmol/l Verapamil	10	0.95±0.22	2.50±0.53	381.67±46.78
100 μmol/l TFP	10	0.96±0.28	2.40±0.70	405.00±66.23
5 μmol/l Gö-6976	6	1.27±0.19	3.17±0.40	394.44±15.47
40 μmol/l myr-PKC_ζ	6	1.28±0.14	3.50±0.43	371.39±15.09
30 μmol/l myr-PKC_θ	6	1.08±0.12	2.67±0.33	430.56±23.34
4 μmol/l trans-PKC_ε	6	1.03±0.11	2.50±0.22	413.89±23.37
100 nmol/l PMA	4	1.08±0.13	2.25±0.25	408.33±49.30
10 μmol/l PKAI 14-22	4	1.00±0.12	2.50±0.58	408.35±48.11
600 ng/ml rhPRL$^+$				
50 μmol/l DRB	12	0.83±0.31	3.33±1.03	241.39±40.14*
70 μmol/l CCH	13	0.89±0.27	3.46±0.88	256.28±36.57*
10 μmol/l Nifedipine	14	0.77±0.22	3.14±0.77	243.45±29.63*
100 nmol/l Verapamil	10	0.92±0.40	3.67±1.37	245.83±34.86*
100 μmol/l TFP	10	0.87±0.16	3.50±0.55	248.61±35.13*
5 μmol/l Gö-6976	6	1.02±0.21	3.83±0.98	268.06±19.62*
40 μmol/l myr-PKC_ζ	6	1.00±0.19	4.50±0.89	225.00±06.80*
30 μmol/l myr-PKC_θ	6	1.13±0.20	4.33±0.71	259.80±08.52*
4 μmol/l trans-PKC_ε	6	0.93±0.19	3.50±1.05	276.94±49.89*
100 nmol/l PMA	4	1.00±0.21	4.00±0.82	250.00±10.21*
10 μmol/l PKAI 14-22	4	0.95±0.13	3.75±0.50	254.17±22.05*

Values are means ± SE. Caco-2 monolayer was exposed to recombinant human prolactin (rhPRL), RNA polymerase II inhibitor [5,6-dichloro-1-β-D-ribobenzimidazole (DRB)], protein synthesis inhibitor [cycloheximide (CCH)], L-type calcium channel blockers (nifedipine and verapamil), plasma membrane Ca^{2+}-ATPase (PMCA) inhibitor [trifluoperazine (TFP)], PKC inhibitors [Gö-6976 for $PKC_{\alpha/\beta}$, myristoylated (myr) pseudosubstrates for $PKC_{\zeta/\theta}$ and translocation (trans) inhibitor peptide for PKC_ε], PKC activator (PMA), myristoylated PKA inhibitor 14-22 amide (PKAI 14-22), or rhPRL plus inhibitors. DMSO (0.3% vol/vol) was used as vehicle for preparation of inhibitors. Mounted monolayer was bathed on both sides with 1.25 mmol/l calcium-containing solution. The apical side was negative with respect to the basolateral side. PD, potential difference; I_{sc}, short-circuit current; TER, transepithelial resistance. $^*P < 0.01$ compared with the control group.

trol and 600 ng/ml rhPRL-treated monolayers were clamped to −25, −10, −5, 0, +5, +10, or +25 mV (the serosal side was considered zero) during 60-min experiment by using EVC-4000 system. Transepithelial calcium fluxes in apical-to-basolateral (A-to-B) and basolateral-to-apical (B-to-A) directions were determined. Net calcium flux was a subtraction of B-to-A flux from A-to-B flux. In some experiments, Caco-2 monolayers ($n = 5$ per each voltage; total 280 Snapwells used) were exposed to 600 ng/ml rhPRL plus PI3K inhibitor (75 μmol/l LY-294002; Tocris Bioscience, Bristol, UK), panspecific PKC inhibitor (1 μmol/l GF-109203X; AG Scientific, San Diego, CA), or ROCK inhibitor (1 μmol/l Y-27632; Calbiochem).

Calcium uptake study. The calcium uptake protocol was modified from the method of Charoenphandhu et al. (6). In brief, Caco-2 cells (1.0×10^6 cells/cm^2) were propagated in 6-well plates for 3 days. Confluent Caco-2 cells were then incubated with 600 ng/ml rhPRL for 60 min until ^{45}Ca was added to obtain a final specific activity of ~500 mCi/mol. After exactly 1-, 3-, 6-, 9-, 12-, 20-, 30-, or 40-min exposure to ^{45}Ca ($n = 5$ per each time interval; total 225 setups used; cells for 0 min were not incubated with ^{45}Ca), cells were immediately washed in ice-cold ^{45}Ca-free solution to stop the physiological processes, placed in 5 mmol/l EGTA-containing solution to eliminate the adsorbed extracellular calcium, centrifuged at 550 *g* for 5 min, and finally lysed by 30% vol/vol Triton X-100. Radioactivity of ^{45}Ca in the homogenate was analyzed by a liquid scintillation spectrophotometer (Packard). Cellular protein was determined by bicinchoninic acid method using a commercial kit (Sigma). In some experiments, 600 ng/ml rhPRL-treated cells were also incubated with 75 μmol/l LY-294002, 1 μmol/l GF-109203X, or 1 μmol/l Y-27632.

Statistical analysis. Results are expressed as means ± SE. Two sets of data were compared using the unpaired Student's *t*-test. One-way analysis of variance with Dunnett's multiple-comparison test was used for multiple sets of data. The level of significance for all statistical tests was $P < 0.05$. The curves of calcium uptake vs. time and of calcium flux vs. voltage were obtained using one-phase association and second-order polynomial equations, respectively (36). Data were analyzed by GraphPad Prism 4.0 for Mac OS X (GraphPad Software, San Diego, CA).

RESULTS

PRL signaling in Caco-2 monolayer was nongenomic and protein synthesis independent. Calcium flux studies using Ussing chamber technique demonstrated that 600 ng/ml rhPRL significantly increased the transcellular calcium transport by ~2.13-fold (Fig. 1), while decreasing TER in Caco-2 monolayer (Table 2). PRL effects occurred within 60 min after treatment. Exposure to PRL plus inhibitors of de novo gene transcription (50 μmol/l DRB) or protein biosynthesis (70 μmol/l cycloheximide) had no effect on the transcellular calcium transport (Fig. 1). DRB or cycloheximide alone were without effect on the basal calcium transport (Fig. 1) and

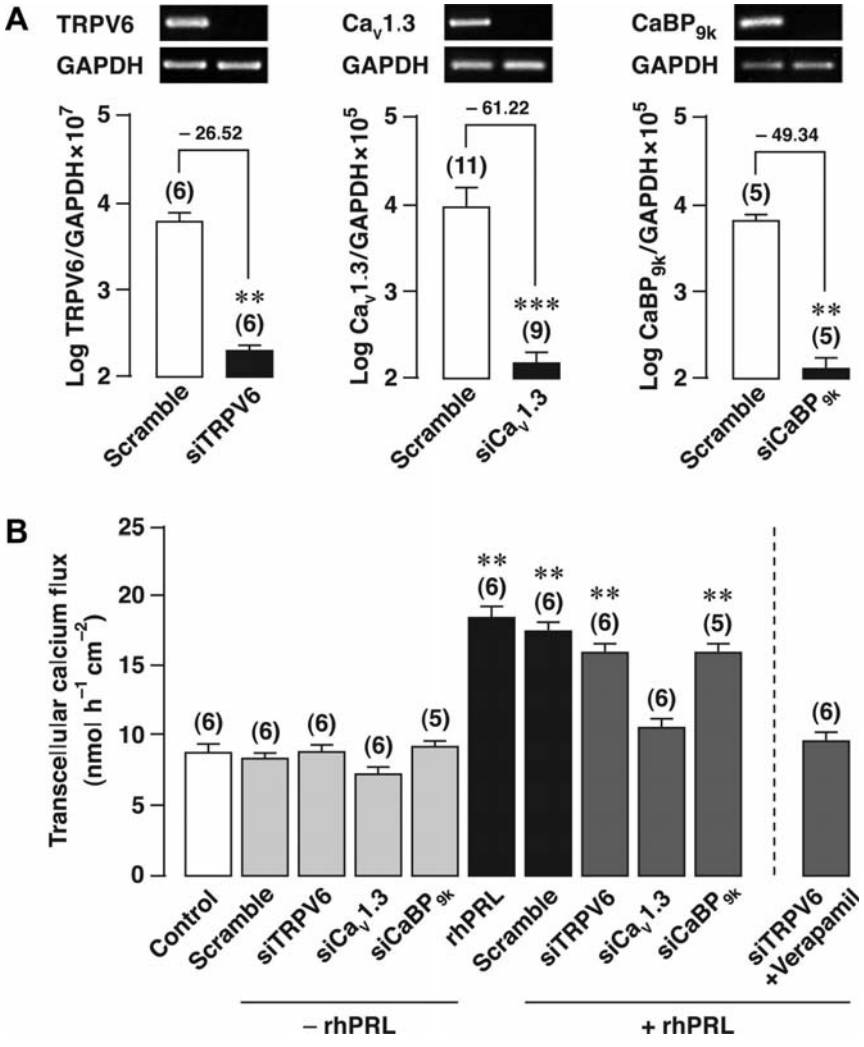

Fig. 2. *A*: expression of transient receptor potential vanilloid family calcium channel 6 (TRPV6), voltage-dependent L-type Ca^{2+} channel 1.3 ($Ca_v1.3$) and calbindin-D_{9k} ($CaBP_{9k}$) in Caco-2 cells transfected with scramble small interfering RNA (siRNA; negative control) or siRNA targeting (si) TRPV6, $Ca_v1.3$, or $CaBP_{9k}$ mRNAs. Quantitative real-time PCR (qRT-PCR) results are expressed as log means ± SE. Representative electrophoretic bands and fold differences between the expression in control and knockdown cells (conventional PCR, 36 cycles) are also presented along with qRT-PCR results. GAPDH was used for normalization. $^{**}P < 0.01$, $^{***}P < 0.001$ compared with scramble. *B*: transcellular calcium transport in TRPV6, $Ca_v1.3$, and $CaBP_{9k}$ knockdown Caco-2 monolayers with (+rhPRL) or without (−rhPRL) 600 ng/ml rhPRL in the basolateral solution. In some experiments, TRPV6 knockdown monolayers were exposed to 600 ng/ml rhPRL plus 100 nmol/l verapamil ($Ca_v1.3$ blocker; on the apical side). Control group denotes normal Caco-2 monolayers (without siRNA transfection). $^{**}P < 0.01$ compared with the control group. Numbers in parentheses represent the number of independent Snapwells.

Table 3. *Epithelial electrical parameters of knockdown Caco-2 monolayers*

Condition	n	Electrical Parameter		
		PD, mV	I_{sc}, μA/cm²	TER, Ω·cm²
Control	6	0.98±0.24	2.33±0.52	427.78±89.24
Scramble	6	0.88±0.54	2.17±1.17	409.72±66.34
siTRPV6	6	0.98±0.43	2.33±0.82	416.67±75.28
si$Ca_v1.3$	6	0.90±0.30	2.60±0.24	391.67±49.16
si$CaBP_{9k}$	5	1.10±0.23	3.17±0.75	351.38±35.13
siPKC_ζ	3	0.87±0.21	2.33±0.58	372.22±25.46
600 ng/ml rhPRL	6	0.84±0.11	3.17±0.98	248.89±27.22*
600 ng/ml rhPRL⁺				
Scramble	6	0.75±0.58	2.83±1.60	250.00±49.55*
siTRPV6	6	0.82±0.37	3.17±1.17	252.22±35.07*
si$Ca_v1.3$	6	0.93±0.62	3.67±1.86	243.06±33.51*
si$CaBP_{9k}$	5	1.00±0.28	4.17±1.17	242.22±34.10*
siTRPV6 + verapamil	6	0.87±0.27	3.83±0.98	225.28±31.10*
siPKC_ζ	3	0.80±0.30	3.33±0.58	236.11±60.28*

Values are means ± SE. Caco-2 cells were transfected with small interfering (si)RNAs targeting (si) TRPV6, $Ca_v1.3$, calbindin-D_{9k} ($CaBP_{9k}$), or PKC_ζ. Mounted monolayer was bathed on both sides with 1.25 mmol/l calcium-containing solution. The apical side was negative with respect to the basolateral side. In some experiments, TRPV6-knockdown monolayers were incubated with 100 nmol/l verapamil, which inhibited $Ca_v1.3$ activity. *$P < 0.01$ compared with the control group.

electrical parameters (Table 2). The effect of DRB were consistent with that reported previously (45). The data indicated that PRL exerted stimulatory effects on the transcellular calcium transport via nongenomic, protein synthesis-independent signaling pathways.

PRL increased transcellular calcium transport via L-type calcium channel $Ca_v1.3$ and PMCA. In the transcellular calcium transport, calcium has been reported to traverse the apical membrane through TRPV6 and $Ca_v1.3$ before binding to calbindin-D_{9k} for cytoplasmic translocation to the basolateral side (18, 31, 34). We therefore generated siRNA-transfected Caco-2 monolayers to verify the significance of each putative protein in the PRL-stimulated calcium transport. We show in Fig. 2 that knockdown of TRPV6, $Ca_v1.3$, and calbindin-D_{9k} markedly reduced mRNA expressions by 26.52-, 61.22-, and 49.34-fold, respectively, with no significant effect on the basal calcium transport or electrical parameters (Table 3). Interestingly, the PRL-enhanced calcium transport was completely abolished in $Ca_v1.3$ knockdown monolayer, and not in the TRPV6 and calbindin-D_{9k} knockdown monolayers (Fig. 2*B*). Exposure to 1, 5, and 10 μmol/l nifedipine, a classical L-type calcium channel blocker (dihydropyridine group), on the apical side, but not the basolateral side, diminished the PRL-stimulated transcellular calcium transport in a concentration-dependent manner (Fig. 3). Similar inhibition was observed after incubating Caco-2 monolayer on the apical side with another L-type calcium channel blocker, verapamil (phenylalkylamine group) (Fig. 3). The involvement of $Ca_v1.3$ in the calcium transport response to PRL was supported by the finding that 100 nmol/l verapamil could prevent the PRL-stimulated calcium transport in TRPV6 knockdown monolayer (Fig. 2*B*). The results, therefore, indicated that $Ca_v1.3$ at the apical membrane was required for calcium entry during the PRL-stimulated transcellular calcium transport. Basolateral calcium extrusion under PRL stimulation was likely to be mediated by PMCA rather than NCX1, since calcium flux was totally abolished by a calmodulin-dependent PMCA inhibitor trifluoperazine (Fig. 3).

PRL stimulated apical calcium uptake via the PKC signaling pathway. Although $Ca_v1.3$, a channel for calcium entry, was required for PRL actions, the effects of PRL on apical calcium uptake in Caco-2 cells as well as responsible signaling pathways were not known. Herein, the calcium uptake study showed that, under normal conditions, the relationship between calcium uptake and time complied with the one-phase association equation ($r^2 = 0.95$), and calcium accumulation in Caco-2 cells ascended to the maximal value (Y_{max}) of ~15 nmol/μg protein with a rate constant of ~0.15 min^{-1} (Fig. 4). Exposure to 600 ng/ml rhPRL did not change Y_{max} value. However, the rate constant that represented the rate of calcium uptake was increased in PRL-treated cells by approximately twofold (Fig. 4*D*).

To demonstrate the PRL signaling pathways for stimulation of apical calcium uptake, Caco-2 cells were incubated with inhibitors for PI3K, PKC, and ROCK, all of which have been reported to mediate PRL actions in intestinal epithelial cells (20, 45). The results showed that PI3K inhibitor (LY-294002) and panspecific PKC inhibitor (GF-109203X), but not ROCK

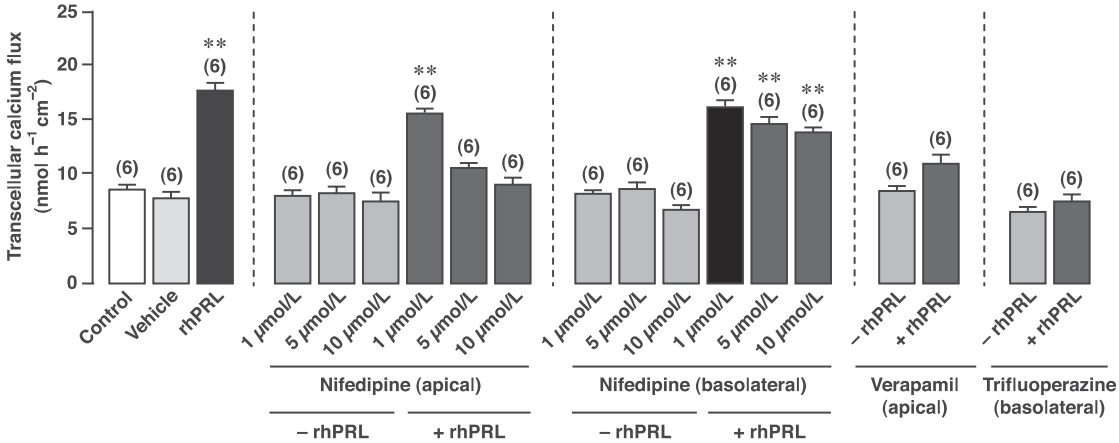

Fig. 3. Transcellular calcium transport in Caco-2 monolayers directly exposed on the apical side to L-type calcium channel blockers (1, 5, and 10 μmol/l nifedipine or 100 nmol/l verapamil), or on the basolateral side to various concentrations of nifedipine or plasma membrane Ca^{2+}-ATPase (PMCA) inhibitor (100 μmol/l trifluoperazine) in the presence (+rhPRL) and absence (−rhPRL) of 600 ng/ml rhPRL. DMSO was used as vehicle for inhibitor preparation. Numbers in parentheses represent the number of independent Snapwells. **$P < 0.01$ compared with the control group.

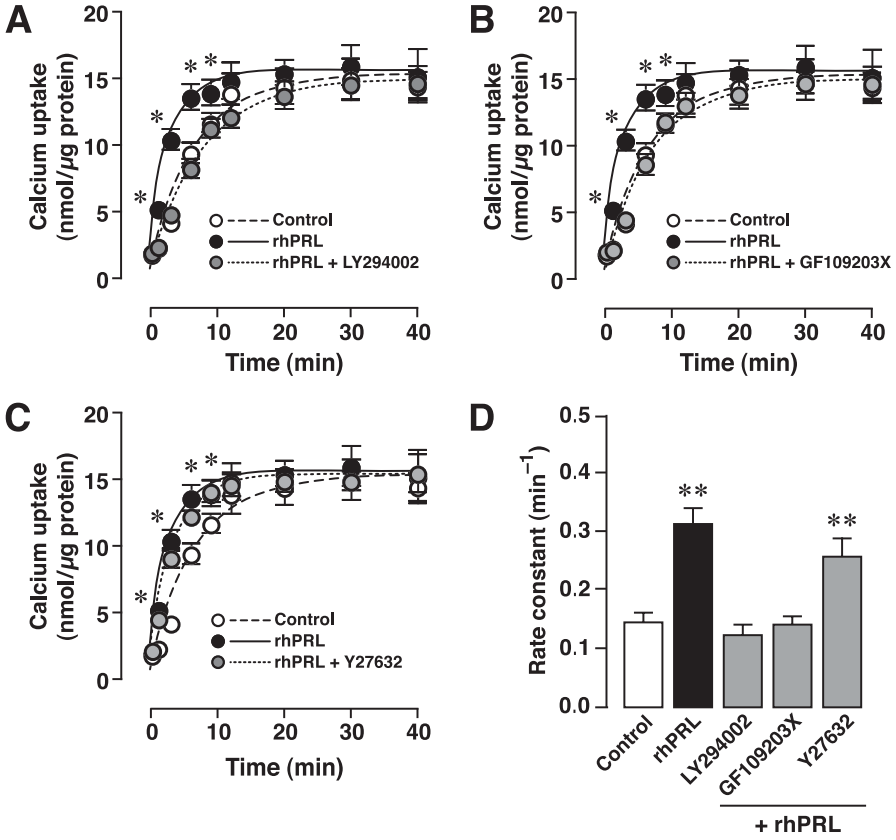

Fig. 4. Calcium uptake in Caco-2 cells (n = 5 per each time interval; total 225 Snapwells used) treated with 600 ng/ml rhPRL, or rhPRL plus phosphoinositide 3-kinase (PI3K) inhibitor (75 μmol/l LY-294002) (*A*), panspecific PKC inhibitor (1 μmol/l GF-109203X) (*B*), or RhoA-associated coiled-coil forming kinase (ROCK) inhibitor (1 μmol/l Y-27632) (*C*). Cells were incubated in ^{45}Ca-containing solution for 0, 1, 3, 6, 9, 12, 20, 30, or 40 min. Control and rhPRL data in *A* were reused in *B* and *C* for better comparison. *$P < 0.01$ rhPRL vs. control. *D*: rate constant, which is indicative of the rate of calcium uptake, in Caco-2 cells exposed to rhPRL or rhPRL plus inhibitors. Data were obtained from the one-phase association curves in *A–C*. **$P < 0.01$ compared with the control group.

inhibitor (Y-27632), could abolish the effect of PRL on calcium uptake (Fig. 4).

The effect of PRL on the transcellular calcium transport was mediated by PKC$_\zeta$. Since the calcium uptake study showed that PKC was required for the PRL-stimulated transcellular calcium transport, we proceeded to identify the responsible PKC isozyme by exposing Caco-2 monolayer to various PKC isozyme inhibitors in the presence or absence of 600 ng/ml rhPRL. We demonstrated that PKC inhibitors alone had no effect on the basal calcium transport (Fig. 5). PKC$_\zeta$ inhibitor, but not inhibitors of PKC$_{\alpha/\beta}$ (Gö-6976), PKC$_\theta$, or PKC$_\varepsilon$, abolished the PRL-enhanced transcellular calcium transport in Caco-2 monolayer (Fig. 5). Since a high concentration of Gö-6976 (5 μmol/l) used in the present study also inhibited PKC$_\mu$ (16), it was likely that PRL action did not involve PKC$_\mu$. A classical PKC activator, phorbol-12-myristate-13-acetate (PMA), which could not activate PKC$_\zeta$, also itself stimulated the transcellular calcium transport but with a smaller magnitude than PRL (Fig. 5). Exposure to 600 ng/ml rhPRL further increased calcium transport in PMA-treated monolayer (Fig. 5). Neither PKC inhibitors nor PMA had effect on the PRL-induced decrease in TER (Table 2).

Since a number of hormones, such as parathyroid hormone and 1,25(OH)$_2$D$_3$, enhanced calcium transport through the

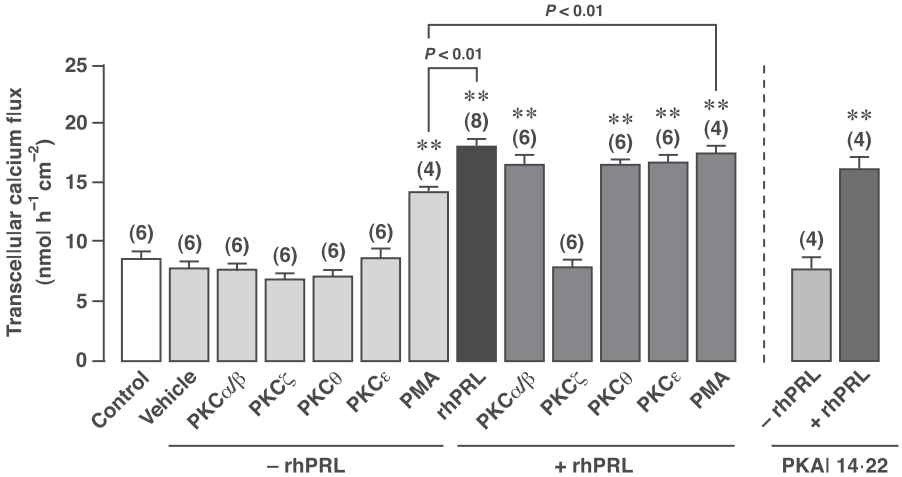

Fig. 5. Transcellular calcium transport in Caco-2 monolayers exposed to selective PKC$_{\alpha/\beta}$ inhibitor (5 μmol/l Gö-6976), 40 μmol/l myristoylated PKC$_\zeta$ pseudosubstrate peptide, 30 μmol/l myristoylated PKC$_\theta$ pseudosubstrate peptide, 4 μmol/l PKC$_\varepsilon$ translocation inhibitor peptide, PKC activator (100 nmol/l phorbol-12-myristate-13-acetate; PMA), or 10 μmol/l myristoylated PKA inhibitor 14-22 amide (PKAI 14-22), in the presence (+rhPRL) or absence (−rhPRL) of 600 ng/ml rhPRL. All cell-permeable inhibitor peptides were dissolved in water. Gö-6976 and PMA were dissolved in DMSO (vehicle). Numbers in parentheses represent the number of independent Snapwells. **$P < 0.01$ compared with the control group.

transcellular route in a protein kinase A (PKA)-dependent manner (10, 11, 23), we examined a possibility of PKA-mediated PRL action. However, exposure to a cell-permeable PKA inhibitor, myristoylated PKA inhibitor 14-22 amide, did not prevent the PRL effect on the transcellular calcium transport (Fig. 5).

PKC_ζ knockdown abolished the PRL-stimulated transcellular calcium transport. To confirm that PRL exerted its actions through PKC_ζ, calcium fluxes were determined in PKC_ζ knockdown Caco-2 monolayer, which manifested a decrease in PKC_ζ mRNA expression by 68.86-fold (Fig. 6*A*). The results showed that 600 ng/ml rhPRL did not increase the transcellular calcium flux in PKC_ζ knockdown monolayer (Fig. 6*B*), while neither scramble siRNA nor PKC_ζ siRNA altered the basal calcium flux (Fig. 6*B*) or electrical parameters (Table 3). However, PKC_ζ knockdown had no effect on the PRL-induced decrease in TER (Table 3).

PRL enhanced the voltage-dependent paracellular calcium via ROCK pathway. In addition to the transcellular pathway, PRL has been reported to augment calcium movement through the paracellular space. However, effects of PRL on the voltage-dependent paracellular calcium transport were not known. Under normal conditions, the voltage-clamp study revealed that the apical-to-basolateral (A-to-B; Fig. 7*A*) calcium fluxes were dramatically increased with positive apical voltage (basolateral voltage was zero), whereas the increase in basolateral-to-apical (B-to-A; Fig. 7*B*) calcium fluxes with negative apical voltage was comparatively much smaller. Given an equal driving force (i.e., transepithelial voltage) of opposite signs, the presence of unidirectional calcium fluxes being larger in one direction than the other suggested that the paracellular space of Caco-2 monolayer possessed a property known as rectification. This phenomenon, therefore, resulted in a large net calcium flux (equivalent to electrical current) at apical voltage positive and a relatively small net calcium flux at voltage negative (Fig. 7, *C* and *F*).

PRL-treated Caco-2 monolayer exhibited significant increases in A-to-B and B-to-A calcium fluxes at the apical voltage ranges of 0 to +25 mV and −25 to −5 mV, respectively, thereby increasing the net calcium fluxes (Fig. 7*C*). Interestingly, after PRL exposure, the B-to-A calcium flux vs. voltage curve nearly became a mirror image of the A-to-B curve. In other words, paracellular space of PRL-treated Caco-2 monolayer no longer exhibited rectification. Such PRL effects on the voltage-dependent paracellular calcium transport were completely abolished by 75 μmol/l LY-294002 (Fig. 7, *A–C*) and 1 μmol/l Y-27632 (Fig. 7, *D–F*), which were PI3K and ROCK inhibitors, respectively.

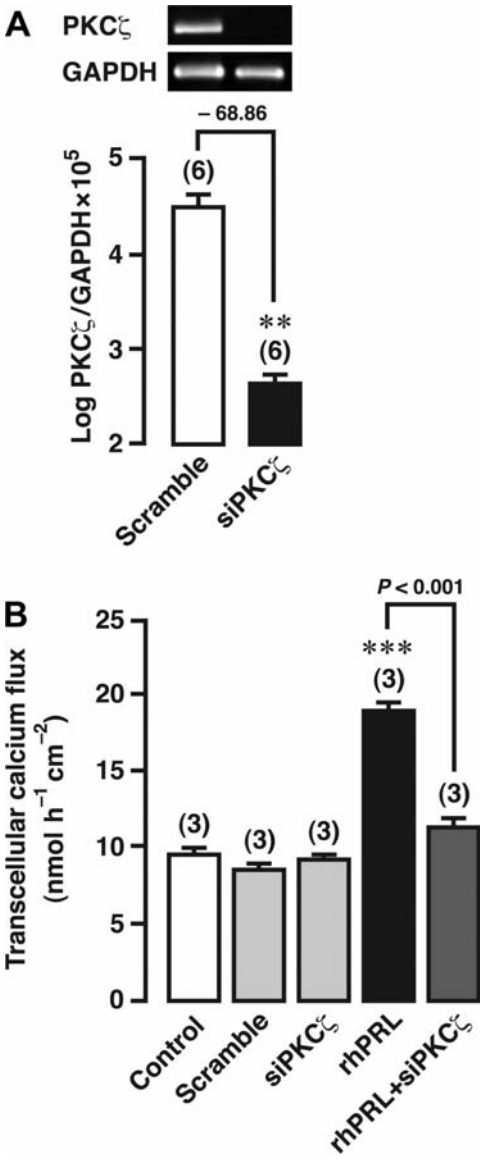

Fig. 6. *A*: expression of PKC_ζ in Caco-2 cells transfected with scramble siRNA (negative control) or siRNA targeting PKC_ζ. qRT-PCR results are expressed as log means ± SE. Representative electrophoretic bands and fold differences between the expression in control and knockdown cells (conventional PCR, 36 cycles) are also presented along with qRT-PCR results. GAPDH was used for normalization. $^{**}P < 0.01$ compared with scramble. *B*: transcellular calcium transport in PKC_ζ knockdown Caco-2 monolayers exposed to 600 ng/ml rhPRL. The control group denotes normal Caco-2 monolayers (without siRNA transfection). $^{***}P < 0.001$ rhPRL vs. rhPRL + $siPKC_\zeta$. Numbers in parentheses represent the number of independent Snapwells.

DISCUSSION

Although the cellular mechanism of PRL action was still not fully understood, a twofold increase in the intestinal calcium absorption both in vivo and in vitro induced by PRL suggested a significant role of this hormone as a regulator of calcium homeostasis in conditions of high circulating PRL levels, such as in pregnancy and lactation (5). In the present study, we provided further information on the cellular mechanism of PRL as well as the possible signaling pathways. Acting via PI3K and PKC_ζ, PRL enhanced the transcellular active calcium transport by increasing calcium entry through $Ca_v1.3$ and the basolateral calcium extrusion by PMCA. PRL also stimulated the voltage-dependent paracellular calcium transport through PI3K and ROCK.

The theoretical concept of the transcellular calcium transport in the intestine was recently challenged by the findings that calbindin-D_{9k} knockout and TRPV6/calbindin-D_{9k} double-knockout mice were normocalcemic and still exhibited active calcium absorption (1, 2, 27). We also found in this study that the rapid nongenomic effects of PRL on the transcellular active calcium transport in Caco-2 monolayer did not require the

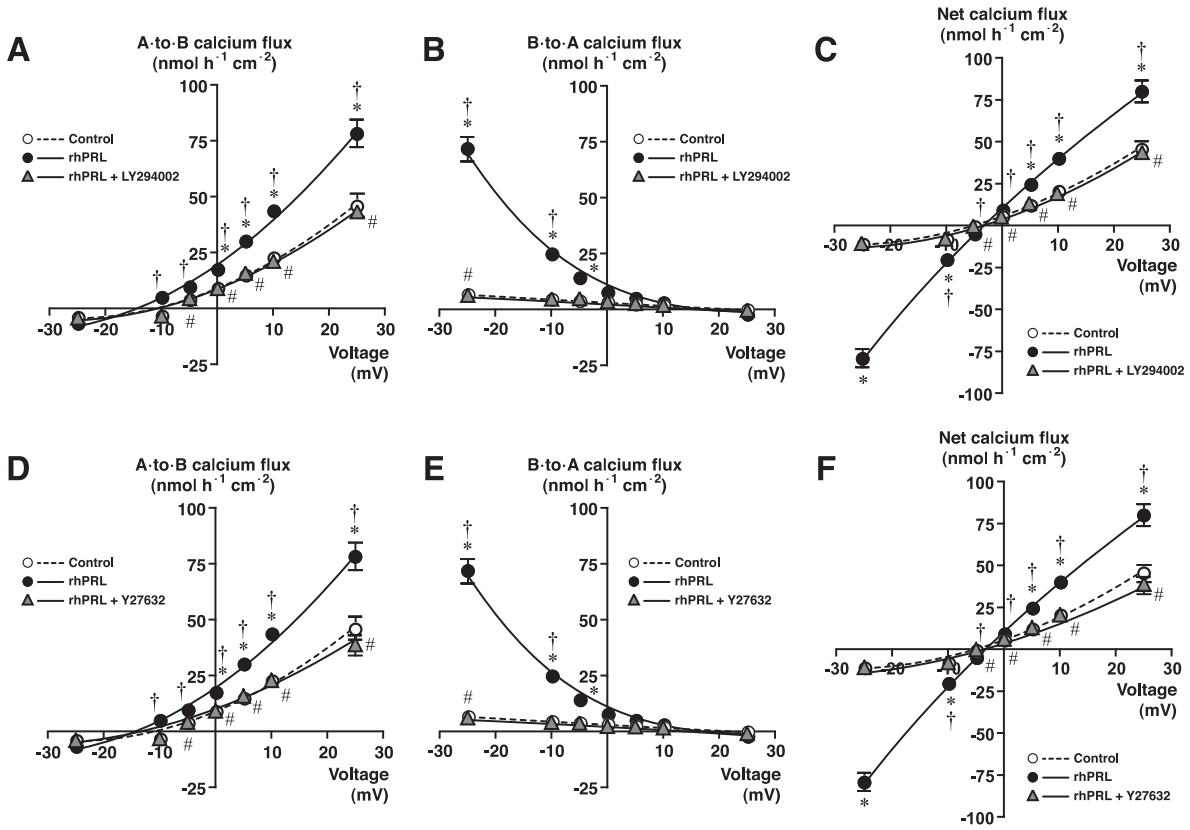

Fig. 7. Effects of PI3K inhibitor (75 μmol/l LY-294002) (*A–C*) and ROCK inhibitor (1 μmol/l Y-27632) (*D–F*) on the PRL-enhanced voltage-dependent paracellular calcium transport across Caco-2 monolayer ($n = 5$ per each voltage point; total 280 Snapwells used). The apical voltage was clamped to −25, −10, −5, 0, +5, +10, or +25 mV, with the basolateral side being a reference. Calcium fluxes in the apical-to-basolateral (A-to-B) (*A* and *D*) and basolateral-to-apical (B-to-A) (*B* and *E*) directions as well as net calcium fluxes (*C* and *F*) are presented. By using paired Snapwells, the net calcium flux was a subtraction of B-to-A flux from A-to-B flux. The mounted Snapwell was bathed on both sides with 1.25 mmol/l Ca^{2+}-containing solution. *$P < 0.01$ rhPRL vs. control. †$P < 0.01$, value of the rhPRL-treated group vs. value of the rhPRL-treated group at −25 mV (for A-to-B and net flux) or +25 mV (for B-to-A). #$P < 0.01$ value of the control group vs. value of the control group at −25 mV (for A-to-B and net flux) or +25 mV (for B-to-A). Values of the control and rhPRL-treated groups in *D*, *E*, and *F* are from those in *A*, *B*, and *C*, respectively.

presence of TRPV6 or calbindin-D_{9k}, although both transport proteins may contribute to the responses to other hormones, such as genomic $1,25(OH)_2D_3$, 17β-estradiol, and glucocorticoids (19, 46). It appeared that redundancy in the mechanisms underlying calcium absorption may involve other calcium channel(s), such as L-type and T-type calcium channels, which could provide alternative route for apical calcium entry (9). Supporting evidence was provided by recent reports that dihydropyridine (nifedipine)- and phenylalkylamine (verapamil)-sensitive L-type calcium channel $Ca_v1.3$ could mediate calcium entry for the transcellular calcium absorption, especially during ingestion of high-calcium diet (31, 34). Nifedipine and verapamil also inhibited the stimulatory effects of parathyroid hormone-related peptide, nongenomic $1,25(OH)_2D_3$, and luminal glucose on intestinal calcium absorption (10, 34, 51). Our previous microarray study has identified several L-type calcium channels upregulated in the duodenal epithelial cells of the pituitary-grafted hyperprolactinemic rats (8). Here, the absence of PRL effect on calcium transport after $Ca_v1.3$ knockdown or nifedipine/verapamil exposure strongly suggested a physiological role of $Ca_v1.3$ during PRL stimulation.

Similar to the apical calcium entry, the cytoplasmic calcium translocation across the intestinal epithelial cells may be mediated by other calcium-binding proteins (CaBP) besides calbindin-D_{9k}, e.g., calmodulin and parvalbumin, as well as vesicular calcium transport (3, 13). Interestingly, the duodenal epithelial cells of hyperprolactinemic rats were found to manifest a ~17-fold increase in parvalbumin mRNA expression as demonstrated by microarray (8), but its physiological significance in calcium transport remains to be investigated. Regarding the basolateral calcium extrusion, ~80–85% of calcium efflux normally occurs through PMCA, whereas the remaining is performed by NCX1 (18, 49). PRL was previously found to increase PMCA activity in purified basolateral membrane vesicles from the duodenum (6); therefore, PMCA was likely to mediate the PRL-enhanced calcium transport.

As for the paracellular pathway, the present results together with that reported by Thongon et al. (45) suggest that PRL augmented the paracellular calcium absorption in a concentration- and voltage-dependent manner. In the study of passive calcium absorption, PRL was found to alter the charge-selective property of tight junction without changing the pore size, thereby increasing calcium permeability and calcium flux through the paracellular route (44, 45). Our present investigation (Fig. 7) further suggests that the paracellular pores for calcium transport are rectifiers. In other words, the paracellular pores can conduct much larger A-to-B calcium flux at apical voltages positive than B-to-A calcium flux at apical voltage

negative even in an absence of the transepithelial calcium gradient, rendering the degree of rectification $J_{i,+25}/J_{o,-25} = 46.23/6.95 \approx 7$ (where J represents calcium flux in $nmol \cdot h^{-1} \cdot cm^{-2}$ at +25 mV or −25 mV; i and o denote A-to-B and B-to-A, respectively). The paracellular rectification could be explained by a model of a channel (or pore) with an energy barrier that impedes calcium movement in a B-to-A direction (for review see Ref. 41). Although the exact paracellular structures acting as the energy barrier have never been identified, we speculated that they might be tight junction proteins, claudins, which had their charge-selective extracellular loops protruding into the paracellular space (47). Several claudins, such as claudin-2, -3, and -12, are known to be involved in the intestinal calcium absorption (7, 15).

After exposure to PRL, the voltage-dependent calcium transport in both A-to-B and B-to-A directions were markedly increased, and the degree of rectification was reduced to ~1, suggesting that an energy barrier or cation-selective barriers of the paracellular pores were removed by PRL. Changes in the paracellular barrier properties could have resulted from the PRL-induced claudin phosphorylation (L. Nakkrasae and N. Charoenphandhu, unpublished observation, 2009). PRL-enhanced voltage-dependent paracellular calcium transport may be of physiological importance, presumably when the intestinal absorptive cells were exposed to nutrients that could alter the transepithelial potential difference, e.g., glucose, short-chain fatty acid, and neutral amino acids (14, 40, 48). Although the modulation of potential difference could also facilitate calcium transport via the transcellular pathway (11), the transcellular calcium transport was much smaller in magnitude when compared with the paracellular calcium transport, particularly in Caco-2 monolayer (7, 45). However, there was a disparity regarding the magnitude of paracellular calcium flux between different models. For example, in perfused intestinal loop, nifedipine inhibited calcium absorption in the presence of 10 mmol/l luminal calcium with similar extent to 1.25 mmol/l calcium, suggesting that the majority of calcium flux in this model was Ca_v mediated rather than diffusive paracellular (35).

The action of PRL on calcium absorption involved the signaling molecules PI3K, PKC, and ROCK (20, 45). PI3K was likely to be the most upstream mediator, which transmitted PRL signals to PKC and ROCK for the transcellular and paracellular calcium transport, respectively (17, 21, 29, 45). In some cells, e.g., L6 muscle cells, PKC_ζ is a key molecule within the PI3K signal cascade (39). PKC is a large family of serine/threonine kinases, consisting of ~12 members (33). Some PKC isozymes, e.g., PKC_α, PKC_β, and PKC_θ, but not PKC_ζ, are activated by diacylglycerol (DAG), rendering them sensitive to DAG analog phorbol ester (i.e., PMA) (33). Several investigators provided evidence that activities of the transcellular calcium transport proteins TRPV6, $Ca_v1.3$, and PMCA could be modulated by PKA and/or PKC, especially $PKC_{\beta II}$ (23, 24, 34). However, PKA and phorbol-sensitive PKCs (e.g., PKC_α, PKC_β, and PKC_θ) were not involved in PRL signaling, since PRL actions were blocked only by an inhibitor or siRNA of PKC_ζ, which is a phorbol-insensitive isozyme (33). The presence of the additive effect of PRL in PMA-treated monolayer also suggested that PRL signaled through another signaling pathway that was not phorbol-sensitive PKCs. The absence of PRL-PMA synergism or truly additive effect, on the other hand, probably indicated that PKC_ζ and phorbol-sensitive PKCs shared some target proteins.

In addition to the calcium gradient-dependent calcium transport, PRL exerted its stimulatory effects on the voltage-dependent calcium transport via ROCK pathway. PRL was previously reported to use the Rho-associated pathway in endothelial cells (28), in which a GTP-bound RhoA activated the serine/threonine kinase ROCK. In T84 colonic adenocarcinoma cell monolayer, the presence of Rho/ROCK activities was essential for a decrease in TER and disassembly of apical junctional complex triggered by extracellular calcium depletion (42). However, it is currently unknown as to why the PRL-induced decrease in TER, which was closely related to the increased paracellular permeability, was not abolished by LY-294002 and Y-27632. It was possible that PRL may have other signaling molecules for modulation of paracellular properties. PKC_ζ might be not involved in the PRL-enhanced calcium transport via the paracellular pathway because PKC_ζ inhibitor was without effect on the PRL-induced decrease in TER.

In conclusion, we demonstrated that PRL stimulated the transcellular active calcium transport via $Ca_v1.3$ and PMCA, but not TRPV6, calbindin-D_{9k}, or NCX1. Such PRL action was mediated by PI3K and phorbol-insensitive PKC_ζ in a nongenomic manner. Moreover, PRL removed the paracellular rectification and enhanced the voltage-dependent paracellular calcium transport via the PI3K and ROCK pathways. The present findings provide more detailed information on the cellular mechanisms of PRL in the intestinal epithelial cells, which could be used to explain how PRL enhances calcium absorption in pregnant and lactating animals.

GRANTS

This research was supported by grants from the Royal Golden Jubilee (RGJ) Program (PHD48K0063 to N. Thongon) and the Faculty of Science, Burapha University (to N. Thongon), the Mahidol University Postdoctoral Fellowship Program (to L. Nakkrasae), the Commission on Higher Education, and the Thailand Research Fund (RSA5180001 to N. Charoenphandhu, and RTA5080008 to N. Krishnamra).

REFERENCES

1. **Akhter S, Kutuzova GD, Christakos S, DeLuca HF.** Calbindin D_{9k} is not required for 1,25-dihydroxyvitamin D_3-mediated Ca^{2+} absorption in small intestine. *Arch Biochem Biophys* 460: 227–232, 2007.
2. **Benn BS, Ajibade D, Porta A, Dhawan P, Hediger M, Peng JB, Jiang Y, Oh GT, Jeung EB, Lieben L, Bouillon R, Carmeliet G, Christakos S.** Active intestinal calcium transport in the absence of transient receptor potential vanilloid type 6 and calbindin-D_{9k}. *Endocrinology* 149: 3196–3205, 2008.
3. **Bindels RJ, Timmermans JA, Hartog A, Coers W, van Os CH.** Calbindin-D_{9k} and parvalbumin are exclusively located along basolateral membranes in rat distal nephron. *J Am Soc Nephrol* 2: 1122–1129, 1991.
4. **Boass A, Lovdal JA, Toverud SU.** Pregnancy- and lactation-induced changes in active intestinal calcium transport in rats. *Am J Physiol Gastrointest Liver Physiol* 263: G127–G134, 1992.
5. **Charoenphandhu N, Krishnamra N.** Prolactin is an important regulator of intestinal calcium transport. *Can J Physiol Pharmacol* 85: 569–581, 2007.
6. **Charoenphandhu N, Limlomwongse L, Krishnamra N.** Prolactin directly enhanced Na^+/K^+- and Ca^{2+}-ATPase activities in the duodenum of female rats. *Can J Physiol Pharmacol* 84: 555–563, 2006.
7. **Charoenphandhu N, Tudpor K, Pulsook N, Krishnamra N.** Chronic metabolic acidosis stimulated transcellular and solvent drag-induced calcium transport in the duodenum of female rats. *Am J Physiol Gastrointest Liver Physiol* 291: G446–G455, 2006.
8. **Charoenphandhu N, Wongdee K, Teerapornpuntakit J, Thongchote K, Krishnamra N.** Transcriptome responses of duodenal epithelial cells

to prolactin in pituitary-grafted rats. *Mol Cell Endocrinol* 296: 41–52, 2008.
9. **Couchourel D, Leclerc M, Filep J, Brunette MG.** Testosterone enhances calcium reabsorption by the kidney. *Mol Cell Endocrinol* 222: 71–81, 2004.
10. **De Boland AR, Norman A.** Evidence for involvement of protein kinase C and cyclic adenosine 3′,5′ monophosphate-dependent protein kinase in the 1,25-dihydroxy-vitamin D_3-mediated rapid stimulation of intestinal calcium transport (transcaltachia). *Endocrinology* 127: 39–45, 1990.
11. **De Boland AR, Norman AW.** Influx of extracellular calcium mediates 1,25-dihydroxyvitamin D_3-dependent transcaltachia (the rapid stimulation of duodenal Ca^{2+} transport). *Endocrinology* 127: 2475–2480, 1990.
12. **Eisenman G, Horn R.** Ionic selectivity revisited: the role of kinetic and equilibrium processes in ion permeation through channels. *J Membr Biol* 76: 197–225, 1983.
13. **Feher JJ, Fullmer CS, Fritzsch GK.** Comparison of the enhanced steady-state diffusion of calcium by calbindin-D_{9K} and calmodulin: possible importance in intestinal calcium absorption. *Cell Calcium* 10: 189–203, 1989.
14. **Ferrante PL, Freeman DE, Whitlock RH, Kronfeld DS.** Effect of D-glucose on in vitro short-circuit current in neonatal calf jejunum and rabbit ileum. *Am J Vet Res* 49: 715–719, 1988.
15. **Fujita H, Sugimoto K, Inatomi S, Maeda T, Osanai M, Uchiyama Y, Yamamoto Y, Wada T, Kojima T, Yokozaki H, Yamashita T, Kato S, Sawada N, Chiba H.** Tight junction proteins claudin-2 and -12 are critical for vitamin D-dependent Ca^{2+} absorption between enterocytes. *Mol Biol Cell* 19: 1912–1921, 2008.
16. **Hill KJ, Webber AC, Hill SJ.** A role of protein kinase Cμ in signalling from the human adenosine A_1 receptor to the nucleus. *Br J Pharmacol* 139: 721–732, 2003.
17. **Hirsch E, Costa C, Ciraolo E.** Phosphoinositide 3-kinases as a common platform for multi-hormone signaling. *J Endocrinol* 194: 243–256, 2007.
18. **Hoenderop JG, Nilius B, Bindels RJ.** Calcium absorption across epithelia. *Physiol Rev* 85: 373–422, 2005.
19. **Huybers S, Naber TH, Bindels RJ, Hoenderop JG.** Prednisolone-induced Ca^{2+} malabsorption is caused by diminished expression of the epithelial Ca^{2+} channel TRPV6. *Am J Physiol Gastrointest Liver Physiol* 292: G92–G97, 2007.
20. **Jantarajit W, Thongon N, Pandaranandaka J, Teerapornpuntakit J, Krishnamra N, Charoenphandhu N.** Prolactin-stimulated transepithelial calcium transport in duodenum and Caco-2 monolayer are mediated by the phosphoinositide 3-kinase pathway. *Am J Physiol Endocrinol Metab* 293: E372–E384, 2007.
21. **Kapus A, Szászi K.** Coupling between apical and paracellular transport processes. *Biochem Cell Biol* 84: 870–880, 2006.
22. **Karbach U, Feldmeier H.** The cecum is the site with the highest calcium absorption in rat intestine. *Dig Dis Sci* 38: 1815–1824, 1993.
23. **Khanal RC, Nemere I.** Endocrine regulation of calcium transport in epithelia. *Clin Exp Pharmacol Physiol* 35: 1277–1287, 2008.
24. **Khanal RC, Nemere I.** Regulation of intestinal calcium transport. *Annu Rev Nutr* 28: 179–196, 2008.
25. **Krishnamra N, Taweerathitam P.** Acute effect of prolactin on active calcium absorption in rats. *Can J Physiol Pharmacol* 73: 1185–1189, 1995.
26. **Krishnamra N, Wirunrattanakij Y, Limlomwongse L.** Acute effects of prolactin on passive calcium absorption in the small intestine by in vivo perfusion technique. *Can J Physiol Pharmacol* 76: 161–168, 1998.
27. **Lee GS, Lee KY, Choi KC, Ryu YH, Paik SG, Oh GT, Jeung EB.** Phenotype of a calbindin-D_{9k} gene knockout is compensated for by the induction of other calcium transporter genes in a mouse model. *J Bone Miner Res* 22: 1968–1978, 2007.
28. **Lee SH, Kunz J, Lin SH, Yu-Lee LY.** 16-kDa prolactin inhibits endothelial cell migration by down-regulating the Ras-Tiam1-Rac1-Pak1 signaling pathway. *Cancer Res* 67: 11045–11053, 2007.
29. **Little D, Dean RA, Young KM, McKane SA, Martin LD, Jones SL, Blikslager AT.** PI3K signaling is required for prostaglandin-induced mucosal recovery in ischemia-injured porcine ileum. *Am J Physiol Gastrointest Liver Physiol* 284: G46–G56, 2003.
30. **Lu Z.** Mechanism of rectification in inward-rectifier K^+ channels. *Annu Rev Physiol* 66: 103–129, 2004.
31. **Mace OJ, Morgan EL, Affleck JA, Lister N, Kellett GL.** Calcium absorption by $Ca_v1.3$ induces terminal web myosin II phosphorylation and apical GLUT2 insertion in rat intestine. *J Physiol* 580: 605–616, 2007.
32. **McLaughlin J, Padfield PJ, Burt JP, O'Neill CA.** Ochratoxin A increases permeability through tight junctions by removal of specific claudin isoforms. *Am J Physiol Cell Physiol* 287: C1412–C1417, 2004.
33. **Mellor H, Parker PJ.** The extended protein kinase C superfamily. *Biochem J* 332: 281–292, 1998.
34. **Morgan EL, Mace OJ, Affleck J, Kellett GL.** Apical GLUT2 and $Ca_v1.3$: regulation of rat intestinal glucose and calcium absorption. *J Physiol* 580: 593–604, 2007.
35. **Morgan EL, Mace OJ, Helliwell PA, Affleck J, Kellett GL.** A role for $Ca_v1.3$ in rat intestinal calcium absorption. *Biochem Biophys Res Commun* 312: 487–493, 2003.
36. **Motulsky H, Christopoulos A.** *Fitting Models to Biological Data Using Linear and Nonlinear Regression: A Practical Guide to Curve Fitting*. New York, NY: Oxford Univ. Press, 2004, p. 312–321.
37. **Murphy EF, Hooiveld GJ, Muller M, Calogero RA, Cashman KD.** Conjugated linoleic acid alters global gene expression in human intestinal-like Caco-2 cells in an isomer-specific manner. *J Nutr* 137: 2359–2365, 2007.
38. **Nakane M, Ma J, Rose AE, Osinski MA, Wu-Wong JR.** Differential effects of vitamin D analogs on calcium transport. *J Steroid Biochem Mol Biol* 103: 84–89, 2007.
39. **Powell DJ, Hajduch E, Kular G, Hundal HS.** Ceramide disables 3-phosphoinositide binding to the pleckstrin homology domain of protein kinase B (PKB)/Akt by a PKC_ζ-dependent mechanism. *Mol Cell Biol* 23: 7794–7808, 2003.
40. **Rexhepaj R, Artunc F, Metzger M, Skutella T, Lang F.** PI3-kinase-dependent electrogenic intestinal transport of glucose and amino acids. *Pflügers Arch* 453: 863–870, 2007.
41. **Sabah NH.** Rectification in biological membranes. *IEEE Eng Med Biol Mag* 19: 106–113, 2000.
42. **Samarin SN, Ivanov AI, Flatau G, Parkos CA, Nusrat A.** Rho/Rho-associated kinase-II signaling mediates disassembly of epithelial apical junctions. *Mol Biol Cell* 18: 3429–3439, 2007.
43. **Tang VW, Goodenough DA.** Paracellular ion channel at the tight junction. *Biophys J* 84: 1660–1673, 2003.
44. **Tanrattana C, Charoenphandhu N, Limlomwongse L, Krishnamra N.** Prolactin directly stimulated the solvent drag-induced calcium transport in the duodenum of female rats. *Biochim Biophys Acta* 1665: 81–91, 2004.
45. **Thongon N, Nakkrasae LI, Thongbunchoo J, Krishnamra N, Charoenphandhu N.** Prolactin stimulates transepithelial calcium transport and modulates paracellular permselectivity in Caco-2 monolayer: mediation by PKC and ROCK pathways. *Am J Physiol Cell Physiol* 294: C1158–C1168, 2008.
46. **Van Abel M, Hoenderop JG, van der Kemp AW, van Leeuwen JP, Bindels RJ.** Regulation of the epithelial Ca^{2+} channels in small intestine as studied by quantitative mRNA detection. *Am J Physiol Gastrointest Liver Physiol* 285: G78–G85, 2003.
47. **Van Itallie CM, Anderson JM.** Claudins and epithelial paracellular transport. *Annu Rev Physiol* 68: 403–429, 2006.
48. **Wall MJ, Declusin RJ, Soergel KH, Baker RD.** The effect of short chain fatty acids on transmural electrical potential across rat small intestine in vivo. *Biochim Biophys Acta* 433: 654–661, 1976.
49. **Wasserman RH, Chandler JS, Meyer SA, Smith CA, Brindak ME, Fullmer CS, Penniston JT, Kumar R.** Intestinal calcium transport and calcium extrusion processes at the basolateral membrane. *J Nutr* 122: 662–671, 1992.
50. **Yee S.** In vitro permeability across Caco-2 cells (colonic) can predict in vivo (small intestinal) absorption in man - fact or myth. *Pharm Res* 14: 763–766, 1997.
51. **Zhou LX, Nemere I, Norman AW.** A parathyroid-related peptide induces transcaltachia (the rapid, hormonal stimulation of intestinal Ca^{2+} transport). *Biochem Biophys Res Commun* 186: 69–73, 1992.
52. **Zweibaum A, Triadou N, Kedinger M, Augeron C, Robine-Leon S, Pinto M, Rousset M, Haffen K.** Sucrase-isomaltase: a marker of foetal and malignant epithelial cells of the human colon. *Int J Cancer* 32: 407–412, 1983.

ARTICLE
Journal of Cellular Biochemistry 107:677–685 (2009)

Journal of Cellular Biochemistry

Evidence for Direct Effects of Prolactin on Human Osteoblasts: Inhibition of Cell Growth and Mineralization

Dutmanee Seriwatanachai,[1,2] Nateetip Krishnamra,[1] and J.P.T.M. van Leeuwen[2*]

[1]*Faculty of Science, Department of Physiology, Mahidol University, Rama VI Road, Bangkok 10400, Thailand*

[2]*Department of Internal Medicine, Erasmus Medical Center, Rotterdam, The Netherlands*

ABSTRACT

Hyperprolactinemia is one of the risk factor of decrease in bone mass which has been believed to be mediated by hypogonadism. However, the presence of prolactin receptor in human osteosarcoma cell line and primary bone cell culture from mouse calvariae supported the hypothesis of a direct prolactin (PRL) action on bone cells. Therefore, the aim of this study was to investigate the role of PRL and its signal transduction pathway in the regulation of bone metabolism via osteoblast differentiation. Human pre-osteoblasts (SV-HFO) that differentiate in a 3-week period from proliferating pre-osteoblasts (days 2–7) to extracellular matrix producing cells (days 7–14) which is eventually mineralized (days 14–21) were used. Concentration of PRL mimicked a lactating period (100 ng/ml) was used to incubate SV-HFO for 21 days in osteogenic medium. Human prolactin receptor mRNA and protein are expressed in SV-HFO. PRL significantly decreased osteoblast number (DNA content) which was due to a decrease in proliferation. PRL increased osteogenic markers, RUNX2 and ALP in early stage of osteoblast differentiation while decreasing it later suggesting a bi-directional effect. Calcium measurement and Alizarin red staining showed a reduction of mineralization by PRL while having neither an effect on osteoblast activity nor RANKL/OPG mRNA ratio. We also demonstrated that PRL action on mineralization was not via PI-3 kinase pathway. The present study provides evidence of a direct effect of prolactin on osteoblast differentiation and in vitro mineralization. J. Cell. Biochem. 107: 677–685, 2009. © 2009 Wiley-Liss, Inc.

KEY WORDS: HYPERPROLACTINEMIA; OSTEOBLAST DIFFERENTIATION; BONE FORMATION; RANKL/OPG

A number of causes have been implicated to physiological and pathological hyperprolactinemia. Pregnancy and lactation produced physiologically high concentration of prolactin (PRL) of ~75–100 and ~200–300 ng/ml [Ritchie et al., 1998; Prentice, 2000], anterior pituitary tumor [Schlechte et al., 1983; Greenspan et al., 1986; Klibanski and Greenspan, 1986] or use of antipsychotic drug in schizophrenia patients elevates prolactin (PRL) levels by dopaminergic inhibition [Naidoo et al., 2003]. Hyperprolactinemia-induced osteoporosis is, so far, believed to be mediated by hypogonadism. However, in hyperprolactinemic women with normal estrogen levels, net bone loss still occurred, but its severity was significantly less than that in hyperprolactinemia without estrogen. PRL is a peptide hormone produced by the lactotrope cells in the anterior pituitary gland and is primarily associated with lactation. We previously found in the in vivo studies that PRL has a significant effect on bone remodeling in lactating rat, stimulating recruitment of calcium for fetal development and breast feeding [Lotinun et al., 1998; Lotinun et al., 2003]. The prolactin receptor (PRLR) knockout mice were shown to have a significant effect on fetal skeletal development suggesting a role for PRL signaling to maintain a normal fetal bone development [Clement-Lacroix et al., 1999]. In addition, the expression PRL receptor (PRLR) in osteoblasts as assessed by PCR and immunohistochemistry suggested a direct effect of PRL on bone remodeling [Bataille-Simoneau et al., 1996; Coss et al., 2000; Seriwatanachai et al., 2008a,b]. However, it is yet not clear whether bone is directly regulated by PRL. The skeletal effects observed in the lactating rats and PRLR knockout mice may still be due to the presence of other hormones in lactating stage and other changes in the PRLR knockout mice. Nevertheless, the expression of PRLR in human fetal osteoblast (hFOB 1.19), osteoblast-like cell, MG-63 and Saos-2 and rat osteoblast suggested a direct effect of PRL on osteoblasts [Bataille-Simoneau et al., 1996; Coss et al., 2000; Seriwatanachai et al., 2008a,b]. There are only few studies focusing on the direct short-term effects of PRL

The authors declare no conflict of interest.

Grant sponsor: Royal Golden Jubilee Program; Grant sponsor: Thailand Research Fund.

*Correspondence to: Prof. Dr. J.P.T.M. van Leeuwen, Department of Internal Medicine, Room Ee585c, Erasmus Medical Center's Gravendijkwal 230, 3015 CE Rotterdam, The Netherlands. E-mail: j.vanleeuwen@erasmusmc.nl

Received 12 February 2009; Accepted 5 March 2009 • DOI 10.1002/jcb.22161 • © 2009 Wiley-Liss, Inc.

Published online 13 April 2009 in Wiley InterScience (www.interscience.wiley.com).

on osteoblast [Coss et al., 2000; Seriwatanachai et al., 2008a,b]. None of them has studied the putative role of human PRL on human osteoblast differentiation and bone formation.

The aim of this study was to assess the impact of PRL and PRL signaling, on human osteoblast differentiation related to bone formation. The expression of PRLR and the effect of PRL on osteoblast activity and matrix mineralization were measured together with studies on PRL signal transduction pathway.

MATERIALS AND METHODS

CELL CULTURE

SV-HFO are human pre-osteoblast [van Driel et al., 2004; Eijken et al., 2006] were cultured in α-MEM (GIBCO, Paisley, UK) supplemented with 20 mM HEPES, pH 7.5, streptomycin/penicillin, 1.8 mM $CaCl_2$ (Sigma, St. Louis, MO) and heat-inactivated FCS (GIBCO, Paisley, UK) at 37°C and 5% CO_2 in a humidified atmosphere. Cells were seeded in a density of 5×10^3 vital cells/cm^3 and pre-cultured for 1 week in the presence of 10% FCS. During this pre-culture, SV-HFO cells remained in an undifferentiated stage. After preculture, cells were seeded in density of 10×10^3 vital cells/cm^2 in osteogenic medium consisting of 2% charcoal-treated FCS supplemented with 10 mM β-glycerophosphate (Sigma) and dexamethasone (Sigma).

Recombinant human PRL (R&D Systems, Inc., Minneapolis, MN) was reconstituted in BSA and HCl following the manufacturer's instruction before being diluted in α-MEM. Medium freshly supplemented with and without PRL was replaced every 2–3 days. For biochemical analysis, medium was collected and stored at −20°C and cells were scraped from the culture dish in PBS containing 0.1% Triton X-100 and stored at −80°C. Cell lysates were sonicated on ice in a sonifier cell disrupter for 2×15 s before analysis.

IMMUNOCYTOCHEMISTRY

To verify and localize the PRLR proteins in osteoblasts, SV-HFO cells were seeded on cover slips in density of 10×10^3 vital cells/cm^2 and incubated with osteogenic medium for 5 and 12 days. Unattached cells were then removed by washing with PBS pH 7.4 twice. The cover slips were removed from the incubator and were fixed with 4% of paraformaldehyde for 10 min at room temperature. Cells were then washed three times with PBS, and permeabilized with 0.15% Triton-X100 in PBS for 5 min at room temperature. Then cells were washed twice with PBS, and nonspecific proteins were blocked with 10% BSA for 30 min at room temperature. Samples were then incubated with the 1:300 diluted rabbit polyclonal anti-PRLR (Santa Cruz, CA) primary antibody for 1 h at room temperature. Cells were further incubated with 1:200 diluted Alexa Fluor 488 conjugated anti-rabbit IgG antibody as a secondary antibody for 1 h at room temperature. Cells were then stained with nuclear DAPI stain for 2 min. Anti-PRLR was digitally captured by using inverted fluorescence microscopy (Bio-Rad MRC1024 MP scanning system mounted on a Nikon Eclipse TE300 fluorescence microscope).

DNA CONTENT

For DNA measurements, 100 μl SV-HFO cell lysates were treated with 200 μl heparin (8 IU/ml in PBS) and 100 μl ribonuclease A (50 μg/ml in PBS) for 30 min at 37°C. This was followed by adding 100 μl ethidium bromide solution (25 μg/ml in PBS). Samples were analyzed on the Wallac 1420 victor2 (Perkin-Elmer, Wellesley, MA) using an extinction filter of 340 nm and an emission filter of 590 nm. For standards, calf thymus DNA (Sigma) was used.

ALKALINE PHOSPHATASE (ALP) ACTIVITY

ALP activity was assayed by determining the release of *p*-nitrophenol from *p*-nitrophenylphosphate (20 mM in 1 M diethanolamine buffer supplemented with 1 mM $MgCl_2$ at pH 9.8) in the SV-HFO cell lysates for 10 min at 37°C. The reaction was stopped by adding 0.06 M NaOH. Absorption was measured at 405 nm. Results were adjusted for DNA content of the cell lysates.

MINERALIZATION

For quantification of the mineral content cell lysates were incubated overnight in 0.24 M HCl at 4°C. Calcium content was colorimetrically determined colorimetrically with a calcium assay kit (Sigma) according to the manufacturer's description. Results were adjusted for DNA content of the cell lysates. For Alizarin Red S staining cell cultures were fixed for 60 min with 70% ethanol on ice. After fixation, cells were washed twice with PBS and stained for 10 min with an anthraquinone derivative, Alizarin Red S solution.

APOPTOSIS ASSAY

Apoptosis was measured through the binding of annexin V and uptake of propidium iodide (PI) by flow cytometry using a Apoptest-FITC kit (Nexins research, Kattendijke, The Netherlands). For analysis 10,000 osteoblasts were counted using a FACScalibur (Becton Dickinson). Percentage total apoptotic cells was calculated by counting apoptotic (annexin V or PI stained) cells.

PROLIFERATION ASSAY

Osteoblast proliferation was examined by using a colorimetric BrdU cell proliferation enzyme-linked immunosorbent assay kit (No. 1 647 229, Roche, Mannheim, Germany). SV-HFO cells were seeded into 96-well plates, in osteogenic medium with and without 100 ng/ml PRL. 100 μM BrdU labeling solution was added to each well giving a final concentration of 10 μM. After 24 h incubation and removal of the culture medium the cells were fixed and DNA was denaturated. Subsequently, the anti-BrdU-peroxidase conjugate was added which binds to the incorporated in newly synthesized DNA. The immune complexes were detected by subsequent reaction with tetramethylbenzidine as substrate for 10 min. The reaction was stopped by addition of 200 μl 1 M H_2SO_4 to each well, and the reaction product was quantified by measuring the absorbance at 450 nm with reference to 690 nm using the Wallac 1420 victor2 (Perkin-Elmer, Wellesley, MA) [Gratzner, 1982].

QUANTIFICATION OF mRNA EXPRESSION

Total RNA was isolated using RNA-Bee solution (Tel-Test, Friendwood, TX) according to the manufacturer's protocol. To remove calcium (derived from extracellular matrix), RNA was precipitated by overnight incubation with 4 M LiCl and 50 mM EDTA at −20°C. After precipitation and centrifugation for 30 min at 14,000 rpm and 4°C, the RNA pellet was washed four times with 70% EtOH and dissolved in H_2O. The total amount of RNA was quantified using the RiboGreen RNA Quantitation Kit (Molecular Probes, Eugene, OR). One microgram total RNA was reverse transcribed into cDNA using 0.2 μg oligo(dT)18 and 0.2 μg random hexamer primers and a cDNA synthesis kit (MBI Fermentas, St. Leon-Rot, Germany).

Quantitative real-time PCR (QPCR) was carried out using an ABI 7700 sequence detection system (Applied Biosystems, Foster City, CA). Reactions were performed in 25 μl volumes using a qPCR core kit (Eurogentec, Seraing, Belgium). Reaction mixes contained 20 ng cDNA, 5 mM $MgCl_2$, 200 μM dNTPs, and 0.025 U/μl Hot GoldStar enzyme. Primer and probe sets were designed, using the Primer Express software (version 1.5; Applied Biosystems), amplicons overlapped at least one exon boundary. Cycling conditions were 50°C for 2 min, 95°C for 10 min, followed by 40 cycles of 95°C for 15 s and 60°C for 1 min. The relative gene expression was calculated by the comparative Ct method of which Ct sample is normalized to endogenous house keeping gene, GAPDH, according to the calculation; relative Ct value $= 2^{-[\text{delta}]Ct_{\text{SAMPLE}} - [\text{delta}]Ct_{\text{GAPDH}}}$

STATISTICS

Data are presented as mean ± SEM and are derived of at least two independent experiments each consisting of at least three cultures. Differences between groups were analyzed by the Student's *t*-test.

RESULTS

EXPRESSION OF HUMAN PROLACTIN RECEPTOR (hPRLR)

hPRLR expression and PRL effects were studied in detail using the SV-HFO osteoblast differentiation model. This human pre-osteoblast model produces an extracellular matrix during culture, which eventually is mineralized in 2–3 weeks time period [Chiba et al., 1993; Eijken et al., 2006], as shown in Figure 1. hPRLR mRNA was found to be expressed in human osteoblasts and the expression remained constant during differentiation (Fig. 2). Incubation with PRL did not significantly change the hPRLR mRNA expression significantly at the various days albeit that at all days tested hPRLR mRNA expression appeared to be lower than in untreated cultures. Also at protein level, the hPRLR was demonstrated in human osteoblasts (Fig. 3).

EFFECTS OF PROLIFERATION AND APOPTOSIS

PRL treatment decreased total cell number as reflected by a decrease in the total amount DNA during osteoblast differentiation (Fig. 4A). The decrease in DNA only became apparent after 7 days of culture. For total protein we found a similar pattern after PRL treatment as observed for total DNA with a reduction from day 7 of culture onwards (data not shown). The reduction in cell number can be due to an increase in apoptosis and/or an inhibition of cell proliferation. PRL did not affect apoptosis of human osteoblasts (Fig. 4B) but inhibited cell proliferation (Fig. 4C).

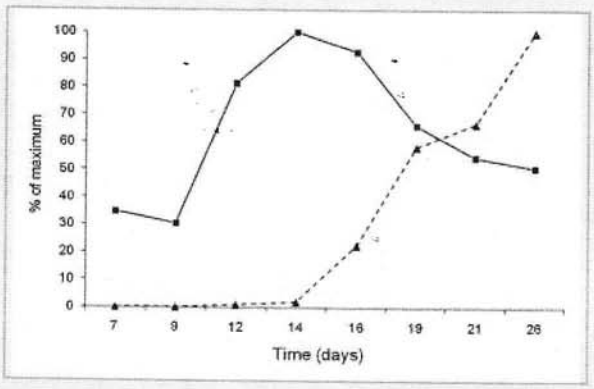

Fig. 1. Temporal pattern of alkaline phosphatase activity (solid line) and mineralization (dashed line) during differentiation of SV-HFO pre-osteoblasts induced by osteogenic medium.

EFFECTS ON HUMAN OSTEOBLAST DIFFERENTIATION

To investigate the role of PRL on osteoblast differentiation, we analyzed the expression of known osteoblast marker genes and the effect of on ALP activity. PRL significantly increased Runx2 at early differentiation, day 5 while decreasing it at the late osteoblast differentiation, day 21 (Fig. 5A). This pattern is similar to that of ALP mRNA expression as shown in Figure 5B. PRL increased collagen type Ia mRNA expression at d5 but did not affect it later on during differentiation (Fig. 5C). ALP activity showed a peak around days 10–12 of culture and in this period the ALP activity in the PRL condition was significantly higher at day 12 while it did not reach significantly at day 10 (Fig. 5D).

PRL EFFECTS ON MINERALIZATION

Next we examined the direct effect of PRL on osteoblast mineralization using Alizarin Red staining at day 14 and day 21.

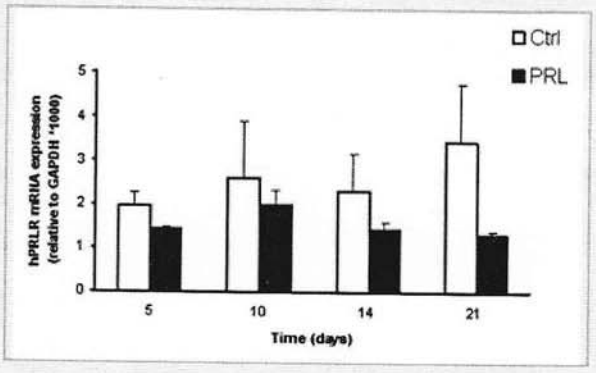

Fig. 2. Expression of hPRLR mRNA (QPCR) during human osteoblast differentiation in control condition (open bars) and after treatment with 100 ng/ml PRL (solid bars).

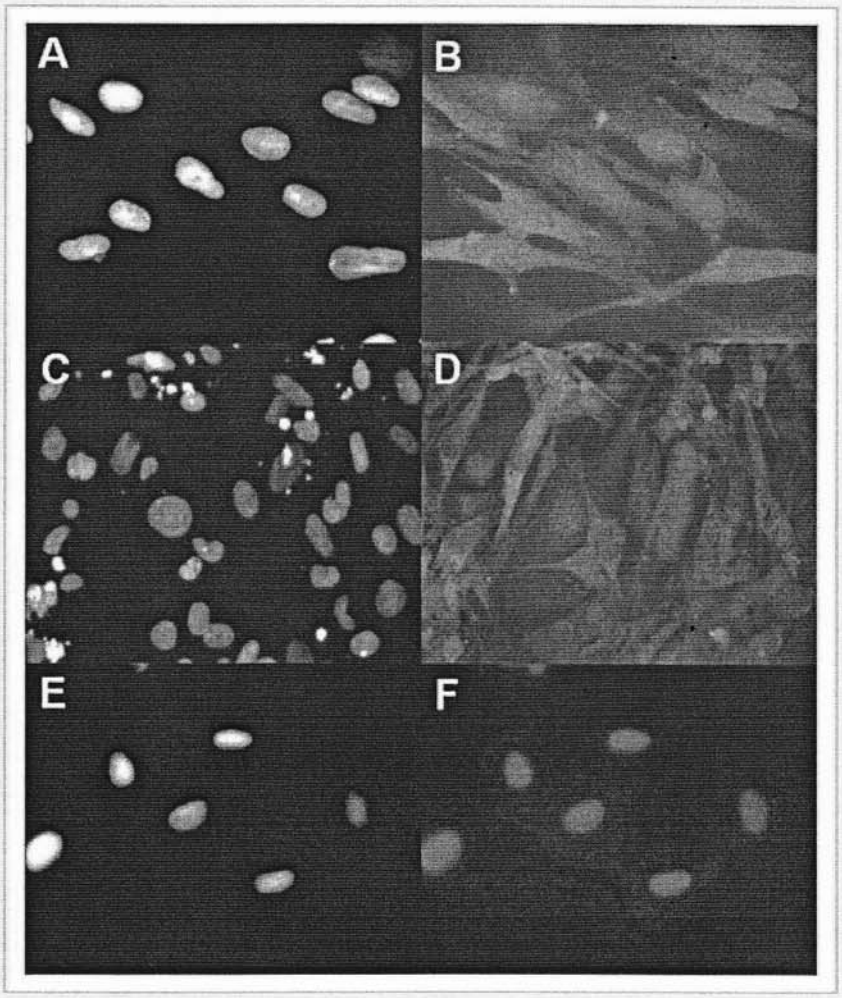

Fig. 3. Immunofluorescent analysis of hPRLR protein expression in SV-HFO cells exposed for 5 days (A,B) and 12 days (C,D) to osteogenic medium (n = 3). A,C,E: DAPI nuclear staining, (B,D,F) double staining with DAPI (blue) and hPRLR antibody conjugated with ALEXA (green). Cells were incubated in the absence (anti-hPRLR) of primary antibody against hPRLR proteins (E,F). Experiments were performed in triplicate, magnification 400×.

We found that PRL visibly reduced the alizarin red staining at day 14 and day 21 (Fig. 6A). In contrast to the control condition, total Ca^{2+} was not yet detectable at d14 in PRL treated group, and at day 21 of culture it was significantly decreased in the PRL condition (Fig. 6B). After correcting the total Ca^{2+} with DNA, it did not change the PRL effect and significance (Fig. 6C).

EFFECTS OF PRL ON RANKL AND OPG EXPRESSION

To elucidate the action of PRL on osteoclastogenesis function of osteoblast, we measured the expression of RANKL and its decoy receptor, OPG. We could not find a significant change in their expression as well as the bone resorption indicator, RANKL/OPG ratio, in PRL-treated group in any given days (Fig. 7A–C).

PI3 KINASE AND PRL ACTION

PI3 kinase pathway is one of the recent pathways reported to be involved in PRL action in many kinds of cells [al Sakkaf et al., 1996; Hugl and Merger, 2007; Jantarajit et al., 2007; Seriwatanachai et al., 2008b]. Our previous report [Seriwatanachai et al., 2008b] also suggested that the shortterm action of PRL on the reduction of osteoblastic ALP activity is via PI-3 kinase activity. We tested the effect of PI3 kinase inhibition by LY294002 in various phases (d0–3, d4–7, and d11–14) during osteoblast differentiation. In general these studies showed that treatment with PRL reduced total DNA (Fig. 8A–C). In none of the phases inhibition of PI-3 kinase alone did effect total DNA level nor did it inhibit the PRL effect (Fig. 8A–C). When LY294002 was added together with PRL at days 11–14 the reduction in DNA was even stronger (Fig. 8C). We confirmed the inhibitory effect of PRL on mineralization (Fig. 8D–F). Inhibition of PI-3 kinase activity in control condition suppressed the mineralization only when added at the early differentiating stage (d0–3 and d4–7) but not when added at the onset of mineralization (d11–14) (Fig. 8D–F). PI-3 kinase inhibition did not block the PRL effect on mineralization, in contrast, when added in the early phases it even augmented the inhibition by PRL (Fig. 8D,E).

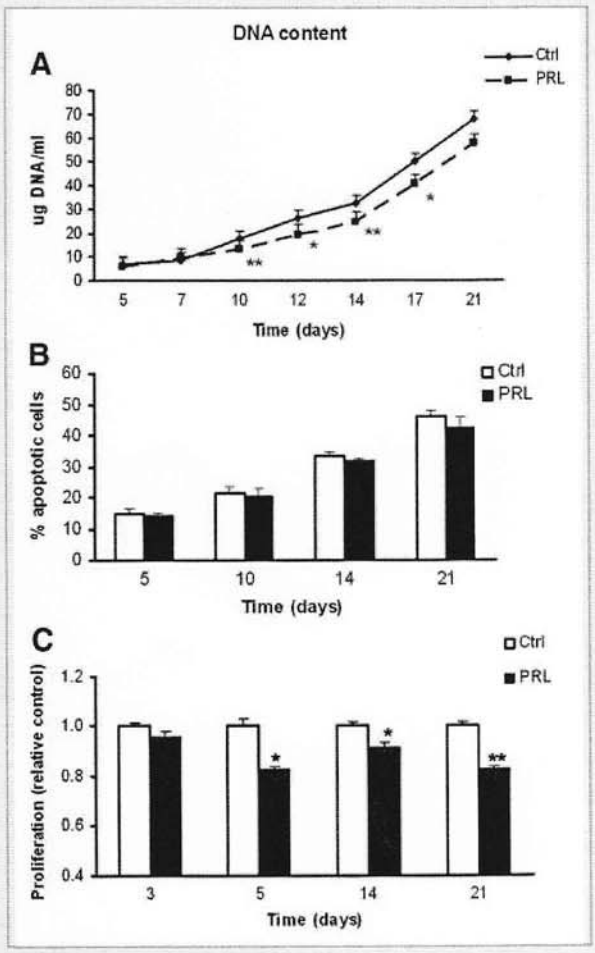

Fig. 4. Effect of PRL treatment on total cell number as reflected by (A) total DNA content, (B) apoptosis, and (C) proliferation. Data shown are mean of two independent cultures performed in triplicate. $^{*}P < 0.05$, and $^{**}P < 0.01$ compared with their respective values of control group.

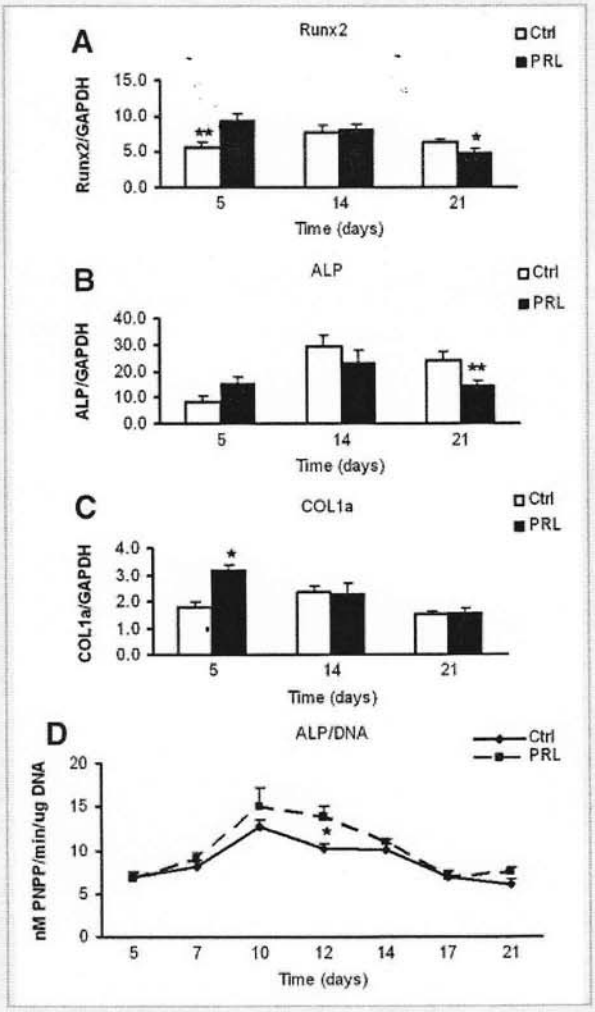

Fig. 5. Effect of PRL on osteoblast differentiation as presented by RUNX2 (A) ALP (B), collagen Type Ia; COL Ia (C) mRNAs expression and ALP/DNA (D). Data shown are mean of two independent cultures performed in triplicate. $^{*}P < 0.05$, and $^{**}P < 0.01$ compared with their respective values of control group.

DISCUSSION

The current study demonstrates for the first time direct effects PRL on human osteoblast differentiation. PRL treatment had a bi-directional effect on osteoblast differentiation and bone formation. PRL reduces human osteoblast proliferation while accelerating its differentiation. However, this acceleration is not accompanied by an enhanced mineralization. Apparently, the accelerated differentiation did not lead to a condition favorable for mineralization. An explanation for this yet elusive but the decrease in total protein may be linked to an insignificant matrix protein production.

Recently, an increased understanding has been acquired with respect to the therapeutic treatment of hyperprolactinemic patients. However, the role of prolactin in the regulation of bone remodeling and the associated bone loss remains largely unclear. Of note was our previous demonstration that PRL receptor is expressed in human fetal osteoblast (hFOB 1.19), osteoblast-like cell (MG-63) and primary rat osteoblast derived from mesenchymal stem cells [Seriwatanachai et al., 2008a,b]. Also other evidence provided osteoblast as a new target of PRL. Deformed skeletal development in PRL receptor knock out pup suggesting an importance role of PRL for maintaining fetal bone development [Clement-Lacroix et al., 1999]. However, so far no data were available on direct effects of PRL on human fetal osteoblast differentiation. We demonstrated hPRLR expression at all stages during differentiation of the human pre-osteoblast cell line, SV-HFO. This model produces an extracellular matrix during culture which eventually is mineralized in 2–3 weeks time period [Chiba et al., 1993; Eijken et al., 2006] therefore, it is suitable for studying PRL effect on human osteoblast differentiation and in vitro bone formation. We presented that in vitro administration of PRL result in a reduction of osteoblast growth. The observation that in PRL-treated osteoblast shows a declinement of osteoblast number as represented by DNA content in a time-dependent manner (Fig. 4A). This finding suggested

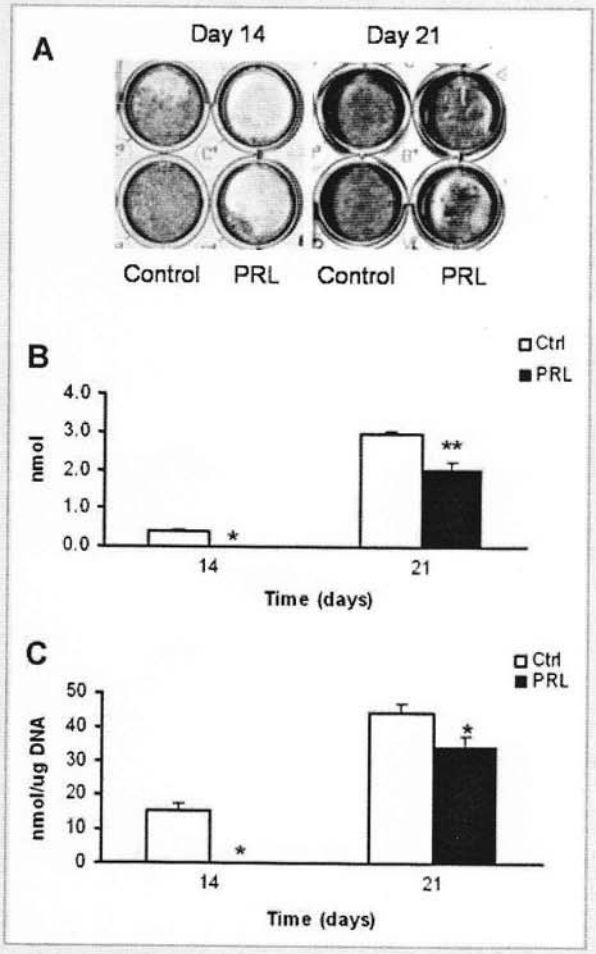

Fig. 6. The effect of PRL on mineralization as presented by mineral Alizarin Red staining (A), total Ca^{+2} (B), and Ca^{+2}/DNA (C). Data shown are mean of two independent cultures performed in triplicate. $^{*}P<0.05$, and $^{**}P<0.01$ compared with their respective values of control group. [Color figure can be viewed in the online issue, which is available at www.interscience.wiley.com.]

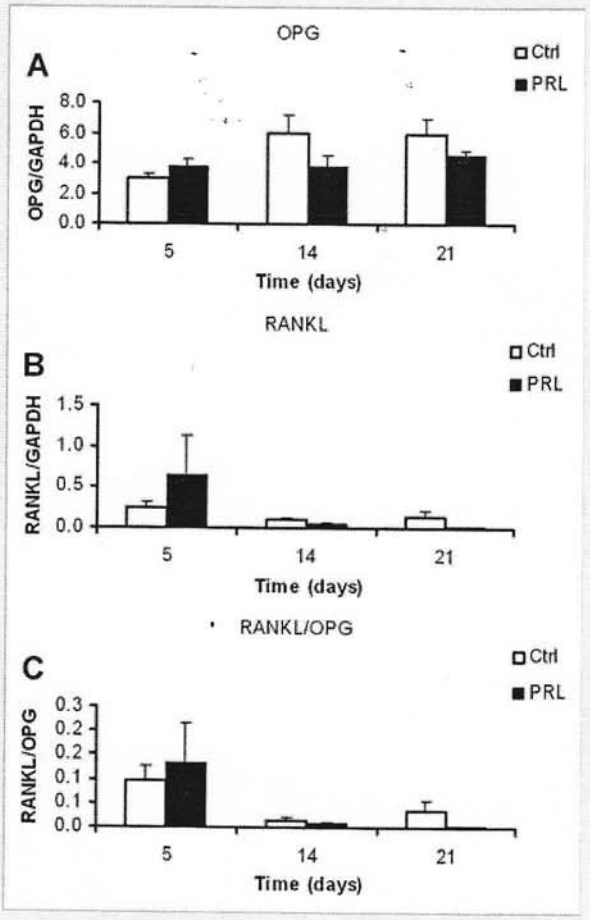

Fig. 7. The effect of 100 ng/ml PRL on the bone resorption-associated parameters which are mRNA expressions of OPG (A) RANKL (B) and the ratios of RANKL/OPG mRNA (C). SV-HFO was exposed to a osteogenic medium (open bar) or with PRL (close bar) for 5, 14, and 21 days. Data shown are mean of two independent cultures performed in triplicate.

that the downregulation of osteoblast quantity is enhanced by PRL action. Therefore, in the next part of the study, we checked whether the reduction of osteoblast quantity regarding the effect of PRL on osteoblast number also could be indirectly manifested through an induction of spontaneous apoptosis or reduction of its proliferation. Indeed, PRL-treated osteoblasts were found reduced proliferation at early phase of osteoblast differentiation, without enhancing a number of apoptosis in PRL treated group. Interestingly, in the present experiment of which tested between vehicle and PRL treated group, and previous observation has found that PRL has no effect on osteoblast-like cell and rat osteoblast proliferation, however, in shortterm PRL administration and in non-osteogenic medium [Coss et al., 2000; Seriwatanachai et al., 2008a,b]. Thus it could simply suggest that change in osteoblast proliferation in bone development influenced by PRL was occurred only in osteogenic medium and in prolonged administration of PRL.

Extensive collagen degradation during a tissue-turnover processes in variety of biological and physiological provides a dynamic cellular activity including proliferation [Hotary et al., 2003; Mott and Werb, 2004; Chun et al., 2006]. Recently, a combined deficiencies in uPARAP/Endo180, a cellular collagen receptor, and MT1-MMP, a principal mesenchymal cell collagenase, mice found to have a severe effect on bone formation and that caused by a proliferative failure and poor survival of bone- and cartilage-forming cells suggesting a necessary of collagen degradation for osteoblast proliferation [Wagenaar-Miller et al., 2007]. In fact, we observed a augmented collagen type I mRNA expression as affected by PRL at early stage of differentiation (d5) which could considerably propose that it could inhibit the early osteoblast proliferation resulting in a certain reduction in DNA accumulating content along culturing period.

The central regulator of bone formation is the Runx2 (also known as Cbfa1/AML3). This transcription factor is required for osteoblastic fate determination, and mediated the complex pathways required for bone formation and turnover [Lian and Stein, 2003; Lian et al., 2004]. We showed that RUNX2 and ALP mRNA were reduced in PRL-treated group in late differentiation suggesting a decrease in

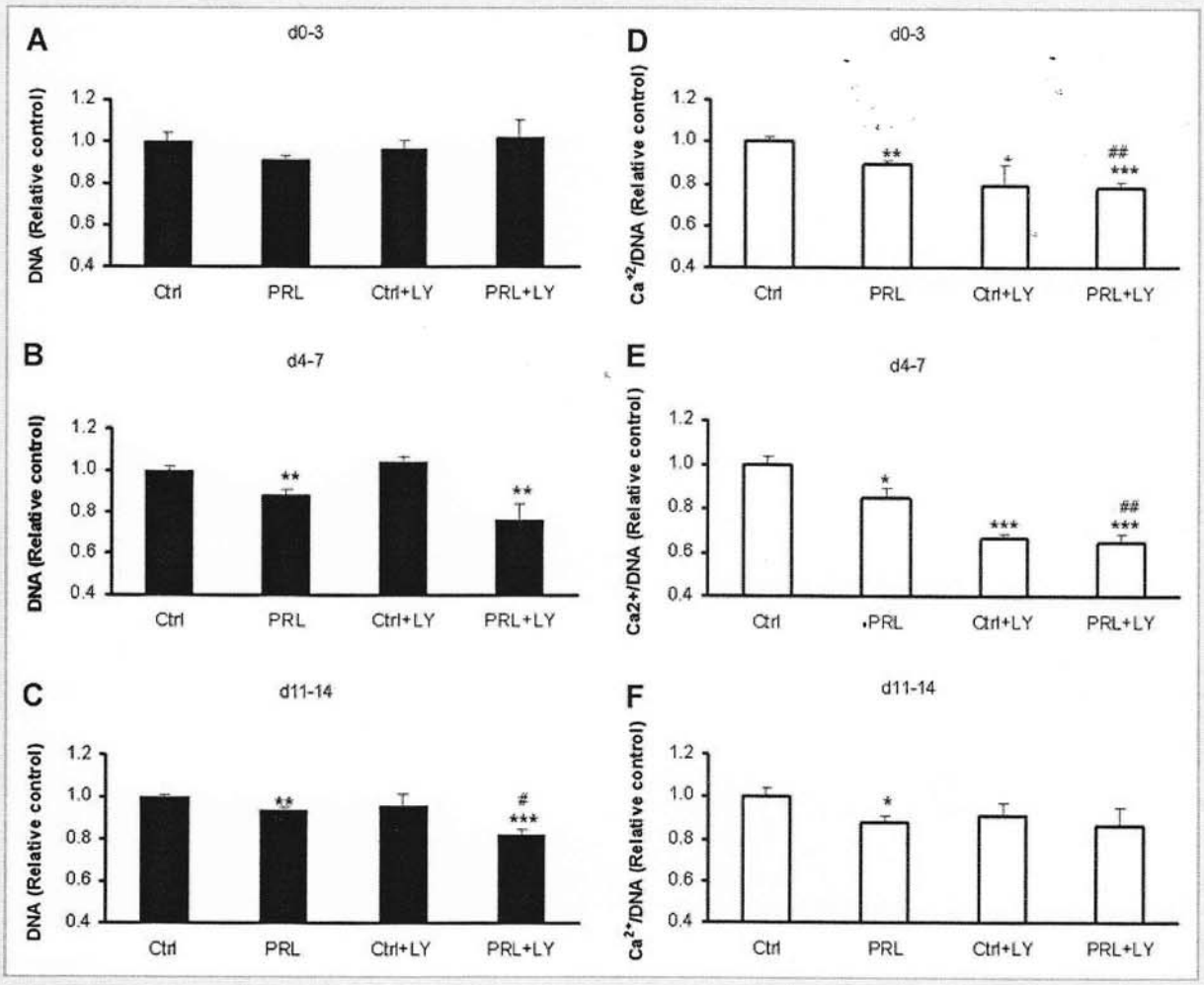

Fig. 8. The combined action of PRL and PI-3 kinase inhibitor (LY294002) on DNA (A–C) and Ca^{2+}/DNA (D–F). LY294002 was added into osteogenic medium with and without PRL at d0–3 (A,D), d4–7 (B,E), and d11–14 (C,F). All plates were harvested at d14 to determine DNA content and Ca^{2+}/DNA. $^{*}P < 0.05$, $^{**}P < 0.01$, and $^{***}P < 0.001$ compared with control group, $^{\#}P < 0.05$ and $^{\#\#}P < 0.01$, compared with PRL group. Data shown are mean of two independent cultures performed in triplicate.

pre-osteoblast differentiation and bone formation. Albeit this should be investigated more detail as RUNX2 has been shown to exert a complex role in osteoblast differentiation, crucial for osteoblast differentiation in early stages but inhibitory in later stages [Liu et al., 2001; Maruyama et al., 2007]. A number of experiments also observed the reduction of osteocalcin, ALP mRNA effected by PRL [Coss et al., 2000; Seriwatanachai et al., 2008b], consistent with our present finding. ALP activity remained unchanged which is possibly due to a reduction of DNA and protein content. Regardless of the reduction of total protein, we similarly found a decrease in its total activity (data not shown), indeed, we showed a significant reduction of ALP mRNA expression. Interestingly, RUNX2 and ALP mRNA expression was found to be enhanced in PRL-treated group at early stage of differentiation (d5). This observation is consistent with the recent report that shortterm PRL administration increases osteocalcin mRNA, a marker of late osteoblast differentiation, while reducing RANKL/OPG ratio in human osteoblast derived from fetal bone tissue favors osteoblast differentiation and bone formation [Seriwatanachai et al., 2008a]. This contradictory finding implies a bi-directional effect of PRL regarding to the stage of osteoblast differentiation. However, the different incubation period, PRL level and medium condition should be also taken into account.

The next step of experiment was concerned about the role of PRL on mineralization since some evidence found a contradictory action according to different model and technical approaches. We observed a decrease in Ca^{2+} content by biochemical assay, and as shown by Alizarin Red staining, which is truly resulted from a reduction of Ca^{2+} content, not secondary to the decrease in DNA content as it is proved by the reduction of Ca^{2+}/DNA content. Indeed, a reduction of bone ossification and mineralizing rate in PRL receptor knockout murine embryo and 8-week-old mouse [Clement-Lacroix et al., 1999] supports a significance role of PRL in fetal and adult bone mineralization.

Up to date, they have been stated of knowledge concerning signal transduction of the PRLR. Nb2 cells are some of the favored models with which to study PRL actions, as shown that PRL induces a rapid tyrosine phosphorylation of IRS-1 and of the 85-kDa subunit of the phosphatidyl-inositol (PI)-3 kinase [al Sakkaf et al., 1996; Berlanga et al., 1997]. Both PI-3 kinase and IRS-1 appear to associate with the

PRLR in a PRL-dependent manner. It has been proposed that a proliferative effect of PRL activation of PI-3 kinase might be mediated by Fyn in Nb2 cells [al Sakkaf et al., 1997] and beta-cell line [Hugl and Merger, 2007]. We previously demonstrated that a certain concentration of PI3 kinase inhibition reverses PRL reduced ALP activity without effecting cell survival in MG-63 and hFOB suggesting PI3 kinase is one of potential PRL pathways in human osteoblast [Seriwatanachai et al., 2008a]. However, the present study found that shortterm administration of PI3 kinase inhibitor did not reverse the inhibitory action of PRL on DNA and Ca^{2+} content suggesting PI3 kinase involved in bone mineralization and osteoblast number is independent to PRL action. Noted, the induction of apoptotis according to the inhibition of PI-3 kinase was ruled out by optimizing the concentration of LY294002, and was not shown to decrease DNA content. However we found that the combination of PRL and PI3 kinase inhibitor constantly induced a decreased in DNA content in d4–7 and d11–14 but not d0–3 confirming the action of PRL on DNA content is not via PI3 kinase pathway. Moreover, data from Ca^{2+} content demonstrated that shortterm PI3 kinase inhibition at proliferative not mineralizing stage is sufficient for inhibiting the mineralization where as the osteoblast number remains unchanged. This time specific manner can also be found in glucocorticoid (dexamethasone) action of which is capable to decrease bone mineralization once cell have not entered to osteoblast differentiation pathway [Eijken et al., 2006].

The results also demonstrated unchanged in OPG, a decoy receptor of RANKL, and RANKL mRNA expression in osteoblast at entire stage of differentiation leading to non-significance RANKL/OPG ratio. Unlikely, the results from osteosarcoma showed that PRL increases RANKL/OPG ratio after administrating PRL in nondexamethasone medium for shortterm incubation. It, however, suggested the cell type specificity and differentiation dependence. Besides, a number of in vivo studies reported the diverse effect of PRL on bone remodeling in which depends on age of animal, weight bearing and connective structure [Krishnamra and Cheeveewattana, 1994; Krishnamra and Seemoung, 1996; Krishnamra et al., 1997]. The combined dimerization of PRL receptor isoforms through its action on bone development and osteoblast differentiation also is not ruled out. Indeed, evidences show that PRL receptor may be crossly combined among isoforms in which gives variety biological effects in a number of kinds of cell [Perrot-Applanat et al., 1997; Qazi et al., 2006]. In conclusion, despite the issues discussed above, the observations of the present study demonstrate that a prolonged incubation of PRL can have an inhibitory effect on osteoblast number, mineralization and differentiation as altered by a reduction of bone precursor marker.

ACKNOWLEDGMENTS

This research was supported by grants from the Royal Golden Jubilee Program (to D.S.) and the Thailand Research Fund (TRF).

REFERENCES

al Sakkaf KA, Dobson PR, Brown BL, 1996. Activation of phosphatidylinositol 3-kinase by prolactin in Nb2 cells. Biochem Biophys Res Commun 221:779–784.

al Sakkaf KA, Dobson PR, Brown BL. 1997. Prolactin induced tyrosine phosphorylation of p59fyn may mediate phosphatidylinositol 3-kinase activation in Nb2 cells. J Mol Endocrinol 19:347–350.

Bataille-Simoneau N, Gerland K, Chappard D, Basle MF, Mercier L. 1996. Expression of prolactin receptors in human osteosarcoma cells. Biochem Biophys Res Commun 229:323–328.

Berlanga JJ, Gualillo O, Buteau H, Applanat M, Kelly PA, Edery M. 1997. Prolactin activates tyrosyl phosphorylation of insulin receptor substrate 1 and phosphatidylinositol-3-OH kinase. J Biol Chem 272:2050–2052.

Chiba H, Sawada N, Ono T, Ishii S, Mori M. 1993. Establishment and characterization of a simian virus 40-immortalized osteoblastic cell line from normal human bone. Jpn J Cancer Res 84:290–297.

Chun TH, Hotary KB, Sabeh F, Saltiel AR, Allen ED, Weiss SJ. 2006. A pericellular collagenase directs the 3-dimensional development of white adipose tissue. Cell 125:577–591.

Clement-Lacroix P, Ormandy C, Lepescheux L, Ammann P, Damotte D, Goffin V, Bouchard B, Amling M, Gaillard-Kelly M, Binart N, Baron R, Kelly PA. 1999. Osteoblasts are a new target for prolactin: Analysis of bone formation in prolactin receptor knockout mice. Endocrinology 140:96–105.

Coss D, Yang L, Kuo CB, Xu X, Luben RA, Walker AM. 2000. Effects of prolactin on osteoblast alkaline phosphatase and bone formation in the developing rat. Am J Physiol Endocrinol Metab 279:E1216–E1225.

Eijken M, Koedam M, van Driel M, Buurman CJ, Pols HA, van Leeuwen JP. 2006. The essential role of glucocorticoids for proper human osteoblast differentiation and matrix mineralization. Mol Cell Endocrinol 248: 87–93.

Gratzner HG. 1982. Monoclonal antibody to 5-bromo- and 5-iododeoxyuridine: A new reagent for detection of DNA replication. Science 218:474–475.

Greenspan SL, Neer RM, Ridgway EC, Klibanski A. 1986. Osteoporosis in men with hyperprolactinemic hypogonadism. Ann Intern Med 104:777–782.

Hotary KB, Allen ED, Brooks PC, Datta NS, Long MW, Weiss SJ. 2003. Membrane type I matrix metalloproteinase usurps tumor growth control imposed by the three-dimensional extracellular matrix. Cell 114: 33–45.

Hugl SR, Merger M. 2007. Prolactin stimulates proliferation of the glucose-dependent beta-cell line INS-1 via different IRS-proteins. JOP 8:739–752.

Jantarajit W, Thongon N, Pandaranandaka J, Teerapornpuntakit J, Krishnamra N, Charoenphandhu N. 2007. Prolactin-stimulated transepithelial calcium transport in duodenum and Caco-2 monolayer are mediated by the phosphoinositide 3-kinase pathway. Am J Physiol Endocrinol Metab 293:E372–E384.

Klibanski A, Greenspan SL. 1986. Increase in bone mass after treatment of hyperprolactinemic amenorrhea. N Engl J Med 315:542–546.

Krishnamra N, Cheeveewattana V. 1994. Studies of acute effect of prolactin on distribution of absorbed calcium and long-term effect on calcium balance in weaned, young, and sexually mature rats. Can J Physiol Pharmacol 72:1521–1527.

Krishnamra N, Seemoung J. 1996. Effects of acute and long-term administration of prolactin on bone 45Ca uptake, calcium deposit, and calcium resorption in weaned, young, and mature rats. Can J Physiol Pharmacol 74:1157–1165.

Krishnamra N, Seemoung J, Limlomwongse L. 1997. Acute effect of prolactin on bone 45Ca accumulation in rats. Endocr J 44:257–264.

Lian JB, Stein GS. 2003. Runx2/Cbfa1: A multifunctional regulator of bone formation. Curr Pharm Des 9:2677–2685.

Lian JB, Javed A, Zaidi SK, Lengner C, Montecino M, van Wijnen AJ, Stein JL, Stein GS. 2004. Regulatory controls for osteoblast growth and differentiation: Role of Runx/Cbfa/AML factors. Crit Rev Eukaryot Gene Expr 14: 1–41.

Liu W, Toyosawa S, Furuichi T, Kanatani N, Yoshida C, Liu Y, Himeno M, Narai S, Yamaguchi A, Komori T. 2001. Overexpression of Cbfa1 in osteoblasts inhibits osteoblast maturation and causes osteopenia with multiple fractures. J Cell Biol 155:157–166.

Lotinun S, Limlomwongse L, Krishnamra N. 1998. The study of a physiological significance of prolactin in the regulation of calcium metabolism during pregnancy and lactation in rats. Can J Physiol Pharmacol 76:218–228.

Lotinun S, Limlomwongse L, Sirikulchayanonta V, Krishnamra N. 2003. Bone calcium turnover, formation, and resorption in bromocriptine- and prolactin-treated lactating rats. Endocrine 20:163–170.

Maruyama Z, Yoshida CA, Furuichi T, Amizuka N, Ito M, Fukuyama R, Miyazaki T, Kitaura H, Nakamura K, Fujita T, Kanatani N, Moriishi T, Yamana K, Liu W, Kawaguchi H, Nakamura K, Komori T. 2007. Runx2 determines bone maturity and turnover rate in postnatal bone development and is involved in bone loss in estrogen deficiency. Dev Dyn 236:1876–1890.

Mott JD, Werb Z. 2004. Regulation of matrix biology by matrix metalloproteinases. Curr Opin Cell Biol 16:558–564.

Naidoo U, Goff DC, Klibanski A. 2003. Hyperprolactinemia and bone mineral density: The potential impact of antipsychotic agents. Psychoneuroendocrinology 28(Suppl 2):97–108.

Perrot-Applanat M, Gualillo O, Pezet A, Vincent V, Edery M, Kelly PA. 1997. Dominant negative and cooperative effects of mutant forms of prolactin receptor. Mol Endocrinol 11:1020–1032.

Prentice A. 2000. Maternal calcium metabolism and bone mineral status. Am J Clin Nutr 71:1312S–1316S.

Qazi AM, Tsai-Morris CH, Dufau ML. 2006. Ligand-independent homo- and heterodimerization of human prolactin receptor variants: Inhibitory action of the short forms by heterodimerization. Mol Endocrinol 20:1912–1923.

Ritchie LD, Fung EB, Halloran BP, Turnlund JR, Van Loan MD, Cann CE, King JC. 1998. A longitudinal study of calcium homeostasis during human pregnancy and lactation and after resumption of menses. Am J Clin Nutr 67:693–701.

Schlechte JA, Sherman B, Martin R. 1983. Bone density in amenorrheic women with and without hyperprolactinemia. J Clin Endocrinol Metab 56: 1120–1123.

Seriwatanachai D, Charoenphandhu N, Suthiphongchai T, Krishnamra N. 2008a. Prolactin decreases the expression ratio of receptor activator of nuclear factor kappaB ligand/osteoprotegerin in human fetal osteoblast cells. Cell Biol Int 32(9): 1126–1135.

Seriwatanachai D, Thongchote K, Charoenphandhu N, Pandaranandaka J, Tudpor K, Teerapornpuntakit J, Suthiphongchai T, Krishnamra N. 2008b. Prolactin directly enhances bone turnover by raising osteoblast-expressed receptor activator of nuclear factor kappaB ligand/osteoprotegerin ratio. Bone 42:535–546.

van Driel M, Pols HA, van Leeuwen JP. 2004. Osteoblast differentiation and control by vitamin D and vitamin D metabolites. Curr Pharm Des 10:2535–2555.

Wagenaar-Miller RA, Engelholm LH, Gavard J, Yamada SS, Gutkind JS, Behrendt N, Bugge TH, Holmbeck K. 2007. Complementary roles of intracellular and pericellular collagen degradation pathways in vivo. Mol Cell Biol 27:6309–6322.

Molecular and Cellular Endocrinology 296 (2008) 41–52

Contents lists available at ScienceDirect

Molecular and Cellular Endocrinology

journal homepage: www.elsevier.com/locate/mce

Transcriptome responses of duodenal epithelial cells to prolactin in pituitary-grafted rats

Narattaphol Charoenphandhu[a,b,*], Kannikar Wongdee[a,c], Jarinthorn Teerapornpuntakit[a], Kanogwun Thongchote[a], Nateetip Krishnamra[a,b]

[a] Consortium for Calcium and Bone Research, Faculty of Science, Mahidol University, Bangkok, Thailand
[b] Department of Physiology, Faculty of Science, Mahidol University, Bangkok, Thailand
[c] Department of Pathobiology, Faculty of Science, Mahidol University, Bangkok, Thailand

ARTICLE INFO

Article history:
Received 5 June 2008
Received in revised form
19 September 2008
Accepted 22 September 2008

Keywords:
Duodenum
Gene ontology
Hyperprolactinemia
Microarray
Pituitary transplantation
Real-time PCR

ABSTRACT

Chronic prolactin (PRL) exposure can affect several functions of duodenal epithelia, especially those associated with fluid and electrolyte transport. However, little is known regarding its molecular mechanism. To identify PRL-regulated genes, microarray analysis was performed on RNA samples from duodenal epithelial cells of anterior pituitary (AP)-grafted hyperprolactinemic rats. Herein, we identified 321 transcripts upregulated and 241 transcripts downregulated after 4 weeks of AP transplantation. Results from real-time PCR analyses of 15 selected genes were consistent with the microarray results. Gene ontology analysis demonstrated pleiotropic effects of PRL on several cellular processes, including cellular metabolic process, cell communication and cell adhesion. Interestingly, 17 upregulated transcripts and 12 downregulated transcripts are involved in the transport of ions and nutrients, e.g., Ca^{2+}, Na^{+}, K^{+}, Cl^{-} and glucose, thus agreeing with the established action of PRL on electrolyte homeostasis. The present results provided fundamental information for further investigations on mechanism of PRL actions in the intestine.

1. Introduction

Prolactin (PRL) is one of the most versatile hormones with respect to its array of actions in vertebrates. The more than 300 PRL actions can be classified into 5 categories, i.e., water and electrolyte balance, growth and development, brain and behavior, reproduction, and immunoregulation (Bole-Feysot et al., 1998). PRL receptors (PRLR) are widely expressed in tissues from all 3 germ layers including the digestive tract where PRL exerts 3 major actions, i.e., ion and nutrient absorption, epithelial cell proliferation, and gastrointestinal motility (Charoenphandhu and Krishnamra, 2007; Bujanover et al., 2002; Chen et al., 1997). Most effects of PRL on the intestinal epithelial cells are genomic and are dependent on de novo gene transcription (Bole-Feysot et al., 1998). However, little is known regarding the PRL-regulated intestinal genes.

Salient actions of PRL on the intestinal epithelial cells are related to ion transport. Duodenum appears to be the most responsive intestinal segment to PRL (Charoenphandhu and Krishnamra, 2007). In pregnant and lactation rats, PRL acts as a Ca^{2+}-regulating hormone that enhances the duodenal Ca^{2+} absorption, thus mitigating massive Ca^{2+} loss from bone for fetal growth and galactopoiesis (Charoenphandhu and Krishnamra, 2007; Boass et al., 1992). Long-term exposure to hyperprolactinemia induced by 4-week anterior pituitary (AP) transplantation was found to increase the transcellular Ca^{2+} transport in rat duodenum by ~2-fold (Tudpor et al., 2005). The direct stimulatory action of PRL on Ca^{2+} absorption has been confirmed by investigations using ex vivo duodenal tissue and the intestinal epithelium-like Caco-2 monolayer (Jantarajit et al., 2007; Thongon et al., 2008). In addition to Ca^{2+}, exposure to PRL for 2 days also increased the intestinal transport of water, Na^{+}, K^{+} and Cl^{-} as well as nutrient molecules, such as glucose and neutral amino acids (e.g., glycine and proline) (Mainoya, 1975a,d). Thus, we hypothesized that a number of duodenal transporter genes involved in ion and nutrient transport may be upregulated in response to long-term hyperprolactinemia.

Besides the transport activities, growth and maturation of the intestinal mucosa is influenced by PRL. In the jejunum of 2-week-old rats, PRL induced proliferation of epithelial cells and ~3-fold increases in maltase and alkaline phosphatase activities (Bujanover et al., 2002). PRL also led to mucosal hypertrophy in pregnant and lactating rats (Mainoya, 1978). Moreover, an increase in the plasma PRL level was reported to stimulate proliferation of the colonic epithelial cells, and could be an unfavorable prognostic

* Corresponding author at: Department of Physiology, Faculty of Science, Mahidol University, Rama VI Road, Bangkok 10400, Thailand. Tel.: +66 2 354 7154; fax: +66 2 354 7154.
E-mail address: naratt@narattsys.com (N. Charoenphandhu).

0303-7207/$ – see front matter © 2008 Elsevier Ireland Ltd. All rights reserved.
doi:10.1016/j.mce.2008.09.025

factor in patients with colonic carcinoma (Bhatavdekar et al., 1995). Regarding PRL effect on the cellular metabolism, PRL increased the activities of UDP-glucuronosyltransferase and glutathione S-transferase in the jejunal epithelial cells of lactating rats (Luquita et al., 1999). Therefore, PRL appeared to exert a variety of actions beyond the scope of ion or nutrient transport, and considerable genomic response of the intestinal epithelial cells to long-term PRL exposure, which could be determined by a genome-wide expression study, was anticipated.

To avoid chronic stress from daily handling and PRL injection, hyperprolactinemia in the present study was induced by AP transplantation. Within 15 days after transplanting two extra AP glands from donors under the renal capsule of the recipient, continuous secretion of PRL from the AP allografts in the absence of the hypothalamic dopaminergic inhibition resulted in a sustained increase in the plasma PRL level (Charoenphandhu et al., 2007; Adler et al., 1989). Four weeks after transplantation, the plasma PRL levels are known to be maintained within the range of 90–100 ng/mL (Piyabhan et al., 2000), which are comparable to the levels attained during pregnancy in humans and rats (Boass et al., 1992). Other AP hormones were not secreted from the grafts due to the absence of their respective trophic factors from the hypothalamus.

The principal objective of this study was to analyze the profile of PRL-regulated genes in the duodenal epithelial cells by using microarray and quantitative real-time PCR (qRT-PCR) techniques. Prior to the profile study, expression of PRLR was determined to show that the duodenal tissue was a target of PRL, and whether hyperprolactinemia induced the downregulation of PRLR. The Illumina's high-performance BeadArray™ technology was used in our microarray study because it has been reported to exhibit high selectivity and sensitivity in gene expression profiling as a result of the high redundancy of each probe built in the bead array (Kuhn et al., 2004; Yan et al., 2008).

2. Materials and methods

2.1. Animals

Eighteen female Sprague–Dawley rats (10-week-old, weighing 200–220 g), were obtained from the National Laboratory Animal Centre, Thailand. They were individually placed in hanging stainless steel cages, fed standard pellets (Perfect Companion, Bangkok, Thailand) and distilled water ad libitum under 12/12 h light/dark cycle. Room temperature was controlled at 23–25 °C, and the relative humidity was about 50–60%. After 7-day acclimatization period, rats were randomly divided into two groups, i.e., sham-operated ($n = 6$) and AP-grafted groups ($n = 4$). Eight rats acted as donors for AP transplantation. This study has been approved by the Institutional Animal Care and Use Committee of the Faculty of Science, Mahidol University, Bangkok, Thailand.

2.2. Anterior pituitary (AP) transplantation

The procedure was modified from the methods of Adler et al. (1989) and Charoenphandhu et al. (2007). In brief, a 1.0 cm paracostal incision was made to expose the left renal capsule of the recipient rat. Two 10-week-old donors were then decapitated to collect the pituitary glands which were immediately inserted into the prepared renal capsule of the recipient rat (i.e., 2 glands/rat) and finally covered with the renal fascia. Muscle and skin were sutured with sterile silk 3/0, and cleaned with 70% ethanol and povidone-iodine. Wound dressing was performed daily. Sham operation consisted of exposure of the left kidney and a gentle touch of the renal fascia with forceps. Visual examination of the well-vascularized hypophyseal graft and immunohistochemical staining for PRL production were performed at the end of the experiments to confirm successful AP transplantation (Charoenphandhu et al., 2007). At 4 weeks after transplantation, plasma PRL levels have been known to increase to 90–100 ng/mL, which are comparable to the levels during pregnancy (Boass et al., 1992).

2.3. Tissue preparation

A median laparotomy was performed under 50 mg/kg sodium pentobarbitone i.p. (Abbott, North Chicago, IL, USA) anesthesia. The hypophyseal grafts were gently dissected from the perirenal tissue for immunohistochemical analysis. The duodenal segment (10 cm) was removed and cut longitudinally along the radix mesenterii to expose the mucosa. Duodenal epithelial cells were collected by scraping the mucosal surface with an ice-cold glass slide, and homogenized at 4 °C with a glass-Teflon Potter-Elvehjem tissue grinder (Wheaton, Millville, NJ, USA) as previously described (Jantarajit et al., 2007). Gene expression profile of each duodenal sample was analyzed separately by microarray.

2.4. Immunohistochemistry for PRL production

Imaging technique was performed to evaluate the viability of AP grafts (e.g., no sign of inflammation or graft rejection) as well as PRL production. Paraffin-embedded 4.0-μm sections were used to detect PRL production in the hypophyseal grafts. After blocking endogenous peroxidase activity and non-specific background with 3% H_2O_2 and 3% horse serum (Sigma, St. Louis, MO, USA), respectively, the sections were incubated for 60 min with 1:300 PRL polyclonal antibody (Dako, Carpinteria, CA, USA) prior to 10-min incubation with biotin-conjugated anti-rabbit secondary antibody and peroxidase-conjugated streptavidin (Dako). The chromogenic reaction was carried out with 3,3′-diaminobenzidine (Dako) to produce a brownish product. The slides were finally counterstained with hematoxylin (Sigma) for 5 min. The normal pituitary gland and perirenal fat pad were used as positive and negative controls, respectively. Hematoxylin–eosin (H&E) staining was also performed to identify structures of the graft. Images were acquired under light microscope (model BX51 TRF; Olympus, Tokyo, Japan).

2.5. Total RNA and cDNA preparation

By using TRIzol reagent (Invitrogen, Carlsbad, CA, USA), the total RNA was prepared from duodenal epithelial cells, as previously described (Thongon et al., 2008). The total RNA was treated with RQ1 DNase (Promega, Madison, WI, USA), and later purified with RNeasy Mini kit (Qiagen, Valencia, CA, USA). Purity of the total RNA was determined by the ratio of absorbance readings at 260 and 280 nm, the ratio of which fell in the range of 1.8–2.0. Integrity of RNA was analyzed by denaturing agarose gel electrophoresis with the 28S rRNA band appearing approximately twice as intense as the 18S rRNA band. Purified total RNA samples were later used for both microarray and qRT-PCR studies. As for qRT-PCR, 1 μg total RNA was reverse-transcribed with the oligo-dT_{15} primer and the iScript kit (Bio-rad, Hercules, CA, USA) to cDNA by a thermal cycler (model MyCycler; Bio-rad). Glyceraldehyde-3-phosphate dehydrogenase (GAPDH), a housekeeping gene, served as a control gene to check the consistency of the reverse transcription (percent coefficient of variation <10%, $n = 10$).

2.6. Microarray

Illumina TotalPrep RNA amplification/in vitro transcription kit (catalog no. IL1791; Ambion, Austin, TX, USA) was used to amplify and generate biotinylated cRNA from 500 ng total RNA for hybridization with Illumina BeadChip array. After purification, biotinylated cRNA was quantified with NanoDrop 1000 spectrophotometer (Thermo Scientific, Waltham, MA, USA). 750 ng of biotinylated cRNA from each duodenal sample was separately hybridized on the RatRef-12 Expression BeadChip (binary manifest file version V1_0_R0_11222119_A; Illumina, San Diego, CA, USA). Each RatRef-12 BeadChip is constructed with BeadArray™ technology, and contains 12 whole-genome gene expression arrays, thus allowing 12 independent samples to be hybridized to a single chip. Each array, which can probe 21,910 genes, consists of 22,523 oligonucleotide probes (50-base gene-specific sequence and 29-base address sequence per probe) selected primarily from the National Center for Biotechnology Information (NCBI) Reference Sequence (RefSeq) database (release 16; http://www.ncbi.nlm.nih.gov/RefSeq). After incubation at 58 °C for 20 h, the BeadChip was washed, blocked and incubated at room temperature with streptavidin-Cy3-containing solution (Illumina) according to the manufacturer's instruction. Fluorescent signals were scanned with BeadStation 500GX Genetic Analysis System (Illumina). Image registration and data extraction were automated with BeadStudio 3.1.3 (Illumina).

2.7. Quantitative real-time PCR (qRT-PCR) and sequencing

Primers used in the present study were designed by OLIGO 6 (Molecular Biology Insights, Cascade, CO, USA) and Primer Validator 1.4 (Naratt Software, Bangkok, Thailand), as shown in Table 1. qRT-PCR and melting curve analyses were performed by Bio-rad MiniOpticon with the iQ SYBR Green SuperMix (Bio-rad) as previously described (Thongon et al., 2008). Gene expression levels were normalized to GAPDH expression. The PCR products were also visualized on 1.5% agarose gel stained with 1.0 μg/mL ethidium bromide under a UV transilluminator (Alpha Innotech, San Leandro, CA, USA). After electrophoresis, all PCR products were extracted by the HiYield Gel/PCR DNA Extraction kit (Real Biotech Corporation, Taipei, Taiwan), and were sequenced by the ABI Prism 3100 Genetic Analyzer (Applied Biosystems, Foster City, CA, USA). qRT-PCR experiments were performed in triplicate.

Table 1
Rattus norvegicus oligonucleotide sequences used in qRT-PCR experiments.

Gene	Accession no.	Primer (forward/reverse)	Product length (bp)
Prolactin receptor			
Short isoform	NM_012630	5′-TTCTACCACCATCGCAAC-3′; 5′-CTGATCTCGTTTGTCATTGAG-3′	120
Long isoform	NM_001034111	5′-TCAAGCAACCGCAGACTC-3′; 5′-CAGTTTAGCCAATCGTTCCA-3′	107
Cell adhesion (GO:0007155)			
Ceacam10	NM_173339	5′-TCTCCTTTGATTGCTCTTCCT-3′; 5′-CTCTGGGGTTCACGAGTG-3′	75
Cellular component organization and biogenesis (GO:0016043)			
Syngr1	NM_019166	5′-TCGGCTCCATTGTGAATGAG-3′; 5′-CTTTCTTGCGGTCCTTGACA-3′	192
Cellular developmental process (GO:0048869)			
Epim	NM_012748	5′-TCCGTAGATTACGTGGAGCA-3′; 5′-AGGACAGCAATGACAGCCA-3′	119
Cellular metabolic process (GO:0044237)			
Cpz	NM_031766	5′-GGATGCGGCCTATAACCAT-3′; 5′-TCCAGGAGAAAGTGCAGCA-3′	114
Kynu	NM_053902	5′-GAGGAGTCGTCTGTGACAAG-3′; 5′-GCAGTAAGCAGTCTGATGAAC-3′	106
Sardh	NM_053664	5′-TTGCTAGGAATCTCCCAGGA-3′; 5′-TGGAACACTCTTCTCAGTGGTG-3′	194
Developmental process (GO:0032502)			
Dbn1	NM_031024	5′-ACCTGTCTGCTTCTCTACCCA-3′; 5′-CTAAGCTACAATCTGGTCTGGG-3′	160
Metabolism (GO:0008152)			
Pon1	NM_032077	5′-TTGAATGAGAAGGAGCCAGC-3′; 5′-TAAACACCTCCACGGTGGA-3′	166
Regulation of biological process (GO:0050789)			
CD40lg	NM_053353	5′-TGGAAAATGGGAGACAACT-3′; 5′-CAGAGGCTGACGATGAAT-3′	118
Gkn1	NM_198972	5′-GACAGCAATGTAGACGGAAGT-3′; 5′-TTTTCATAGTCCCAGAGGC-3′	119
Inhba	NM_017128	5′-GAATGAACTCATGGAGCAGACC-3′; 5′-TGCTGAAACAGACGGATGGT-3′	195
Syn2	NM_019159	5′-GTAATGGCATTGCAGTAGGTCC-3′; 5′-AACATGCCGTCAGCACTGAG-3′	181
Transport (GO:0006810)			
Cacnb1	NM_017346	5′-AGGACTTCCTGCACATCAAGG-3′; 5′-TTGTCACCTGACTTGCTGGAG-3′	175
Clcnkb	NM_173103	5′-CTCCACATTCACCTCTCCC-3′; 5′-GCAGCAGACAACCCTAGAAG-3′	104
Slc22a17	NM_177421	5′-GTCGTGGGATTGTACTGCTGA-3′; 5′-CATCAGGTAGACACCAAGGTCA-3′	146
Housekeeping gene			
GAPDH	NM_017008	5′-AGTCTACTGGCGTCTTCAC-3′; 5′-TCATATTTCTCGTGGTTCAC-3′	133

GAPDH, glyceraldehyde-3-phosphate dehydrogenase; full names of other genes are presented in Tables 2 and 3. Gene ontology (GO) identifiers are presented in parentheses.

2.8. Data analysis

Unless otherwise specified, differential gene expression of microarray and qRT-PCR were considered statistically significant when there was a 2-fold or greater difference in expression between the sham-operated and AP-grafted groups (Sigala et al., 2008). Microarray data were analyzed by BeadStudio Gene Expression Module 3.2.6 and Genome Viewer 3.2.7 (Illumina). The Illumina's Cubic-Spline normalization algorithm was applied to adjust sample signals to minimize the effects of variation arising from non-biological factors. False discovery checks were performed with the "compute false discovery rate" function of the BeadStudio. Comparison between two groups of samples (sham-operated vs. AP-grafted) was done with the *t*-test differential expression algorithm. $P < 0.05$ was used as the criterion for statistical significance. Gene Ontology (GO) analysis for characterizing the biological properties of gene products was performed according to the GO Consortium's instruction at the GO website (http://www.geneontology.org). The used GO search engines were AmiGO (http://amigo.geneontology.org), High-Throughput GoMiner (http://discover.nci.nih.gov/gominer), and Ensembl (http://www.ensembl.org). Gene symbol and full name of gene can be searched from the Rat Genome Database (http://rgd.mcw.edu). The qRT-PCR results compared by using $2^{-\Delta\Delta C_T}$ method (Livak and Schmittgen, 2001) are expressed as $\log_2$ means ± S.E. Graphics were performed with GraphPad Prism 5 (GraphPad Software, San Diego, CA, USA).

3. Results

3.1. Immunohistochemical analysis showed PRL production in the hypophyseal allograft

At 4 weeks after AP transplantation, the two implanted glands were removed from the perirenal connective tissues, and were analyzed for their viability and function histologically and immunohistochemically. The excised grafts were highly vascularized reddish-gray tissue with an average diameter of 1.5–2.5 mm ($n = 4$). H&E staining demonstrated a group of cells of varying size, arranged in irregular cords and clusters (Fig. 1A), agreeing with the histological morphology of normal pituitary gland. Numerous thin-walled sinusoidal networks with richly fenestrated endothelia were seen between the clusters of cells. Immunohistochemical analysis revealed the presence of PRL inside the pars distalis of the implanted glands (Fig. 1B and C), similar to that seen in normal pituitary gland (Fig. 1D). The adjacent fat tissues, fascia, and pars intermedia (negative control) did not show PRL immunoreactivity. Active signs of microvascular endothelial damage and lymphoid proliferation were not seen, suggesting the absence of graft rejection and allograft vasculopathy. The results corroborated that the AP-grafted rats possessed two healthy ectopic pituitary glands which actively produced extra PRL.

3.2. Chronic PRL exposure downregulated PRLR in the duodenal epithelial cells

PRLR mRNA expression was demonstrated by PCR. Since chronic exposure to PRL did not change GAPDH expression (Fig. 2A), mRNA expression levels were first normalized by GAPDH expression. In the present study, both short (-S) and long (-L) isoforms of PRLRs were strongly expressed in the duodenal epithelial cells (Fig. 2B), suggesting that these cells could be target of PRL action. The electrophoretic bands obtained were of expected sizes (Fig. 2B), and amplicon sequencing confirmed qRT-PCR findings. Since prolonged exposure to a high level of PRL could downregulate its receptor (Bowen et al., 2000; Swaminathan et al., 2008), a study of PRLR expression after AP transplantation was performed. qRT-PCR demonstrated (Fig. 2C) that the duodenal epithelial cells from AP-grafted rats showed a decrease in PRLR-L expression by −2.146-fold ($P < 0.05$). In contrast, the expression levels of PRLR-S in both sham-operated and AP-grafted rats were comparable.

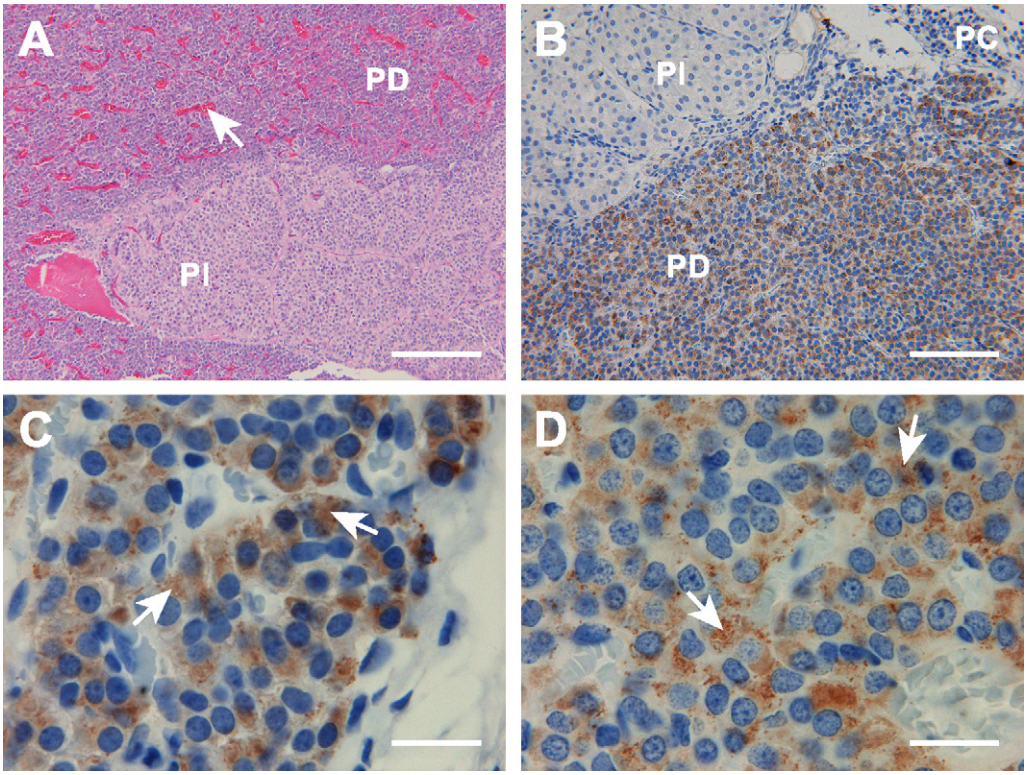

Fig. 1. Representative data of the immunohistochemical analysis for PRL production ($n = 4$–6). (A) Hematoxylin–eosin (H&E) staining of the pars distalis (PD) and pars intermedia (PI) of a hypophyseal allograft dissected from a 4-week AP-grafted rat. The arrow indicates a thin-walled sinusoid filled with numerous erythrocytes. Scale bar, 200 μm. (B) Immunohistochemical staining of an implanted pituitary gland with anti-PRL antibody. The PD is strongly labelled with brownish products of peroxidase, whereas the PI used as a negative control is not stained. The perirenal connective tissues (PC) do not show PRL immunoreactivity. Scale bar, 100 μm. (C) PRL-producing cells (arrows) in a hypophyseal allograft. Scale bar, 20 μm. (D) PRL-producing cells (arrows) in a normal pituitary gland, which is used as a positive control. This gland was dissected from the pituitary fossa of a sham-operated rat. Scale bar, 20 μm.

3.3. Microarray study revealed transcriptome responses of the duodenal epithelial cells after 4 weeks of AP transplantation

Among the 21,910 genes, the microarray analysis detected a total of 321 genes upregulated by more than 2-fold (287 known genes and 34 unknown genes) and 241 genes downregulated by lower than −2-fold (210 known genes and 31 unknown genes) in the duodenal epithelial cells of AP-grafted rats (Fig. 3A and B, and Supplemental Tables S1 and S2). All known genes which were upregulated by more than 10-fold or downregulated by less than −10-fold are listed in order of fold change in Tables 2 and 3, respectively. As shown in Fig. 3, analysis of the distribution of fold changes demonstrated that one half of the PRL-altered genes were increased in the range of 2- to 4-fold (156 known genes and 25 unknown genes), or were decreased in the range of −2 to −4-fold (111 known genes and 18 unknown genes). There were 8 upregulated genes, i.e., Kynu, Clcnkb, Kcnab2, Rup2, Clstn2, Prlpd, Sardh and Epim, and 4 downregulated genes, i.e., Apoa2, S100a9, Mfap4 and Grik3, the expression levels of which were changed by a factor of 100 or higher (Tables 2 and 3).

Furthermore, we searched the GO and Ensembl databases to obtain functional classification of each PRL-altered gene. Only the genes changed by more than 10-fold or less than −10-fold were categorized into 14 major GO groups, each with unique GO identifier, as depicted in Fig. 4A. There were a total of 49 annotated genes in the upregulated set, and 37 annotated genes in the downregulated set (Table 4). The upregulated genes (Fig. 4B) were predominantly involved in the molecular function (11 genes, 20.75% of >10-fold upregulated genes), cellular metabolic process (10 genes, 18.87%), regulation of biological process (7 genes, 13.21%), transport (5 genes, 9.43%) and cellular component (4 genes, 7.55%). Within the downregulated group (Fig. 4C), the majority of genes were involved in the regulation of biological process (8 genes, 20% of <−10-fold downregulated genes), cell communication (7 genes, 17.50%) and molecular function (6 genes, 15%).

Since the effects of PRL on ion and nutrient transport have been well established in the intestine, especially in the duodenum (Charoenphandhu and Krishnamra, 2007; Mainoya, 1975a,b), we further analyzed all upregulated and downregulated genes in the transport category (GO identifier 0006810). The results showed that PRL changed the expression of several genes involved in the transport of Ca^{2+}, Na^{+}, K^{+}, Cl^{-}, H^{+}, Zn^{2+}, Cu^{2+}, HCO_3^{-}, phosphate, glucose, neutral amino acid, organic cation, and organic anion (Tables 5 and 6). Interestingly, the majority of the PRL-altered transporter genes were involved in K^{+} transport (Fig. 5A and B), i.e., 5 upregulated transcripts (29.41% of upregulated transcripts in the transport category) and 3 downregulated transcripts (25%). PRL also altered the expression of two genes which are subunits of Na^{+}/K^{+}-ATPase, a known target protein of PRL (Laborde et al., 1992; Charoenphandhu et al., 2006), i.e., Atp1a2 and Atp1a3 by 2.023- and −7.244-fold (Tables 5 and 6), respectively.

Moreover, PRL increased the expression of several duodenal genes reported to be involved in ion and nutrient transport in the intestine and/or the total body water and electrolyte homeostasis, such as Klk7, Avp, Npb, Kng1, Ren1, Trpc2, Npy2r, Nppc and Gcgr (Supplemental Table S1), while decreasing the expression of others, such as Npy1r, Npy5r, Chrm1, P2ry12, Galr3, Hrh2, Npr2 and Drd3 (Supplemental Table S2). PRL also upregulated Pthr1 encoding parathyroid hormone receptor 1 by 2.015-fold, and downregulated Calca encoding calcitonin/calcitonin-related polypeptide

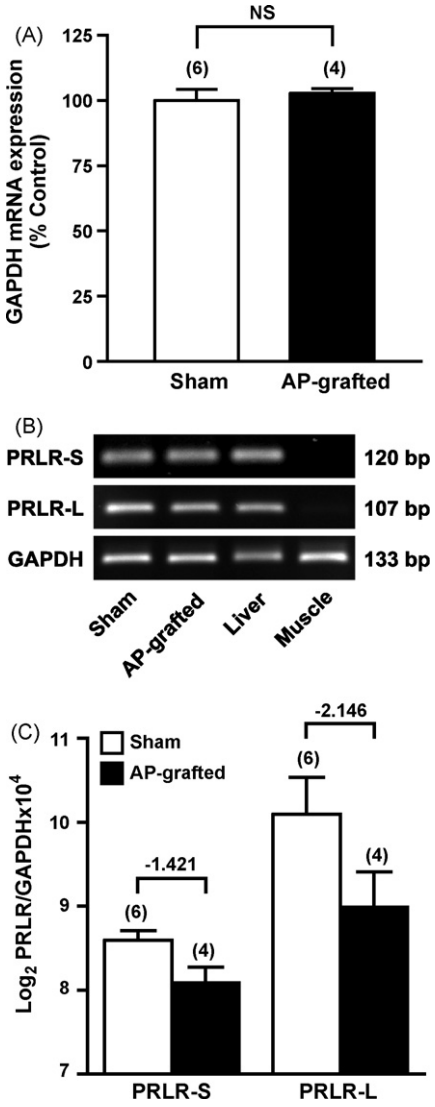

Fig. 2. (A) Expression of GAPDH, the housekeeping gene used for normalization in the qRT-PCR study, in the duodenal epithelial cells of sham-operated (Sham) and AP-grafted rats. Results were obtained from qRT-PCR and expressed as means ± S.E. NS, not significant. (B) Representative electrophoretic bands of short (-S) and long (-L) isoforms of PRLR in the duodenal epithelial cells of Sham and AP-grafted rats. Liver and gastrocnemius muscle from a Sham rat were used as positive and negative controls, respectively. Data were obtained from conventional RT-PCR at 36 cycles. (C) Expression of PRLR-S and -L in the duodenal epithelial cells of Sham and AP-grafted rats as determined by qRT-PCR. GAPDH is a housekeeping gene used for normalization. Results are expressed as $\log_2$ means ± S.E. Fold changes of PRLR-S and PRLR-L expression are presented above their respective columns. Numbers in parentheses represent the number of animals.

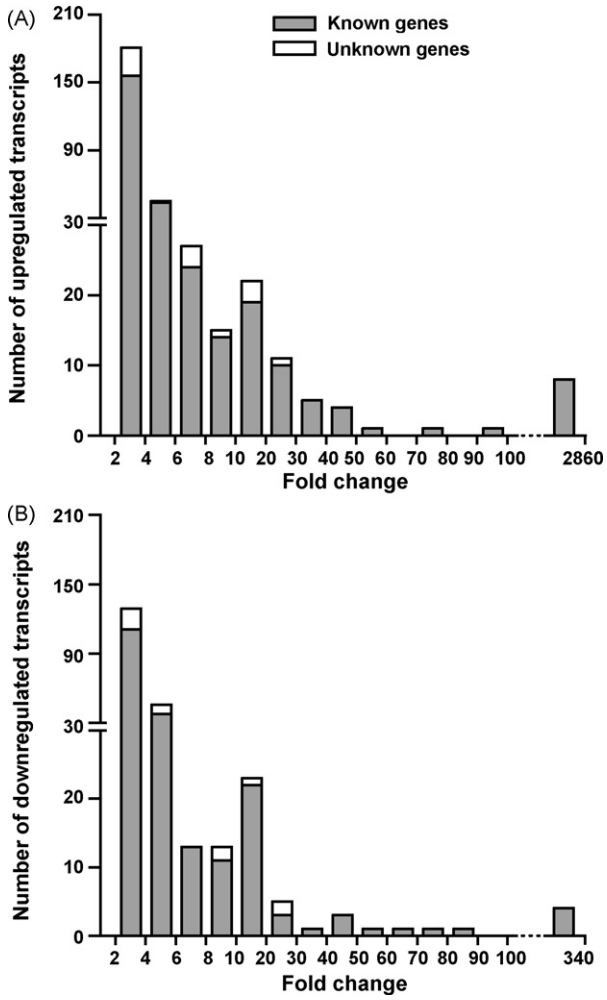

Fig. 3. Distribution of fold changes of genes upregulated (A) and downregulated (B) in the duodenal epithelial cells of AP-grafted rats as determined by microarray. This data set includes transcripts with expression levels changed by more than 2-fold or less than −2-fold.

α by −2.300-fold, both of which have been known to regulate intestinal Ca^{2+} transport and/or Ca^{2+} homeostasis.

Finally, we used qRT-PCR to verify changes in gene expression demonstrated by microarray. We selected genes to be tested by qRT-PCR according to their biological functions, i.e., 1–3 genes per each category (Table 1). As shown in Fig. 6, the qRT-PCR results of 15 studied transcripts were all consistent with the microarray results in response to hyperprolactinemia.

4. Discussion

In the present study, we demonstrated, for the first time, the transcriptome responses of the duodenal epithelial cells to hyperprolactinemia using the highly sensitive Illumina microarray. There was a good quantitative correlation between the fold changes determined by microarray and qRT-PCR. The present results supported the hypothesis that PRL could exert its actions on the duodenal epithelium in a genomic manner. Gene ontology analysis also suggested pleiotropic actions of PRL on a number of cellular processes, especially the transport function, thus confirming the previous studies both in vitro at the tissue level and in vivo that PRL regulated the body electrolyte homeostasis by controlling the rates of intestinal ion transport. Although the samples were collected by scraping and may contain other mucosal cells, e.g., goblet cells, there has been no report on the effect of PRL on other mucosal cell types. It was, therefore, implicated that our results represented the expression profile of the duodenal absorptive cells.

The presence of PRLR in the duodenal epithelial cells indicated that these cells could be direct targets of PRL actions. Our results were consistent with several previous investigations which showed PRLR expression in the duodenum at both transcriptional and translational levels (Jantarajit et al., 2007). However, nothing is known pertaining duodenal PRLR expression under either physiological (e.g., pregnancy and lactation) or pathological (e.g., prolactinoma) hyperprolactinemia. As demonstrated by our qRT-PCR, chronic exposure to PRL could downregulate duodenal PRLR, similar to that typically seen in other cells, such as luteal cells and human

Table 2
Known genes upregulated in the duodenal epithelial cells of AP-grafted rats.

Gene name	Gene symbol	Accession no.	Fold change
Kynureninase (L-kynurenine hydrolase)	Kynu	NM_053902	2859.417
Chloride channel Kb	Clcnkb	NM_173103	397.970
Potassium voltage-gated channel, shaker-related subfamily, beta member 2	Kcnab2	NM_017304	213.821
Urinary protein 2	Rup2	NM_001034950	147.546
Calsyntenin 2	Clstn2	NM_134377	136.802
Prolactin-like protein D	Prlpd	NM_022537	134.864
Sarcosine dehydrogenase	Sardh	NM_053664	123.675
Epimorphin	Epim	NM_012748	100.643
Pyrimidinergic receptor P2Y, G-protein coupled, 6	P2ry6	NM_057124	93.969
Carboxypeptidase Z	Cpz	NM_031766	75.040
Solute carrier family 38, member 5	Slc38a5	NM_138854	52.576
Toll-like receptor 4	Tlr4	NM_019178	46.702
Cholinergic receptor, muscarinic 2	Chrm2	NM_031016	42.014
Paraoxonase 1	Pon1	NM_032077	41.760
Fatty acid binding protein 3	Fabp3	NM_024162	40.893
Insulin 2	Ins2	NM_019130	39.318
Protease, serine, 2	Prss2	NM_012729	39.121
CEA-related cell adhesion molecule 10	Ceacam10	NM_173339	34.794
Kallikrein 7	Klk7	NM_012593	33.569
Mitogen-activated protein kinase 15	Mapk15	NM_173331	32.832
Drebrin 1	Dbn1	NM_031024	28.679
Synapsin II, transcript variant 2	Syn2	NM_019159	28.674
Pregnancy upregulated non-ubiquitously expressed CaM kinase	Pnck	NM_017275	27.032
Synaptogyrin 1	Syngr1	NM_019166	27.020
GTP binding protein 3	Gtpbp3	NM_001011919	25.783
Sex hormone binding globulin	Shbg	NM_012650	22.897
Nuclear factor of activated T-cells, cytoplasmic, calcineurin-dependent 2 interacting protein	Nfatc2ip	NM_001007692	22.859
Syncollin	Sycn	NM_139086	22.518
Formin binding protein 1	Fnbp1	NM_138914	22.349
Unc-5 homolog A (*C. elegans*)	Unc5a	NM_022206	21.680
Parvalbumin	Pvalb	NM_022499	17.373
Zinc finger protein 382	Znf382	NM_144749	16.306
Hemochromatosis type 2 (juvenile) homolog (human)	Hfe2	NM_001012080	16.123
FSH primary response 1	Fshprh1	NM_012955	15.476
GATA binding protein 3	Gata3	NM_133293	15.366
Sodium channel, voltage-gated, type I, alpha	Scn1a	NM_030875	14.246
MAD homolog 9 (*Drosophila*)	Smad9	NM_138872	14.104
Growth arrest specific 8	Gas8	NM_001039030	13.856
Calcium channel, voltage-dependent, beta 1 subunit	Cacnb1	NM_017346	12.633
CD40 ligand	Cd40lg	NM_053353	12.457
Zona pellucida glycoprotein 4	Zp4	NM_172330	12.451
Insulin 1	Ins1	NM_019129	12.398
Protamine 3	Prm3	NM_001002855	12.356
Outer dense fiber of sperm tails 4	Odf4	NM_001007670	11.871
FYVE, RhoGEF and PH domain containing 1	Fgd1	NM_001037546	11.434
Mitochondrial hepatocellular carcinoma-downregulated carrier protein	Hdmcp	NM_001001509	11.245
Calpain 6	Capn6	NM_031808	10.646
Calpain 3	Capn3	NM_017117	10.388
SH3-domain GRB2-like 3	Sh3gl3	NM_031238	10.101

Results are expressed as fold difference in signal intensity. This data set includes mRNAs whose levels changed by more than 10-fold in response to hyperprolactinemia. The complete list of the upregulated transcripts (more than 2-fold) is presented as supplemental data (Table S1).

embryo kidney 293T cells (Bowen et al., 2000; Swaminathan et al., 2008). However, despite the downregulation of PRLR, the duodenum appeared to be responsive to PRL since the stimulatory effect of PRLR on the transepithelial Ca^{2+} absorption in the duodenum of AP-grafted rats was still detectable (Tudpor et al., 2005). Moreover, similar to the results in luteal cells (Bowen et al., 2000), chronic PRL exposure predominantly downregulated PRLR-L, but not PRLR-S. The exact explanation of the differential PRLR isoform expression is not fully understood. Generally, PRLR-S and -L are expressed as cell surface receptors, and both isoforms possess comparable binding affinities (Bole-Feysot et al., 1998). It is suggested that PRL exerts its actions through PRLR-L, whereas PRLR-S does not mediate the transcriptional activation (Lesueur et al., 1991), or may even block the signal transduction of PRLR-L (Hu et al., 2001). Nevertheless, overexpression of PRLR-S completely rescued mammopoiesis in the heterozygous PRLR ($PRLR^{+/-}$) mice (Binart et al., 2003), indicating possible role of PRLR-S in the mammary gland in vivo. In the intestine, known direct PRL actions are presumably mediated by PRLR-L, especially those involved in water, electrolyte and nutrient absorption (Thongon et al., 2008). The absence of change in the duodenal PRLR-S expression after AP transplantation suggested that PRL exerted its actions predominantly via PRLR-L.

Microarray analysis revealed several PRL-regulated genes in the transport category. Functions of PRL as an osmoregulatory and calciotropic hormone are conserved throughout the evolution from fishes to mammals (Sakamoto and McCormick, 2006; Charoenphandhu and Krishnamra, 2007; Norris, 2007). In rats, PRL has long been known to stimulate Ca^{2+}, Na^+ and Cl^- transport in the duodenum (Tudpor et al., 2005; Mainoya, 1975d), and its Ca^{2+}-regulating action becomes more significant during pregnancy and lactation (Boass et al., 1992). Herein, we found that PRL altered the expression of Na^+/K^+-ATPase α polypeptides Atp1a2 and Atp1a3, which are subunits of Na^+/K^+-ATPase essential for the transcellular Na^+ transport and the solvent drag-induced paracellular transport

Table 3
Known genes downregulated in the duodenal epithelial cells of AP-grafted rats.

Gene name	Gene symbol	Accession no.	Fold change
Apolipoprotein A-II	Apoa2	NM_013112	−333.239
S100 calcium binding protein A9 (calgranulin B)	S100a9	NM_053587	−184.269
Microfibrillar-associated protein 4	Mfap4	NM_001034124	−132.304
Glutamate receptor, ionotropic, kainate 3	Grik3	NM_181373	−103.219
Kinesin 13B	Kif13B	NM_213626	−81.392
Inhibin beta-A	Inhba	NM_017128	−75.430
Phosphate cytidylyltransferase 1, choline, beta isoform	Pcyt1b	NM_173151	−69.764
Kringle containing transmembrane protein 1	Kremen1	NM_053649	−55.434
Dyslexia susceptibility 1 candidate 1 homolog (human)	Dyx1c1	NM_001007010	−44.282
Potassium inwardly rectifying channel, subfamily J, member 16	Kcnj16	NM_053314	−43.750
Mast cell protease 8	Mcpt8	NM_021598	−43.715
Connector enhancer of kinase suppressor of Ras 2	Cnksr2	NM_021686	−36.672
Ataxin 1	Atxn1	NM_012726	−24.906
Olfactory receptor 1078	Olr1078	NM_207597	−21.566
Dynein, axonemal, light intermediate polypeptide 1	Dnali1	NM_001031647	−21.532
Patched homolog 1 (*Drosophila*)	Ptch1	NM_053566	−19.512
T-complex protein 11 (mouse)	Tcp11	NM_001007695	−19.249
Sterol O-acyltransferase 1	Soat1	NM_031118	−19.244
Neurogenic differentiation 3	Neurod3	NM_019207	−18.431
Src-related kinase lacking C-terminal regulatory tyrosine and N-terminal myristylation sites	Srms	NM_001011961	−16.639
p21 (CDKN1A)-activated kinase 3	Pak3	NM_019210	−15.416
Taste receptor, type 2, member 10	Tas2r10	NM_023995	−14.844
PR-Vbeta1	VCS-beta1	NM_001017497	−14.458
Vomeronasal 1 receptor, B9	V1rb9	NM_173297	−13.607
CNDP dipeptidase 2 (metallopeptidase M20 family)	Cndp2	NM_001010920	−13.014
Solute carrier family 9, member 4	Slc9a4	NM_173098	−12.871
Succinate receptor 1	Sucnr1	NM_001001518	−12.769
Ly49 inhibitory receptor 5	Ly49i5	NM_001009501	−12.573
Tumor necrosis factor receptor superfamily, member 8	Tnfrsf8	NM_019135	−12.454
Surfactant associated protein D	Sftpd	NM_012878	−12.059
Gamma-aminobutyric acid (GABA-A) receptor, subunit alpha 4	Gabra4	NM_080587	−12.047
Profilin 2	Pfn2	NM_030873	−11.924
Prostaglandin D receptor	Ptgdr	NM_022241	−11.867
Erythrocyte protein band 4.1-like 1, transcript variant 2	Epb4.1l1	NM_021681	−11.439
G protein-coupled receptor 44	Gpr44	NM_001012070	−11.342
Trace-amine-associated receptor 7e	Taar7e	NM_175590	−10.730
Inter-alpha trypsin inhibitor, heavy chain 3	Itih3	NM_017351	−10.660

Results are expressed as fold difference in signal intensity. This data set includes mRNAs whose levels changed by less than −10-fold in response to hyperprolactinemia. The complete list of the downregulated transcripts (lower than −2-fold) is presented as supplemental data (Table S2).

of ions and nutrients (Charoenphandhu et al., 2006; Tanrattana et al., 2004). Na^+/K^+-ATPase is a principal target protein of PRL in several tissues of vertebrates, e.g., branchial epithelium of marine teleost (Pickford et al., 1970), ascending limb and distal convoluted tubule of rat kidneys (Laborde et al., 1992), and duodenal epithelium of rats (Charoenphandhu et al., 2006). Furthermore, PRL changed the expression of the voltage-dependent Ca^{2+} channel (Ca_v) subunits. Since the transepithelial Ca^{2+} flux exhibited a good correlation with L-type Ca_v activity and the L-type Ca_v blocker verapamil could block intestinal Ca^{2+} absorption (Morgan et al., 2007; Pento and Johnson, 1983), the altered Ca_v expression could explain the PRL-enhanced transepithelial calcium transport. In addition to Ca^{2+}, Na^+ and Cl^-, some investigators demonstrated a stimulatory effect of PRL on the intestinal transport of K^+, glucose and neutral amino acids (Mainoya, 1975a,b,c). The effect of PRL on K^+ transport is indeed predominant in the colon where it inhibits the Ca^{2+}-dependent K^+ secretion (Puntheeranurak et al., 2007). Physiological significance of the PRL-regulated K^+ transport in the rat duodenum is currently not known, but it may be essential for maternal K^+ homeostasis since the expression of eight K^+-related genes were altered by PRL. Furthermore, the PRL-induced downregulation of Zn^{2+} transporter Slc30a3 supported the previous finding reported by Travaglini and co-workers (1991) that hyperprolactinemia from prolactinoma led to a decrease in serum Zn^{2+} levels, which could be normalized by administration of bromocriptine, an inhibitor of pituitary PRL secretion. As for the intestinal transport of Cu^{2+}, HCO_3^-, phosphate, organic cations and organic anions, the effect of PRL on their transporters have never been demonstrated functionally either in vitro or in vivo, although the expression of the related genes were altered quite significantly by PRL.

Moreover, PRL also upregulated several genes known to regulate the intestinal ion transport and/or total body fluid and electrolyte homeostasis, e.g., kallikrein 7 (Klk7), arginine vasopressin (Avp), neuropeptide B (Npb), kininogen 1 (Kng1), renin 1 (Ren1), transient receptor potential cation channel (Trpc2), neuropeptide Y receptors (Npy1r, Npy2r and Npy5r), natriuretic peptide precursor type C (Nppc), glucagon receptor (Gcgr), muscarinic cholinergic receptor 1 (Chrm1), purinergic receptors (P2rx2 and P2ry12), galanin receptor 3 (Galr3), histamine receptor H2 (Hrh2), natriuretic peptide receptor 2 (Npr2) and dopamine receptor D3 (Drd3) (Antunes-Rodrigues et al., 2004; Cox, 2007; Hirota and McKay, 2006; Kinoshita et al., 2006; Margolius et al., 1985; Norris, 2007; Schultheiss et al., 2006; Walling et al., 1977; Zhang et al., 2007). Avp encoding arginine vasopressin not only plays a major role in osmoregulation, but also increases the duodenal motility (Li et al., 2007a). Thus, Avp upregulation could partially explain the PRL-induced increase in the gastrointestinal emptying time during lactation (Chen et al., 1997). Regarding Klk7 as a member of the kallikrein-kinin system, products of this system were found to stimulate Na^+ transport across the basolateral membrane of the intestinal absorptive cells (Moriwaki and Fujimori, 1979). Some natriuretic peptide-related genes, e.g., natriuretic peptide precursor type C (Nppc) and natriuretic peptide receptor 2 (Npr2), as well as renin-angiotensin system-related genes, e.g., renin (Ren1), are widely accepted as regulators of water

Table 4
Identification of PRL-altered transcripts in each gene ontology category.

Upregulated transcripts		Downregulated transcripts	
GO:000815 Biological process		GO:000815 Biological process	
GO:0007155 Cell adhesion		GO:0007155 Cell adhesion	
Ceacam10	(34.794)	Mfap4	(−132.304)
GO:0007154 Cell communication		GO:0007154 Cell communication	
Clstn2	(136.802)	Grik3	(−103.219)
Chrm2	(42.014)	Cnksr2	(−36.672)
Fshprh1	(15.476)	Olr1078	(−21.566)
		Pak3	(−15.416)
		Sucnr1	(−12.769)
		Gabra4	(−12.047)
			(−10.730)
		Taar7e	
GO:0016043 Cellular component organization and biogenesis		GO:0016043 Cellular component organization and biogenesis	
Syngr1	(27.020)	Kif13B	(−81.392)
Hdmcp	(11.245)		
GO:0048869 Cellular developmental process			
Epim	(100.643)		
GO:0044237 Cellular metabolic process		GO:0044237 Cellular metabolic process	
Carbohydrate metabolism		Lipid metabolism	
Ins2	(39.318)	Apoa2	(−333.239)
Ins1	(12.398)	Pcyt1b	(−69.764)
Lipid metabolism		Soat1	(−19.244)
Fabp3	(40.893)	Amine metabolism	
Nucleic acid metabolism		Itih3	(−10.660)
Gtpbp3	(25.783)		
Protein metabolism			
Kynu	(2859.417)		
Sardh	(123.675)		
Cpz	(75.040)		
Mapk15	(32.832)		
Pnck	(27.032)		
Capn3	(10.388)		
GO:0032502 Developmental process		GO:0032502 Developmental process	
Dbn1	(28.679)	Kremen1	(−55.434)
		Sftpd	(−12.059)
		Ptgdr	(−11.867)
GO:0008152 Metabolism			
Pon1	(41.760)		
GO:0050789 Regulation of biological process		GO:0050789 Regulation of biological process	
Syn2	(28.674)	S100a9	(−184.269)
Nfatc2ip	(22.859)	Inhba	(−75.430)
Sycn	(22.518)	Atxn1	(−24.906)
Znf382	(16.306)	Ptch1	(−19.512)
Smad9	(14.104)	Neurod3	(−18.431)
Cd40lg	(12.457)	Tnfrsf8	(−12.454)
Fgd1	(11.434)	Pfn2	(−11.924)
		Gpr44	(−11.342)
GO:0042221 Response to chemical stimulus			
Prss2	(39.121)		
GO:0006950 Response to stress			
Tlr4	(46.702)		
GO:0005575 Cellular component		GO:0005575 Cellular component	
Hfe2	(16.123)	Mcpt8	(−43.715)
Gas8	(13.856)	Dnali1	(−21.532)
Prm3	(12.356)	VCS-beta1	(−14.458)
Odf4	(11.871)		
GO:0003674 Molecular function		GO:0003674 Molecular function	
Calcium ion binding		Protein binding	
Pvalb	(17.373)	Epb4.1l1	(−11.439)
Protein binding		Peptidase activity	
Shbg	(22.897)	Cndp2	(−13.014)
Fnbp1	(22.349)	Receptor activity	
Zp4	(12.451)	Tcp11	(−19.249)
Sh3gl3	(10.101)	Tas2r10	(−14.844)
Hormone activity		V1rb9	(−13.607)
Prlpd	(134.864)	Ly49i5	(−12.573)
Peptidase activity			
Klk7	(33.569)		
Capn6	(10.646)		
Receptor activity			
P2ry6	(93.969)		
Unc5a	(21.680)		
Transcription factor activity			
Gata3	(15.366)		
Unknown		Unknown	

Table 4 (*Continued*)

Upregulated transcripts		Downregulated transcripts	
Rup2	(147.546)	Dyx1c1	(−44.282)
MGC108778	(23.930)	RN.13478	(−22.425)
LOC363483	(19.150)	LOC312102	(−20.541)
LOC497899	(18.844)	Srms	(−16.639)
RN.37544	(17.404)	RN.3886	(−12.456)

Numbers in parentheses represent fold changes of corresponding transcripts. Each category is accompanied by a unique GO identifier supplied by the GO search engines. Within each category, transcripts are listed in order of fold change. This data set includes mRNAs with the expression levels changed by more than 10-fold or less than −10-fold in response to hyperprolactinemia.

Table 5
PRL-upregulated transcripts in the transport category (GO:0006810).

Gene name	Gene symbol	Accession no.	Fold change
Calcium transport			
Calcium channel, voltage-dependent, beta 1 subunit	Cacnb1	NM_017346	12.633
Calcium channel, voltage-dependent, T type, alpha 1H subunit	Cacna1h	NM_153814	8.392
Calcium channel, voltage-dependent, T type, alpha 1G subunit	Cacna1g	NM_031601	7.017
Phosphate transport			
Solute carrier family 17 (sodium-dependent inorganic phosphate cotransporter), member 7	Slc17a7	NM_053859	3.582
Sodium transport			
Sodium channel, voltage-gated, type I, alpha	Scn1a	NM_030875	14.246
Amiloride-sensitive cation channel 3	Accn3	NM_173135	2.084
ATPase, Na^+/K^+ transporting, alpha 2 polypeptide	Atp1a2	NM_012505	2.023
Chloride transport			
Chloride channel Kb	Clcnkb	NM_173103	397.970
Potassium transport			
Potassium voltage-gated channel, shaker-related subfamily, beta member 2	Kcnab2	NM_017304	213.821
Potassium voltage-gated channel, Isk-related subfamily, member 1	Kcne1	NM_012973	5.314
Potassium inwardly rectifying channel, subfamily J, member 5	Kcnj5	NM_017297	2.547
Potassium voltage-gated channel, subfamily H (eag-related), member 2	Kcnh2	NM_053949	2.209
Potassium voltage-gated channel, subfamily Q, member 3	Kcnq3	NM_031597	2.049
Bicarbonate transport			
Solute carrier family 4, sodium bicarbonate cotransporter, member 9	Slc4a9	NM_152938	2.353
Copper transport			
ATPase, Cu^{2+} transporting, beta polypeptide	Atp7b	NM_012511	4.160
Organic cation transport			
Solute carrier family 22 (organic cation transporter), member 17	Slc22a17	NM_177421	2.646
Neutral amino acid transport			
Solute carrier family 38, member 5	Slc38a5	NM_138854	52.576

Results are expressed as fold difference in signal intensity. This data set includes mRNAs with the expression levels changed by more than 2-fold in response to hyperprolactinemia.

Table 6
PRL-downregulated transcripts in the transport category (GO:0006810).

Gene name	Gene symbol	Accession no.	Fold change
Calcium transport			
Calcium channel, voltage-dependent, L type, alpha 1E subunit	Cacna1e	NM_019294	−2.424
Sodium transport			
Solute carrier family 9, member 4	Slc9a4	NM_173098	−12.871
ATPase, Na^+/K^+ transporting, alpha 3 polypeptide	Atp1a3	NM_012506	−7.244
Potassium transport			
Potassium inwardly rectifying channel, subfamily J, member 16	Kcnj16	NM_053314	−43.750
Potassium voltage-gated channel, subfamily H (eag-related), member 1	Kcnh1	NM_031742	−2.297
Potassium voltage-gated channel, subfamily G, member 3, transcript variant 1	Kcng3	NM_133426	−2.061
Hydrogen ion transport			
ATPase, H^+ transporting, V0 subunit D, isoform 2	Atp6v0d2	NM_001011972	−4.735
ATPase, H^+ transporting, V1 subunit G isoform 2	Atp6v1g2	NM_212490	−3.151
Zinc transport			
Solute carrier family 30 (zinc transporter), member 3	Slc30a3	NM_001013243	−2.737
Organic anion transport			
Solute carrier organic anion transporter family, member 6c1	Slco6c1	NM_173338	−2.767
Kidney specific organic anion transporter	Slc21a4	NM_030837	−2.473
Glucose transport			
Solute carrier family 2 (facilitated glucose transporter), member 4	Slc2a4	NM_012751	−2.137

Results are expressed as fold difference in signal intensity. This data set includes mRNAs with the expression levels changed by lower than −2-fold in response to hyperprolactinemia.

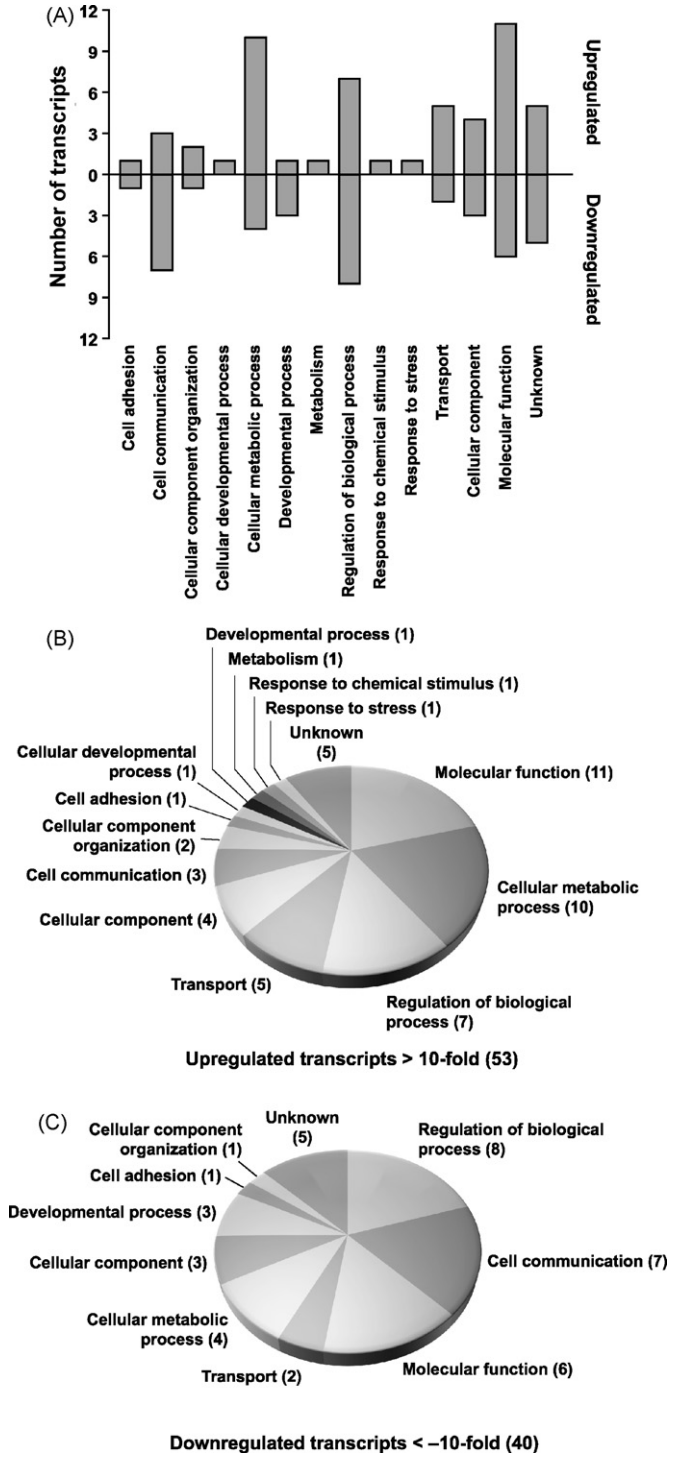

Fig. 4. (A) Distribution of genes in each gene ontology category. Columns above the abscissa represent transcripts that were upregulated at 4 weeks after AP transplantation, whereas columns below the abscissa represent downregulated transcripts. All transcripts were functionally classified according to known cellular functions by using GO search engines. (B) A pie chart shows proportional distribution of upregulated genes in each gene ontology category. (C) A pie chart shows proportional distribution of downregulated genes in each category. Numbers in parentheses represent the number of upregulated or downregulated transcripts. This data set includes transcripts whose levels changed by more than 10-fold or less than −10-fold.

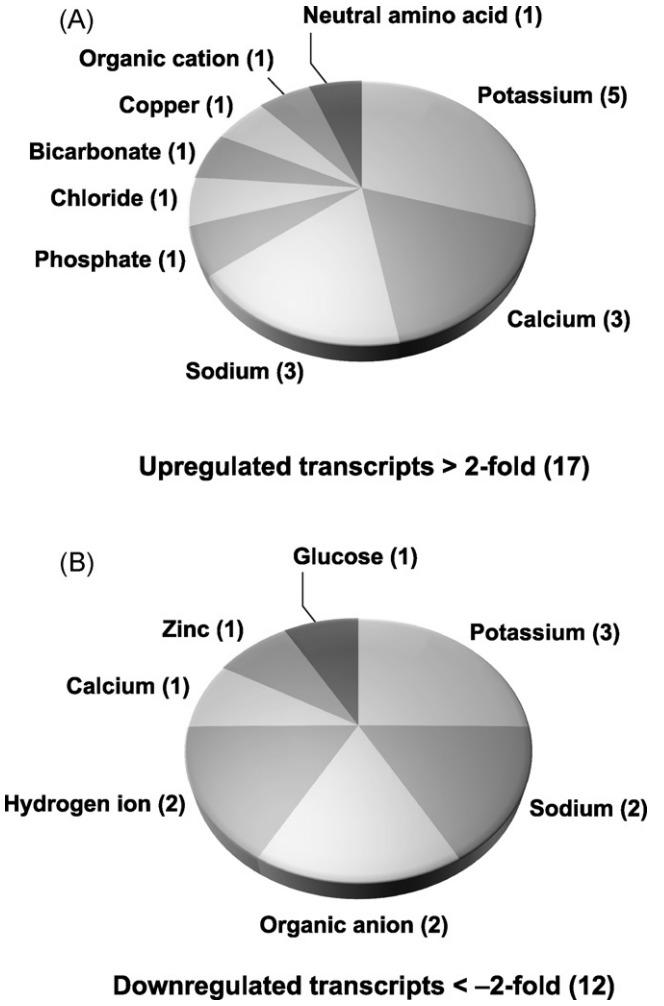

Fig. 5. Pie charts show proportional distributions of upregulated (A) and downregulated (B) genes in the transport category (GO:0006810). The transcripts were functionally classified according to the transported ions or substances. Numbers in parentheses represent the number of upregulated or downregulated transcripts. This data set includes transcripts with expression levels changed by more than 2-fold or less than −2-fold.

and Na^+ balance (Antunes-Rodrigues et al., 2004), whereas the muscarinic cholinergic receptors (Chrm) and neuropeptide Y receptors (e.g., Npy1r, Npy2r and Npy5r) are capable of modulating intestinal fluid secretion (Cox, 2007; Hirota and McKay, 2006). Downregulation of galanin receptor 3 (Galr3) possibly affected the intestinal transport activity, since galanin could increase the active Na^+ and Cl^- absorption in the rabbit ileum (Homaidan et al., 1994).

Of interest is the finding of the PRL-induced upregulation of Pthr1 encoding parathyroid hormone receptor 1 and the downregulation of Calca encoding calcitonin/calcitonin-related polypeptide α, a hypocalcemic hormone. Although the actions of both proteins on the duodenal epithelium have never been reported, we postulate that such actions might be part of the indirect mechanism by which PRL regulates the duodenal Ca^{2+} absorption and/or Ca^{2+} balance. Nemere and Norman (1986) previously reported that parathyroid hormone 1–34, which could bind to Pthr1, significantly stimulated Ca^{2+} transport in the perfused, isolated duodenal loops.

Besides the genes related to electrolyte homeostasis, PRL also altered a number of genes in other categories, including cell adhesion, cell communication, cellular developmental process, and cellular metabolic process, as shown in Table 4. Although most PRL-altered genes are of unknown functions in the intestine,

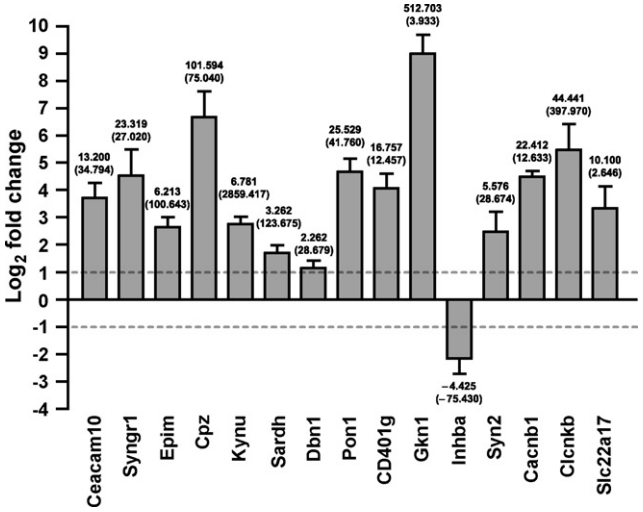

Fig. 6. Fold changes in the expression levels of 15 transcripts selected from various GO categories in the duodenal epithelial cells of AP-grafted rats ($n = 4$) vs. sham-operated rats ($n = 6$). Gene expression was normalized by GAPDH. Twofold upregulation or downregulation are indicated by the two dashed lines. Fold change value of each gene from qRT-PCR is presented on its respective column. Corresponding microarray data are given in parentheses. Full names of genes are shown in Tables 2 and 3.

alteration of some transcripts, such as epimorphin (Epim), zinc finger protein 382 (Znf382), kringle-containing transmembrane protein 1 (Kremen1), purinergic receptor (P2rx2), and insulin (Ins1 and Ins2), might explain PRL actions on the intestinal cell proliferation and maturation (Coutinho-Silva et al., 2005; Gebelein et al., 1998; Iizuka et al., 2007; Ménard et al., 1999). Mainoya (1978) demonstrated that, during pregnancy and lactation, the intestinal weight of rats was markedly increased, and such effect could be abolished by bromocriptine. Hence, the lactation-induced intestinal hypertrophy could be attributed to the proliferative effect of PRL. In contrast, Muller and Dowling (1981) could not detect intestinal hypertrophy in hyperprolactinemic rats with serum PRL of 870 ng/mL. This discrepancy could be due to the typical biphasic action of PRL, in which excess PRL molecules bind to PRLRs as non-functional 1:1 PRL-PRLR complex instead of a functional 1:2 complex (Fuh et al., 1993). To induce intestinal hypertrophy, we speculate that PRL may do so by increasing the expression of a morphogenic protein epimorphin (Epim) or purinergic receptor P2X (P2rx2), both of which have been reported to enhance survival of intestinal epithelial cells (Iizuka et al., 2007; Coutinho-Silva et al., 2005). Alternatively, PRL may induce production of certain local growth factors, such as insulin (Ins1 and Ins2), which can stimulate proliferation of jejunal epithelial cells (Ménard et al., 1999). Other upregulated transcripts in the regulation of biological process and molecular function categories, e.g., mothers against decapentaplegic homolog 9 (Smad9), also appear to be essential for growth and development of the intestinal epithelium.

PRL is also involved in the biotransformation of certain exogenous and endogenous compounds, e.g., *p*-nitrophenol and androgenic steroids (Luquita et al., 1999). Since the intestinal epithelia are normally exposed to drugs and toxic substances, an elevated plasma PRL in lactating animals may help neutralize these chemicals at the absorptive sites, thereby reducing the amount of their toxic metabolites in milk. It is possible that the upregulation of UDP-glucuronosyltransferase (Udpgtr2) gene of the cellular metabolic process category (Supplemental Tables S1) could be important for the PRL-regulated phase II biotransformation of drugs and steroid hormones during lactation. Luquita and co-workers (1999) demonstrated that 1–3 mg/kg/day) PRL administration over 4 days increased UDP-glucuronosyltransferase activity in the jejunum of ovariectomized rats. Consistent with a previous report on a high activity of an antioxidative protein paraoxonase in lactating animals (Turk et al., 2005), paraoxonase (Pon1) expression was increased in our microarray study by ~41-fold (Table 2). In addition, other genes, e.g., nuclear factor of activated T-cells, cytoplasmic, calcineurin-dependent 2 interacting protein (Nfatc2ip) and GATA binding protein 3 (Gata3), may also function in the modulation of the immunoprotective or barrier function of the intestinal epithelium (Li et al., 2007b; Kiwamoto et al., 2006).

In summary, the present study demonstrated that PRL altered the expression of a number of genes related to fluid and electrolyte homeostasis (especially for Ca^{2+}, Na^{+}, K^{+} and Cl^{-} transport) and cell proliferation, both of which are well-established functions of PRL in the intestine. However, the precise functions of these PRL-regulated genes in the duodenal epithelial cells as well as the association between PRL and the functions of those genes are currently unknown. Our results thus provide direction for further investigations into the mechanism of PRL actions in the intestine during pregnancy and lactation.

Conflict of interest

None.

Acknowledgments

This research was supported by grants from the Commission on Higher Education, and the Thailand Research Fund (RSA5180001 to N. Charoenphandhu and RTA5080008 to N. Krishnamra).

Appendix A. Supplementary data

Supplementary data associated with this article can be found, in the online version, at doi:10.1016/j.mce.2008.09.025.

References

Adler, R.A., Farrell, M.E., Krieg, R.J., Deiss, W.P., 1989. Hypogonadism does not mediate urinary calcium loss in pituitary-grafted rats. Metabolism 38, 805–809.
Antunes-Rodrigues, J., de Castro, M., Elias, L.L., Valenca, M.M., McCann, S.M., 2004. Neuroendocrine control of body fluid metabolism. Physiol. Rev. 84, 169–208.
Bhatavdekar, J.M., Patel, D.D., Shah, N.G., Karelia, N.H., Vora, H.H., Ghosh, N., Suthar, T.P., Balar, D.B., 1995. Prognostic value of insulin-like growth factor-1 receptors in patients with colon/rectal cancer: correlation with plasma prolactin. Eur. J. Surg. Oncol. 21, 23–26.
Binart, N., Imbert-Bolloré, P., Baran, N., Viglietta, C., Kelly, P.A., 2003. A short form of the prolactin (PRL) receptor is able to rescue mammopoiesis in heterozygous PRL receptor mice. Mol. Endocrinol. 17, 1066–1074.
Boass, A., Lovdal, J.A., Toverud, S.U., 1992. Pregnancy- and lactation-induced changes in active intestinal calcium transport in rat. Am. J. Physiol. 263, G127–G134.
Bole-Feysot, C., Goffin, V., Edery, M., Binart, N., Kelly, P.A., 1998. Prolactin (PRL) and its receptor: actions, signal transduction pathways and phenotypes observed in PRL receptor knockout mice. Endocr. Rev. 19, 225–268.
Bowen, J.M., Telleria, C.M., Towns, R., Keyes, P.L., 2000. Downregulation of long-form prolactin receptor mRNA during prolactin-induced luteal regression. Eur. J. Endocrinol. 143, 285–292.
Bujanover, Y., Wollman, Y., Reif, S., Golander, A., 2002. A possible role of prolactin on growth and maturation of the gut during development in the rat. J. Pediatr. Endocrinol. Metab. 15, 789–794.
Charoenphandhu, N., Krishnamra, N., 2007. Prolactin is an important regulator of intestinal calcium transport. Can. J. Physiol. Pharmacol. 85, 569–581.
Charoenphandhu, N., Limlomwongse, L., Krishnamra, N., 2006. Prolactin directly enhanced Na^{+}/K^{+}- and Ca^{2+}-ATPase activities in the duodenum of female rats. Can. J. Physiol. Pharmacol. 84, 555–563.
Charoenphandhu, N., Tudpor, K., Thongchote, K., Saengamnart, W., Puntheeranurak, S., Krishnamra, N., 2007. High-calcium diet modulates effects of long-term prolactin exposure on the cortical bone calcium content in ovariectomized rats. Am. J. Physiol. Endocrinol. Metab. 292, E443–E452.
Chen, T.S., Doong, M.L., Wang, S.W., Tsai, S.C., Lu, C.C., Shih, H.C., Chen, Y.H., Chang, F.Y., Lee, S.D., Wang, P.S., 1997. Gastric emptying and gastrointestinal transit during lactation in rats. Am. J. Physiol. 272, G626–G631.

Coutinho-Silva, R., Stahl, L., Cheung, K.K., de Campos, N.E., de Oliveira Souza, C., Ojcius, D.M., Burnstock, G., 2005. P2X and P2Y purinergic receptors on human intestinal epithelial carcinoma cells: effects of extracellular nucleotides on apoptosis and cell proliferation. Am. J. Physiol. Gastrointest. Liver Physiol. 288, G1024–G1035.

Cox, H.M., 2007. Neuropeptide Y receptors; antisecretory control of intestinal epithelial function. Auton. Neurosci. 133, 76–85.

Fuh, G., Colosi, P., Wood, W.I., Wells, J.A., 1993. Mechanism-based design of prolactin receptor antagonists. J. Biol. Chem. 268, 5376–5381.

Gebelein, B., Fernandez-Zapico, M., Imoto, M., Urrutia, R., 1998. KRAB-independent suppression of neoplastic cell growth by the novel zinc finger transcription factor KS1. J. Clin. Invest. 102, 1911–1919.

Hirota, C.L., McKay, D.M., 2006. Cholinergic regulation of epithelial ion transport in the mammalian intestine. Br. J. Pharmacol. 149, 463–479.

Homaidan, F.R., Tang, S.H., Donowitz, M., Sharp, G.W., 1994. Effects of galanin on short circuit current and electrolyte transport in rabbit ileum. Peptides 15, 1431–1436.

Hu, Z.Z., Meng, J., Dufau, M.L., 2001. Isolation and characterization of two novel forms of the human prolactin receptor generated by alternative splicing of a newly identified exon 11. J. Biol. Chem. 276, 41086–41094.

Iizuka, M., Sasaki, K., Hirai, Y., Shindo, K., Konno, S., Itou, H., Ohshima, S., Horie, Y., Watanabe, S., 2007. Morphogenic protein epimorphin protects intestinal epithelial cells from oxidative stress by the activation of EGF receptor and MEK/ERK, PI3 kinase/Akt signals. Am. J. Physiol. Gastrointest. Liver Physiol. 292, G39–G52.

Jantarajit, W., Thongon, N., Pandaranandaka, J., Teerapornpuntakit, J., Krishnamra, N., Charoenphandhu, N., 2007. Prolactin-stimulated transepithelial calcium transport in duodenum and Caco-2 monolayer are mediated by the phosphoinositide 3-kinase pathway. Am. J. Physiol. Endocrinol. Metab. 293, E372–E384.

Kinoshita, N., Takahashi, T., Tada, S., Shinozuka, K., Mizuno, N., Takahashi, K., 2006. Activation of P2Y receptor enhances high-molecular compound absorption from rat ileum. J. Pharm. Pharmacol. 58, 195–200.

Kiwamoto, T., Ishii, Y., Morishima, Y., Yoh, K., Maeda, A., Ishizaki, K., Iizuka, T., Hegab, A.E., Matsuno, Y., Homma, S., Nomura, A., Sakamoto, T., Takahashi, S., Sekizawa, K., 2006. Transcription factors T-bet and GATA-3 regulate development of airway remodeling. Am. J. Respir. Crit. Care Med. 174, 142–151.

Kuhn, K., Baker, S.C., Chudin, E., Lieu, M.H., Oeser, S., Bennett, H., Rigault, P., Barker, D., McDaniel, T.K., Chee, M.S., 2004. A novel, high-performance random array platform for quantitative gene expression profiling. Genome Res. 14, 2347–2356.

Laborde, K., Bussieres, L., Dechaux, M., Shahedi, M., Sachs, C., 1992. Effects of prolactin on Na^+/K^+-ATPase activity in the nephron during maturation in the rat. Pediatr. Res. 31, 207–210.

Lesueur, L., Edery, M., Ali, S., Paly, J., Kelly, P.A., Djiane, J., 1991. Comparison of long and short forms of the prolactin receptor on prolactin-induced milk protein gene transcription. Proc. Natl. Acad. Sci. U.S.A. 88, 824–828.

Li, L., Kong, X., Liu, H., Liu, C., 2007a. Systemic oxytocin and vasopressin excite gastrointestinal motility through oxytocin receptor in rabbits. Neurogastroenterol. Motil. 19, 839–844.

Li, S.Z., McDill, B.W., Kovach, P.A., Ding, L., Go, W.Y., Ho, S.N., Chen, F., 2007b. Calcineurin-NFATc signaling pathway regulates AQP2 expression in response to calcium signals and osmotic stress. Am. J. Physiol. Cell Physiol. 292, C1606–C1616.

Livak, K.J., Schmittgen, T.D., 2001. Analysis of relative gene expression data using real-time quantitative PCR and the $2^{-\Delta\Delta C_T}$ method. Methods 25, 402–408.

Luquita, M.G., Catania, V.A., Sánchez Pozzi, E.J., Vore, M., Veggi, L.M., Pellegrino, J.M., Mottino, A.D., 1999. Induction of phase II biotransformation reactions in rat jejunum during lactation. Possible involvement of prolactin. Biochim. Biophys. Acta 1472, 82–92.

Mainoya, J.R., 1975a. Effect of prolactin on sugar and amino acid transport by the rat jejunum. J. Exp. Zool. 192, 149–154.

Mainoya, J.R., 1975b. Further studies on the action of prolactin on fluid and ion absorption by the rat jejunum. Endocrinology 96, 1158–1164.

Mainoya, J.R., 1975c. Analysis of the role of endogenous prolactin on fluid and sodium chloride absorption by the rat jejunum. J. Endocrinol. 67, 343–349.

Mainoya, J.R., 1975d. Effects of bovine growth hormone, human placental lactogen and ovine prolactin on intestinal fluid and ion transport in the rat. Endocrinology 96, 1165–1170.

Mainoya, J.R., 1978. Possible influence of prolactin on intestinal hypertrophy in pregnant and lactating rats. Experientia 34, 1230–1231.

Margolius, H.S., Halushka, P.V., Chao, J., Miller, D.H., Cuthbert, A.W., Spayne, J.A., 1985. Studies of the kallikrein-kinin system and prostaglandins in epithelial ion transport. Soc. Gen. Physiol. Ser. 39, 121–133.

Ménard, D., Corriveau, L., Beaulieu, J.F., 1999. Insulin modulates cellular proliferation in developing human jejunum and colon. Biol. Neonate 75, 143–151.

Morgan, E.L., Mace, O.J., Affleck, J., Kellett, G.L., 2007. Apical GLUT2 and $Ca_v1.3$: regulation of rat intestinal glucose and calcium absorption. J. Physiol. 580, 593–604.

Moriwaki, C., Fujimori, H., 1979. Effect of kallikrein-kinin system on ion transport across rat small intestine. Adv. Exp. Med. Biol. 120A, 461–471.

Muller, E., Dowling, R.H., 1981. Prolactin and the small intestine. Effect of hyperprolactinaemia on mucosal structure in the rat. Gut 22, 558–565.

Nemere, I., Norman, A.W., 1986. Parathyroid hormone stimulates calcium transport in perfused duodena from normal chicks: comparison with the rapid (transcaltachic) effect of 1,25-dihydroxyvitamin D_3. Endocrinology 119, 1406–1408.

Norris, D.O., 2007. Bioregulation of calcium and phosphate homeostasis. In: Norris, D.O. (Ed.), Vertebrate Endocrinology. Elsevier, San Diego, pp. 486–511.

Pento, J.T., Johnson, M.E., 1983. The influence of verapamil on calcium transport and uptake in segments of rat intestine. Pharmacology 27, 343–349.

Pickford, G.E., Griffith, R.W., Torretti, J., Hendlez, E., Epstein, F.H., 1970. Branchial reduction and renal stimulation of Na^+, K^+-ATPase by prolactin in hypophysectomized killifish in fresh water. Nature 228, 378–379.

Piyabhan, P., Krishnamra, N., Limlomwongse, L., 2000. Changes in the regulation of calcium metabolism and bone calcium content during growth in the absence of endogenous prolactin and during hyperprolactinemia: a longitudinal study in male and female Wistar rats. Can. J. Physiol. Pharmacol. 78, 757–765.

Puntheeranurak, S., Schreiber, R., Spitzner, M., Ousingsawat, J., Krishnamra, N., Kunzelmann, K., 2007. Control of ion transport in mouse proximal and distal colon by prolactin. Cell. Physiol. Biochem. 19, 77–88.

Sakamoto, T., McCormick, S.D., 2006. Prolactin and growth hormone in fish osmoregulation. Gen. Comp. Endocrinol. 147, 24–30.

Schultheiss, G., Hennig, B., Schunack, W., Prinz, G., Diener, M., 2006. Histamine-induced ion secretion across rat distal colon: involvement of histamine H1 and H2 receptors. Eur. J. Pharmacol. 546, 161–170.

Sigala, S., Bodei, S., Missale, C., Zani, D., Simeone, C., Cunico, S.C., Spano, P.F., 2008. Gene expression profile of prostate cancer cell lines: effect of nerve growth factor treatment. Mol. Cell. Endocrinol. 284, 11–20.

Swaminathan, G., Varghese, B., Thangavel, C., Carbone, C.J., Plotnikov, A., Kumar, K.G., Jablonski, E.M., Clevenger, C.V., Goffin, V., Deng, L., Frank, S.J., Fuchs, S.Y., 2008. Prolactin stimulates ubiquitination, initial internalization, and degradation of its receptor via catalytic activation of Janus kinase 2. J. Endocrinol. 196, R1–R7.

Tanrattana, C., Charoenphandhu, N., Limlomwongse, L., Krishnamra, N., 2004. Prolactin directly stimulated the solvent drag-induced calcium transport in the duodenum of female rats. Biochim. Biophys. Acta 1665, 81–91.

Thongon, N., Nakkrasae, L.I., Thongbunchoo, J., Krishnamra, N., Charoenphandhu, N., 2008. Prolactin stimulates transepithelial calcium transport and modulates paracellular permselectivity in Caco-2 monolayer: mediation by PKC and ROCK pathways. Am. J. Physiol. Cell Physiol. 294, C1158–C1168.

Travaglini, P., Mocchegiani, E., De Min, C., Re, T., Fabris, N., Faglia, G., 1991. Zinc and bromocriptine long-term administration in patients with prolactinomas: effects on prolactin and thymulin circulating levels. Int. J. Neurosci. 59, 119–125.

Tudpor, K., Charoenphandhu, N., Saengamnart, W., Krishnamra, N., 2005. Long-term prolactin exposure differentially stimulated the transcellular and solvent drag-induced calcium transport in the duodenum of ovariectomized rats. Exp. Biol. Med. (Maywood) 230, 836–844.

Turk, R., Juretić, D., Geres, D., Turk, N., Rekić, B., Simeon-Rudolf, V., Robić, M., Svetina, A., 2005. Serum paraoxonase activity in dairy cows during pregnancy. Res. Vet. Sci. 79, 15–18.

Walling, M.W., Brasitus, T.A., Kimberg, D.V., 1977. Effects of calcitonin and substance P on the transport of Ca, Na and Cl across rat ileum in vitro. Gastroenterology 73, 89–94.

Yan, J., Barnes, B.M., Kohl, F., Marr, T.G., 2008. Modulation of gene expression in hibernating arctic ground squirrels. Physiol. Genomics 32, 170–181.

Zhang, G.H., Zhu, J.X., Xue, H., Fan, J., Chen, X., Tsang, L.L., Chung, Y.W., Xing, Y., Chan, H.C., 2007. Dopamine stimulates Cl^- absorption coupled with HCO_3^- secretion in rat late distal colon. Eur. J. Pharmacol. 570, 188–195.

ELSEVIER

Cell Biology International 32 (2008) 1126–1135

Cell Biology International

www.elsevier.com/locate/cellbi

Prolactin decreases the expression ratio of receptor activator of nuclear factor κB ligand/osteoprotegerin in human fetal osteoblast cells

Dutmanee Seriwatanachai [a], Narattaphol Charoenphandhu [a,c,*], Tuangporn Suthiphongchai [b,c], Nateetip Krishnamra [a,c,*]

[a] *Department of Physiology, Faculty of Science, Mahidol University, Rama VI Road, Bangkok 10400, Thailand*
[b] *Department of Biochemistry, Faculty of Science, Mahidol University, Rama VI Road, Bangkok 10400, Thailand*
[c] *Consortium for Calcium and Bone Research, Faculty of Science, Mahidol University, Rama VI Road, Bangkok 10400, Thailand*

Received 18 December 2007; revised 28 March 2008; accepted 30 April 2008

Abstract

Prolactin (PRL) enhanced bone remodeling leading to net bone loss in adult and net bone gain in young animals. Studies in PRL-exposed osteoblasts derived from adult humans revealed an increase in the expression ratio of receptor activator of nuclear factor κB ligand (RANKL) and osteoprotegerin (OPG), thus supporting the previous finding of PRL-induced bone loss in adults. This study thus investigated the effects of PRL on the osteoblast functions and the RANKL/OPG ratio in human fetal osteoblast (hFOB) cells which strongly expressed PRL receptors. After 48 h incubation, PRL increased osteocalcin expression, but had no effect on cell proliferation. However, the alkaline phosphatase activity was decreased in a dose–response manner within 24 h. The effect of PRL on alkaline phosphatase was abolished by LY294002, a phosphoinositide 3-kinase (PI3K) inhibitor. PRL also decreased the RANKL/OPG ratio by downregulating RANKL and upregulating OPG expression, implicating a reduction in the osteoblast signal for osteoclastic bone resorption. It could be concluded that, unlike the osteoblasts derived from adult humans, PRL-exposed hFOB cells exhibited indices suggestive of bone gain, which could explain the in vivo findings in young rats. The signal transduction of PRL in osteoblasts involved the PI3K pathway.

Keywords: Alkaline phosphatase; hFOB; OPG; Osteocalcin; PI3K; Prolactin receptor; RANKL

1. Introduction

Pregnant and lactating mammals use prolactin (PRL) as a calcium-regulating hormone to stimulate intestinal calcium absorption and mobilize calcium from bone for fetal development and milk production (Charoenphandhu and Krishnamra, 2007; Lotinun et al., 1998; Thongon et al., 2008). However, PRL action on calcium metabolism was also reported in non-pregnant/lactating rats, in which PRL induced a positive calcium balance by directly stimulating the intestinal calcium absorption and renal calcium reabsorption (Jantarajit et al., 2007; Piyabhan et al., 2000). Interestingly, young rats were more responsive to PRL than adult and aging rats (Krishnamra et al., 1993; Krishnamra and Seemoung, 1996).

Studies of the in vivo effects of PRL on bone are generally complicated by chronic estrogen deficiency caused by PRL-induced hypogonadism (Wang and Chan, 1982; Wang et al., 1980). However, osteoblasts have been known to express PRL receptors (PRLR), which indicated that bone cells are direct targets of PRL (Coss et al., 2000). Our in vivo studies using bone histomorphometry in adult rats showed that PRL exerted an estrogen-independent action by enhancing bone turnover with a greater effect on bone resorption (Seriwatanachai et al., 2008). At the cellular level, PRL directly decreased osteocalcin expression and alkaline phosphatase activity in an osteoblast cell line (MG-63) derived from an adult human,

* Corresponding authors. Department of Physiology, Faculty of Science, Mahidol University, Rama VI Road, Bangkok 10400, Thailand. Tel./fax: +66 2354 7154.
E-mail addresses: naratt@narattsys.com (N. Charoenphandhu), scnks@mahidol.ac.th (N. Krishnamra).

1065-6995/$ - see front matter © 2008 International Federation for Cell Biology. Published by Elsevier Ltd. All rights reserved.
doi:10.1016/j.cellbi.2008.04.026

thus supporting the in vivo findings of PRL-induced bone loss (Seriwatanachai et al., 2008). Interestingly, the effects of PRL on bone varied with age. In contrast to adult rats (more than 8 weeks old), PRL stimulated calcium deposition and induced net bone gain in femur, tibia and sternum of 3-week-old young rats (Krishnamra and Seemoung, 1996). We therefore hypothesized that, unlike its action in MG-63 osteoblasts derived from adult humans, PRL may increase the cellular activities of osteoblasts derived from young humans leading to bone formation. Although the expression of PRLR in human fetal osteoblast (hFOB) cell lines had not been reported, we herein used differentiated hFOB cells, which had minimal chromosome aberration and exhibited the matrix-producing properties of normal differentiated osteoblasts (Harris et al., 1995; Subramaniam et al., 2002), in the investigation of PRL actions. In addition, undifferentiated hFOB cells have recently been shown to possess multilineage differentiation potential (Yen et al., 2007), suggesting that they retained the characteristics of fetal cells.

Bone turnover is a coupled process of the osteoblastic bone formation and osteoclastic bone resorption. Since osteoclasts did not express PRLR (Coss et al., 2000; Kelly et al., 2001), enhanced bone resorption in hyperprolactinemic rats could be due to changes in the osteoblast-expressed mediators, the receptor activator of nuclear factor κB ligand (RANKL) and osteoprotegerin (OPG). Binding of RANKL to its receptors on osteoclasts stimulated bone resorption, whereas binding to its decoy receptors, OPG, decreased bone resorption (Kostenuik, 2005). Thus, the RANKL/OPG ratio determined osteoclast activity, bone resorption as well as bone turnover (Abdallah et al., 2005; Grimaud et al., 2003; Kostenuik, 2005). Our recent findings of the PRL-induced increase in the RANKL/OPG ratio in MG-63 cells and decrease in the OPG expression in primary osteoblasts from adult rats supported the in vivo report of net bone loss in adult hyperprolactinemic rats (Seriwatanachai et al., 2008). Hence, it was possible that hFOB cells may respond to PRL by decreasing the RANKL/OPG expression ratio.

Nothing is known regarding PRL signaling in osteoblasts. The putative signaling pathway of PRL in mammary epithelia was the Janus kinase (JAK2) pathway (Bole-Feysot et al., 1998), whereas the phosphoinositide 3-kinase (PI3K) pathway was reported in non-mammary tissues, e.g., liver, duodenum, colon, pancreatic islets, and Nb2 lymphoma cells (Amaral et al., 2004; Bishop et al., 2006; Jantarajit et al., 2007; Puntheeranurak et al., 2007; Yamauchi et al., 1998). We recently demonstrated that the PRL-stimulated transepithelial calcium transport in the duodenum was via the PI3K, and not the JAK2 pathway (Jantarajit et al., 2007). Therefore, signal transduction of PRL in osteoblasts may also occur via the PI3K.

The objectives of the present study were (i) to demonstrate the expression of PRLR in hFOB cells; (ii) to study the effect of PRL on functions of hFOB cells, including cell proliferation, osteocalcin expression, and alkaline phosphatase activity; (iii) to show whether there was a change in the expression ratio of RANKL/OPG in PRL-exposed hFOB cells; and (iv) to investigate whether PRL signaling in hFOB cells involved the PI3K pathway.

2. Materials and methods

2.1. Cell culture

Human fetal osteoblast 1.19 (hFOB) cells (ATCC No. CRL-11372), an immortalized cell line, were propagated in DMEM/F-12 media, supplemented with 10% fetal bovine serum (FBS), 100 U/mL penicillin/streptomycin, and 0.25 μL/mL amphotericin B (Sigma, St. Louis, MO, USA). Cells were cultured in 75-cm^2 T-flasks at 37 °C in a 5% CO_2 in air humidified incubator. Culture medium was changed every 2 days, and the cultures were split 1:10 when cells had reached 80% confluence. Cells were counted using a hemocytometer and trypan blue dye exclusion.

Osteoblast-like MG-63 cells (ATCC No. CRL-1427; a kind gift from Dr Suttatip Kamolmatyakul, Prince of Songkla University, Thailand), derived from human osteosarcoma, were cultured in 75-cm^2 T-flasks with α-MEM supplemented with 10% FBS, 100 U/mL penicillin/streptomycin, and 0.25 μL/mL amphotericin B (Sigma). To induce maximal expression of PRLR, 1 μM dexamethasone and 0.1 μM 1,25-$(OH)_2D_3$ (Sigma) were also added to the medium, as previously described (Bataille-Simoneau et al., 1996). Cells were incubated at 37 °C with 5% CO_2, and subcultured according to the ATCC's protocol.

2.2. Immunofluorescent analysis

hFOB cells were cultured on a coverslip at 10^5 cells/coverslip in the presence of 0.2% FBS for 16 h. Cells were fixed for 10 min with 3% paraformaldehyde and 2% sucrose at 25 °C, washed 3 times with PBS, and permeabilized for 5 min with 0.5% Triton X-100 in PBS at 25 °C. Non-specific sites were blocked with 10% FBS for 30 min at room temperature. Samples were then incubated overnight at 4 °C with 1:300 rabbit polyclonal anti-PRLR primary antibody (Santa Cruz Biotechnology, Santa Cruz, CA, USA), and finally with 1:200 Alexa Fluor 488-conjugated goat anti-rabbit secondary antibody (Molecular Probes, Eugene, OR, USA). Images were captured with an inverted fluorescent microscope (model Eclipse TE2000-U; Nikon, Tokyo, Japan).

2.3. Cell proliferation assay

hFOB cells were inoculated in a 96-well culture plate (5000 cells/well). After 48 h incubation with 1, 10, 100, 1000 ng/mL PRL, the culture medium was replaced by a medium containing 10% 3-(4,5-dimethylthiazol-2-yl)-2,5-diphenyltetrazolium bromide (MTT) (Sigma). After 3 h incubation with MTT at 37 °C, the absorbance of each well was determined at 540 nm by a microplate reader (model Multiscan EX; Thermo Labsystems, Cergy-Pontoise, France), as described previously (Mosmann, 1983). The absorbance of control cells was considered to be 100%. The relative proliferation of PRL-exposed cells was presented as a percent of control. Each sample was an average of 6 replications, and the relative proliferation of each n was averaged from 3 independent samples (triplicate).

2.4. Alkaline phosphatase activity assay

MG-63 or hFOB cells were cultured in 6-well culture plates (10^5 cells/well). Alkaline phosphatase activity was determined by the conversion of *p*-nitrophenyl phosphate to *p*-nitrophenol, as previously described (Coss et al., 2000). In brief, cells were washed twice with PBS pH 7.4, and incubated for 1 h with 2 mL solution containing (in mM) 100 Na_2CO_3, 10 $MgCl_2$, 20 *p*-nitrophenyl phosphate (Sigma), pH 10.3. Thereafter, 1 mL of 5 M NaOH was added. Color development was quantified immediately at 410 nm.

2.5. Preparation of total RNA and RT-PCR

As previously described (Charoenphandhu et al., 2007; Seriwatanachai et al., 2008), the total RNA of hFOB cells was prepared by using the RNeasy mini kit (Qiagen, Valencia, CA, USA). Two micrograms of the total RNA were reverse-transcribed with the oligo-dT_{20} primer and SuperScript III kit (Invitrogen, Carlsbad, CA, USA) to cDNA by a thermal cycler (model Minicycler; MJ Research, Watertown, MA, USA). Sense and antisense primers for PRLR, osteocalcin, RANKL, OPG, and glyceraldehyde-3-phosphate dehydrogenase (GAPDH) are shown in Table 1. GAPDH served as a control gene to check the consistency of the reverse transcription and to normalize values between samples. After amplification with Taq polymerase (Qiagen), the PCR products were visualized on a 1% agarose gel stained with 1.0 μg/mL ethidium bromide under a trans-UV system (model Quantity One 2000; BioRad, Hercules, CA, USA). The cycle-band intensity curve was plotted for each gene to obtain an optimal PCR cycle which fell in the exponential phase. For a semi-quantitative analysis, the expression of a studied gene in the control group was considered to be 100%, while that in the experimental group was calculated as a percent change relative to the value of the control group.

2.6. Western blot analysis

hFOB cells were lysed in a lysis buffer (150 mM Tris–HCl pH 7.4, 150 mM NaCl, 0.1% SDS, 1% Triton X-100, 1% Nonidet P-40, protease inhibitor, 1 M NaF, 1 M β-glycerophosphate, 0.5 M Na_3VO_4, 1 M DTT, 1% sodium deoxycholate, and 5 mM EDTA) (Sigma). After 30 min incubation at 4 °C, lysates were sonicated and centrifuged at 12,000 × *g* for 10 min at 4 °C, and heated for 5 min at 95 °C before being loaded on a gel. Proteins (100 μg/well) were separated by sodium dodecylsulfate polyacrylamide gel electrophoresis (SDS-PAGE), and subsequently transferred to a nitrocellulose membrane (Amersham, Buckinghamshire, UK) by electroblotting. Non-specific binding sites on the membrane were blocked for 1 h at room temperature by 5% skim milk in TBS containing 0.1% Tween-20. Membranes were probed overnight at 4 °C with 1:2000 rabbit polyclonal anti-RANKL or anti-OPG primary antibodies (Santa Cruz), and re-probed with 1:5000 mouse anti-β-actin antibody (Santa Cruz). After 1 h incubation at 25 °C with 1:2000 goat anti-rabbit or anti-mouse secondary antibodies (Santa Cruz), blots were visualized using the enhanced chemiluminescence (ECL Plus) kit (Amersham). Expression of each protein in the control group was considered as 100%.

2.7. Experimental protocols

Protocol 1

The objective of this protocol was to determine the expression of PRLR in hFOB cells. Normally, osteoblasts constitutively express PRLR; however, some osteoblastic cell lines, e.g., MG-63 cells, require mediators such as vitamin D or dexamethasone for PRLR expression (Bataille-Simoneau et al., 1996). Therefore, hFOB cells were cultured in the presence of 0.2% and 10% fetal bovine serum (FBS; controls), 0.1 μM 1,25-$(OH)_2D_3$ (Vit D) (Sigma), 1 μM dexamethasone (DEX) (Sigma), or a combination of Vit D and DEX. Expression of PRLR transcripts was determined by RT-PCR, and expression of PRLR proteins was demonstrated by immunofluorescent imaging.

Protocol 2

To investigate the direct effects of PRL on osteoblast functions, hFOB cells were incubated in normal media (control) or medium containing 1, 10, 100 or 1000 ng/mL recombinant human PRL (rhPRL) (purity >97% as determined by SDS-PAGE; R&D Systems, Minneapolis, MN, USA) at 37 °C for

Table 1
Homo sapiens oligonucleotide sequences used in the PCR experiment

Gene	Reference or accession no.	Primer (forward/reverse)	Product length (bp)	Cycle
PRLR	[a]	5′-AAATGTGGCATCTGCAACCGTTTTCAC-3′ 5′-GCACTTGCTTGATGTTGCAGTGAAGTT-3′	1790	30
OC	[a]	5′-GGCCAGGCAGGTGCGAAGC-3′ 5′-GCCAGGCCAGCAGAGCGACAC-3′	271	30
RANKL	[a]	5′-GCCAGTGGGAGATGTTAG-3′ 5′-TTAGCTGCAAGTTTTCCC-3′	486	33
OPG	[a]	5′-GCTAACCTCACCTTCGAG-3′ 5′-TGATTGGACCTGGTTACC-3′	324	22
GAPDH[b]	NM_002046	5′-CACCCACTCCTCCACCTTTG-3′ 5′-CCACCACCCTGTTGCTGTAG-3′	110	20

PRLR, prolactin receptor; OC, osteocalcin; RANKL, receptor activator of nuclear factor κB ligand; OPG, osteoprotegerin; GAPDH, glyceraldehyde-3-phosphate dehydrogenase.

[a] Seriwatanachai et al., 2008.

[b] Custom-design primer.

0, 0.5, 3, 6, 12, 24 and 48 h prior to determination of alkaline phosphatase activity. The maximal suppression of alkaline phosphatase activity by PRL was seen at 48 h similar to that reported previously by Seriwatanachai et al. (2008). Therefore, the 48 h incubation period was used to demonstrate the effects of PRL on osteoblast proliferation and functions, including osteocalcin mRNA expression and RANKL/OPG mRNA and protein expression. Expression of mRNAs and proteins was determined in triplicate by RT-PCR and Western blot analysis, respectively.

Protocol 3

Since one of the signaling pathways of PRL was the PI3K pathway (Jantarajit et al., 2007; Puntheeranurak et al., 2007), this protocol aimed to demonstrate whether PRL affected osteoblast activity via this pathway. hFOB or MG-63 cells were incubated at 37 °C for 48 h with normal media (control) or media containing 0.3% dimethyl sulfoxide (DMSO; vehicle; Sigma), 100 nM LY294002 (PI3K inhibitor; Sigma), 100 ng/mL rhPRL, or 100 ng/mL rhPRL plus 100 nM LY294002. Finally, the alkaline phosphatase activity was determined.

2.8. Statistical analysis

Results are expressed as mean ± SEM. Multiple comparisons were performed by one-way analysis of variance (ANOVA) with Newman–Keuls post-test. The level of significance for all statistical tests was $P < 0.05$. Data were analyzed by GraphPad Prism 4.0 for Mac OS X (GraphPad Software, San Diego, CA, USA).

3. Results

3.1. hFOB cells expressed mRNAs and proteins of PRLR

Our RT-PCR study revealed a constitutive expression of PRLR in hFOB cells under the control condition (Fig. 1A). In contrast to the previous report on MG-63 cells (Seriwatanachai et al., 2008), the expression of PRLR in hFOB cells was not altered by 1,25-$(OH)_2D_3$, dexamethasone or the combination of both. Both agents were known to upregulate PRLR in other osteoblast cell lines, e.g., MG-63 and Saos-2 cells (Bataille-Simoneau et al., 1996). Immunofluorescent analysis confirmed that hFOB cells strongly expressed PRLR proteins (Fig. 1B). These findings indicated that this fetal osteoblast cell line served as a target of PRL.

3.2. PRL upregulated osteocalcin expression in hFOB cells

Since PRL stimulates bone growth and bone calcium deposition in young animals, we studied osteoblast functions that were associated with bone formation. We found that PRL had no effect on hFOB cell proliferation (Fig. 2A). However, 100 and 1000 ng/mL rhPRL increased the expression of osteocalcin mRNA from the control level (100.00 ± 5.74%) to 155.27 ± 13.02% ($n = 5$, $P < 0.05$) and 174.73 ± 12.08 ($n = 5$, $P < 0.01$), respectively. The results implied the stimulatory effect of PRL on osteoblastic functions in fetal osteoblasts.

3.3. PRL decreased alkaline phosphatase activity in hFOB cells

In contrast to the osteocalcin expression, the activity of alkaline phosphatase was decreased by 100 and 1000 ng/mL rhPRL to 83.31 ± 2.97% ($n = 5$, $P < 0.05$) and 77.70 ± 5.07% ($n = 5$, $P < 0.01$), respectively (Fig. 3A). A time-dependent study showed a significant decrease in alkaline phosphatase activity at 24 h after exposure to 1000 ng/mL rhPRL (Fig. 3B).

3.4. PRL decreased the expression ratio of RANKL/OPG in hFOB cells

Effects of rhPRL exposure on the markers of osteoblast-mediated activation of bone resorption are presented in Fig. 4. The expression ratio of RANKL and OPG, both of which were

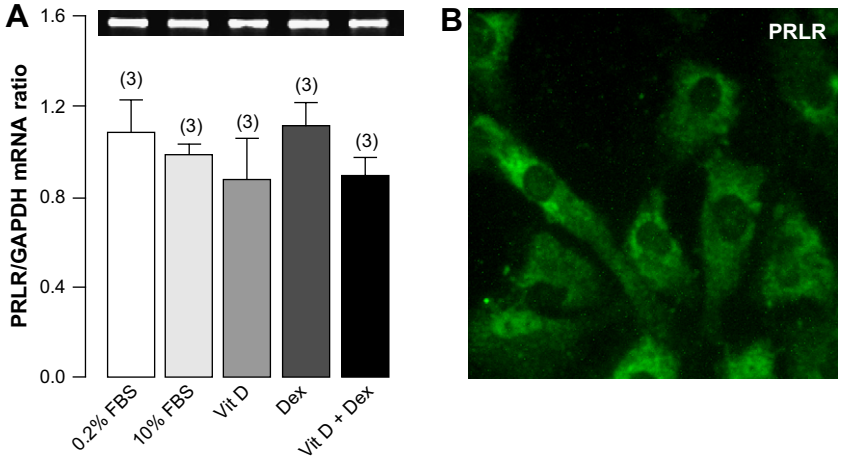

Fig. 1. (A) Expression of PRLR transcripts in hFOB cells exposed for 48 h to 0.2% and 10% fetal bovine serum (FBS, control), 0.1 μM 1,25-$(OH)_2D_3$ (Vit D), 1 μM dexamethasone (DEX), or a combination of Vit D and DEX (Vit D + DEX). A representative electrophoretic image of PRLR is also demonstrated. Numbers in parentheses are numbers of independent flasks. (B) A representative immunofluorescent image showing PRLR protein expression in hFOB cells ($n = 5$), magnification ×400.

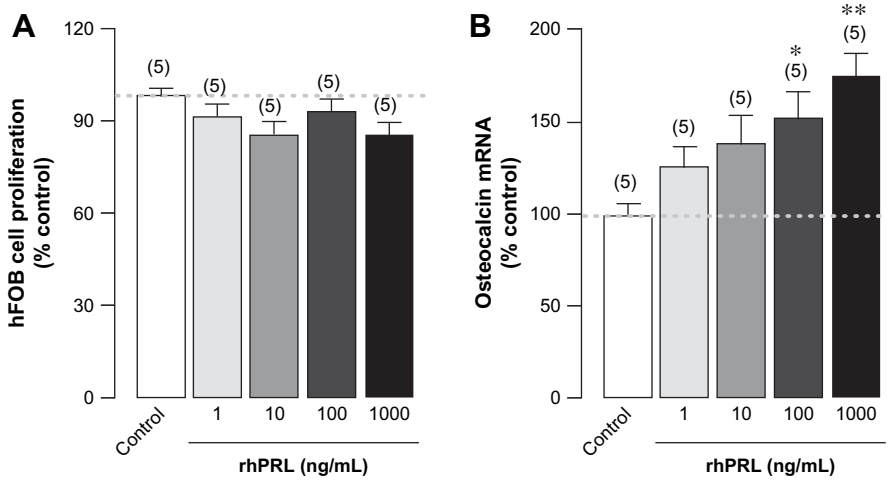

Fig. 2. Dose-dependent changes in (A) cell proliferation and (B) osteocalcin mRNA expression in hFOB cells incubated for 48 h with 1, 10, 100 or 1000 ng/mL rhPRL. Values of the control groups were normalized to 100%. *$P < 0.05$, **$P < 0.01$ compared with the control group. Numbers in parentheses are numbers of independent flasks. Experiments were performed in triplicate.

synthesized by osteoblasts, represented bone resorption (Kostenuik, 2005). Expression of RANKL transcripts were decreased by 10, 100 and 1000 ng/mL rhPRL to 76.56 ± 4.97% ($n = 3, P < 0.05$), 76.81 ± 3.96% ($n = 3, P < 0.05$) and 57.58 ± 7.73% ($n = 3, P < 0.01$) of the control level, respectively, while RANKL protein was decreased by 100 and 1000 ng/mL rhPRL to 71.53 ± 2.79% ($n = 7, P < 0.01$) and 64.78 ± 6.46% ($n = 7, P < 0.01$). Although PRL did not change the expression of OPG transcripts, 100 and 1000 ng/mL rhPRL upregulated expression of OPG protein to 122.96 ± 5.42% ($n = 5, P < 0.05$) and 140.12 ± 7.53% ($n = 5, P < 0.001$), respectively. Therefore, the ratios of RANKL/OPG mRNAs in hFOB cells were significantly decreased by 24, 21 and 43% after 48 h exposure to 10, 100 and 1000 ng/mL rhPRL, respectively, while the ratios of RANKL/OPG proteins were decreased by 41% and 56% after 100 and 1000 ng/mL rhPRL exposure. The decreased RANKL/OPG ratio implicated a suppression of the osteoclast-mediated bone resorption by PRL.

3.5. PRL-mediated decreases in alkaline phosphatase activity in hFOB and MG-63 cells were completely blocked by a PI3K inhibitor

Because the PI3K pathway was one of the signaling pathways of PRL, we investigated whether PRL used this pathway in osteoblasts (i.e., hFOB and MG-63 cells). We found that LY294002, a specific PI3K inhibitor, at concentrations ranging from 10 nM to 1 μM did not affect the viability or the proliferation rate of hFOB and MG-63 cells (Fig. 5A,B). Exposure to 100 ng/mL rhPRL decreased alkaline phosphatase activity in both hFOB and MG-63 cells; however, this PRL action was completely abolished by 100 nM LY294002 (Fig. 5C,D). DMSO, a vehicle for LY294002 preparation, and 100 nM LY294002 alone had no effect on the alkaline phosphatase activity in both cell lines. The results suggested that PRL decreased the osteoblastic alkaline phosphatase activity via the PI3K pathway.

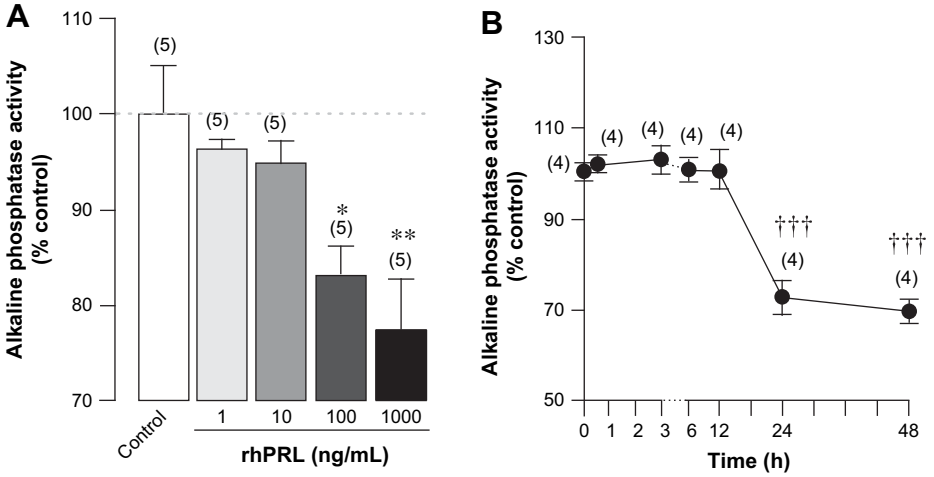

Fig. 3. Dose-dependent changes in alkaline phosphatase activity (A) in hFOB cells incubated for 48 h with 1, 10, 100 or 1000 ng/mL rhPRL. Values of the control groups were normalized to 100%. *$P < 0.05$, **$P < 0.01$ compared with the control group. (B) Time-dependent changes in alkaline phosphatase activity in hFOB cells exposed to 1000 ng/mL rhPRL. The value at 0 h was normalized to 100%. $^{\dagger\dagger\dagger}P < 0.001$ compared with the values at 0 h. Numbers in parentheses are numbers of independent flasks. Experiments were performed in triplicate.

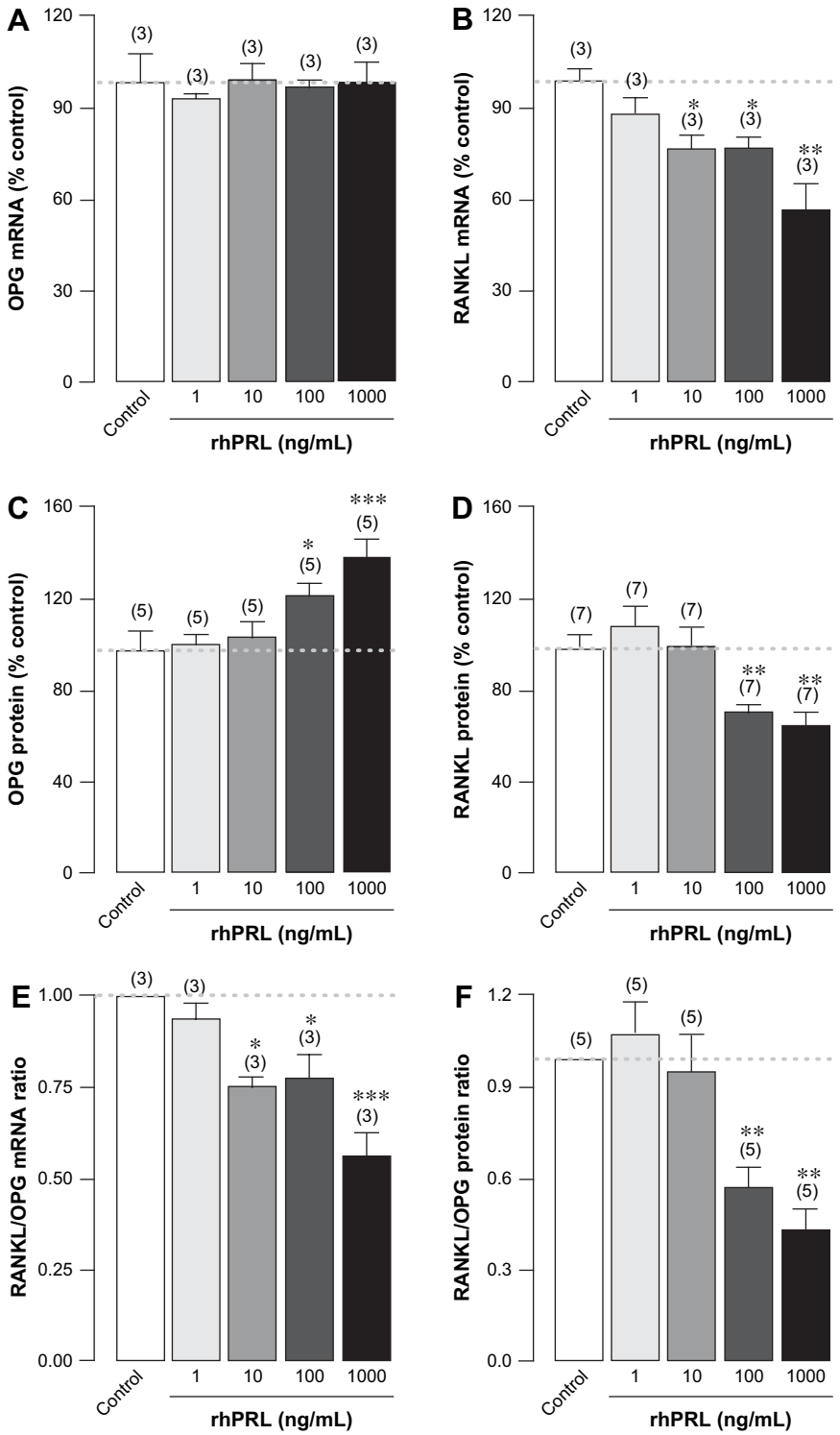

Fig. 4. Dose-dependent changes in the mRNA expressions of OPG (A) and RANKL (B), protein expressions of OPG (C) and RANKL (D), and the ratios of RANKL/OPG mRNA (E) and protein (F) expressions in hFOB cells incubated for 48 h with 1, 10, 100 or 1000 ng/mL rhPRL. Values of the control groups were normalized to 100%. $^{*}P < 0.05$, $^{**}P < 0.01$, $^{***}P < 0.001$ compared with the control group. Numbers in parentheses are numbers of independent flasks. Experiments were performed in triplicate.

4. Discussion

In adult animals, high bone turnover is a characteristic of both physiological and pathological hyperprolactinemia (Krishnamra et al., 1997; Lotinun et al., 2003; Meaney et al., 2004). Generally, high bone turnover accelerates bone loss, especially when the resorption cavities are incompletely replaced. However, under certain conditions, such as during growth hormone administration, the increased bone turnover shifts the balance between bone formation and resorption

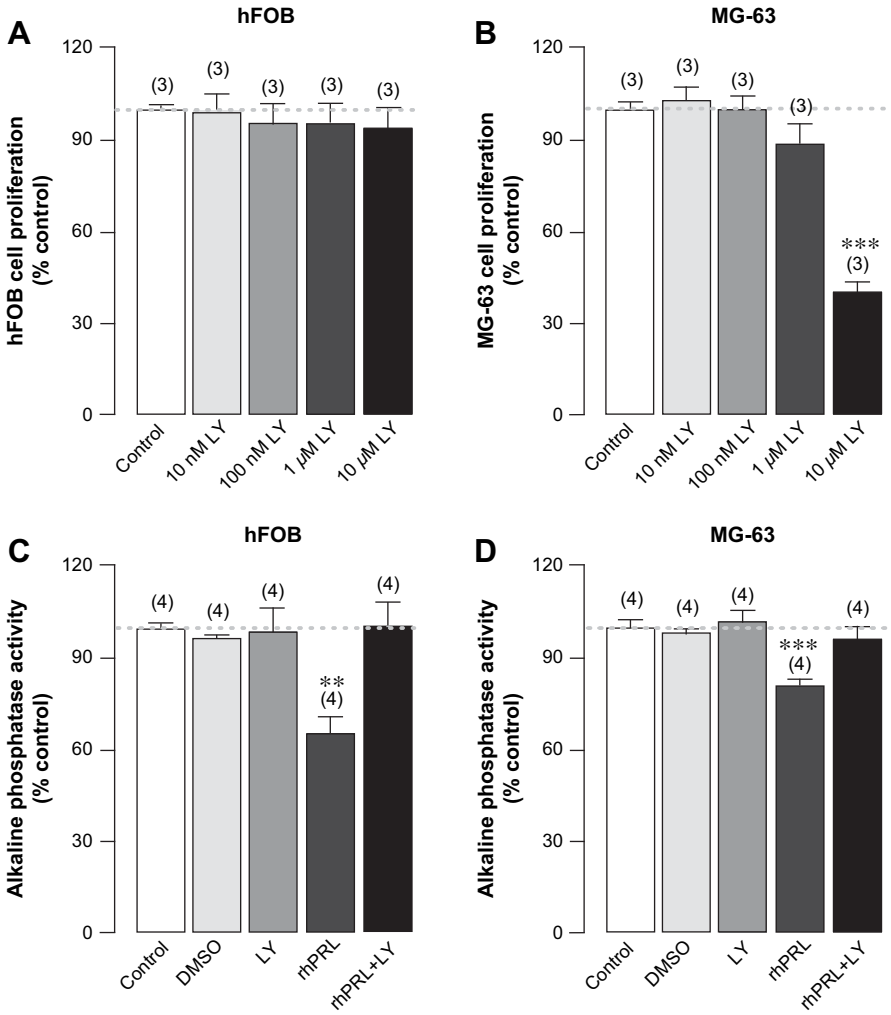

Fig. 5. (A,B) Proliferation of hFOB and MG-63 cells after incubation for 48 h with 10 nM, 100 nM, 1 μM or 10 μM LY294002 (LY, PI3K inhibitor). (C,D) Alkaline phosphatase activity in hFOB and MG-63 cells incubated for 48 h in normal culture media (control) or media containing 0.3% DMSO (vehicle), 100 nM LY294002, 100 ng/mL rhPRL, or 100 ng/mL rhPRL plus 100 nM LY294002. Values of the control groups were normalized to 100%. $^{**}P < 0.01$, $^{***}P < 0.001$ compared with the control group. Numbers in parentheses are numbers of independent flasks. Experiments were performed in triplicate.

toward net bone calcium deposition (Parfitt, 1991). Although high physiological PRL of ∼75−100 ng/mL during pregnancy did not produce a significant bone loss, transient osteopenia was reported after 3 months of lactation when plasma PRL ranged between 200 and 350 ng/mL (Prentice, 2000; Ritchie et al., 1998). Furthermore, high PRL levels (up to ∼1000 ng/mL) found in several pathological conditions, e.g., prolactinomas or prolonged antipsychotic drug use, induced massive bone loss and overt osteopenia (Biller et al., 1992; Crosignani, 2006; Meaney et al., 2004). Thus, PRL exposure in adult animals and humans, depending on the PRL concentrations, could lead to bone loss. On the other hand, by using the in vivo ^{45}Ca kinetic study, Krishnamra and Seemoung (1996) reported that young rats responded differently to PRL, i.e., by enhancing bone gain instead of bone loss despite the presence of high bone turnover. Moreover, PRL administration in 3-week-old weaned rats resulted in a dose-dependent increase in the calcium content of femur, tibia and vertebrae (Krishnamra and Seemoung, 1996). The present investigation showed an increase in osteocalcin expression and a decrease in the RANKL/OPG ratio in hFOB cells which indicated that PRL-exposed osteoblasts derived from immature animals could potentially induce bone gain.

Indeed, the in vivo osteopenic action of PRL had long been explained by estrogen deficiency due to PRL-induced hypogonadism (Meaney et al., 2004; Wang et al., 1980). However, the PRLR knockout mice manifested a 60% decrease in the rate of bone formation (Clément-Lacroix et al., 1999), and PRL-exposed rats exhibited high bone turnover with different histomorphometric patterns from those seen in ovariectomized (Ovx) rats, i.e., higher mineral apposition rate and bone formation rate (Seriwatanachai et al., 2008). It is possible that PRL could also exert a direct estrogen-independent action on bone cells. The finding of PRLR in osteoblasts also supported this hypothesis. Although the levels of PRLR transcript in MG-63 cells were significantly elevated in the presence of 1,25-$(OH)_2D_3$ and dexamethasone (Bataille-Simoneau et al., 1996), the expression of PRLR mRNAs and proteins in hFOB cells similar to that in the primary rat osteoblasts (Seriwatanachai et al., 2008) was constitutive and independent of both hormones.

We further investigated the effect of PRL on hFOB cell functions and found that PRL stimulated osteocalcin expression in hFOB cells without affecting cell proliferation. This effect of PRL agreed with the recent report on neonatal osteoblasts (Seriwatanachai et al., 2008), and was also consistent with the action of other hormones, such as leptin which enhanced osteoblast differentiation but not proliferation (Thomas et al., 1999). On the other hand, MG-63 cells derived from adult humans showed a decrease in osteocalcin expression after a 48-h PRL exposure (Seriwatanachai et al., 2008). The PRL-induced increase in the activity of hFOB cells supported our hypothesis that PRL could increase bone formation in osteoblasts derived from young animals.

Similar to the primary neonatal rat osteoblasts (Coss et al., 2000) and MG-63 cells (Seriwatanachai et al., 2008), PRL-exposed hFOB cells manifested a decrease in alkaline phosphatase activity. Although alkaline phosphatase is a classical marker of bone formation (Stein et al., 1996), its expression depends on the developmental stage of osteoblasts (Owen et al., 1990). Normally, osteoblasts have roles in all 3 steps of bone formation, i.e., cell proliferation, extracellular matrix maturation, and mineralization (Owen et al., 1990). Responses of osteoblast proliferation, gene expression and enzyme activities to various humoral factors depend on the stage of development of the cells. For example, transforming growth factor β and its downstream protein Smad3 inhibited osteoblast proliferation, but enhanced alkaline phosphatase activity, mineralization, and expression of bone matrix proteins (Sowa et al., 2002). Generally, alkaline phosphatase expression is increased immediately after cessation of cell proliferation, while the expression of osteocalcin, which is important for the formation of hydroxyapatite crystal lattices (Hoang et al., 2003), is increased later during matrix maturation near the onset of mineralization (Owen et al., 1990). Therefore, a disparate relationship between osteocalcin expression and alkaline phosphatase activity could be observed during the development of osteoblasts.

Since PRL enhanced osteocalcin expression in the matrix maturation step (Fig. 2B) without affecting the in vitro mineralization of primary rat osteoblasts (Charoenphandhu et al., 2008), it appeared that PRL increased bone calcium deposition in young rats by downregulating RANKL and upregulating OPG, thereby decreasing the RANKL/OPG ratio. Similar to PRL, growth hormone which increases bone turnover and bone gain (Brixen et al., 2000; Landin-Wilhelmsen et al., 2003; Schlemmer et al., 1991) also stimulates OPG synthesis in hFOB cells (Mrak et al., 2007). In contrast, MG-63 cells responded to 48-h PRL exposure by increasing the RAN KL/OPG ratio (Seriwatanachai et al., 2008). An increase in this ratio has been associated with osteopenic conditions, such as hyperparathyroidism and aging (Cao et al., 2003; Stilgren et al., 2004). In the transgenic mice, overexpression of RANKL increased the cortical porosity, whereas overexpression of OPG prevented bone loss and improved cortical bone strength (Kostenuik, 2005; Mizuno et al., 2002). The ~50% decrease in RANKL/OPG ratio in the present study implied that PRL could potentially suppress bone resorption, thus supporting the earlier report of greater calcium deposition in bones of PRL-treated young rats (Krishnamra and Seemoung, 1996).

Although the direct actions of PRL in osteoblasts have been demonstrated, nothing was known regarding its signaling pathway. PRL binding to PRLRs triggers dimerization of PRLRs and activation of the downstream signals (Bole-Feysot et al., 1998). In the mammary epithelia, PRL-PRLR complex used the JAK2 signaling pathway in the stimulation of milk production (Bole-Feysot et al., 1998). However, in other tissues, such as liver and calcium-transporting epithelia, e.g., duodenum and colon, mitogen-activated protein kinase (MAPK) and PI3K pathways have been reported (Amaral et al., 2004; Yamauchi et al., 1998). We recently showed that PRL directly stimulated duodenal calcium absorption (Jantarajit et al., 2007), and inhibited colonic Ca^{2+}-dependent Cl^- and K^+ secretion via the PI3K pathway (Puntheeranurak et al., 2007). By using a potent inhibitor of PI3K (LY294002), the present study showed that the suppressive effect of PRL on alkaline phosphatase activity in hFOB cells was completely abolished. Therefore, the PI3K pathway could be one of the signaling pathways of PRL in osteoblasts. The detailed signaling cascade, however, remains to be investigated.

It can be concluded that hFOB cells strongly and constitutively express PRLR. PRL directly increases osteocalcin mRNA expression, and decreases the RANKL/OPG ratio in these cells, indicating the stimulation of bone formation and suppression of bone resorption, respectively. PRL also decreases alkaline phosphatase activity, in part, via the PI3K signaling pathway. Our in vitro study supported the previous in vivo findings that, unlike mature rats, PRL enhances bone calcium deposition and bone gain in young rats.

Acknowledgements

We thank Dr Sinee Disthabanchong from the Faculty of Medicine, Ramathibodi Hospital, Mahidol University, for her technical guidance and helpful comments. We thank Dr Suttatip Kamolmatyakul from the Prince of Songkla University, Thailand, for a kind gift of MG-63 cells. This research was supported by grants from the Royal Golden Jubilee Program (to DS), the Thailand Research Fund (TRF) and the National Center for Genetic Engineering and Biotechnology (BIOTEC).

References

Abdallah BM, Stilgren LS, Nissen N, Kassem M, Jorgensen HR, Abrahamsen B. Increased RANKL/OPG mRNA ratio in iliac bone biopsies from women with hip fractures. Calcif Tissue Int 2005;76:90–7.

Amaral ME, Cunha DA, Anhê GF, Ueno M, Carneiro EM, Velloso LA, et al. Participation of prolactin receptors and phosphatidylinositol 3-kinase and MAP kinase pathways in the increase in pancreatic islet mass and sensitivity to glucose during pregnancy. J Endocrinol 2004;183:469–76.

Bataille-Simoneau N, Gerland K, Chappard D, Basle MF, Mercier L. Expression of prolactin receptors in human osteosarcoma cells. Biochem Biophys Res Commun 1996;229:323–8.

Biller BM, Baum HB, Rosenthal DI, Saxe VC, Charpie PM, Klibanski A. Progressive trabecular osteopenia in women with hyperprolactinemic amenorrhea. J Clin Endocrinol Metab 1992;75:692–7.

Bishop JD, Nien WL, Dauphinee SM, Too CK. Prolactin activates mammalian target-of-rapamycin through phosphatidylinositol 3-kinase and stimulates phosphorylation of p70S6K and 4E-binding protein-1 in lymphoma cells. J Endocrinol 2006;190:307–12.

Bole-Feysot C, Goffin V, Edery M, Binart N, Kelly PA. Prolactin (PRL) and its receptor: actions, signal transduction pathways and phenotypes observed in PRL receptor knockout mice. Endocr Rev 1998;19:225–68.

Brixen K, Hansen TB, Hauge E, Vahl N, Jorgensen JO, Christiansen JS, et al. Growth hormone treatment in adults with adult-onset growth hormone deficiency increases iliac crest trabecular bone turnover: a 1-year, double-blind, randomized, placebo-controlled study. J Bone Miner Res 2000;15:293–300.

Cao J, Venton L, Sakata T, Halloran BP. Expression of RANKL and OPG correlates with age-related bone loss in male C57BL/6 mice. J Bone Miner Res 2003;18:270–7.

Charoenphandhu N, Krishnamra N. Prolactin is an important regulator of intestinal calcium transport. Can J Physiol Pharmacol 2007;85: 569–81.

Charoenphandhu N, Teerapornpuntakit J, Methawasin M, Wongdee K, Thongchote K, Krishnamra N. Prolactin decreases expression of Runx2, osteoprotegerin and RANKL in primary osteoblasts derived from tibiae of adult female rats. Can J Physiol Pharmacol 2008;86:240–8.

Charoenphandhu N, Wongdee K, Tudpor K, Pandaranandaka J, Krishnamra N. Chronic metabolic acidosis upregulated claudin mRNA expression in the duodenal enterocytes of female rats. Life Sci 2007;80:1729–37.

Clément-Lacroix P, Ormandy C, Lepescheux L, Ammann P, Damotte D, Goffin V, et al. Osteoblasts are a new target for prolactin: analysis of bone formation in prolactin receptor knockout mice. Endocrinology 1999;140: 96–105.

Coss D, Yang L, Kuo CB, Xu X, Luben RA, Walker AM. Effects of prolactin on osteoblast alkaline phosphatase and bone formation in the developing rat. Am J Physiol Endocrinol Metab 2000;279:E1216–25.

Crosignani PG. Current treatment issues in female hyperprolactinaemia. Eur J Obstet Gynecol Reprod Biol 2006;125:152–64.

Grimaud E, Soubigou L, Couillaud S, Coipeau P, Moreau A, Passuti N, et al. Receptor activator of nuclear factor κB ligand (RANKL)/osteoprotegerin (OPG) ratio is increased in severe osteolysis. Am J Pathol 2003;163: 2021–31.

Harris SA, Enger RJ, Riggs BL, Spelsberg TC. Development and characterization of a conditionally immortalized human fetal osteoblastic cell line. J Bone Miner Res 1995;10:178–86.

Hoang QQ, Sicheri F, Howard AJ, Yang DS. Bone recognition mechanism of porcine osteocalcin from crystal structure. Nature 2003;425:977–80.

Jantarajit W, Thongon N, Pandaranandaka J, Teerapornpuntakit J, Krishnamra N, Charoenphandhu N. Prolactin-stimulated transepithelial calcium transport in duodenum and Caco-2 monolayer are mediated by the phosphoinositide 3-kinase pathway. Am J Physiol Endocrinol Metab 2007;293:E372–84.

Kelly PA, Binart N, Freemark M, Lucas B, Goffin V, Bouchard B. Prolactin receptor signal transduction pathways and actions determined in prolactin receptor knockout mice. Biochem Soc Trans 2001;29:48–52.

Kostenuik PJ. Osteoprotegerin and RANKL regulate bone resorption, density, geometry and strength. Curr Opin Pharmacol 2005;5:618–25.

Krishnamra N, Lotinun S, Limlomwongse L. Acute effect and mechanism of action of prolactin on the in situ passive calcium absorption in rat. Bone Miner 1993;23:253–66.

Krishnamra N, Seemoung J. Effects of acute and long-term administration of prolactin on bone ^{45}Ca uptake, calcium deposit, and calcium resorption in weaned, young, and mature rats. Can J Physiol Pharmacol 1996;74: 1157–65.

Krishnamra N, Seemoung J, Limlomwongse L. Acute effect of prolactin on bone ^{45}Ca accumulation in rats. Endocr J 1997;44:257–64.

Landin-Wilhelmsen K, Nilsson A, Bosaeus I, Bengtsson BA. Growth hormone increases bone mineral content in postmenopausal osteoporosis: a randomized placebo-controlled trial. J Bone Miner Res 2003;18:393–405.

Lotinun S, Limlomwongse L, Krishnamra N. The study of a physiological significance of prolactin in the regulation of calcium metabolism during pregnancy and lactation in rats. Can J Physiol Pharmacol 1998;76:218–28.

Lotinun S, Limlomwongse L, Sirikulchayanonta V, Krishnamra N. Bone calcium turnover, formation, and resorption in bromocriptine- and prolactin-treated lactating rats. Endocrine 2003;20:163–70.

Meaney AM, Smith S, Howes OD, O'Brien M, Murray RM, O'Keane V. Effects of long-term prolactin-raising antipsychotic medication on bone mineral density in patients with schizophrenia. Br J Psychiatry 2004; 184:503–8.

Mizuno A, Kanno T, Hoshi M, Shibata O, Yano K, Fujise N, et al. Transgenic mice overexpressing soluble osteoclast differentiation factor (sODF) exhibit severe osteoporosis. J Bone Miner Metab 2002;20:337–44.

Mosmann T. Rapid colorimetric assay for cellular growth and survival: application to proliferation and cytotoxicity assays. J Immunol Methods 1983;65:55–63.

Mrak E, Villa I, Lanzi R, Losa M, Guidobono F, Rubinacci A. Growth hormone stimulates osteoprotegerin expression and secretion in human osteoblast-like cells. J Endocrinol 2007;192:639–45.

Owen TA, Aronow M, Shalhoub V, Barone LM, Wilming L, Tassinari MS, et al. Progressive development of the rat osteoblast phenotype in vitro: reciprocal relationships in expression of genes associated with osteoblast proliferation and differentiation during formation of the bone extracellular matrix. J Cell Physiol 1990;143:420–30.

Parfitt AM. Growth hormone and adult bone remodelling. Clin Endocrinol (Oxf) 1991;35:467–70.

Piyabhan P, Krishnamra N, Limlomwongse L. Changes in the regulation of calcium metabolism and bone calcium content during growth in the absence of endogenous prolactin and during hyperprolactinemia: a longitudinal study in male and female Wistar rats. Can J Physiol Pharmacol 2000; 78:757–65.

Prentice A. Calcium in pregnancy and lactation. Annu Rev Nutr 2000;20: 249–72.

Puntheeranurak S, Schreiber R, Spitzner M, Ousingsawat J, Krishnamra N, Kunzelmann K. Control of ion transport in mouse proximal and distal colon by prolactin. Cell Physiol Biochem 2007;19:77–88.

Ritchie LD, Fung EB, Halloran BP, Turnlund JR, Van Loan MD, Cann CE, et al. A longitudinal study of calcium homeostasis during human pregnancy and lactation and after resumption of menses. Am J Clin Nutr 1998;67:693–701.

Schlemmer A, Johansen JS, Pedersen SA, Jorgensen JO, Hassager C, Christiansen C. The effect of growth hormone (GH) therapy on urinary pyridinoline cross-links in GH-deficient adults. Clin Endocrinol (Oxf) 1991;35:471–6.

Seriwatanachai D, Thongchote K, Charoenphandhu N, Pandaranandaka J, Tudpor K, Teerapornpuntakit J, et al. Prolactin directly enhances bone turnover by raising osteoblast-expressed receptor activator of nuclear factor κB ligand/osteoprotegerin ratio. Bone 2008;42:535–46.

Sowa H, Kaji H, Yamaguchi T, Sugimoto T, Chihara K. Smad3 promotes alkaline phosphatase activity and mineralization of osteoblastic MC3T3-E1 cells. J Bone Miner Res 2002;17:1190–9.

Stein GS, Lian JB, Stein JL, Van Wijnen AJ, Montecino M. Transcriptional control of osteoblast growth and differentiation. Physiol Rev 1996;76: 593–629.

Stilgren LS, Rettmer E, Eriksen EF, Hegedus L, Beck-Nielsen H, Abrahamsen B. Skeletal changes in osteoprotegerin and receptor activator of nuclear factor-κB ligand mRNA levels in primary hyperparathyroidism: effect of parathyroidectomy and association with bone metabolism. Bone 2004;35:256–65.

Subramaniam M, Jalal SM, Rickard DJ, Harris SA, Bolander ME, Spelsberg TC. Further characterization of human fetal osteoblastic hFOB 1.19 and hFOB/ERα cells: bone formation in vivo and karyotype analysis using multicolor fluorescent in situ hybridization. J Cell Biochem 2002;87: 9–15.

Thomas T, Gori F, Khosla S, Jensen MD, Burguera B, Riggs BL. Leptin acts on human marrow stromal cells to enhance differentiation to osteoblasts and to inhibit differentiation to adipocytes. Endocrinology 1999;140: 1630–8.

Thongon N, Nakkrasae LI, Thongbunchoo J, Krishnamra N, Charoenphandhu N. Prolactin stimulates transepithelial calcium transport and modulates paracellular permselectivity in Caco-2 monolayer: Mediation by PKC and ROCK pathways. Am J Physiol Cell Physiol 2008;294:C1158–68.

Wang C, Chan V. Divergent effects of prolactin on estrogen and progesterone production by granulosa cells of rat Graafian follicles. Endocrinology 1982;110:1085–93.

Wang C, Hsueh AJ, Erickson GF. Prolactin inhibition of estrogen production by cultured rat granulosa cells. Mol Cell Endocrinol 1980;20:135–44.

Yamauchi T, Kaburagi Y, Ueki K, Tsuji Y, Stark GR, Kerr IM, et al. Growth hormone and prolactin stimulate tyrosine phosphorylation of insulin receptor substrate-1, -2, and -3, their association with p85 phosphatidylinositol 3-kinase (PI3-kinase), and concomitantly PI3-kinase activation via JAK2 kinase. J Biol Chem 1998;273:15719–26.

Yen ML, Chien CC, Chiu IM, Huang HI, Chen YC, Hu HI, et al. Multilineage differentiation and characterization of the human fetal osteoblastic 1.19 cell line: a possible in vitro model of human mesenchymal progenitors. Stem Cells 2007;25:125–31.

Histochem Cell Biol (2008) 130:79–90
DOI 10.1007/s00418-008-0419-6

ORIGINAL PAPER

Osteoblasts express claudins and tight junction-associated proteins

Kannikar Wongdee · Jantarima Pandaranandaka · Jarinthorn Teerapornpuntakit · Kukiat Tudpor · Jirawan Thongbunchoo · Narongrit Thongon · Walailak Jantarajit · Nateetip Krishnamra · Narattaphol Charoenphandhu

Accepted: 12 March 2008 / Published online: 26 March 2008

Abstract Osteoblasts were previously reported to form tight junctions, which may play an important role in the regulation of ion transport across the epithelial-like bone membrane. However, the evidence for the presence of tight junction-associated proteins in osteoblasts is lacking. We therefore studied the expression of tight junction-associated genes in primary rat osteoblasts and bone tissues. Quantitative real-time PCR showed that osteoblasts expressed ZO-1, -2, -3, cingulin, occludin, claudin-1 to -12, -14 to -20, -22 and -23. By using western blot analyses of selected claudins, expression of claudin-5, -11, -14 and -15, but not claudin-3, were identified in osteoblasts. A confocal immunofluorescent study in undecalcified tibial sections confirmed that claudin-16 was localized on the trabecular surface, normally covered by osteoblasts and bone-lining cells. In addition, immunohistochemical studies in decalcified tibial sections demonstrated the expression of claudin-5, -11, -14, -15 and -16 in bone-lining cells (inactive osteoblasts). Primary osteoblasts cultured in the Snapwell for 19–26 days were found to form a monolayer with measurable transepithelial resistance of ~110–180 Ωcm^2, confirming the presence of barrier functions of the tight junction. It was concluded that osteoblasts expressed several tight junction-associated proteins, which possibly regulated ion transport across the bone membrane.

Keywords Bone membrane · Claudin · Confocal microscope · Occludin · Real-time PCR

K. Wongdee · J. Pandaranandaka · K. Tudpor · J. Thongbunchoo · N. Krishnamra · N. Charoenphandhu
Consortium for Calcium and Bone Research (COCAB), Faculty of Science, Mahidol University, Rama VI Road, Bangkok 10400, Thailand

K. Wongdee
Department of Pathobiology, Faculty of Science, Mahidol University, Rama VI Road, Bangkok 10400, Thailand

J. Teerapornpuntakit · N. Thongon · W. Jantarajit · N. Krishnamra · N. Charoenphandhu (✉)
Department of Physiology, Faculty of Science, Mahidol University, Rama VI Road, Bangkok 10400, Thailand
e-mail: naratt@narattsys.com

J. Pandaranandaka
Faculty of Medicine, Thammasat University, Pathumthani 12120, Thailand

Introduction

Besides the skeletal function, bone acts as an ion exchange system which maintains differential ion compositions, such as Ca^{2+} and K^+, between the two fluid compartments, i.e., plasma and bone extracellular fluid (BECF) (Armstrong and Singer 1965; Marenzana et al. 2005; Rubinacci et al. 2000). The Ca^{2+} efflux from BECF was important for a rapid or short-term correction of the plasma Ca^{2+} without the activation of bone remodeling, while high K^+ concentration in BECF may control bone mineralization (Bushinsky et al. 1997; Marenzana et al. 2005; Rubinacci et al. 2000). It was evident that, to maintain an ionic gradient, osteoblasts and bone-lining cells (inactive osteoblasts) formed a bone membrane to actively control the paracellular exchange of specific ions between the two fluid compartments in an epithelial-like manner (Bushinsky et al. 1989; Rubinacci et al. 2000; Trumbore et al. 1980). In typical epithelia, such processes require the presence of tight junctions which help restrict the paracellular ion movement and maintain membrane integrity, as indicated by the presence of transepithelial resistance (TER) (Furuse and Tsukita

2006; Greger 1996; Shu et al. 2006). Interestingly, several investigators reported that osteoblasts and osteocytes could form tight junctions both in vivo and in vitro (Weinger and Holtrop 1974; Prêle et al. 2003), suggesting a presence of bone membrane with its possible role in the regulation of ion compositions of the BECF.

The expression profiles of tight junction proteins in osteoblasts have never been studied. In simple epithelia lining the cavities and surfaces of structures such as intestinal epithelium and renal tubular epithelium, the tight junction consists of cytoplasmic proteins, e.g., zonula occludens (ZO)-1, -2, -3 and cingulin, and transmembrane proteins, e.g., occludin and claudin-1 to -24 (Furuse and Tsukita 2006). The cytoplasmic proteins are involved in the signaling pathways that alter the tight junction permeability and expression of tight junction-related genes (Guillemot and Citi 2006; Ikari et al. 2004). On the other hand, the transmembrane proteins, especially claudins, form a continuous network of cell–cell contacts that maintain cell adhesion and regulate paracellular transport of ions. Since claudins possess several charged amino acids on their extracellular loops, claudin-expressing epithelial cells manifest charge-, size- and/or ion-selective properties, and permit ion movement in a channel-like fashion (Furuse and Tsukita 2006; Van Itallie and Anderson 2006). Among the 24 claudins, claudin-16 is of particular interest because its functions are specifically related to the transepithelial Ca^{2+} and Mg^{2+} transport. Thus, we hypothesize that osteoblasts, which can form tight junctions and exhibit ion-selective paracellular transport, also express claudins and other tight junction-related genes.

The objectives of this study were (1) to demonstrate the expression patterns of tight junction-related genes in primary rat osteoblasts and bone tissues, and (2) to show that osteoblasts could form a monolayer that generated TER which was indicative of the barrier property of the tight junction. The epithelial-like monolayer of osteoblasts was obtained by seeding osteoblasts on a Snapwell, which is a compartmentalized permeable support. A standard method, namely Ussing chamber technique, allowed us to determine the TER (Greger 1996), which represents the ability of cells to restrict the paracellular ion movement across the monolayer, and is measurable only when tight junctions are formed.

Materials and methods

Animals

Female 8-week-old Sprague–Dawley rats weighing 180–200 g were obtained from the Animal Centre of Thailand. They were placed in hanging stainless steel cages, fed standard pellets (Perfect Companion, Bangkok, Thailand) and distilled water ad libitum under 12/12 h light/dark cycle. Room temperature was controlled at 23–25°C, and relative humidity was about 50–60%. This study has been approved by the Institutional Animal Care and Use Committee of the Faculty of Science, Mahidol University, Bangkok, Thailand.

Primary osteoblast culture

The culture technique was modified from the method of Bakker and Klein-Nulend (2003). Tibiae and femora were removed from a rat by sterile surgical technique. After removing the connective tissues and marrow cells, bones were cut into small dice, and cultured in a 25-cm^2 T flask (Corning, NY, USA) with DMEM supplemented with 15% FBS, 100 U/mL penicillin/streptomycin and 100 µg/mL ascorbate-2-phosphate (all purchased from Sigma, St Louis, MO, USA). Cells were incubated at 37°C with 5% CO_2, and subcultured every 3 days until day 9. The medium was changed daily. Confluent cells from the same rat in six flasks were pooled together for the total RNA preparation. Morphology and nine markers of osteoblast differentiation, i.e., expression of osteocalcin, osteopontin, *runt*-related transcription factor (Runx) 2, osterix, distal-less homeobox 5 (Dlx5), *msh* homeobox homolog 2 (Msx2), AJ18, osteoprotegerin (OPG), and receptor activator of nuclear factor κB ligand (RANKL), were carefully checked. Since morphology and viability of primary osteoblasts became altered after the fourth passage, we used only confluent cells from the first and second passages in this study.

As for the electrical measurements, a confluent osteoblast monolayer was prepared by seeding cells (2×10^5 cells/cm^2) on a polyester Snapwell (compartmentalized permeable support) with 12-mm diameter and 0.4-µm pore size (Corning). The medium was changed daily after 48 h of seeding. Monolayers were incubated at 37°C for 19, 21, 23 or 26 days in a humidified atmosphere containing 5% CO_2. Morphology of the monolayer was visualized by scanning electron microscopy.

Total RNA and cDNA preparation

By using TRIzol reagent (Invitrogen, Carlsbad, CA, USA), total RNA was prepared from calvarial homogenate, primary osteoblasts, kidney, duodenum and distal colon of rats, as previously described (Charoenphandhu et al. 2007). The total RNA was treated with RQ1 DNase (Promega, Madison, WI, USA), and later purified with RNeasy Mini kit (Qiagen, Valencia, CA, USA). Purity of the total RNA was determined by the ratio of absorbance readings at 260 and 280 nm, the ratio of which fell in the range of 1.8–2.0. Integrity of RNA was analyzed by denaturing agarose gel

electrophoresis with the 28S rRNA band appearing approximately twice as intense as the 18S rRNA band. A total of 1 μg of the total RNA was reverse-transcribed with the oligo-dT_{15} primer and the iScript kit (Bio-Rad, Hercules, CA, USA) to cDNA by a thermal cycler (model MyCycler; Bio-Rad). Glyceraldehyde-3-phosphate dehydrogenase (GAPDH), a housekeeping gene, served as a control gene to check the consistency of the reverse transcription (percent coefficient of variation <1%, $n = 30$).

Quantitative real-time PCR (qRT-PCR) and sequencing

Primers used in the present study were designed by OLIGO 6 (Molecular Biology Insights, Cascade, CO, USA) and Primer Validator 1.4 (Naratt Software, Bangkok, Thailand), as shown in Table 1. qRT-PCR was performed by Bio-rad MiniOpticon with the iQ SYBR Green SuperMix (Bio-rad). As for the absolute qRT-PCR of claudin-16, the LightCycler 480 System (Roche, Mannheim, Germany) with high-resolution melting curve analysis was used. The PCR products were also visualized on a 2% agarose gel stained with 1.0 μg/mL ethidium bromide under a UV transilluminator (Alpha Innotech, San Leandro, CA, USA). After electrophoresis, all PCR products were extracted by the HiYield Gel/PCR DNA Extraction kit (Real Biotech Corporation, Taipei, Taiwan), and were sequenced by the ABI Prism 3100 Genetic Analyzer (Applied Biosystems, Foster City, CA, USA). qRT-PCR experiments were performed in triplicate.

Plasmid construction

Claudin-16 from the rat kidneys was amplified by a thermal cycler (model MyCycler; Bio-Rad) with the GoTaq Green Master Mix (Promega). After amplicon sequencing, PCR fragments were cloned into the pGEM-T Easy vector (Promega) and introduced into *Escherichia coli* (JM109; Promega). Thereafter, cultured bacteria were harvested, and the plasmid was purified with the HiYield Plasmid kit (Real Biotech Corporation), sequenced and quantified by using a spectrophotometer at 260/280 nm (model UV-2550; Shimadzu, Kyoto, Japan). Cloned claudin-16 fragments were used to create a standard curve for absolute qRT-PCR of claudin-16.

Western blot analysis

Primary osteoblasts were lysed in lysis buffer (0.5 mM Tris pH 7.5, 1.5 M NaCl, 10% NP-40, 5% DOC, 10 mM Na EDTA, 1 mM PMSF, 1 μg/mL leupeptin, 1 μg/mL aprotinin, 1 μg/mL pepstatin A) (Sigma). After 20-min incubation at 4°C, lysates were sonicated, centrifuged at 12,000×*g* for 10 min, and then heated for 5 min at 95°C. Proteins were separated by SDS–PAGE, and transferred to a polyvinylidene fluoride membrane (Amersham, Buckinghamshire, UK) by electroblotting. After being blocked at 25°C for 4 h with 5% non-fat milk, membranes were probed overnight at 4°C with 1:500 anti-claudin-3, -5, -11, -14, -15 and -16 polyclonal antibodies (Santa Cruz Biotechnology, Santa Cruz, CA, USA). Membranes were later re-probed with 1:5,000 mouse anti-rat *β*-actin monoclonal antibodies (Santa Cruz). After 2-h incubation at 25°C with 1:20,000 secondary antibodies (Santa Cruz), blots were visualized by enhanced chemiluminescence (ECL Plus; Amersham). Band density was measured by FluorChem SP 4.1 (Alpha Innotech, San Leandro, CA, USA). *β*-actin was used for normalization.

Immunohistochemistry

Tibiae from five rats were dissected and fixed in 4% paraformaldehyde in 0.1 M PBS at 4°C overnight. They were then washed in cold PBS pH 7.4 and decalcified in 20% w/v EDTA at 4°C for 15 days. Decalcifying solution was replaced every 3 days. The success of decalcification was confirmed by dual-energy X-ray absorptiometry (model Lunar PIXImus2; GE Medical Systems, Madison, WI, USA) with X-ray energy of 80/35 kVp at 500 μA. Thereafter, decalcified bones were embedded in paraffin, and cut into 7-μm sections by a microtome. After deparaffinization in xylene and graded ethanol, sections were incubated at 37°C for 5 min in the antigen retrieval solution containing 0.01 mg/mL proteinase K, 50 mM Tris–HCl pH 7.5, 5 mM EDTA, and later incubated in 3% H_2O_2 for 30 min to reduce the endogenous peroxidase activity. Non-specific binding was blocked by incubating the sections with 4% BSA in 0.1 M PBS for 2 h. After blocking, the sections were incubated at 4°C overnight with 1:200 polyclonal antibodies against claudin-14, -15 or -16. Then, they were washed with 0.1 M PBS, incubated for 1 h with biotinylated goat anti-rabbit antibody (Zymed, South San Francisco, CA, USA), and finally incubated for 1 h at room temperature with streptavidin-conjugated horseradish peroxidase (Zymed). Color was developed with 3,3′-diaminobenzidine (Pierce, Rockford, IL, USA) as a chromogenic peroxidase substrate. Sections were eventually counterstained with hematoxylin and examined under a light microscope (Olympus, Tokyo, Japan) and Image-Pro Plus 5 (Media Cybernetics, Bethesda, MD, USA). Signal intensity was quantified by the method of Lehr et al. (1999).

Confocal laser-scanning microscopy

Immunofluorescent technique was described previously (Jantarajit et al. 2007). Tibiae from three rats were dehydrated with sequential ethanol (70, 95, and 100%), and

Table 1 *Rattus norvegicus* oligonucleotide sequences used in qRT-PCR experiments

Gene	Accession no.	Primer (forward/reverse)	Product length (bp)
Osteoblast-related proteins			
Osteocalcin	J04500	5′–CACAGGGAGGTGTGTGAG–3′ 5′–TGTGCCGTCCATACTTTC–3′	203
Osteopontin	NM_012881	5′–TTCACTGCCAGCACACAA–3′ 5′–TTTGACCTCAGTCCGTAAGC–3′	101
Runx2	XM_001066909	5′–TAACGGTCTTCACAAATCCTC–3′ 5′–GGCGGTCAGAGAACAAACTA–3′	135
Osterix	AY177399	5′–GCCTACTTACCCGTCTGA–3′ 5′–CTCCAGTTGCCCACTATT–3′	139
Dlx5	NM_012943	5′–CTCTCTAGGACTGACGCAAAC–3′ 5′–GAGTTACACGCCATAGGGTC–3′	135
Msx2	NM_012982	5′–TAGACCTGTGCTTCCCAT–3′ 5′–ACAAACATCCATCCTAGAGTG–3′	114
AJ18	AF321874	5′–GTCCCTGGTATGTATCAC–3′ 5′–GAAGACTTTGGCTAAAAC–3′	133
Osteoprotegerin	NM_012870	5′–ATTGGCTGAGTGTTCTGGT–3′ 5′–CTGGTCTCTGTTTTGATGC–3′	140
RANKL	NM_057149	5′–TCGCTCTGTTCCTGTACT–3′ 5′–AGTGCTTCTGTGTCTTCG–3′	145
Transmembrane tight junction proteins			
Cldn-1	NM_031699	5′–AGGTCTGGCGACATTAGTGG–3′ 5′–TGGTGTTGGGTAAGAGGTTG–3′	202
Cldn-2	XM_236535	5′–TCTGGATGGAGTGTGCGAC–3′ 5′–AGTGGCAAGAGGCTGGGC–3′	467
Cldn-3	NM_031700	5′–GCACCCACCAAGATCCTCTA–3′ 5′–AGGCTGTCTGTCCTCTTCCA–3′	246
Cldn-4	NM_001012022	5′–TGGATGAACTGCGTGGTGC–3′ 5′–CCCTACGACTGAGAGAAGC–3′	153
Cldn-5	NM_031701	5′–CGCTTGTGGCACTCTTTGT–3′ 5′–ACTCCCGGACTACGATGTTG–3′	168
Cldn-6	XM_001055688	5′–GGAGGGGCTATGGATGTC–3′ 5′–GCAGATGGGAATGAGGGT–3′	271
Cldn-7	NM_031702	5′–ACTACTGGGCTTTTCAATGGC–3′ 5′–CACCGAGTCGTACATTTTGC–3′	190
Cldn-8	NM_001037774	5′–GCTGGAATCATCTTCTTCAT–3′ 5′–CATCCACCAGCGGGTTGTAG–3′	100
Cldn-9	NM_001011889	5′–CTTCATTGGCAACAGCATCG–3′ 5′–CCTTGGCACCTTCGTCCTC–3′	242
Cldn-10	XM_001074876	5′–CATATTGTCAGGTCTGTGTTC3′ 5′–TGGGTGTTTTGTTGTTGTC–3′	200
Cldn-11	NM_053457	5′–ATTGGCATCATCGTCACAAC–3′ 5′–ATGTCCACCAGGGGCTTG–3′	158
Cldn-12	XM_001067932	5′–CCTTCAAGTCTTCGGTGCC–3′ 5′–CAGGAGGATGGGAGTACAG–3′	312
Cldn-14	NM_001013429	5′–CTGTACCTGGGCTTCATC–3′ 5′–CACACATAGTCATTCAACCTG–3′	230
Cldn-15	XM_222085	5′–GCTGTGCCACCGACTCCC–3′ 5′–CAGAGCCCAGTTCATACTTG–3′	330
Cldn-16	NM_131905	5′–ATCTTCTTCAGTACGCTGCC–3′ 5′–CGATGAGTAATACGGTCCC–3′	372
Cldn-17	XM_221711	5′–CTCCAGTGAGAGGGTCAAAG–3′ 5′–AGCAGCAGTATCCACAGAGC–3′	236
Cldn-18	NM_001014096	5′–CCGTTCAGACCAGGTACAC–3′ 5′–CTCCAGGCTTATAGGCAAC–3′	180

Table 1 continued

Gene	Accession no.	Primer (forward/reverse)	Product length (bp)
Cldn-19	NM_001008514	5′–TGCTGAAGGACCCATCTG–3′ 5′–TGTGCTTGCTGTGAGAACTG–3′	129
Cldn-20	XM_973727	5′–GCACTCTAAAATACTCCATTC–3′ 5′–TGAAGCAGACTCCTCCAGC–3′	186
Cldn-22	XM_001059255	5′–ATGGGCTTAGTCTTCCGAAC–3′ 5′–TGGATGACGCAGGATTTC–3′	170
Cldn-23	NM_001033062	5′–GTGGAACTACTTCGGGACTC–3′ 5′–CCCAGCACCAGACTGTAGC–3′	285
Occludin	NM_031329	5′–CACGTTCGACCAATGC–3′ 5′–CCCGTTCCATAGGCTC–3′	188
Cytoplasmic tight junction proteins			
ZO-1	XM_218747	5′–GTATCCGATTGTTGTGTTCC–3′ 5′–TCACTTGTAGCACCATCCGC–3′	270
ZO-2	NM_053773	5′–TCTGAAGGTGAACACACAA–3′ 5′–CCAGGATGTCTCTATACACG–3′	134
ZO-3	XM_001069839	5′–TGCTAATGAGACCGCTAAAG–3′ 5′–GACACTCCGTTGATCTGTAA–3′	169
Cingulin	XM_001059265	5′–ATCGGGAACTCCAGTCAAC–3′ 5′–TGACGGGAACGGCTAAAG–3′	121
Housekeeping gene			
GAPDH	NM_017008	5′–AGTCTACTGGCGTCTTCAC–3′ 5′–TCATATTTCTCGTGGTTCAC–3′	133

Runx runt-related transcription factor, *Dlx5* distal-less homeobox 5, *Msx2 msh* homeobox homolog 2, *RANKL* receptor activator of nuclear factor κB ligand, *Cldn* claudin, *ZO* zonula occludens, *GAPDH* glyceraldehyde-3-phosphate dehydrogenase

embedded in methyl methacrylate resin. The embedded tibiae were cut longitudinally at a thickness of 7 μm with a RM2255 microtome (Leica, Nussloch, Germany). After deplastination, the sections were incubated overnight at 4°C with 1:200 goat anti-claudin-16 antibody (Santa Cruz). Thereafter, they were incubated for 3 h at 20°C with 1:200 FITC-conjugated donkey anti-goat secondary antibody (green signal; Santa Cruz). Nuclei were stained with 1:1000 TO-PRO-3 (red signal; Molecular Probes, Eugene, OR, USA). Negative control was obtained by incubating a tissue section with a secondary antibody in the absence of a primary antibody. Samples were examined for fluorescent signals by using a FV1000 confocal microscope (Olympus).

As for the immunocytochemistry in primary osteoblasts, cells were plated on a coverslip in six-well culture discs (10^4 cells/cm^2), and maintained for 2 days before being fixed for 5 min in 3% paraformaldehyde and 2% sucrose. After blocking non-specific bindings, cells were incubated overnight at 4°C with 1:200 rabbit anti-claudin-5, -11, -14 and -15 polyclonal antibodies (Santa Cruz), and were later incubated with 1:200 Alexa Fluor 488-conjugated mouse anti-rabbit secondary antibody (green signal; Molecular Probes) at 20°C. Negative controls were incubated with an equivalent volume of PBS instead of the anti-claudin antibodies. Nuclei were stained with 1:500 TO-PRO-3 (red signal). Images were captured with a confocal microscope.

Scanning electron microscopy (SEM)

Primary osteoblasts were seeded on a Snapwell at a density of 2×10^5 cells/cm^2. After 21 days of culture, Snapwell-cultured osteoblasts were fixed with 2.5% glutaraldehyde in 0.1 M PBS pH 7.2 and 2.5 mM $MgCl_2$ for 2 h at 4°C. Samples were dehydrated in graded ethanols (50, 70, 80, 90, 95 and 100%) for 10 min each. The fixed samples were freeze-dried, coated with a thin layer of platinum and palladium, and examined under SEM (model S-2500; Hitachi, Tokyo, Japan).

Electrical measurements

Three electrical parameters, i.e., epithelial potential difference (PD), short-circuit current (Isc) and transepithelial resistance (TER), were determined by Ussing chamber technique as previously described (Jantarajit et al. 2007). This technique allowed us to determine whether tight junctions were formed. A Snapwell was mounted in the chamber for 40-min electrical measurements. The monolayer was bathed on both sides with buffer containing (in mM) 118 NaCl, 4.7 KCl, 1.1 $MgCl_2$, 1.25 $CaCl_2$, 23 $NaHCO_3$, 12 D-glucose and 2 mannitol (Sigma), and continuously gassed with humidified 5% CO_2 in 95% O_2. A pair of Ag/AgCl electrodes connected to agar bridges (3.0 M KCl per 4 g % agar) was located near each surface of the Snapwell for

measurement of PD. The other ends of the PD-sensing electrodes were connected to a pre-amplifier (model EVC-4000; World Precision Instruments, Sarasota, FL, USA), and finally to a PowerLab 4/30 operated with a software Chart 5.4 (ADInstruments, Colorado Springs, CO., USA). Another pair of Ag/AgCl electrodes was placed at the end of each chamber to supply Isc, which was also measured by a PowerLab 4/30 connected in series to the EVC-4000 current-generating unit. TER was calculated by the Ohm's equation.

Statistical analysis

Results are expressed as means ± SE. Multiple comparisons were performed by one-way analysis of variance (ANOVA) with the Dunnett post-test. Data were analyzed by GraphPad Prism 4 (GraphPad Software, San Diego, CA, USA).

Results

Prior to the investigation on the tight junction protein expression, we performed an experiment to confirm that the cultured cells obtained from tibiae and femora of rats were differentiated osteoblasts. As shown in Fig. 1, primary osteoblasts and cells in the rat calvaria strongly expressed all markers of osteoblast differentiation, i.e., osteocalcin, osteopontin, Runx2, osterix, Dlx5, Msx2, AJ18, OPG and RANKL (Kostenuik 2005; Owen et al. 1990; Zhang et al. 2006).

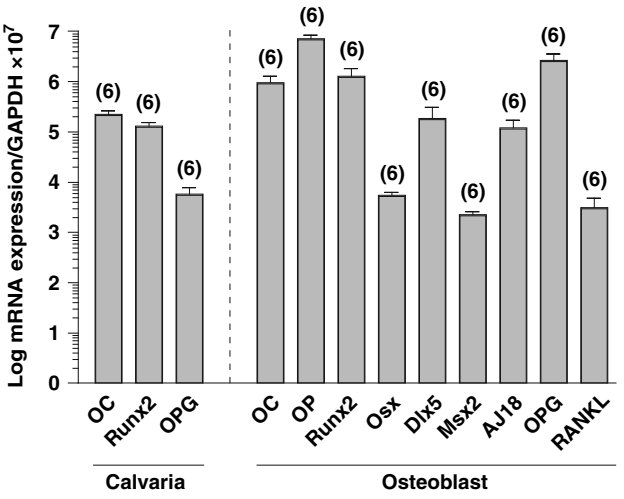

Fig. 1 Expression of the marker genes related to osteoblast differentiation, namely osteocalcin (*OC*), osteopontin (*OP*), Runx2, osterix (*Osx*), Dlx5, Msx2, AJ18, OPG and RANKL, in calvaria and primary osteoblasts. GAPDH is a housekeeping gene for normalization. *Numbers* in parentheses represent the number of animals in each group

In the investigation on the expression of tight junction genes, we used qRT-PCR to demonstrate the expression of the cytoplasmic tight junction genes, ZO-1, -2, -3 and cingulin, as well as the transmembrane tight junction gene, occludin in the calvarial homogenate (Fig. 2a) and primary rat osteoblasts (Fig. 2b). Moreover, as depicted in Fig. 3, both primary osteoblasts and calvarial cells exhibited mRNA expression of claudin-1 to -12, -14 to -20, -22 and -23. Expression of claudin-3, -5 and -8 in osteoblasts were very low. We did not study the expression of claudin-13, -21 and -24 as these genes have never been reported in rats (Charoenphandhu et al. 2007).

Although claudin-16 was previously known to be expressed exclusively in the thick ascending limb of the loop of Henle (Simon et al. 1999), it was also identified in primary osteoblasts (Fig. 3b). We further performed absolute qRT-PCR to compare the expression of claudin-16 in primary osteoblasts with those in the kidney (positive control) and calvaria as well as in other Ca^{2+}-transporting epithelia, i.e., duodenum and distal colon. The results confirmed that primary osteoblasts and all three tissues expressed claudin-16 mRNA, but the levels in the kidney were ~600 times higher than others ($P < 0.01$, Fig. 4a).

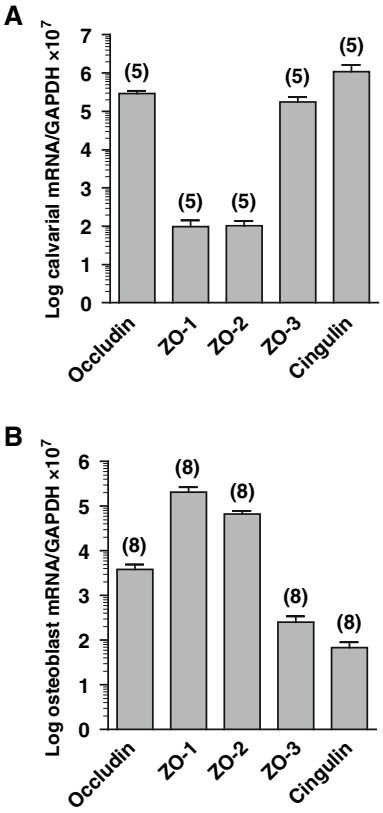

Fig. 2 Expression of genes of tight junction proteins, including occludin, ZO-1, -2, -3 and cingulin, in calvaria (**a**) and primary rat osteoblasts (**b**). GAPDH is a housekeeping gene for normalization. *Numbers* in parentheses represent the number of animals in each group

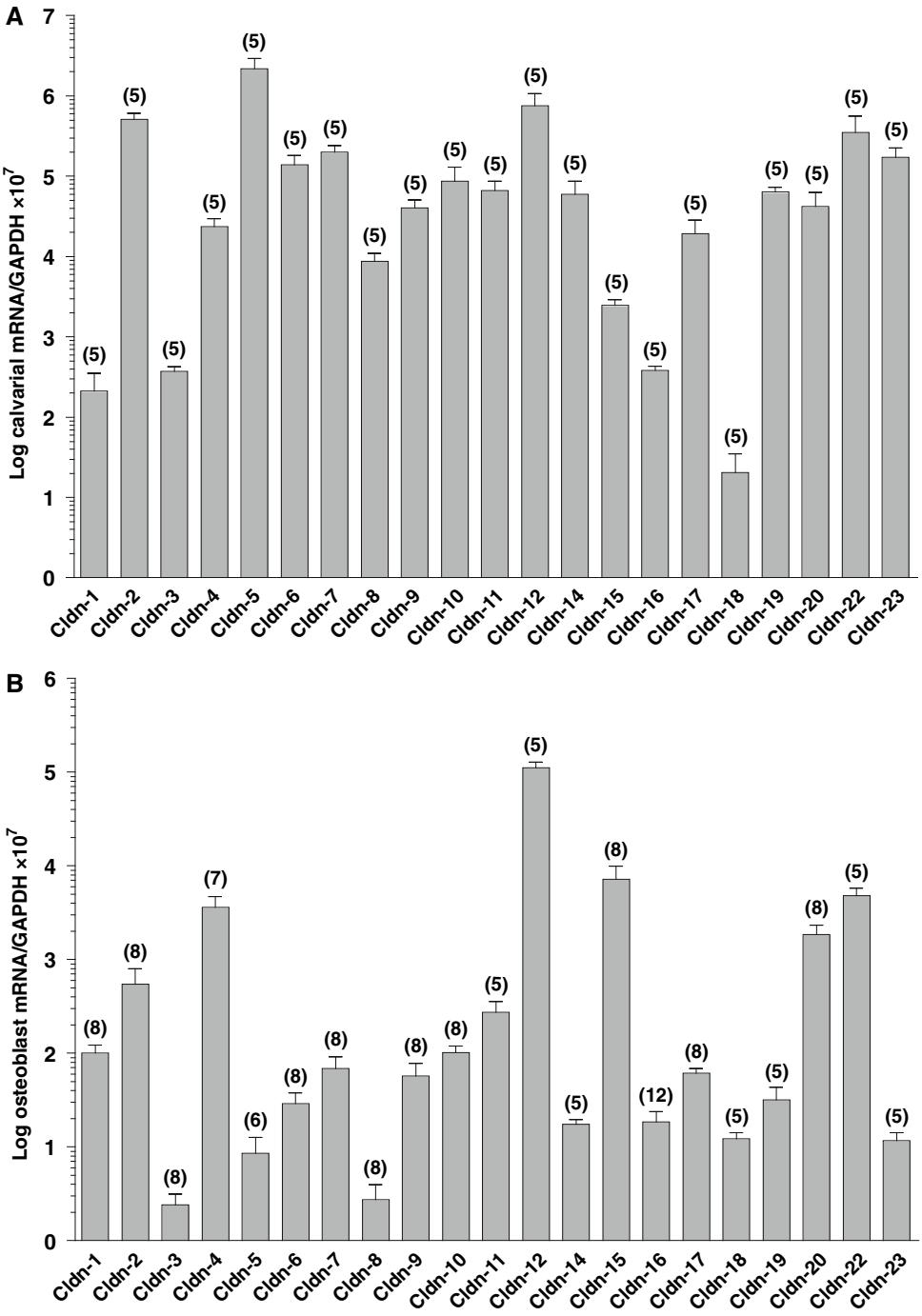

Fig. 3 Expression of claudin mRNAs in calvaria (**a**) and primary rat osteoblasts (**b**). Claudin-13, -21 and -24 were not studied, because they have never been reported in rats. GAPDH is a housekeeping gene for normalization. *Numbers* in parentheses represent the number of animals in each group

Interestingly, the expression of claudin-16 proteins in osteoblasts and kidneys were comparable (Fig. 4b).

Furthermore, protein expression of claudin-5, -11, -14, -15 and -16, but not claudin-3, were demonstrated in the primary rat osteoblasts by western blot analysis (Fig. 4c, d) and confocal immunofluorescent technique (Fig. 5a). In the methyl methacrylate-embedded tibial sections, claudin-16 localization was confined to the metaphyseal trabecular surfaces, where osteoblasts and bone-lining cells were present, but not in the cortical parts or the marrow cavities (Fig. 5b). By using immunohistochemical localization in the decalcified tibial sections, expression of claudin-5, -11, -14, -15 and -16, but not claudin-3, were visualized in bone-lining cells (arrows; Fig. 6), which are inactive osteoblasts lining the bone matrix.

After being cultured in Snapwell for 19, 21, 23 or 26 days, the tibia-derived cells formed a homogeneous monolayer that strongly expressed osteocalcin, osteopontin, Runx2, osterix, Dlx5, Msx2, AJ18, OPG and RANKL (data not shown) similar to osteoblasts cultured

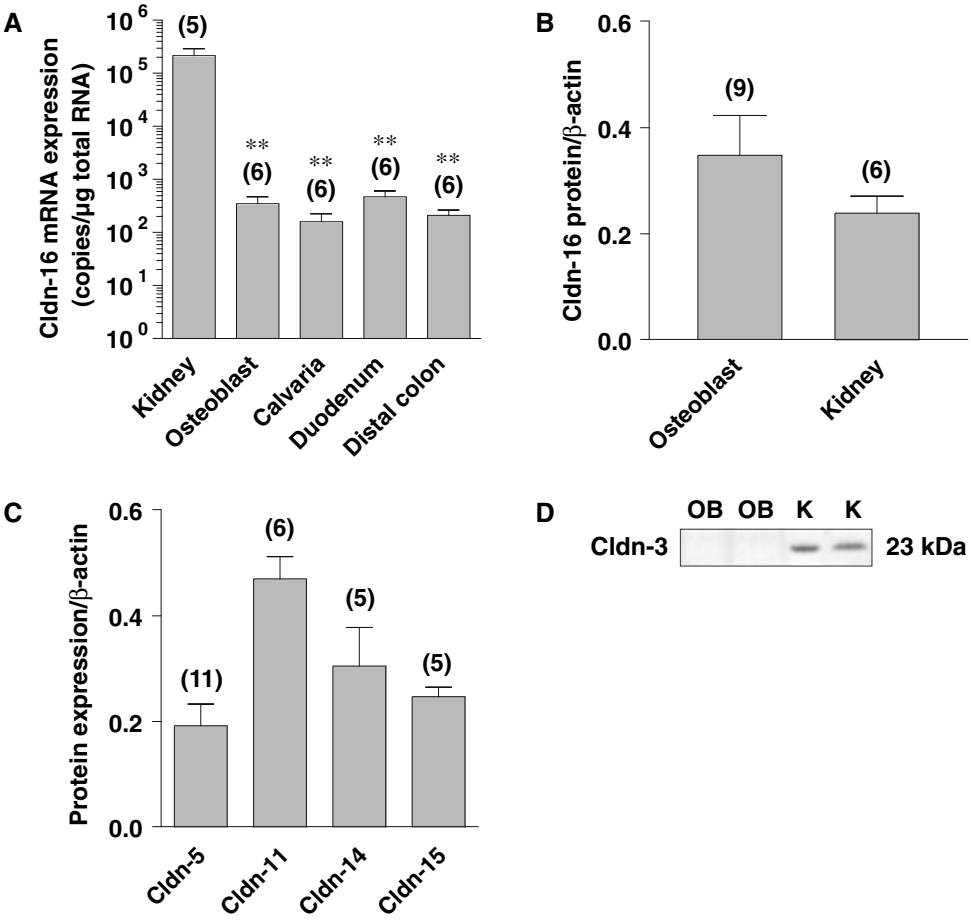

Fig. 4 **a** Absolute qRT-PCR analysis of claudin-16 expression in kidney (positive control), primary osteoblasts, calvaria, duodenum and distal colon. $^{**}P < 0.01$ compared with kidney. **b** Western blot analysis of claudin-16 expression in the kidney and primary rat osteoblasts. **c** Protein expression of claudin-5, -11, -14 and -15 in primary rat osteoblasts. *β*-actin is a housekeeping protein for normalization. *Numbers* in parentheses represent the number of animals in each group. **d** Representative electrophoretic bands of the western blot analysis of claudin-3 expression ($n = 5$). Claudin-3 protein was not expressed in the osteoblasts (*OB*), but was strongly expressed in the kidney (*K*). Experiments were performed in duplicate

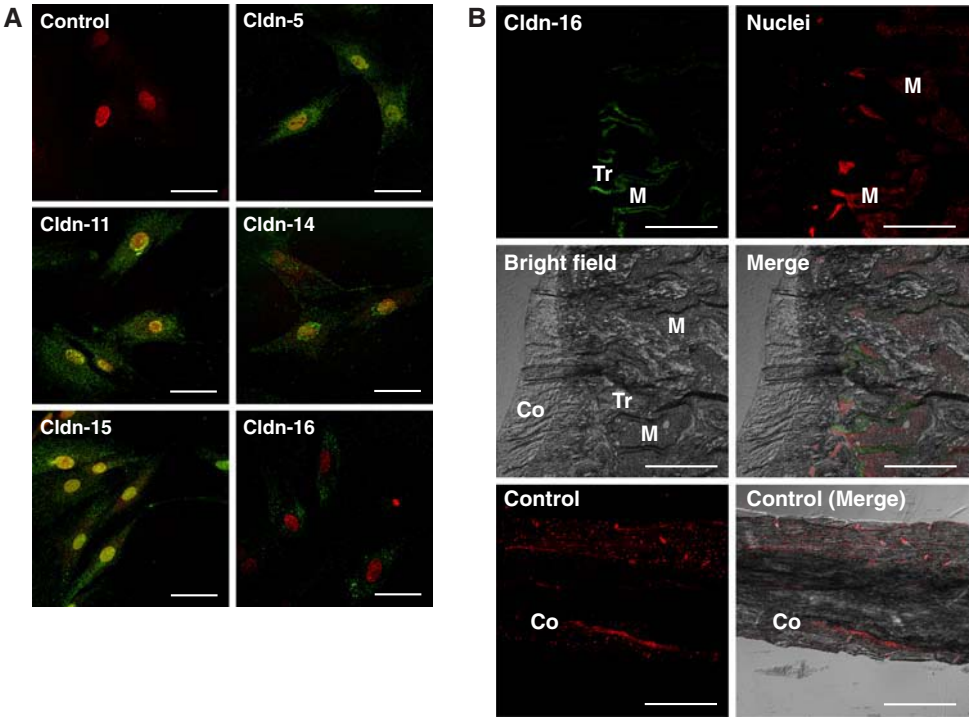

Fig. 5 **a** Expression of claudin-5, -11, -14, -15 and -16 (*green signals*) in primary rat osteoblasts ($n = 5$) as demonstrated by the confocal immunofluorescent technique. Nuclei are stained in *red*. Control image was obtained by incubating osteoblasts in the absence of anti-claudin antibodies. *Bars* 10 µm. **b** Representative confocal immunofluorescent images of claudin-16 localization in a methyl methacrylate-embedded section of the tibial metaphysis ($n = 3$). Positive signals (*green*) are visible on the surfaces of the trabeculae (*Tr*), but not on the cortical regions (*Co*) or marrow cavities (*M*). Nuclei are labeled in *red*. Control images were obtained by incubating tissue sections in the absence of anti-claudin-16 antibody. *Bars* 400 µm

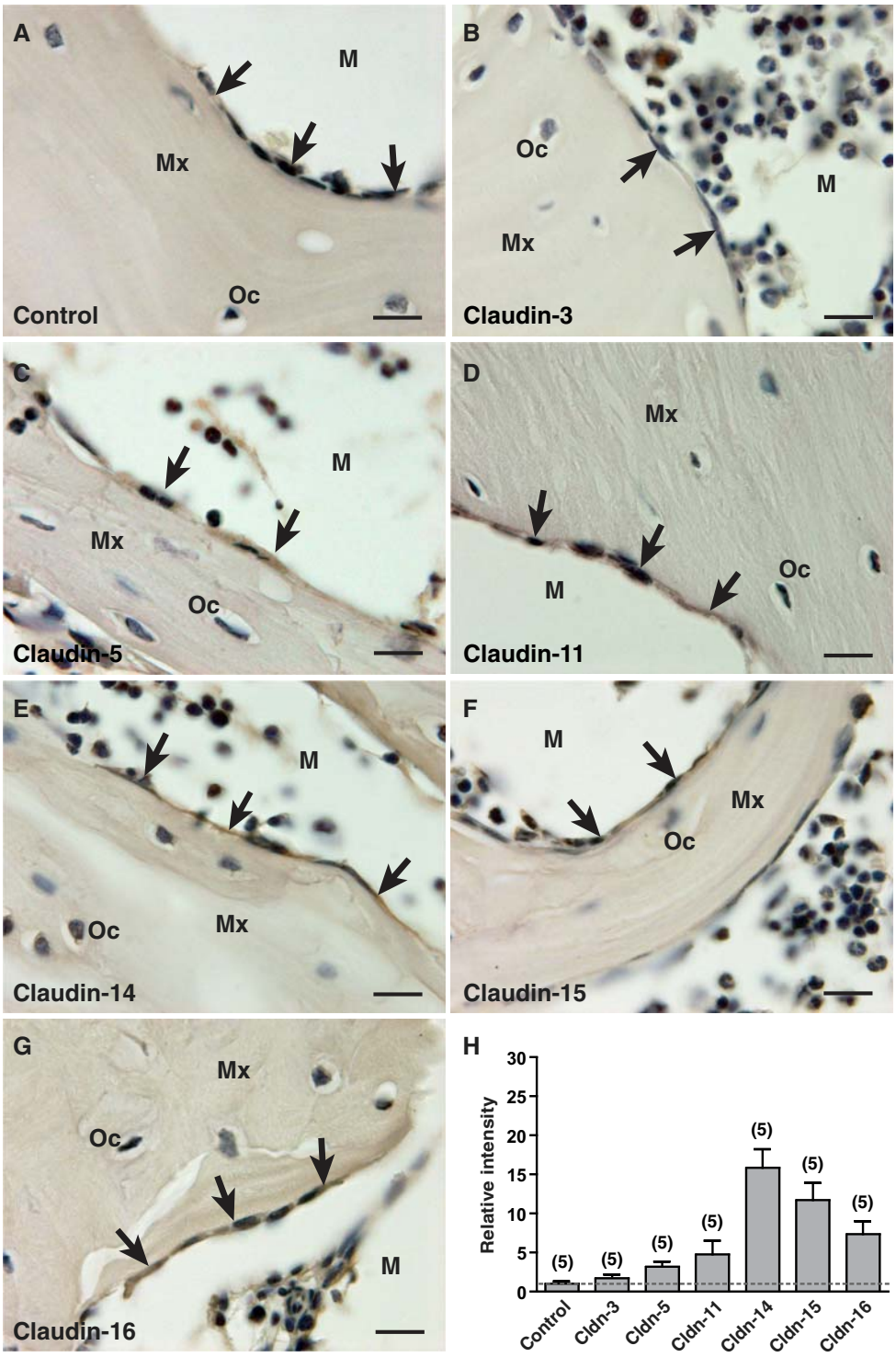

Fig. 6 **a–g** Immunohistochemical localization of claudin-5, -11, -14, -15 and -16 in decalcified tibiae ($n = 5$). Claudin-3 was not detected, whereas the positive signals for other claudins were seen in bone-lining cells (inactive flat osteoblasts; *arrows*), which covered the bone matrix (*Mx*). No signal was found in osteocytes (*Oc*) or marrow (*M*). Images of negative controls (without anti-claudin antibody) did not show immunoreactive signal. *Bars* 10 μm. **h** Relative signal intensity of claudin expression in decalcified tibial sections. The intensities of controls were normalized to 1. *Numbers* in parentheses represent the number of animals

in flasks, indicating that these cells were differentiated osteoblasts. SEM showed cells with well-developed pseudopodia firmly attached to the Snapwell forming a monolayer (Fig. 7). Electrical parameters, i.e., PD, Isc and TER, of the monolayer were measurable on day 19–26 after seeding (Table 2). The presence of TER suggested that these osteoblasts could form the tight junction in Snapwell.

Discussion

In the present study, we reported, for the first time, that osteoblasts and bone tissues of rats expressed claudins and other tight junction-associated proteins at the transcriptional and translational levels. Moreover, osteoblasts could form epithelial-like monolayers when grown on the compartmentalized permeable supports.

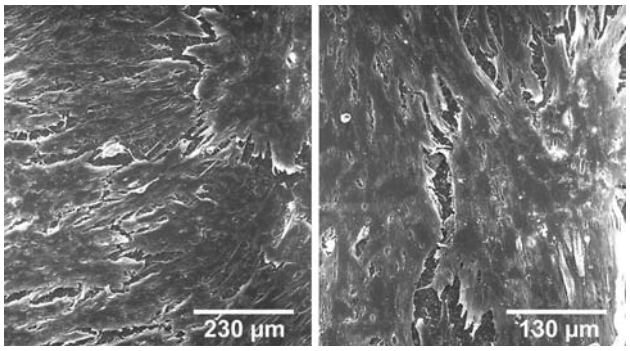

Fig. 7 Scanning electron micrographs of primary osteoblasts at day 21 of culture ($n = 6$). Cells firmly attached to Snapwell and formed a monolayer

Since the tight junction is the most important barrier which restricts ion and water from passing freely through the paracellular space, the expression of tight junction proteins in osteoblasts supports the previous hypothesis that osteoblasts and bone-lining cells, which cover 90% of bone surface, form an epithelial-like bone membrane to regulate ion transport and maintain differential ion compositions between the plasma and BECF (Bushinsky et al. 1989; Marenzana et al. 2005; Peterson et al. 1985; Trumbore et al. 1980). Normally, concentrations of Ca^{2+}, Mg^{2+} and K^{+} in BECF are approximately 0.5, 0.4 and 25 mM, whereas those in plasma are 1.25, 0.7 and 4.5 mM, respectively (Armstrong and Singer 1965; Trumbore et al. 1980). These ionic gradients were thought to be actively maintained by bone membrane, and were dissipated in dead tissue or in the presence of inhibitors of ATP production (Marenzana et al. 2005; Rubinacci et al. 2002). By using the three-dimensional scanning Ca^{2+}-selective electrode technique, Marenzana et al. (2005) demonstrated Ca^{2+} efflux from bone surface through the paracellular route. Although our techniques could not show the localization of claudin expression at the tight junction, the evidence of the intensely expressed claudin-16, which is known to control the paracellular Ca^{2+} transport (Ikari et al. 2004), along the trabecular surface of the tibia suggested the transport function of the tight junctions in bone membrane. Moreover, we showed that several markers of the epithelial cells, e.g., ZO-3, cingulin and claudins, which are highly specific to the tight junction formation (Citi et al. 1991; Inoko et al. 2003) were also expressed in osteoblasts. Therefore, our findings corroborated the formation of tight junctions in osteoblasts and an existence of an epithelial-like bone membrane.

Herein, we studied the mRNA expression of the cytoplasmic tight junction proteins, ZO-1, -2, -3 and cingulin, and the transmembrane proteins, occludin and claudin-1 to -23, in calvaria and osteoblasts. Although calvarial homogenate contained mRNAs from many cell types, such as osteoblasts, osteoclasts and osteocytes, our results provided suggestive evidence that bone expressed tight junction genes. In normal epithelia, ZO-1, a member of the membrane-associated guanylate kinase-like homologues (MAGUK), directly binds to occludin, claudin-1 to -8 and -16 to modulate the assembly of the tight junction (Inoko et al. 2003; McNeil et al. 2006). Cingulin, on the other hand, is not required for the tight junction assembly, but is important for the signaling pathways that control the expression of several claudins, such as claudin-2, -6 and -7 (Guillemot and Citi 2006). Since cingulin was previously detected only in epithelial tissues, the presence of cingulin in the osteoblasts strongly suggested that osteoblasts and/or their lineages, e.g., bone-lining cells, possess epithelial characteristics.

Regarding the transmembrane protein occludin, despite being one of the tight junction-associated proteins, it may not be essential for the tight junction assembly or the paracellular ion transport, since enterocytes of the occludin-knockout mice exhibited normal morphology of the tight junction and normal epithelial barrier function (Saitou et al. 2000). The exact function of occludin, therefore, remains controversial. Among other transmembrane proteins, claudins have been widely accepted as the key proteins for the regulation of the paracellular transport of ions, water-soluble nutrients and drugs in a size- and charge-specific fashion in the gastrointestinal tract, renal tubule, respiratory tract and blood–brain barrier (Furuse and Tsukita 2006; Van Itallie and Anderson 2006). Each claudin consists of four transmembrane domains and two extracellular loops, which contain charged amino acids and also interact with those of the adjacent cells to form a paracellular barrier (Van Itallie et al. 2003). Some claudins, e.g., claudin-8, -10, -14, -16 and -19, were suggested to form arrays of tight junctional pores or channel-like structures which, in turn,

Table 2 Electrical parameters of the osteoblast monolayers grown on Snapwells for 19, 21, 23 and 26 days

Conditions	n	Electrical parameters		
		PD (mV)	Isc (μA cm^{-2})	TER (Ω cm^2)
19-Day-monolayer	6	0.59 ± 0.21	8.61 ± 1.87	114.77 ± 8.58
21-Day-monolayer	12	0.76 ± 0.25	3.47 ± 0.70	150.67 ± 26.48
23-Day-monolayer	6	1.11 ± 0.47	3.89 ± 1.29	161.63 ± 13.59
26-Day-monolayer	4	0.66 ± 0.18	3.82 ± 0.87	184.43 ± 47.55

Values are means ± SE

regulated the paracellular ion transport and were responsible for the size- and/or charge-selective properties of the tight junction (Angelow et al. 2007; Ben-Yosef et al. 2003; Ikari et al. 2004; Van Itallie et al. 2006; Yu et al. 2003). Since different types of cells expressed different fingerprints of claudin patterns, and co-localization and co-polymerization of different claudins could affect the paracellular ion movement (Furuse and Tsukita 2006), the unique transport property of each epithelium could have resulted from its distinctive pattern of claudins. Therefore, to further explore the possible epithelial-like functions of osteoblasts, information on claudin profile, as provided by the present study, was indispensable. We speculate that bone membrane may use a specific set of claudins to regulate ion transport across the paracellular channel.

Primary osteoblasts and calvaria were shown to express mRNAs of claudin-1 to -12, -14 to -20, -22 and -23. Due to a limited availability of commercial claudin antibodies suitable for bone staining, we studied protein expression of only some selected claudins, namely claudin-3, -5, -11, -14, -15 and -16, all known to be important for the charge selectivity of the renal tubular and intestinal epithelia (Ben-Yosef et al. 2003; Ikari et al. 2004; Van Itallie and Anderson 2006). As shown in the results, only claudin-3 protein was not detected in primary osteoblasts, possibly due to its low mRNA levels. Claudin-5, -11, -14, -15 and -16 were identified in primary osteoblasts and bone-lining cells by confocal microscopy and immunohistochemistry, respectively. However, we were not able to demonstrate claudin expression in the osteoblast monolayer cultured on Snapwell due to a technical limitation caused by the shape and opaqueness of Snapwell. As for the primary osteoblasts cultured on coverslips, claudins were dispersed over the plasma membrane instead of localizing around the tight junctions.

Interestingly, primary osteoblasts, calvaria and tibiae of rats expressed mRNA and protein of claudin-16, which was important for the paracellular Ca^{2+} and Mg^{2+} reabsorption in the thick ascending limb (TAL) of the loop of Henle (Simon et al. 1999). Several investigators previously suggested that claudin-16 was strongly expressed only in the TAL and distal convoluted tubules of the kidneys (Simon et al. 1999). However, our results as well as reports of claudin-16 expression in lung (Hirano et al. 2000), mammary glands (Markov et al. 2006) and salivary glands (Kriegs et al. 2007) confirmed the presence of claudin-16 in the extrarenal tissues. Moreover, as demonstrated by the present absolute qRT-PCR, mucosal cells of duodenum and distal colon, both being Ca^{2+}-transporting epithelia, also expressed claudin-16 mRNAs, but the levels were not as high as those in the kidneys.

The functions of claudin-1, -2, -4, -8, -15, and -19 have been well characterized in MDCK cells. Expression of claudin-1, -8 and -19 increased TER, while claudin-2, -4 and -15 regulated the paracellular permeability to ions (Angelow et al. 2007; McCarthy et al. 2000; Van Itallie et al. 2001, 2003; Yu et al. 2003). Because of the fact that the barrier functions of claudins (or tight junction) could be evaluated by measurement of TER, the osteoblast monolayer was grown on a compartmentalized permeable support, i.e., Snapwell. The compartmentalized culture environment is known to induce formation of the monolayer by other cell types, such as rat monoclonal bone marrow stem cells (Shu et al. 2006). As shown in Fig. 7, the primary rat osteoblasts that formed a monolayer in Snapwell did retain the osteoblast phenotypes. The presence of TER of $\sim$110–180 Ωcm^2, which is comparable to the TER reported in the duodenum (Charoenphandhu et al. 2006), confirmed that the primary rat osteoblasts were able to form a functional epithelial-like membrane in vitro with the barrier property of tight junctions. In addition, other electrical parameters, i.e., PD and Isc, implicated ion fluxes across the monolayer (Shu et al. 2006; Trumbore et al. 1980). Besides the barrier function, tight junctions of osteoblasts could play an important role in the vesicular trafficking of bone matrix proteins to the surface of bone and in maintaining the polarity of matrix-secreting osteoblasts, thereby resulting in an organized matrix deposition in bone tissue (Prêle et al. 2003).

Finally, it could be concluded that the primary osteoblasts and bone tissues expressed several tight junction proteins, thus supporting the existence of a functional epithelial-like bone membrane, its regulation of the paracellular ion transport, and the maintenance of BECF ion compositions. The osteoblast monolayer cultured on Snapwell, similar to normal epithelia, exhibited electrical parameters, i.e., PD and TER, which are indicative of the ion transport activity and barrier function of the tight junction, respectively. These novel findings are fundamental and provide the basis for further investigation to explain how osteoblasts form bone membrane in vivo, and how bone membranes regulate the ionic compositions of BECF and the paracellular transport of ions.

Acknowledgments This research was supported by grants from the Strategic Consortia for Capacity Building of University Faculties and Staff, Commission on Higher Education, Thailand (to K.W.), and the Thailand Research Fund (to N.C. and N.K.).

References

Angelow S, El-Husseini R, Kanzawa SA, Yu AS (2007) Renal localization and function of the tight junction protein, claudin-19. Am J Physiol Renal Physiol 293:F166–F177

Armstrong WD, Singer L (1965) Composition and constitution of the mineral phase of bone. Clin Orthop Relat Res 38:179–190

Bakker A, Klein-Nulend J (2003) Osteoblast isolation from murine calvariae and long bones. In: Helfrich MH, Ralston SH (eds)

Methods in molecular medicine: bone research protocols. Humana Press, New Jersey, pp 19–28

Ben-Yosef T, Belyantseva IA, Saunders TL, Hughes ED, Kawamoto K, Van Itallie CM, Beyer LA, Halsey K, Gardner DJ, Wilcox ER, Rasmussen J, Anderson JM, Dolan DF, Forge A, Raphael Y, Camper SA, Friedman TB (2003) Claudin 14 knockout mice, a model for autosomal recessive deafness DFNB29, are deaf due to cochlear hair cell degeneration. Hum Mol Genet 12:2049–2061

Bushinsky DA, Chabala JM, Levi-Setti R (1989) Ion microprobe analysis of mouse calvariae in vitro: evidence for a "bone membrane". Am J Physiol 256:E152–E158

Bushinsky DA, Riordon DR, Chan JS, Krieger NS (1997) Decreased potassium stimulates bone resorption. Am J Physiol 272:F774–F780

Charoenphandhu N, Tudpor K, Pulsook N, Krishnamra N (2006) Chronic metabolic acidosis stimulated transcellular and solvent drag-induced calcium transport in the duodenum of female rats. Am J Physiol Gastrointest Liver Physiol 291:G446–G455

Charoenphandhu N, Wongdee K, Tudpor K, Pandaranandaka J, Krishnamra N (2007) Chronic metabolic acidosis upregulated claudin mRNA expression in the duodenal enterocytes of female rats. Life Sci 80:1729–1737

Citi S, Amorosi A, Franconi F, Giotti A, Zampi G (1991) Cingulin, a specific protein component of tight junctions, is expressed in normal and neoplastic human epithelial tissues. Am J Pathol 138:781–789

Furuse M, Tsukita S (2006) Claudins in occluding junctions of humans and flies. Trends Cell Biol 16:181–188

Greger R (1996) Epithelial transport. In: Greger R, Windhorst U (eds) Comprehensive human physiology: from cellular mechanisms to integration. Springer, Berlin, pp 1217–1232

Guillemot L, Citi S (2006) Cingulin regulates claudin-2 expression and cell proliferation through the small GTPase RhoA. Mol Biol Cell 17:3569–3577

Hirano T, Kobayashi N, Itoh T, Takasuga A, Nakamaru T, Hirotsune S, Sugimoto Y (2000) Null mutation of PCLN-1/Claudin-16 results in bovine chronic interstitial nephritis. Genome Res 10:659–663

Ikari A, Hirai N, Shiroma M, Harada H, Sakai H, Hayashi H, Suzuki Y, Degawa M, Takagi K (2004) Association of paracellin-1 with ZO-1 augments the reabsorption of divalent cations in renal epithelial cells. J Biol Chem 279:54826–54832

Inoko A, Itoh M, Tamura A, Matsuda M, Furuse M, Tsukita S (2003) Expression and distribution of ZO-3, a tight junction MAGUK protein, in mouse tissues. Genes Cells 8:837–845

Jantarajit W, Thongon N, Pandaranandaka J, Teerapornpuntakit J, Krishnamra N, Charoenphandhu N (2007) Prolactin-stimulated transepithelial calcium transport in duodenum and Caco-2 monolayer are mediated by the phosphoinositide 3-kinase pathway. Am J Physiol Endocrinol Metab 293:E372–E384

Kostenuik PJ (2005) Osteoprotegerin and RANKL regulate bone resorption, density, geometry and strength. Curr Opin Pharmacol 5:618–625

Kriegs JO, Homann V, Kinne-Saffran E, Kinne RK (2007) Identification and subcellular localization of paracellin-1 (claudin-16) in human salivary glands. Histochem Cell Biol 128:45–53

Lehr HA, van der Loos CM, Teeling P, Gown AM (1999) Complete chromogen separation and analysis in double immunohistochemical stains using Photoshop-based image analysis. J Histochem Cytochem 47:119–126

Marenzana M, Shipley AM, Squitiero P, Kunkel JG, Rubinacci A (2005) Bone as an ion exchange organ: evidence for instantaneous cell-dependent calcium efflux from bone not due to resorption. Bone 37:545–554

Markov AG, Shadrin LV, Veshnyakova AU, Amasheh S, Fromm M (2006) The tight junction proteins claudin-2 and -16 expression in mammary epithelium of mice. Ross Fiziol Zh Im I M Sechenova 92:1382–1386

McCarthy KM, Francis SA, McCormack JM, Lai J, Rogers RA, Skare IB, Lynch RD, Schneeberger EE (2000) Inducible expression of claudin-1-myc but not occludin-VSV-G results in aberrant tight junction strand formation in MDCK cells. J Cell Sci 113:3387–3398

McNeil E, Capaldo CT, Macara IG (2006) Zonula occludens-1 function in the assembly of tight junctions in Madin–Darby canine kidney epithelial cells. Mol Biol Cell 17:1922–1932

Owen TA, Aronow M, Shalhoub V, Barone LM, Wilming L, Tassinari MS, Kennedy MB, Pockwinse S, Lian JB, Stein GS (1990) Progressive development of the rat osteoblast phenotype in vitro: reciprocal relationships in expression of genes associated with osteoblast proliferation and differentiation during formation of the bone extracellular matrix. J Cell Physiol 143:420–430

Peterson DR, Heideger WJ, Beach KW (1985) Calcium homeostasis: the effect of parathyroid hormone on bone membrane electrical potential difference. Calcif Tissue Int 37:307–311

Prêle CM, Horton MA, Caterina P, Stenbeck G (2003) Identification of the molecular mechanisms contributing to polarized trafficking in osteoblasts. Exp Cell Res 282:24–34

Rubinacci A, Benelli FD, Borgo E, Villa I (2000) Bone as an ion exchange system: evidence for a pump-leak mechanism devoted to the maintenance of high bone K^+. Am J Physiol Endocrinol Metab 278:E15–E24

Rubinacci A, Covini M, Bisogni C, Villa I, Galli M, Palumbo C, Ferretti M, Muglia MA, Marotti G (2002) Bone as an ion exchange system: evidence for a link between mechanotransduction and metabolic needs. Am J Physiol Endocrinol Metab 282:E851–E864

Saitou M, Furuse M, Sasaki H, Schulzke JD, Fromm M, Takano H, Noda T, Tsukita S (2000) Complex phenotype of mice lacking occludin, a component of tight junction strands. Mol Biol Cell 11:4131–4142

Shu C, Li TY, Tsang LL, Fok KL, Lo PS, Zhu JX, Ho LS, Chung YW, Chan HC (2006) Differentiation of adult rat bone marrow stem cells into epithelial progenitor cells in culture. Cell Biol Int 30:823–828

Simon DB, Lu Y, Choate KA, Velazquez H, Al-Sabban E, Praga M, Casari G, Bettinelli A, Colussi G, Rodriguez-Soriano J, McCredie D, Milford D, Sanjad S, Lifton RP (1999) Paracellin-1, a renal tight junction protein required for paracellular Mg^{2+} resorption. Science 285:103–106

Trumbore DC, Heideger WJ, Beach KW (1980) Electrical potential difference across bone membrane. Calcif Tissue Int 32:159–168

Van Itallie CM, Anderson JM (2006) Claudins and epithelial paracellular transport. Annu Rev Physiol 68:403–429

Van Itallie C, Rahner C, Anderson JM (2001) Regulated expression of claudin-4 decreases paracellular conductance through a selective decrease in sodium permeability. J Clin Invest 107:1319–1327

Van Itallie CM, Fanning AS, Anderson JM (2003) Reversal of charge selectivity in cation or anion-selective epithelial lines by expression of different claudins. Am J Physiol Renal Physiol 285:F1078–F1084

Van Itallie CM, Rogan S, Yu A, Vidal LS, Holmes J, Anderson JM (2006) Two splice variants of claudin-10 in the kidney create paracellular pores with different ion selectivities. Am J Physiol Renal Physiol 291:F1288–F1299

Weinger JM, Holtrop ME (1974) An ultrastructural study of bone cells: the occurrence of microtubules, microfilaments and tight junctions. Calcif Tissue Res 14:15–29

Yu AS, Enck AH, Lencer WI, Schneeberger EE (2003) Claudin-8 expression in Madin–Darby canine kidney cells augments the paracellular barrier to cation permeation. J Biol Chem 278:17350–17359

Zhang X, Yang M, Lin L, Chen P, Ma KT, Zhou CY, Ao YF (2006) Runx2 overexpression enhances osteoblastic differentiation and mineralization in adipose-derived stem cells in vitro and in vivo. Calcif Tissue Int 79:169–178

Regulation of electrolyte transport across cultured endometrial epithelial cells by prolactin

Chatsri Deachapunya, Sutthasinee Poonyachoti[1] and **Nateetip Krishnamra**[2,3]

Department of Physiology, Faculty of Medicine, Srinakharinwirot University, Sukhumvit 23, Wattana, Bangkok 10110, Thailand
[1]Department of Physiology, Faculty of Veterinary Science, Chulalongkorn University, Henri-Dunant Road, Bangkok 10330, Thailand
[2]Department of Physiology and [3]Consortium for Calcium and Bone Research, Faculty of Science, Mahidol University, Rama VI Road, Bangkok 10400, Thailand
(Correspondence should be addressed to C Deachapunya; Email: chatsri@swu.ac.th)

Abstract

The effect of prolactin (PRL) on ion transport across the porcine glandular endometrial epithelial cells was studied in primary cell culture using the short-circuit current technique. Addition of 1 μg/ml PRL either to the apical solution or to the basolateral solution produced a peak followed by a sustained increase in Isc, but with a lesser response when PRL was added apically. Basolateral addition of PRL increased the Isc in a concentration-dependent manner with a maximum effect at 1 μg/ml and an effective concentration value of 120 ng/ml. The PRL-stimulated Isc was significantly reduced by pretreatment with an apical addition of 5-nitro-2-(3-phenylpropylamino) benzoic acid (200 μM), diphenylamine-2-carboxylic acid (1 mM) or 4,4′-diisothiocyanatostilbene-2,2′-disulfonic acid (200 μM), Cl^- channel blockers, but not by amiloride (10 μM), a Na^+ channel blocker. In addition, pretreatment with bumetanide (200 μM), a Na^+–K^+–$2Cl^-$ cotransporter inhibitor, in the basolateral solution significantly reduced the PRL-stimulated Isc. Replacement of Cl^- or HCO_3^- in the bathing solutions also decreased the Isc response to PRL. Pretreatment of the monolayer with AG490 (50 μM), an inhibitor of JAK2 activity significantly inhibited the PRL-induced increase in Isc. Western blot analysis of the porcine endometrial epithelial cells revealed the presence of short isoform of PRL receptor (PRLR-S) that could be regulated by 17β-estradiol. The results of this investigation showed that PRL acutely stimulated anion secretion across the porcine endometrial epithelial cells possibly through PRLR-S present in both apical and basolateral membranes. The PRL response appeared to be mediated by the JAK2-dependent pathway.
Journal of Endocrinology (2008) **197,** 575–582

Introduction

Endometrial epithelial cells play an important role in the regulation of fluid and electrolyte volume and composition within the uterine cavity, providing an optimal intrauterine environment for implantation and embryo development. The transport-related activities of the surface and glandular epithelial cells have been shown to be regulated by several hormones, growth factors, cytokines, and a number of signaling molecules. Electrophysiological studies of cultured human endometrial epithelial cells (Matthews *et al.* 1993) and the intact porcine endometrial epithelium (Vetter & O'Grady 1996) have provided direct evidence for the regulation of Na^+ absorption and K^+ secretion. In the primary culture of mouse and porcine endometrial epithelial cells, prostaglandins (PGs) especially PGE2, adrenaline, ATP, and UTP were found to activate anion secretion (Chan *et al.* 1997, Fong *et al.* 1998, Deachapunya & O'Grady 1998, Palmer-Densmore *et al.* 2002). These epithelial cells also exhibited Na^+ transport that was activated by insulin and insulin-like growth factor, and inhibited by epidermal growth factor (Deachapunya *et al.* 1999, Deachapunya & O'Grady 2001).

Prolactin (PRL) is synthesized and secreted from the anterior pituitary gland, as well as the extrapituitary tissues including myometrium, deciduas, and mammary epithelial cells (Freeman *et al.* 2000). It exerts a wide variety of biological actions, such as the regulation of water and electrolyte balance, growth of mammary gland, milk production, and secretion. Recently, PRL has been reported to stimulate the intestinal Ca^{2+} absorption (Jantarajit *et al.* 2007), especially under conditions of high calcium demand such as pregnancy and lactation (Charoenphandhu & Krishnamra 2007).

In human endometrium, PRL receptors (PRL-R) and its mRNA have been identified in glandular epithelial and stromal cells (Jabbour *et al.* 1998, Tseng & Zhu 1998). PRL-R belongs to the superfamily of the cytokine class-1 receptor (Kelly *et al.* 1991). Several isoforms, i.e. short, intermediate, and long isoforms and the soluble PRL-binding protein have been identified in many tissues (Clevenger & Kline 2001). Binding of PRL to its transmembrane receptors induces receptor

DOI: 10.1677/JOE-08-0077
0022–0795/08/0197–575 Online version via http://www.endocrinology-journals.org

dimerization, tyrosine phosphorylation, and activation of the JAK, which leads to phosphorylation of other associated regulatory proteins especially the STAT proteins. The phosphorylated STAT proteins dimerize and translocate to the nucleus to bind to the PRL-responsive genes, resulting in target gene transcription and biological responses. Other signaling pathways involving mitogen-activated protein kinase (MAPK), insulin-receptor substrate (IRS-1), phosphoinositide 3 (PI-3) kinase, PLC, PKC, and intracellular Ca^{2+} have also been reported to mediate PRL actions (Bole-Feysot *et al.* 1998, Gubbay *et al.* 2002).

Although PRL is known as an important regulator of water and electrolyte transport in lower vertebrates (Bern 1975, Sakamoto & McCormick 2006), there were very few reports on its transport-related effect in the mammalian epithelial cells. Several studies using the everted intestinal sac technique have demonstrated the stimulatory effect of PRL on fluid and NaCl absorption in the rat, hamster, and guinea pig jejunum, but not in guinea pig ileum or rat colon (Mainoya *et al.* 1974). In the rabbit mammary glands, PRL decreased epithelial membrane permeability to sucrose, suggesting a decrease in the permeability of the tight junction (Linzell *et al.* 1975). From the studies using the mouse mammary epithelial cells grown on floating collagen gels, PRL treatment for 3 days was found to increase the short-circuit current (Isc) and transepithelial potential difference (PD), which indicated an increase in net active Na^+ absorption, probably with some Cl^- secretion (Bisbee *et al.* 1979). In the mouse mammary epithelial cell line HC11, PRL acutely increased Cl^- transport through the JAK–STAT system (Selvaraj *et al.* 2000). Eventhough PRL seemed to play an important role in the regulation of transepithelial ion transport in a variety of epithelia, its effect on the ion transport function of the endometrial epithelium has not been investigated. Since we have previously shown that the primary cultured porcine endometrial epithelial cells possessed the transport machinery capable of Na^+ absorption and Cl^- secretion (Deachapunya & O'Grady 1998, Deachapunya *et al.* 1999), the objectives of the present study were to investigate the regulatory mechanism of PRL on the ion transport across these epithelial cells.

Materials and Methods

Materials

PRL, insulin, amiloride, 5-nitro-2-(3-phenylpropylamino) benzoic acid (NPPB), diphenylamine-2-carboxylic acid (DPC), 4,4′-diisothiocyanatostilbene-2,2′-disulfonic acid (DIDS), bumetanide, acetazolamide, PGE2, 8-chloro-phenylthio-3′,5′-cyclicmonophosphate (8cpt-cAMP), non-essential amino acids, and high-purity grade salts were obtained from Sigma Chemical Co. Dulbecco's modified Eagle's medium (DMEM), Dulbecco's PBS (DPBS), fetal bovine serum (FBS), collagenase (type 1), kanamycin, penicillin–streptomycin, and fungizone were purchased from Gibco (Grand Island, NY).

Cell isolation and culture

Porcine uterine tissues collected from 5- to 6-month-old pig were obtained from the Metropolitan slaughterhouse, Klongtoey, Bangkok, under the supervision of the Department of Livestock Development, Ministry of Agriculture and Cooperatives, Thailand. The tissue was placed in an ice-cold porcine Ringer solution containing (mM): 130 NaCl, 6 KCl, 3 $CaCl_2$, 0·7 $MgCl_2$, 20 $NaHCO_3$, 0·3 NaH_2PO_4, and 1·3 Na_2HPO_4 (pH 7·4). After removal of the serosal muscle layer, the tissue fragments were cut into small pieces and digested overnight with collagenase. The epithelial glands were then isolated as described previously (Deachapunya & O'Grady 1998), and suspended in DMEM supplemented with 3·7 g/l $NaHCO_3$, 10% FBS, 850 nM (5 μg/ml) insulin, 1% non-essential amino acid, 5 μg/ml fungizone, 100 U/ml penicillin, 100 μg/ml streptomycin, and 100 μg/ml kanamycin (standard media). They were then plated onto the cell culture dishes and incubated at 37 °C in a humidified atmosphere of 5%CO_2 in air. Culture medium was changed after 24 h and then every 2–3 days. After 80% confluence (within 2–3 days), the epithelial cells were subcultured onto 24 mm (4·5 cm^2) transparent permeable membrane filters (Costar, Cambridge, MA, USA). Using this method of isolation, the purity of epithelial cells was greater than 90% as assessed by staining the isolated cells with cytokeratin (Deachapunya & O'Grady 1998). Cell monolayers were fed every 2 days and maintained in the standard media for about 7 days before the beginning of the experiment.

Measurement of electrical parameters

Before studying ion transport, the transepithelial resistance of the cell monolayer was measured with an epithelial voltohmmeter (EVOM) coupled to Ag/AgCl 'chopstick' electrodes (World Precision Instruments, Serasota, FL, USA). Monolayer with high resistance ($\approx$3000 Ωcm^2) was then mounted in Ussing Chamber, bathed in both sides with the standard porcine Ringer solution, which was maintained at 37 °C and bubbled with 95%O_2–5%CO_2. Transepithelial PD and Isc were measured with the use of voltage-clamp circuitry (EVC-4000, World Precision Instruments) with Ag/AgCl electrodes connected to the bathing solution via agar bridges. Tissue conductance (G) was calculated using Ohm's law (G = Isc/PD). The monolayer was continuously short circuited, except for a brief interval of open-circuited readings for PD measurement before and after adding any chemical. Data from the voltage clamp were connected to a MacLab 4S A/D converter and recorded with a 400 MHz PowerPC Macintosh. After mounting, the cell monolayer was equilibrated for at least 20 min to achieve a stable Isc before addition of chemicals. Positive Isc corresponded to the movement of anions in the serosal to mucosal direction or the movement of cations in the mucosal to serosal direction or a combination of both. In the anion replacement experiments, gluconate salts were substituted for chloride

and HEPES were substituted for bicarbonate. The experiment under HCO_3^- free condition was performed in the presence of 100 μM acetazolamide and bubbled with 100% O_2.

Western blot analysis

Porcine endometrial epithelial cells seeded in the 100 mm cell culture dish were allowed to grow in the standard medium up to 80% confluence. In some experiments, the medium was switched to the serum-free and phenol red-free DMEM alone or supplemented with 10^{-8} M 17β-estradiol for 48 h. Cells were then harvested and suspended in lysis buffer containing 50 mM Tris–HCl, 1% NP-40, 0·25% sodium deoxycholate, 150 mM NaCl, 1 mM EGTA, 1 mM phenylmethylsulfonyl fluoride, 20 μg aprotinin, and 1 mM NaF (pH 7·4). The supernatant was collected and protein concentrations were determined using the BCA protein assay kit (Pierce Biotechnology, Inc., Rockford, IL, USA). Protein samples (20 μg) were separated by 10% SDS-PAGE and electrically transferred to a polyvinylidene difluoride membrane (Hybond-P, Amersham Biosciences) in Tris–glycine buffer. Blotted membranes were washed and then blocked with 5% nonfat powdered milk in Tris-buffered saline for 4 h at room temperature with constant agitation. The membrane was incubated overnight at 4 °C with 1 μg/ml primary antibody, which is anti-rat PRL receptor monoclonal antibody generated against the extracellular domain of PRL receptor (clone U5, Affinity BioReagents). The membrane was then washed and incubated for 1 h at room temperature with a 1:10 000 horseradish peroxidase (HRP)-conjugated goat anti-mouse secondary antibody (Zymed Laboratories Inc., San Francisco, CA, USA). After washing, the immunoreactive protein bands were visualized using the enhanced chemiluminescence (ECL) detection system (Santa Cruz Biotechnology Inc., Santa Cruz, CA, USA) according to the manufacturer's instructions. The membranes were exposed to film (Hyperfilm-ECL, Amersham Biosciences) for adequate duration to visualize the chemiluminescent bands. To confirm equal loading, the membranes were stripped and reprobed with a 1:300 000 anti-β-actin monoclonal antibody (clone AC-15, Sigma Co.) followed by a 1:10 000 HRP-conjugated anti-mouse antibody. The intensity of the protein bands was determined using densiotometry analysis (Scion Image; Scion Cooperation, Frederick, MD, USA). Band intensity of the PRL-R from each treatment was normalized to the β-actin intensity and expressed as the PRL-R/β-actin ratio.

Data analyses

All values are presented as mean ± S.E.M. and n is the number of monolayers from at least three different uterine tissue cultures. The differences between control and experimental means were analyzed using a Student's t-test or ANOVA where appropriate. The difference between treatment and control means following a significant ANOVA was identified by Dunnett's test (Prism 3.0, GraphPad Software, Inc., San Diego, CA, USA). A value of $P<0·05$ was considered statistically significant. The effective concentration (EC_{50}) value was determined using a four-parameter logistic function to fit the data (Prism 3.0; GraphPad Software Inc.).

Results

Effect of PRL on Isc

Under basal condition, after an equilibrating period of 30 min, the porcine endometrial epithelial monolayer exhibited average Isc, PD (lumen negative), and tissue conductance of 30·68 ± 2·49 μA, −27·22 ± 3·89 mV, and 1·47 ± 0·25 mS ($n=17$) respectively. Addition of 1 μg/ml PRL to the apical or basolateral solution produced an increase in Isc that reached a peak within 2–3 min before decreasing slightly and was maintained at a level above baseline (Fig. 1A). In some experiments, the PRL-stimulated Isc gradually decreased to the baseline level. The peak Isc response to apical addition of 1 μg/ml PRL was 3·45 ± 0·94 μA ($n=4$), while the subsequent basolateral addition of 1 and 5 μg/ml PRL led

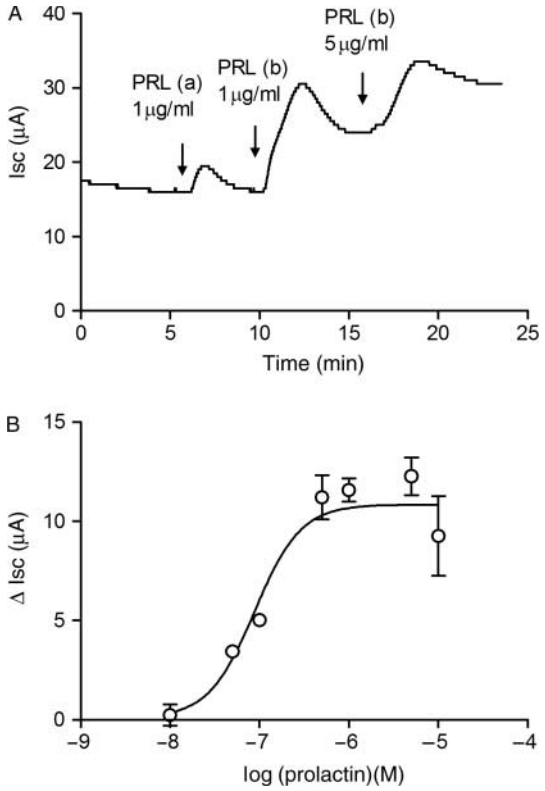

Figure 1 Effect of PRL on the basal Isc in the endometrial epithelial monolayers. (A) A representative Isc tracing responded to an addition of 1 μg/ml PRL to (a) the apical solution followed by 1 and 5 μg/ml PRL added to (b) the basolateral solution. (B) Concentration–response relationships showing the increase in Isc following basolateral treatment with various concentrations of PRL. The EC_{50} value was 120 ng/ml ($n=6$).

to a peak Isc of 11·00±0·98 μA (n=17) and 14·36±1·37 μA (n=12) respectively. Basolateral addition of PRL increased the Isc in a concentration-dependent manner with a maximum response with 1 μg/ml PRL and a half maximum EC_{50} value of 120 ng/ml (n=6, Fig 1B).

Ionic basis of the PRL-stimulated Isc

To determine the ionic basis of the Isc response induced by PRL, we examined the effect of PRL in the presence of pharmacological ion channel blockers and ion substitution solutions. An apical application of the Na^+ channel blocker amiloride at 10 μM inhibited the basal Isc by 35% (Fig. 2A). However, it did not affect the Isc response induced by PRL (1 μg/ml), which was 12·21±1·39 μA (n=5), when compared with the control value of 11·44±1·22 μA (n=12) (Fig. 2E). By contrast, the PRL-stimulated Isc was significantly decreased in the presence of Cl^- channel blockers, NPPB, DPC, and DIDS in the apical solution. NPPB and DPC have been widely used to block CFTR,

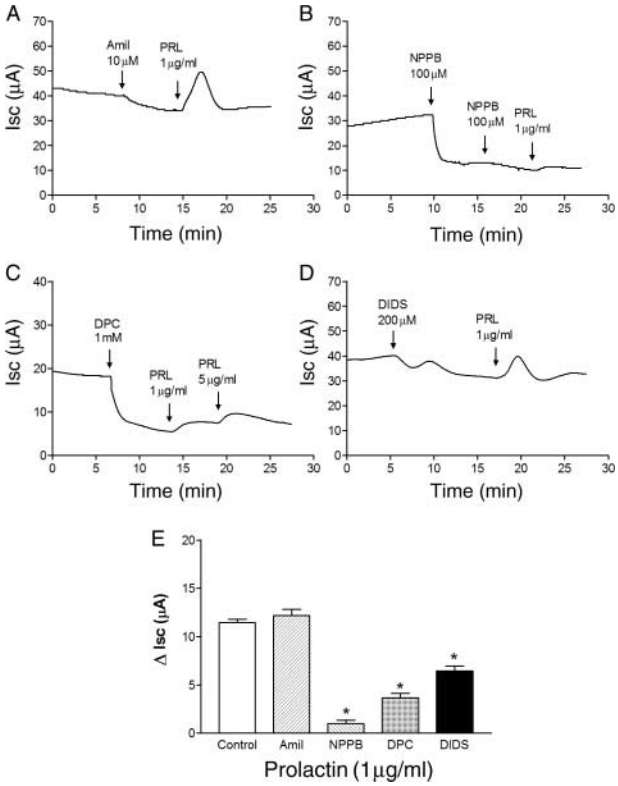

Figure 2 Effect of ion channel blockers on the PRL-stimulated Isc. (A) A representative Isc tracing showing that an apical addition of amiloride (Amil, 10 μM) produced a small decrease in basal Isc. A subsequent addition of PRL (1 μg/ml) into the basolateral solution produced an increase in Isc. (B) An apical addition of NPPB (100 μM), (C) DPC (1 mM), or (D) DIDS (200 μM) decreased the basal Isc and reduced the PRL response. (E) Bar graph illustrating the average maximal increases in Isc response produced by prolactin alone (control) and in the presence of amiloride, NPPB, DPC, or DIDS. Values represent means±S.E.M. *P<0·01 when compared with the control value by ANOVA.

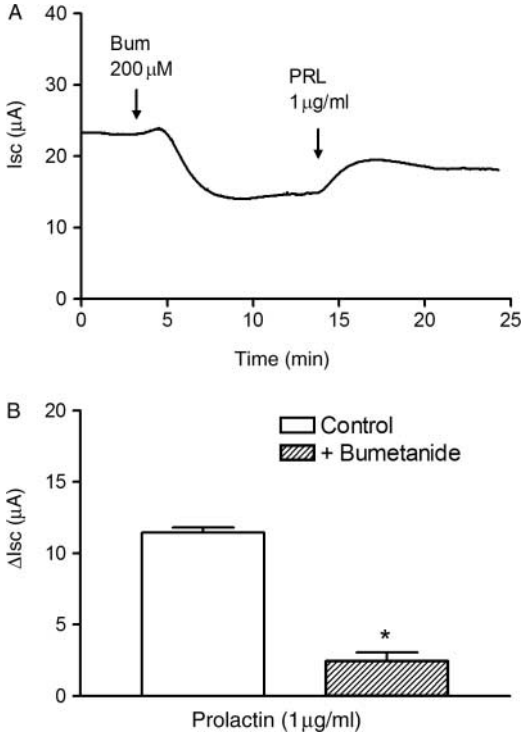

Figure 3 Effect of Na^+–K^+–$2Cl^-$ cotransporter blockers on the PRL-stimulated Isc. (A) A representative Isc tracing showing that a basolateral addition of bumetanide (200 μM) produced a decrease in basal Isc. A subsequent addition of PRL (1 μg/ml) into the basolateral solution produced a slightly increase in Isc. (B) Bar graph illustrating the average maximal increases in Isc response produced by prolactin alone (control) and in the presence of bumetanide. Values represent means±S.E.M. *P<0·01 when compared with the control value by Student's t-test.

whereas DIDS blocks the Ca^{2+}-activated Cl^- channels with no effect on the activity and conductance of CFTR (Anderson *et al.* 1992). As shown in Fig. 2B and C, pretreatment with 100 μM NPPB or 1 mM DPC reduced the basal Isc by 60 and 75% and decreased the Isc response to PRL to 1·00±0·71 μA (n=4) and 3·65±0·95 μA (n=5) respectively. An apical addition of 200 μM DIDS reduced the basal Isc by 17% and reduced the Isc response to PRL to 6·43±1·20 μA (n=4) (Fig. 2D). In addition, pretreatment with 200 μM bumetanide, a Na^+–K^+–$2Cl^-$ cotransporter inhibitor, in the basolateral solution abolished most of the PRL-induced increase in Isc from 11·44±1·22 μA (n=12) to 2·48±1·17 μA (P<0·01, n=4) (Fig. 3). Replacement of Cl^- or HCO_3^- in both the apical and the basolateral solutions markedly reduced the maximal Isc response to 1 μg/ml PRL to 1·63±1·06 μA (n=5) and 0·9±0·3 μA (n=3) respectively (Fig. 4).

Intracellular signaling pathways of PRL-induced increase in Isc

The major signaling pathway involved in PRL action is the JAK–STAT pathway which was shown to mediate Cl^-

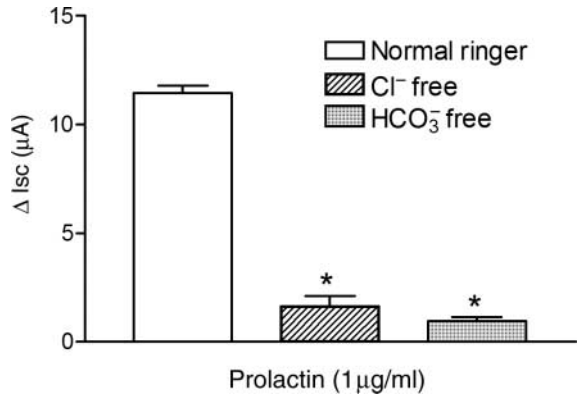

Figure 4 Effects of anion substitution on the maximal Isc response to PRL. In standard Ringer's solution, PRL (1 μg/ml) produced a mean increase in Isc of 11·44±1·22 μA (n=12). Replacement of Cl^- and HCO_3^- in both the apical and basolateral solutions significantly inhibited the maximal Isc response to PRL by 86% (n=4) and 92% (n=4) respectively. *P<0·01 when compared with the control value by ANOVA.

secretion in the mammary cell line, HC11 (Selvaraj *et al.* 2000). Phosphorylations of JAK2, STAT1, and STAT5 have been demonstrated in response to PRL stimulation (200 ng/ml) in human endometrium (Jabbour *et al.* 1998). To determine whether JAK2 was involved in the PRL-induced increase in Isc, we examined the effect of AG490, an inhibitor of JAK2 activity, on PRL action. As shown in Fig 5A, pretreatment with 50 μM AG490, added to both the basolateral and apical solutions, reduced the basal Isc by 55% from 26·21±4·99 to 11·75±4·01 μA (P<0·01, n=5). Sequential additions of 1 and 5 μg/ml PRL slightly increased the Isc response by 3·70±3·09 and 0·80±0·66 μA (n=5) respectively. However, the presence of AG490 did not affect the Isc response to 100 μM 8cpt-cAMP, which was 22·80±2·14 μA (n=4) when compared with the control value of 18·99±1·59 μA (n=5), but slightly decreased the Isc response to 3 μM PGE2 to 12·08±0·87 μA (n=4), which was not statistically significant from that of control (16·84±1·55 μA, n=7, Fig. 5B).

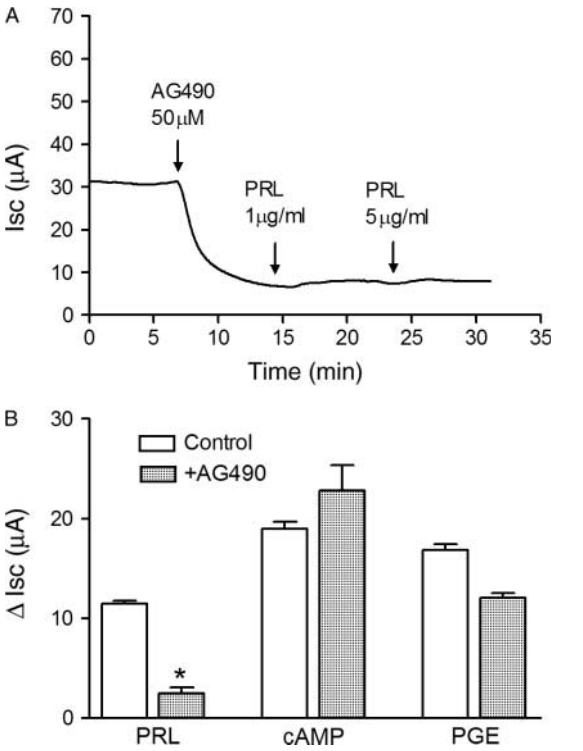

Figure 5 Effect of JAK2 activity inhibitor on the PRL-stimulated Isc. (A) A representative Isc tracing showing that an addition of AG490 (50 μM), an inhibitor of JAK2 activity, to both apical and basolateral solutions completely inhibited both basal and PRL-induced increase in Isc. (B) Bar graph illustrating the average maximal increases in Isc response produced by PRL (1 μg/ml), 8cpt-cAMP (cAMP, 100 μM), or prostaglandin E_2 (PGE, 3 μM) in the absence and presence of AG490 (50 μM). Values represent means ±S.E.M. *P<0·01 when compared with the corresponding control value by Student's t-test.

Expression of PRL receptor

To confirm the functional significance of PRL in the regulation of ion transport, the expression of PRL-R was determined using western blot analysis. A representative western blot as presented in Fig. 6A demonstrated the presence of proteins with an approximate molecular mass of 36 kDa in porcine endometrial epithelial cells as well as in the human mammary gland cancer cell MCF-7 and human endometrial cancer cell RL-95. The 36 kDa protein band corresponded to the short form of PRL-R. Replacement of the standard medium of the endometrial epithelial cells with the serum-free and phenol red-free medium reduced the expression of the protein, whereas addition of 17β-estradiol (10^{-8} M) in the serum-free medium up-regulated the PRL protein expression. Based on the densitometry analysis, the PRL-R/β-actin ratio was significantly decreased from 5·67±0·79 in the standard medium to 1·15±0·09 (P<0·05, n=4) in the serum-free medium. Treatment with 17β-estradiol increased the PRL-R/β-actin ratio by twofold to 2·35±0·12.

Discussion

A previous study in mouse mammary epithelial cells demonstrated that the PRL-induced increase in Isc was predominately mediated by Na^+ absorption (Mainoya *et al.* 1974). However, in another study in the mouse mammary epithelial cell line HC11, it was Cl^- transport that was acutely stimulated by PRL (Selvaraj *et al.* 2000). Using cultured porcine endometrial epithelial cells that possessed the machinery for Na^+ and Cl^- transports, we showed that PRL acutely stimulated anion secretion without affecting Na^+ absorption. This was further supported by the findings that the PRL-induced increase in Isc was blocked by Cl^- channel

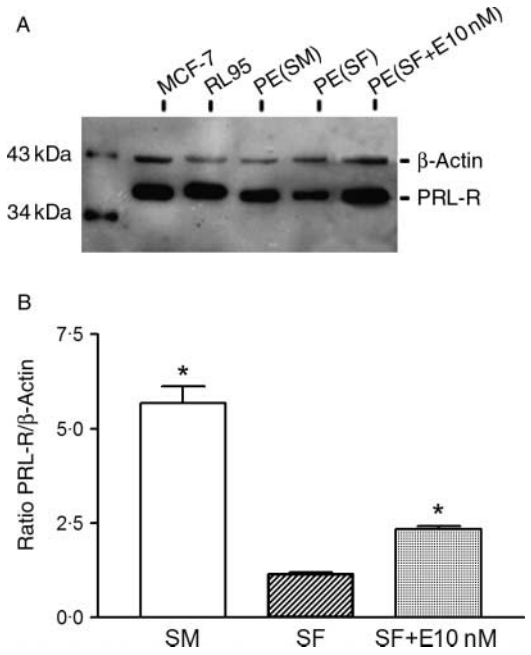

Figure 6 Expression of PRL receptor protein in porcine endometrial epithelial cells. (A) Western blot analysis of PRL receptor (PRL-R). A 36 kDa band of PRL-R was detected in human mammary gland cancer cell MCF-7, human endometrial cancer cell RL-95, and porcine endometrial epithelial cells (PE) under standard medium (SM), serum-free medium (SF) alone, or supplemented with 10^{-8} M 17β-estradiol (SF+E 10 nM). The internal control of 43 kDa band of β-actin was also detected in all samples. (B) Bar graph illustrating the ratio of PRL-R to β-actin protein expression in the endometrial epithelial cells, based on the densitometry of immunoblots obtained from SM, SF, and SF+E10 nM ($n=4$). Values represent means± S.E.M. *$P<0{\cdot}05$ when compared with the serum-free medium condition by Student's *t*-test.

blockers, NPPB, DPC, and DIDS, but not by Na^+ channel blocker, amiloride. In addition, the basolateral pretreatment with bumetanide, a blocker of Na^+–K^+–$2Cl^-$ cotransporter, or replacement of Cl^- or HCO_3^- significantly inhibited the PRL-stimulated Isc. PRL added to the basolateral solution of the high-resistance monolayer produced a greater increase in the Isc response than when added to the apical solution, suggesting that PRL receptors were predominately located at the basolateral membrane. Western blot analysis revealed the expression of a 36 kDa protein band, which corresponded to the short form of PRL-R, indicating the role of this PRL receptor isoform in the mediation of transepithelial anion secretion in the porcine endometrial epithelium.

The basal electrical properties of cultured epithelial cells used in the present study have been described previously (Deachapunya & O'Grady 1998). Under the basal condition, these cells exhibited substantial Isc that was due to a greater Cl^- secretion than Na^+ absorption. Application of PRL produced a concentration-dependent increase in the anion transport with a maximal effect seen at 1 μg/ml PRL and an EC_{50} value of 120 ng/ml. In addition, the maximal PRL response observed within 3–5 min after application, implied a non-genomic action. At PRL concentration of 1 μg/ml, which could be considered a hyperprolactinemic level, PRL was also found to maximally stimulate Cl^- transport in the mammary epithelial HC11 cells (Selvaraj *et al.* 2000). This effective concentration of PRL was comparable with the circulating levels during pregnancy and lactation in the human and the rat (Handwerger & Freemark 1987, Arbogast & Voogt 1998). Like in many other epithelia, Cl^- secretion across the endometrial epithelial cells requires activation of the apical membrane Cl^- channels and the basolateral membrane K^+ channels with the basolateral Na^+–K^+–$2Cl^-$ cotransporters serving as the Cl^- loading step. Since two types of Cl^- channels, cAMP-activated cystic fibrosis transmembrane conductance regulator (CFTR) and Ca^{2+}-activated Cl^- channels have been identified in a variety of epithelia including endometrial epithelial cells (Deachapunya & O'Grady 1998, Palmer-Densmore *et al.* 2002), NPPB and DPC, inhibitors of anion channels including CFTR, and DIDS, an inhibitor of Ca^{2+}-activated Cl^- channels, were used to elucidate PRL action. As the present results showed that the PRL-induced increase in Isc was nearly completely inhibited by DPC and NPPB, it was most likely that CFTR was the primary target of the PRL-stimulated Cl^- secretion. However, the 40% inhibition of the PRL-stimulated Isc by DIDS indicated that the Ca^{2+}-activated Cl^- channels may also be partially involved in the PRL activation of Cl^- secretion. In addition, the PRL-stimulated increase in Isc was also diminished by bumetanide, an inhibitor of Na^+–K^+–$2Cl^-$ cotransporter, which was not surprising since the bumetanide-sensitive Cl^- uptake probably served as the Cl^- loading step for PRL-stimulated Cl^- secretion. The finding that Isc response to PRL was abolished in the Cl^-free solution further confirmed the PRL activation of Cl^- secretion. Since the electronic HCO_3^- secretion used the cAMP- and Ca^{2+}-activated Cl^- channels (Illek *et al.* 1999), a marked reduction of Isc response to PRL in the HCO_3^- free solution suggested a substantial contribution of HCO_3^- to the PRL-induced increase in Isc. Altogether, the results suggest a possible involvement of $Cl^- - HCO_3^-$ exchangers as well as $Na^+ - Na^+ - HCO_3^-$ cotransporters in the PRL-dependent HCO_3^- secretion. However, it was noted that the replacement of HCO_3^- itself, could have produced the intracellular acidification, which could affect the transport pathways or the signaling mechanisms that regulate anion secretion. Taken together, it could be stated that PRL-induced anion secretion by stimulating the apical Cl^- efflux through CFTR as the major channel type and through some Ca^{2+}-activated Cl^- channels, concurrently with the increase in the basolateral Cl^- uptake through the bumetanide-sensitive Na^+–K^+–$2Cl^-$ cotransporter. Although not being investigated in this study, the basolateral K^+ channels that provide the driving force for Cl^- exit across the apical membrane, could also be a target of PRL action, and are subject to further investigation.

Several signaling pathways mediating the multiple actions of PRL have been demonstrated in a variety of tissues with the

JAK–STAT pathway being most extensively studied. Previous evidence of the phosphorylation of JAK2, STAT1, and STAT5 in response to PRL stimulation in the human endometrium (Jabbour *et al.* 1998) and the PRL-stimulated Cl^- transport through the JAK2 cascade pathway in mouse mammary epithelial cell line HC11 (Selvaraj *et al.* 2000) suggested that JAK2 is a likely mediator of PRL-stimulating effect on the anion transport in the porcine endometrial epithelial cells. In the present study, pretreatment with AG490, an inhibitor of JAK2 activity inhibited both the basal Isc and the PRL-induced increase in Isc. Regarding the basal Isc, since the basal Isc of the cultured porcine endometrial epithelial cells has been shown to be generated mainly by Cl^- secretion (Deachapunya & O'Grady 1998), the fact that AG490 could inhibit the basal Isc within 10 min suggested that a constitutive JAK2 activity was responsible for the basal active Cl^- secretion. Although no direct association between JAK2 activity and Cl^- transport mechanism has been reported, the fact that tyrosine-phosphorylated proteins could regulate the basal Cl^- secretion in human colonic epithelial cell line, T84 (Uribe *et al.* 1996) suggested that the JAK2 inhibitors inhibited Cl^- secretion by interfering with the tyrosine phosphorylation of the regulatory transport proteins. Furthermore, based on the findings that i) Cl^- secretion could still be activated by 8cpt-cAMP in the presence of JAK2 inhibitor, ii) the inhibition of the basal Isc did not affect the PGE2-stimulated Isc response, and iii) the PGE2-stimulated Cl^- secretion was via the cAMP-dependent pathway (Deachapunya & O'Grady 1998), it is likely that the cAMP-dependent Cl^- secretion did not involve JAK2 pathway.

In contrast to the PGE2-stimulated Cl^- secretion, the PRL-stimulated Cl^- secretion was probably mediated by the JAK2 pathway because the PRL-induced increase in Isc was significantly inhibited by AG490. These findings were consistent with a report of AG490 blocking phosphorylation of STAT5 and PRL-induced Cl^- secretion, but not the PGE1-induced Cl^- secretion in mouse mammary cell line (Selvaraj *et al.* 2000). The effect of AG490 was more specific to PRL action, since tyrosine kinase inhibitor genistein had no effect on the PRL-stimulated Isc (data not shown).

PRL-R and its mRNA have been identified in human glandular epithelial and stromal cells (Jabbour *et al.* 1998, Tseng & Zhu 1998). Two isoforms of PRL-R, short and long, have been identified in several rat tissues including liver, ovary, thymus, and spleen (Gunes & Mastro 1996, Telleria *et al.* 1997). In the present study, we examined the expression of PRL-R protein in the endometrial epithelial cells by western blot analysis. The monoclonal antibody used in the present study detected protein with molecular mass of about 36 kDa, which corresponded to the short form of the PRL-R, similar to the predominant short isoforms expressed in the rat spleen and brain (Shingo *et al.* 2003). By contrast, the long form of PRL-R is the major receptor isoforms in the rat liver and mammary gland (Jahn *et al.* 1991, Selvaraj *et al.* 2000). Although at least two isoforms of PRL-R mRNA have been found in the reproductive tissues (Telleria *et al.* 1997), the present data indicated that the short form PRL-R was the functional PRL-R in the porcine endometrial epithelial cells, and that the PRL-stimulated Cl^- secretion in the porcine endometrial epithelial cells was mediated through the short form of PRL receptors located predominately at the basolateral membrane.

Generally, PRL is synthesized by the decidualized endometrial stromal cells during the late secretory phase of the menstrual cycle and throughout pregnancy. The level of PRL is apparently much higher in the blood and amniotic fluid during pregnancy (Golander *et al.* 1978, Daly *et al.* 1983). After conception, a continuous increase in PRL production in the decidual cells leads to an accumulation of PRL in the amniotic fluid up to 2–3 μg/ml (Golander *et al.* 1978, Daly *et al.* 1983). Concomitantly, the PRL receptor expression and its mRNA are up-regulated toward the secretory phase of the menstrual cycle (Jabbour *et al.* 1998, Jones *et al.* 1998) and maintained throughout pregnancy (Maaskant *et al.* 1996). The level of PRL receptor mRNA is much higher in the glandular cells than in the stromal cells (Jabbour *et al.* 1998, Jones *et al.* 1998). Although the exact role of PRL in the human endometrium remains to be clarified, the pattern of secretion and expression supports a role of PRL in implantation and placentation. In agreement with those reports, the presence of PRL-R protein that was up-regulated by 17β-estradiol (Fig. 6) in the cultured porcine endometrial epithelial cells strongly suggested the physiological role of PRL in pregnancy. This speculation was consistent with the report that the blastocyst implantation and the maintenance of pregnancy were impaired in the PRL and PRL-R knockout mice (Jikihara *et al.* 1996). The next question is what is the exact role of PRL in the pregnant uterus. It is known that specific concentrations of electrolytes and pH within the uterine lumen are important for implantation and embryo development. In the rhesus monkey, PRL has been shown to regulate the amniotic and fetal extracellular fluid and electrolyte balance by decreasing the water flux from the amniotic side of the fetal membrane (Josimovich *et al.* 1977). Concomitant with the present finding of PRL role in the stimulation of anion secretion across the endometrial epithelial cells, and that active secretion of Cl^- and HCO_3^- provides the driving force for fluid secretion and the regulation of luminal fluid pH, it is likely that PRL exerts endocrine and paracrine actions to regulate the volume and composition of the fluid within the uterine cavity, thus providing an optimal condition for implantation and development of the embryo.

In conclusion, this study shows for the first time the regulation of the transepithelial anion secretion by PRL in the endometrium. The results showed that PRL acutely stimulated anion secretion across the porcine endometrial epithelial cells through the short isoform of PRL receptor and the JAK–STAT-dependent pathway. The PRL-stimulated anion secretion was mostly a result of the activation of DPC- and NPPB-sensitive Cl^- channels, and bumetanide-sensitive Na^+–K^+–$2Cl^-$ cotransport. Further investigation is required to define the physiological and pharmacological significance of PRL action in the endometrium. In addition, the PRL-signaling mechanisms, i.e. intracellular Ca^{2+}, cAMP, or other signaling molecules remain to be elucidated.

Acknowledgements

The authors wish to thank Miss Norathee Buathong for her help with primary cell preparation and some of the experiments, and Dr Narattaphol Charoenphandhu for his valuable comments of the manuscript. This work was fully supported by the Thailand Research Fund (Contract grant number: TRA4780008) awarded to N M. The authors declare that there is no conflict of interest that would prejudice the impartiality of this scientific work.

References

Anderson MP, Sheppard DN, Berger HA & Welsh MJ 1992 Chloride channels in the apical membrane of normal and cystic fibrosis airway and intestinal epithelia. *American Journal of Physiology* **263** L1–L14.

Arbogast LA & Voogt JL 1998 Endogenous opioid peptides contribute to suckling-induced prolactin release by suppressing tyrosine hydroxylase activity and messenger ribonucleic acid levels in tuberoinfundibular dopaminergic neurons. *Endocrinology* **139** 2857–2862.

Bern HA 1975 Prolactin and osmoregulation. *American Zoologists* **15** 937–949.

Bisbee CA, Machen TE & Bern HA 1979 Mouse mammary epithelial cells on floating collagen gels: transepithelial ion transport and effects of PRL. *PNAS* **76** 536–540.

Bole-Feysot C, Goffin V, Edery M, Binart N & Kelly PA 1998 Prolactin (PRL) and its receptor: actions, signal transduction pathways and phenotypes observed in PRL receptor knockout mice. *Endocrine Reviews* **19** 225–268.

Chan HC, Liu CQ, Fong SK, Law SH, Wu LJ, So E, Chung YW, Ko WH & Wong PYD 1997 Regulation of Cl^- secretion by extracellular ATP in cultured mouse endometrial epithelium. *Journal of Membrane Biology* **156** 45–52.

Charoenphandhu N & Krishnamra N 2007 Prolactin is an important regulator of intestinal calcium transport. *Canadian Journal of Physiology and Pharmacology* **85** 569–581.

Clevenger CV & Kline JB 2001 Prolactin receptor signal transduction. *Lupus* **10** 706–718.

Daly DC, Maslar IA & Riddick DH 1983 Prolactin production during *in vitro* decidualization of proliferative endometrium. *American Journal of Obstetrics and Gynecology* **145** 672–678.

Deachapunya C & O'Grady SM 1998 Regulation of chloride secretion across porcine endometrial epithelial cells by prostaglandin E_2. *Journal of Physiology* **508** 31–47.

Deachapunya C & O'Grady SM 2001 EGF regulates the transition from basal sodium absorption to anion secretion in cultured endometrial epithelial cells. *Journal of Cell Physiology* **186** 243–250.

Deachapunya C, Palmer-Densmore M & O'Grady SM 1999 Insulin stimulates transepithelial sodium transport by activation of a protein phosphatase that increases Na-K ATPase activity in endometrial epithelial cells. *Journal of General Physiology* **114** 561–574.

Fong SK, Liu CQ & Chan HC 1998 Cellular mechanisms of adrenaline-stimulated anion secretion by the mouse endometrium epithelium. *Biology of Reproduction* **59** 1342–1348.

Freeman ME, Kanyicsky B, Lerant A & Nagy G 2000 Prolactin: structure, function, and regulation of secretion. *Physiological Reviews* **80** 1523–1631.

Golander A, Hurley T, Barrett J, Hizi A & Handwerger S 1978 Prolactin synthesis by human chorion decidual tissue: a possible source of prolactin in the amniotic fluid. *Science* **202** 311–313.

Gubbay O, Critchley HOD, Bowen JM, King A & Jabbour HN 2002 Prolactin induces ERK phosphorylation in epithelial and CD56+ natural killer cells of the human endometrium. *Journal of Clinical Endocrinology and Metabolism* **87** 2329–2335.

Gunes H & Mastro AM 1996 Prolectin receptor gene expression in rat splenocytes and thymocytes from birth to adulthood. *Molecular and Cellular Endocrinology* **117** 41–52.

Handwerger S & Freemark M 1987 Role of placental lactogen and prolactin in human pregnancy. *Advances in Experimental Medicine and Biology* **219** 399–420.

Illek B, Tam AW, Fischer H & Machen TE 1999 Anion selectivity of apical membrane conductance of Calu 3 human airway epithelium. *Pflügers Archiv* **437** 812–822.

Jabbour HN, Critchley HO & Boddy SC 1998 Expression of functional prolactin receptors in nonpregnant human endometrium: janus kinase-2, signal transducer and activator of transcription-1 (STAT1), and STAT5 proteins are phosphorylated after stimulation with prolactin. *Journal of Clinical Endocrinology and Metabolism* **83** 2545–2553.

Jahn GA, Edery M, Belair L, Kelly PA & Djiane J 1991 Prolactin receptor gene expression in rat mammary gland and liver during pregnancy and lactation. *Endocrinology* **128** 2976–2984.

Jantarajit W, Thongon N, Pandaranandaka J, Teerapornpuntakit J, Krishnamra N & Charoenphandhu N 2007 Prolactin-stimulated transepithelial calcium transport in duodenum and Caco-2 monolayer are mediated by the phosphoinositide 3-kinase pathway. *American Journal of Physiology. Endocrinology and Metabolism* **293** 372–384.

Jikihara H, Kessler CA, Cedars MI & Bra AK 1996 Up-regulation of the human prolactin receptor in the endometrium. *Journal of Endocrinology* **5** 157–162.

Jones RL, Critchley HO, Brooks J, Jabbour HN & McNeilly AS 1998 Localization and temporal expression of prolactin recptor in human endometrium. *Journal of Clinical Endocrinology and Metabolism* **83** 258–262.

Josimovich JB, Merisko K & Boccella L 1977 Amniotic prolactin control over amniotic and fetal extracellular fluid water and electrolytes in the rhesus monkey. *Endocrinology* **100** 564–570.

Kelly PA, Djiane J, Postel-Vinay MC & Edery M 1991 The prolactin/growth hormone receptor family. *Endocrine Reviews* **12** 235–251.

Linzell JL, Peaker M & Taylor JC 1975 The effects of prolactin and oxytocin on milk secretion and on the permeability of the mammary epithelium in the rabbit. *Journal of Physiology* **253** 547–563.

Maaskant RA, Bogic LV, Gilger S, Kelly PA & Bryant-Greenwood GD 1996 The human prolactin receptor in the fetal membranes, decidua, and placenta. *Journal of Clinical Endocrinology Metabolism* **81** 396–405.

Mainoya JR, Bern HA & Regan JW 1974 Influence of ovine prolactin on transport of fluid and sodium chloride by the mammalian intestine and gall bladder. *Journal of Endocrinology* **63** 311–317.

Matthews CJ, Thomas EJ, Redfern CPF & Hirst BH 1993 Ion transport by human endometrium *in vitro*. *Human Reproduction* **8** 1510–1575.

Palmer-Densmore M, Deachapunya C & O'Grady SM 2002 UTP-dependent inhibition of Na absorption requires activation of PKC in endometrial epithelial cells. *Journal of General Physiology* **120** 897–906.

Sakamoto T & McCormick SD 2006 Prolactin and growth hormone in fish osmoregulation. *General and Comparative Endocrinology* **147** 24–30.

Selvaraj NG, Omi E, Gibori G & Rao MC 2000 Janus kinase 2 (JAK2) regulates prolactin-mediated chloride transport in mouse mammary epithelial cells through tyrosine phosphorylation of Na^+–K^+–$2Cl^-$ cotransporter. *Molecular Endocrinology* **14** 2054–2065.

Shingo T, Gregg C, Enwere E, Fujikawa H, Hassam R, Geary C, Cross JC & Weiss S 2003 Pregnancy-stimulated neurogenesis in the adult female forebrain mediated by prolactin. *Science* **299** 117–120.

Telleria CM, Parmer TG, Zhong L, Clarke DL, Albarracin CT, Duan WR, Linzer DI & Gibori G 1997 The different forms of the prolactin receptor in the rat corpus luteum: developmental expression and hormonal regulation in pregnancy. *Endocrinology* **138** 4812–4820.

Tseng L & Zhu HH 1998 Progestin induces prolactin receptor in human endometrial stromal cells. *Journal of the Society for Gynecologic Investigation* **5** 149–155.

Uribe JM, Keely SJ, Traynor-Kaplan AE & Barrett KE 1996 Phosphatidyl-inositol 3-kinase mediates the inhibitory effect of epidermal growth factor on calcium-dependent chloride secretion. *Journal of Biological Chemistry* **271** 26588–26595.

Vetter AE & O'Grady SM 1996 Mechanisms of electrolyte transport across the endometrium I. Regulation by PGF2 and cAMP. *American Journal of Physiology. Cell Physiology* **270** 663–672.

Received in final form 29 March 2008
Accepted 4 April 2008
Made available online as an Accepted Preprint
4 April 2008

Prolactin stimulates transepithelial calcium transport and modulates paracellular permselectivity in Caco-2 monolayer: mediation by PKC and ROCK pathways

Narongrit Thongon, La-iad Nakkrasae, Jirawan Thongbunchoo, Nateetip Krishnamra and Narattaphol Charoenphandhu

Am J Physiol Cell Physiol 294:C1158-C1168, 2008. First published 19 March 2008; doi:10.1152/ajpcell.00020.2008

AJP - Cell Physiology is dedicated to innovative approaches to the study of cell and molecular physiology. It is published 12 times a year (monthly) by the American Physiological Society, 9650 Rockville Pike, Bethesda MD 20814-3991. ISSN: 0363-6143, ESSN: 1522-1563. Visit our website at http://www.the-aps.org/.

Am J Physiol Cell Physiol 294: C1158–C1168, 2008.
First published March 19, 2008; doi:10.1152/ajpcell.00020.2008.

Prolactin stimulates transepithelial calcium transport and modulates paracellular permselectivity in Caco-2 monolayer: mediation by PKC and ROCK pathways

Narongrit Thongon,[1] La-iad Nakkrasae,[2] Jirawan Thongbunchoo,[2] Nateetip Krishnamra,[1,2] and Narattaphol Charoenphandhu[1,2]

[1]*Department of Physiology and* [2]*Consortium for Calcium and Bone Research, Faculty of Science, Mahidol University, Bangkok, Thailand*

Submitted 15 January 2008; accepted in final form 18 March 2008

Thongon N, Nakkrasae L-I, Thongbunchoo J, Krishnamra N, Charoenphandhu N. Prolactin stimulates transepithelial calcium transport and modulates paracellular permselectivity in Caco-2 monolayer: mediation by PKC and ROCK pathways. *Am J Physiol Cell Physiol* 294: C1158–C1168, 2008. First published March 19, 2008; doi:10.1152/ajpcell.00020.2008.—Prolactin (PRL) was previously demonstrated to rapidly enhance calcium absorption in rat duodenum and the intestine-like Caco-2 monolayer. However, its mechanism was not completely understood. Here, we investigated nongenomic effects of PRL on the transepithelial calcium transport and paracellular permselectivity in the Caco-2 monolayer by Ussing chamber technique. PRL increased the transcellular and paracellular calcium fluxes and paracellular calcium permeability within 60 min after exposure but decreased the transepithelial resistance of the monolayer. The effects of PRL could not be inhibited by RNA polymerase II inhibitor (5,6-dichloro-1-β-D-ribobenzimidazole), confirming that PRL actions were nongenomic. Exposure to protein kinase C (PKC) or RhoA-associated coiled-coil forming kinase (ROCK) inhibitors (GF-109203X and Y-27632, respectively) abolished the stimulatory effect of PRL on transcellular calcium transport, whereas ROCK inhibitor, but not PKC inhibitor, diminished the PRL effect on paracellular calcium transport. Knockdown of the long isoform of PRL receptor (PRLR-L) also prevented the enhancement of calcium transport by PRL. In addition, PRL markedly increased paracellular sodium permeability and the permeability ratio of sodium to chloride, which are indicators of the paracellular charge-selective property and are known to be associated with the enhanced paracellular calcium transport. The permeability of other cations in the alkali metal series was also increased by PRL, and such increases were abolished by ROCK inhibitor. It could be concluded that PRL stimulated transepithelial calcium transport through PRLR-L and increased paracellular permeability to cations in the Caco-2 monolayer. These nongenomic actions of PRL were mediated by the PKC and ROCK signaling pathways.

charge selectivity; dilution potential; paracellular transport; phosphoinositide 3-kinase; protein kinase C; long form of prolactin receptor; RhoA; short interference RNA; transcellular transport

DURING PREGNANCY and lactation, prolactin (PRL) is a calcium-regulating hormone that mitigates negative calcium balance by increasing intestinal calcium absorption (10). In vivo studies in normal rats suggested that PRL stimulated both transcellular active and paracellular passive calcium transport in the duodenum and proximal jejunum (10, 33). Exposure to high physiological levels of PRL of 400–600 ng/ml, which are comparable to the levels attained during lactation and suckling (2), rapidly enhanced transepithelial calcium transport in isolated duodenal epithelium and intestine-like Caco-2 monolayer in a dose-dependent manner (25). However, the signaling pathways of PRL in the intestinal absorptive cells and the detailed mechanisms of the PRL-enhanced calcium transport were not completely understood.

Calcium traverses the intestinal epithelium via both transcellular and paracellular pathways (22). Transcellular active calcium transport is a metabolically energized process, consisting of apical calcium entry via the transient receptor potential vanilloid family Ca^{2+} channel 6 (TRPV6), cytoplasmic calcium translocation in a calbindin-D_{9K}-bound form, and basolateral calcium extrusion via the plasma membrane Ca^{2+}-ATPase (PMCA) (22). On the other hand, paracellular passive calcium transport is dependent on the transepithelial calcium gradient and transepithelial resistance (TER) and is absent when both sides of the epithelium contain equal calcium concentration (12, 29). In normal intestinal epithelia, movement of ions and nutrients across the paracellular pathway is generally regulated by the size- and charge-selective properties of the tight junction, which contains several charge-selective claudin proteins arranged in arrays of channellike barriers (32, 49, 54). Several mediators, e.g., phosphoinositide 3-kinase (PI3K), protein kinase C (PKC), and RhoA-associated coiled-coil forming kinase (ROCK), can modulate permselectivity of the paracellular pathway (5, 15, 25, 47).

Our recent investigation (25) demonstrated that the Caco-2 monolayer, which strongly expressed short and long isoforms of the PRL receptor (PRLR-S and -L, respectively), responded to PRL by increasing both transcellular and paracellular calcium transport. However, little was known regarding the effect of PRL on the paracellular permselectivity and electrical properties of the epithelium. Moreover, it was not known whether PRLR-S or PRLR-L was responsible for PRL signaling in the intestinal absorptive cells, but there was a report that in mammary epithelia PRL augmented galactopoiesis and electrolyte transport through PRLR-L, whereas PRLR-S silenced those actions (3, 6, 24, 42). The signaling pathway of PRL in Caco-2 cells, in contrast to mammary epithelial cells, may be nongenomic since the actions were observed very rapidly within 60 min after PRL exposure (25). Interestingly, in Caco-2 cells and duodenal epithelium, the nongenomic actions

Address for reprint requests and other correspondence: N. Charoenphandhu, Dept. of Physiology, Faculty of Science, Mahidol Univ., Rama VI Road, Bangkok 10400, Thailand (e-mail: naratt@narattsys.com).

The costs of publication of this article were defrayed in part by the payment of page charges. The article must therefore be hereby marked "*advertisement*" in accordance with 18 U.S.C. Section 1734 solely to indicate this fact.

of PRL were mediated by the PI3K pathway, but not the putative Janus kinase (JAK)2 or mitogen-activated protein kinase (MAPK) pathways (25). PI3K is the ultimate upstream kinase to several downstream targets, including PKC and ROCK, which are known to modulate transepithelial calcium transport and increase paracellular permeability, respectively (4, 21, 28, 36, 47). Thus PKC and ROCK pathways may mediate the actions of PRL.

In the present study, we used Caco-2 cells to demonstrate PRL-enhanced calcium absorption. Despite being human colorectal adenocarcinoma cells, confluent Caco-2 monolayers have been used widely in the studies of calcium and drug absorption because they have functional similarity to the small intestine, including the presence of brush border, expression of sucrase-isomaltase enzymes, and expression of the transcellular calcium transporters and charge-selective paracellular proteins, e.g., TRPV6, calbindin-D_{9K}, PMCA, and claudin-1, -2, -3, and -5 (37–39, 57, 58). The Caco-2 monolayer also responds to PRL in a dose-dependent manner, with a maximal effective concentration of 600 ng/ml, similar to that seen in duodenal epithelium (25). However, the normal paracellular passive calcium transport and cationic permselectivity of the Caco-2 monolayer as well as its response to PRL by altering paracellular calcium transport have not been fully characterized.

Therefore, the objectives of this study were *1*) to demonstrate that the rapid stimulatory effects of PRL on transepithelial calcium transport in the Caco-2 monolayer are nongenomic, *2*) to show that PRL signaling involves the PKC and ROCK pathways, *3*) to elucidate the normal characteristics of the paracellular calcium transport and cationic permselectivity of the Caco-2 monolayer, as well as the effects of PRL on these parameters, and *4*) to demonstrate that PRLR-L is required for the PRL-enhanced calcium absorption.

MATERIALS AND METHODS

Cell culture. Caco-2 cells [American Type Culture Collection (ATCC) no. HTB-37] were grown in Dulbecco's modified Eagle's medium (DMEM; Sigma, St. Louis, MO) supplemented with 15% fetal bovine serum (FBS; GIBCO, Grand Island, NY), 1% L-glutamine (GIBCO), 1% nonessential amino acid (Sigma), and 100 U/ml penicillin-streptomycin. Cells were propagated in 75-cm^2 T flasks (Corning) under a humidified atmosphere containing 5% CO_2 at 37°C and subcultured as described in the ATCC protocol. Confluent Caco-2 monolayers were prepared by seeding cells on polyester Snapwell inserts with 12-mm diameter and 0.4-μm pore size (catalog no. 3801; Corning) at 5×10^5 cells/well. Culture medium was changed daily after 48 h of seeding. Monolayers were incubated at 37°C for 14 days in a humidified atmosphere containing 5% CO_2.

On the experimental day, the Snapwell was mounted in a modified Ussing chamber with an exposed surface area of 1.13 cm^2 to measure electrical parameters, calcium fluxes, and/or ion permeability, as previously described (25). The monolayer was incubated for 20 min in the chamber before the 60-min experiment was carried out.

Bathing solution. The bathing solution for the Ussing chamber experiments contained (in mmol/l) 118 NaCl, 4.7 KCl, 1.1 $MgCl_2$, 1.25 $CaCl_2$, 23 $NaHCO_3$, 12 D-glucose, and 2 mannitol (all purchased from Sigma). The solution, continuously gassed with humidified 5% CO_2 in 95% O_2, was maintained at 37°C and pH 7.4 and had an osmolality of 290–293 mosmol/kgH_2O as measured by a freezing point-based osmometer (model 3320; Advanced Instruments, Norwood, MA). Water used in the present work had a resistance >18.3 MΩ·cm and a free ionized calcium concentration <2.5 nmol/l.

Short interference RNA transfection. Two short interference RNA (siRNA) sequences targeted for human PRLR-L, i.e., 5′-GGGCUAUAGCAUGGUGACCTT-3′ and 5′-GGUCACCAUGCUAUAGCCCTT-3′, scrambled siRNAs, and the transfection reagent kit were supplied by Ambion (Austin, TX). Caco-2 cells were seeded in Snapwells at 5×10^5 cells/well for 12 days. Thereafter, in vitro transfection was performed with the 1:400 siPORT amine transfection reagent (Ambion) according to the manufacturer's instruction. The siRNAs were added in the culture medium to obtain a final concentration of 1 nmol/l. Control cells were treated with siPORT without siRNA. After a 48-h transfection, the PRL-stimulated calcium transport across the PRLR-L knockdown monolayer was measured. The siRNA efficiency was determined by quantitative real-time PCR (qRT-PCR). This PRLR-L knockdown study was approved by the Institutional Biosafety Committee (IBC) of the Faculty of Science, Mahidol University.

mRNA isolation, qRT-PCR, and sequencing. With the use of TRIzol reagent (Invitrogen, Carlsbad, CA), total RNA was prepared from the PRLR-L knockdown Caco-2 cells as previously described (13). One microgram of the total RNA was reverse-transcribed with the iScript kit (Bio-Rad, Hercules, CA). Glyceraldehyde-3-phosphate dehydrogenase (GAPDH), a housekeeping gene, served as a control gene to check the consistency of reverse transcription (% coefficient of variation <1%; $n = 20$). Sense and antisense primers of PRLRs and GAPDH were designed by OLIGO 6 (Molecular Biology Insights, Cascade, CO) and Primer Validator 1.4 (Naratt Software, Bangkok, Thailand), as shown in Table 1. The amplification reaction using real-time PCR (model MiniOpticon; Bio-Rad) was performed with the iQ SYBR Green SuperMix (Bio-Rad). Relative expression of PRLR over GAPDH was calculated from the threshold cycle (C_t) values by the $2^{\Delta Ct}$ method. After qRT-PCR, the PCR products were also visualized on a 1.5% agarose gel stained with 1.0 μg/ml ethidium bromide. Thereafter, all PCR products were extracted with the HiYield Gel/PCR DNA Extraction kit (Real Biotech, Taipei, Taiwan) and were sequenced with the ABI Prism 3100 Genetic Analyzer (Applied Biosystems, Foster City, CA).

Measurement of electrical parameters. Three electrical parameters, i.e., potential difference (PD), short-circuit current (I_{sc}), and TER, were determined as previously described (12). In brief, a pair of Ag/AgCl electrodes connected to agar bridges (3.0 mol/l KCl per 4 g% agar) was located near each surface of the mounted Snapwell for measurement of PD. The other ends of the PD-sensing electrodes were connected to a preamplifier (model EVC-4000; World Precision Instruments, Sarasota, FL). Another pair of Ag/AgCl electrodes connected in series to the EVC-4000 current-generating unit was placed at the end of each hemichamber to supply I_{sc}. TER and conductance (G; $G = 1/\text{TER}$) were calculated from Ohm's equation.

Measurement of calcium, mannitol, and polyethylene glycol fluxes. Calcium transport across Caco-2 monolayer was determined by the method of Charoenphandhu et al. (12). After 20-min incubation, the Ussing chamber was filled with fresh bathing solution containing

Table 1. *Homo sapiens oligonucleotide sequences used in qRT-PCR experiments*

Name	Accession No.	Primer (forward/reverse)	Product Length, bp
PRLR-S	AF416619	5′-GGTGACCCCTTGATGTTG-3′ 5′-TTCTGGTATATGCTCTTCAGC-3′	145
PRLR-L	NM_000949	5′-ACTTGCCTCTTTCTCCAG-3′ 5′-TCCCTCAAGAATACTAAGCAG-3′	100
GAPDH	NM_002046	5′-CTGGTAAAGTGGATATTGTTG-3′ 5′-GAGGCTGTTGTCATACTTCTC-3′	359

qRT-PCR, quantitative RT-PCR; PRLR-S, short isoform of prolactin receptor; PRLR-L, long isoform of prolactin receptor; GAPDH, glyceraldehyde-3-phosphate dehydrogenase.

$^{45}CaCl_2$ (final specific activity of 500 mCi/mol; Amersham, Little Chalfont, UK). Radioactivity of ^{45}Ca was analyzed with a liquid scintillation spectrophotometer (model Tri-Carb 3100 TR; Perkin-Elmer, Shelton, CT). Total calcium concentration was analyzed by atomic absorption spectroscopy (model SpectrAA-300; Varian Techtron, Victoria, Australia). Unidirectional flux ($J_{H\rightarrow C}$, nmol·h^{-1}·cm^{-2}) of calcium from the hot side (H) to the cold side (C) was calculated with *Eqs. 1* and *2*.

$$J_{H\rightarrow C} = R_{H\rightarrow C}/(S_H \times A) \quad (1)$$

$$S_H = C_H/C_T \quad (2)$$

where $R_{H\rightarrow C}$ is the rate of tracer appearance in the cold side (cpm/h); S_H is the specific activity in the hot side (cpm/nmol); A is the surface area of the Snapwell (cm^2); C_H is the mean radioactivity in the hot side (cpm); and C_T is the total calcium in the hot side (nmol).

Calcium fluxes in the absence of calcium concentration gradient (i.e., bathing solution in both hemichambers contained equal calcium concentration) represented the transcellular active calcium transport (12). The calcium gradient-dependent paracellular passive transport was studied by determining calcium fluxes in the presence of varying apical calcium concentrations (12), i.e., 1.25, 2.5, 5, 10, 20, 40, and 80 mmol/l.

In some experiments, the Caco-2 monolayer was bathed on both sides with solution containing 1 mmol/l mannitol and 1 mmol/l polyethylene glycol (PEG). Paracellular markers [^{3}H]mannitol (Amersham; molecular weight 180; molecular radius ~350 pm) and [^{14}C]PEG (Amersham; molecular weight 4,000; molecular radius ~2.5 nm) were added in the bathing solution to obtain final specific activities of 750 and 500 mCi/mol, respectively. Transepithelial mannitol flux and PEG flux were then measured.

In an Ussing chamber, the Caco-2 monolayer was directly exposed on the basolateral side for 60 min to 600 ng/ml recombinant human PRL (rhPRL) (purity >97%; catalog no. 682-PL; R&D Systems, Minneapolis, MN), which is the maximal effective concentration reported by Jantarajit et al. (25), or rhPRL plus inhibitors, which were an RNA polymerase II inhibitor [50 μmol/l 5,6-dichloro-1-β-D-ribobenzimidazole (DRB); Calbiochem, La Jolla, CA], a panspecific PKC inhibitor (0.8 or 1 μmol/l GF-109203X; A. G. Scientific, San Diego, CA), and a selective ROCK inhibitor (1 μmol/l Y-27632; Calbiochem).

Permeability measurement. Permeability of sodium (P_{Na}) and chloride (P_{Cl}) were determined by the dilution potential technique, modified from the methods of Kahle et al. (26) and Hou et al. (23). In brief, Caco-2 monolayer was equilibrated for 20 min in normal bathing solution containing 145 mmol/l NaCl before the apical solution was replaced with 72.5 mmol/l NaCl-containing solution. Osmolality was maintained by an equivalent amount of mannitol. Changes in the electrical parameters before and after solution replacement were recorded until stable. The ion permeability ratio (P_{Na}/P_{Cl}) was calculated from the dilution potential (V_δ) with *Eq. 3* (45)

$$V_\delta = \frac{RT}{F} \ln \frac{P_{Na} C_a + P_{Cl} C_b}{P_{Na} C_b + P_{Cl} C_a} \quad (3)$$

where P_{Na} is the absolute permeability of sodium; P_{Cl} is the absolute permeability of chloride; C_a is the apical NaCl concentration; C_b is the basolateral NaCl concentration; and R, T, and F are the gas constant, temperature, and the Faraday constant.

When given $\rho = P_{Na}/P_{Cl}$, $\phi = C_b/C_a$, and $\nu = FV_\delta/RT$, *Eq. 3* is rewritten as

$$\rho = (\phi - e^\nu)/(\phi e^\nu - 1) \quad (4)$$

According to the Kimizuka-Koketsu equation (31),

$$G = \frac{F^2}{RT}(P_{Na} C_b + P_{Cl} C_a) \quad (5)$$

where G is the transepithelial conductance and P_{Na} and P_{Cl} are calculated from G and ρ by using *Eqs. 6* and *7*, respectively.

$$P_{Na} = \frac{GRT}{C_a F^2} \times \frac{\rho}{1+\rho} \quad (6)$$

$$P_{Cl} = P_{Na}/\rho \quad (7)$$

To study the permeability ratios of metal ions in the Group 1 series (alkali metals), i.e., P_X/P_{Cl} (X^+ is Li^+, Na^+, K^+, Rb^+, or Cs^+ in the form of chloride salt; all purchased from Sigma), Na^+ as the primary conductor in the bathing solution was substituted with X^+, while pH was maintained with 10 mmol/l HEPES (Sigma). The solution used was titrated with 1 mol/l mannitol until the osmolality of 290 mosmol/kgH_2O was obtained. During the experimental period, the Caco-2 monolayer was equilibrated for 20 min in normal bathing solution containing 145 mmol/l NaCl before the apical solution was replaced with 100 mmol/l X^+-containing solution. Thereafter, the concentration of X^+ was diluted to 50 mmol/l to create diffusion (dilution) potential. P_X/P_{Cl} was calculated as described previously (45).

Calcium permeability (P_{Ca}) of the Caco-2 monolayer via the paracellular pathway was calculated from *Eq. 8* (12)

$$P_{Ca} = J_{Ca}/\Delta C \quad (8)$$

where J_{Ca} is the paracellular passive calcium flux and ΔC is the difference between the apical and basolateral calcium concentrations.

In some experiments, the monolayer was exposed to 1 μmol/l GF-109203X, 1 μmol/l Y-27632, or 75 μmol/l LY-294002 (PI3K inhibitor; Tocris Bioscience, Bristol, UK).

Statistical analyses. Results are expressed as means ± SE. Two sets of data were compared with the unpaired Student's *t*-test. Multiple comparisons were performed by one-way analysis of variance (ANOVA) with Dunnett's posttest. Linear regression with slope analysis was performed to obtain the apical calcium concentration-calcium flux and TER relationships. Nonlinear regression was performed with the one-phase exponential decay equation to demonstrate the Δcalcium-calcium permeability relationship as previously described (12). The level of significance for all statistical tests was $P < 0.05$. Data were analyzed by GraphPad Prism 4.0 for Mac OS X (GraphPad Software, San Diego, CA).

RESULTS

Nongenomic action of PRL on transcellular active calcium transport involves PKC and ROCK pathways. As shown in Fig. 1, 600 ng/ml rhPRL significantly stimulated the transcellular active calcium transport in Caco-2 monolayer from the control value of 9.22 ± 0.48 ($n = 10$) to 18.04 ± 0.51 nmol·h^{-1}·cm^{-2} ($n = 12$, $P < 0.01$). PRL concurrently decreased the TER of the monolayer by ~30% (Table 2). Here, 50 μmol/l DRB, a classic RNA polymerase II inhibitor, was used to inhibit gene transcription. DRB has been used to demonstrate nongenomic effects of several hormones, including vitamin D (43). Since the effect of PRL occurred within 60 min and was not inhibited by DRB, PRL exerted its rapid action via nongenomic signaling pathway(s).

In the presence of 0.8 μmol/l GF-109203X (PKC inhibitor) and 1 μmol/l Y-27632 (ROCK inhibitor), the effect of PRL on the transcellular active calcium transport was diminished (Fig. 1), while only Y-27632 inhibited the action of PRL on the TER (Table 2), suggesting that both PKC and ROCK pathways were involved in the signal transduction of PRL. A higher concentration of GF-109203X, i.e., 1 μmol/l, was used to confirm that

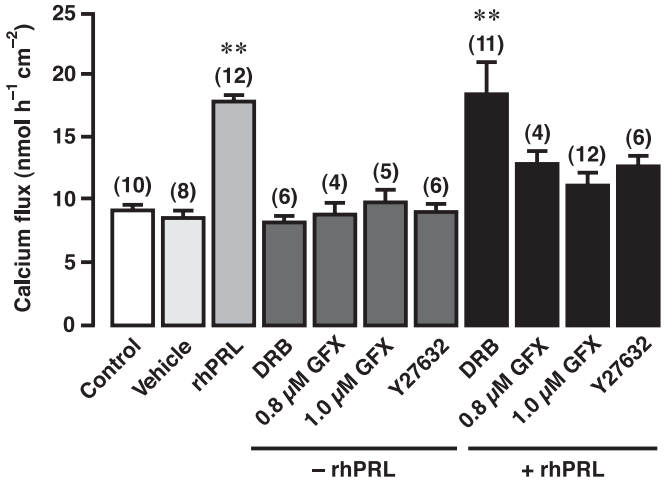

Fig. 1. Transcellular active calcium fluxes in Caco-2 monolayer exposed to RNA polymerase II inhibitor (50 μmol/l 5,6-dichloro-1-β-D-ribobenzimidazole; DRB), protein kinase C (PKC) inhibitor (0.8 and 1 μmol/l GF-109203X; GFX), or RhoA-associated coiled-coil forming kinase (ROCK) inhibitor (1 μmol/l Y-27632) in the presence (+rhPRL) or absence (−rhPRL) of 600 ng/ml recombinant human prolactin (rhPRL). DMSO 0.3% (vol/vol) was used as vehicle for preparation of inhibitors. $^{**}P < 0.01$ compared with control group. Numbers in parentheses represent the number of independent Snapwells.

inhibition of PKC completely abolished the effect of PRL on the transcellular calcium transport. Neither inhibitor alone nor 0.3% (vol/vol) DMSO, a vehicle for the preparation of inhibitors, had an effect on the transcellular active calcium flux or TER (Fig. 1).

PRL stimulates paracellular passive calcium transport via ROCK pathway. The relationship between apical calcium concentrations (C_{Ca}), which created the transepithelial calcium gradient (Δcalcium), and calcium flux (J_{Ca}) in Caco-2 monolayer shows linearity ($r^2 = 0.964$, Fig. 2, *A* and *B*). J_{Ca} under this condition represents the Δcalcium gradient-dependent paracellular passive transport. After exposure to rhPRL, J_{Ca} at all C_{Ca} (1.25–80 mmol/l) were significantly increased compared with their respective controls ($r^2 = 0.956$, $P < 0.01$). The slope, but not the *y*-intercept, of the PRL-exposed graph is higher than that of the control, i.e., 3.76 ± 0.13 vs. 6.41 ± 0.24 × 10^{-3} cm/h ($P < 0.001$). Interestingly, incubation of Caco-2 monolayer with rhPRL plus 1 μmol/l GF-109203X did not affect the paracellular passive calcium transport (Fig. 2*A*), whereas Y-27632 completely abolished the effect of PRL on this mode of calcium transport (Fig. 2*B*). In addition, rhPRL increased the paracellular P_{Ca}, and this effect was abolished by Y-27632 but not 1 μmol/l GF-109203X (Fig. 2, *C* and *D*).

Since tight junctions of several epithelia, as an array of channellike structures, show a conductance block after exposure to divalent cations, including calcium (49), we measured the TER of the monolayer in the presence of transepithelial calcium gradient. As depicted in Fig. 3, increases in apical C_{Ca} led to an increase in TER with linear correlation ($r^2 = 0.882$). Exposure to rhPRL, on the other hand, decreased the TER of the monolayer ($P < 0.01$) compared with the corresponding control values at the respective C_{Ca}. However, the TER of the PRL-exposed monolayer was still increased with the apical C_{Ca} ($r^2 = 0.842$). The slopes of both regression lines are significantly different, i.e., 6.71 ± 0.43 vs. 3.67 ± 0.28 Ω·cm^2·l·mmol^{-1} ($P < 0.001$). A reduction in TER after PRL exposure explained the PRL-stimulated paracellular passive calcium transport.

The ROCK inhibitor (Fig. 3*B*), but not the PKC inhibitor (Fig. 3*A*), abolished the effect of PRL on the apical calcium-induced alteration in TER. Since we recently reported (25) that PI3K inhibitor (75 μmol/l LY-294002) also compromised the paracellular passive calcium transport in Caco-2 monolayer, the effect of this inhibitor on the apical calcium-induced alteration in TER was also examined. Figure 3*C* shows that PI3K inhibitor, similar to ROCK inhibitor, totally abolished the effect of PRL on TER. Inhibitor alone or 0.3% (vol/vol) DMSO had no effect on the paracellular passive calcium transport and did not alter TER (data not shown).

PRL alters charge-selective property of paracellular pathway via ROCK pathway. Increased paracellular transport of calcium is usually associated with alterations in the size- and charge-selective properties of the tight junction, which is the principal barrier for paracellular ion transport (53, 54). However, in the present study, transepithelial fluxes of mannitol and PEG-4000, which are indicators of the widening of the tight junction or change in size selectivity (50), were not affected by PRL (Table 3), suggesting that charge selectivity rather than size selectivity was the determinant of the paracellular transport in the presence of PRL.

The paracellular charge selectivity is determined by P_{Na}, P_{Cl}, and P_{Na}/P_{Cl}. By using the dilution potential technique, we found that rhPRL increased P_{Na} (Fig. 4*A*), but not P_{Cl} (Fig. 4*B*), of Caco-2 monolayer from the control value of 7.81 ± 0.32 ($n = 8$) to 10.96 ± 0.42 × 10^{-6} cm/s ($n = 8$, $P < 0.01$), thereby increasing P_{Na}/P_{Cl} from 3.73 ± 0.23 ($n = 8$) to 8.07 ± 0.82 ($n = 8$, $P < 0.01$) (Fig. 4*C*). The effects of PRL on P_{Na} and P_{Na}/P_{Cl} were completely abolished by Y-27632, but not by 1 μmol/l GF-109203X. Inhibitor alone or vehicle had no effect on the charge selectivity.

Furthermore, we investigated permselectivity of the paracellular pathway to other cations in the alkali metal series with

Table 2. *Epithelial electrical parameters for Caco-2 monolayer*

Condition	*n*	PD, mV	I_{sc}, μA/cm^2	TER, Ω·cm^2
Control	15	0.89±0.12	2.53±0.40	368.17±11.44
Vehicle	10	0.95±0.12	2.40±0.31	381.67±9.11
600 ng/ml rhPRL	15	0.94±0.06	3.67±0.27	255.67±7.10*
Inhibitors				
50 μmol/l DRB	12	0.81±0.11	2.17±0.27	371.53±23.49
1 μmol/l GF-109203X	13	0.95±0.18	2.62±0.47	348.97±19.80
1 μmol/l Y-27632	14	0.63±0.08	2.00±0.30	373.81±18.55
600 ng/ml rhPRL+				
50 μmol/l DRB	14	0.96±0.14	3.71±0.53	261.71±11.52*
1 μmol/l GF-109203X	15	0.79±0.15	3.07±0.51	249.44±13.64*
1 μmol/l Y-27632	14	0.85±0.10	2.29±0.28	377.38±18.54

Values are means ± SE for transepithelial potential difference (PD), short-circuit current (I_{sc}), and transepithelial resistance (TER) in Caco-2 monolayer directly exposed to recombinant human prolactin (rhPRL), RNA polymerase II inhibitor [5,6-dichloro-1-β-D-ribobenzimidazole (DRB)], protein kinase C (PKC) inhibitor (GF-109203X), RhoA-associated coiled-coil forming kinase (ROCK) inhibitor (Y-27632), or rhPRL plus inhibitors. DMSO 0.3% (vol/vol) was used as vehicle for preparation of inhibitors. The monolayer was bathed on both sides with 1.25 mmol/l calcium-containing solution. The apical side was negative with respect to the basolateral side. *$P < 0.01$ vs. control group.

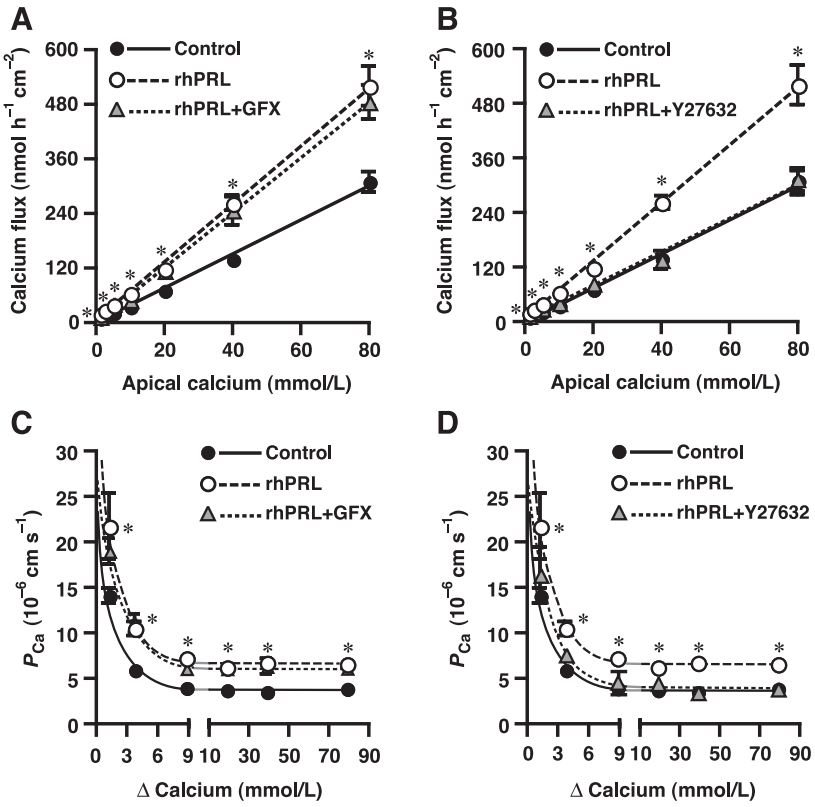

Fig. 2. Gradient-dependent paracellular passive calcium fluxes (*A* and *B*) and calcium permeability (P_{Ca}; *C* and *D*) in Caco-2 monolayer directly exposed to 600 ng/ml rhPRL, PKC inhibitor (1 μmol/l GFX), or ROCK inhibitor (1 μmol/l Y-27632). The apical bathing solution contained a calcium concentration of 1.25, 2.5, 5, 10, 20, 40, or 80 mmol/l. Inhibitors alone or vehicle (DMSO) had no effect on either calcium flux or permeability (data not shown). This experiment was performed on 210 independent Snapwell setups ($n = 5$ per value of apical calcium concentration). Control and rhPRL data in *A* and *C* were reused in panels *B* and *D*, respectively, for better presentation. *$P < 0.01$, control vs. rhPRL.

ionic radii ranging from 90 to 181 pm (ionic radii of Na^+ and Ca^{2+} are 114 and 116 pm, respectively). Under normal conditions, the Caco-2 monolayer showed relative permeability to alkali metal ions as follows: $P_{Na} > P_K > P_{Rb} > P_{Cs} > P_{Li}$ (Fig. 5*A*). rhPRL also increased P_X/P_{Cl} (where X^+ is Li^+, K^+, Rb^+, or Cs^+) of all other alkali metal ions (Fig. 5, *B*, *D–F*), i.e., P_{Li}/P_{Cl} from 1.09 ± 0.02 to 1.86 ± 0.09 ($n = 6$, $P < 0.01$), P_K/P_{Cl} from 2.14 ± 0.07 to 3.41 ± 0.17 ($n = 6$, $P < 0.01$), P_{Rb}/P_{Cl} from 1.75 ± 0.07 to 2.18 ± 0.15 ($n = 6$, $P < 0.01$), and P_{Cs}/P_{Cl} from 1.70 ± 0.03 to 1.91 ± 0.08 ($n = 6$, $P < 0.05$). The effect of PRL on P_X/P_{Cl} was diminished by Y-27632 and LY-294002, but not by 1 μmol/l GF-109203X. Therefore, the PRL-induced alteration in the cationic permselectivity in Caco-2 monolayer involved the ROCK pathway as well as the PI3K pathway.

In another series of experiments, we investigated whether the TER-reducing action of PRL could be applied to other cations of variable sizes. The monolayer was bathed on both sides with solution containing the alkali metal ion of interest, while TER was measured simultaneously. Under control conditions, the TER-ionic radius graph showed a V-shaped relationship, with the lowest TER (or the highest conductance) when Na^+ was used as the primary conductor (Fig. 6). Exposure to PRL significantly decreased TER (or increased ion conductance) no matter which alkali ion was used as the primary conductor. Similar to the permeability studies, this

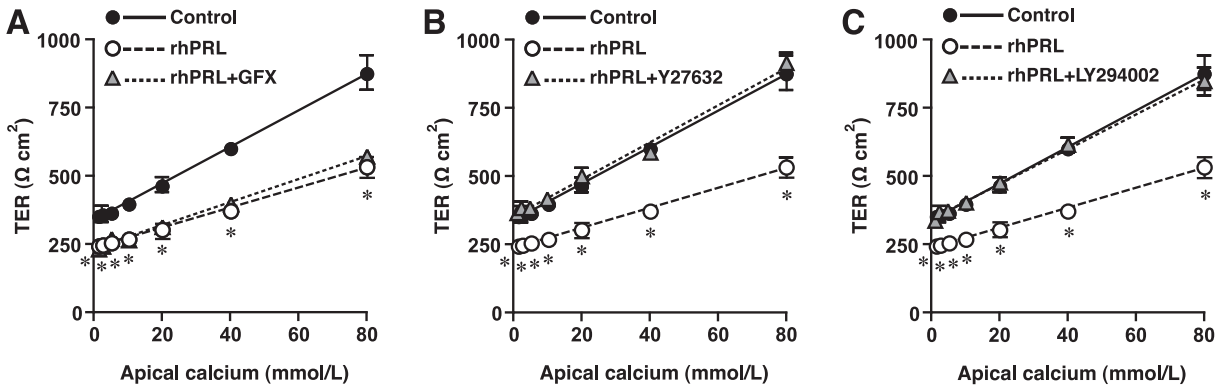

Fig. 3. Effect of 600 ng/ml rhPRL on the relationship between apical calcium concentration and transepithelial resistance (TER) in Caco-2 monolayer ($n = 5$ per value of apical calcium concentration) incubated with PKC inhibitor (1 μmol/l GFX; *A*), ROCK inhibitor (1 μmol/l Y-27632; *B*), or phosphoinositide 3-kinase (PI3K) inhibitor (75 μmol/l LY-294002; *C*). Inhibitors alone or vehicle (DMSO) had no effect on TER (data not shown). Control and rhPRL data in *A* were reused in *B* and *C* for better comparison. *$P < 0.01$, control vs. rhPRL.

Table 3. *Transepithelial mannitol and PEG-4000 fluxes*

Condition	n	Mannitol, nmol·h^{-1}·cm^{-2}	PEG-4000, nmol·h^{-1}·cm^{-2}
Control	7	5.60±0.27	3.89±0.58
600 ng/ml rhPRL	7	5.36±0.34	3.96±0.28

Values are mean ± SE transepithelial fluxes. Caco-2 monolayer was bathed with ^{3}H-labeled mannitol- and ^{14}C-labeled polyethylene glycol (PEG)-containing solution, with or without 600 ng/ml rhPRL. Both mannitol and PEG-4000 are exclusively transported via the paracellular channel and can be used to demonstrate the widening of the tight junction or change in size selectivity.

effect of PRL was abolished by Y-27632 (Fig. 6*B*) and LY-294002 (Fig. 6*C*), but not by 1 μmol/l GF-109203X (Fig. 6*A*).

PRL exerts its stimulatory action on transepithelial calcium transport via PRLR-L. Since PRL normally uses PRLR-L to exert its actions, especially on the mammary gland epithelia (3), we investigated whether PRLR-L is required for the action of PRL in Caco-2 cells with a PRLR-L siRNA knockdown technique. After 48-h incubation with PRLR-L siRNA, expression of PRLR-L mRNA in Caco-2 cells was abolished ($n = 5$, $P < 0.01$) (Fig. 7, *A* and *C*), while the expression of PRLR-S was unaltered (Fig. 7, *A* and *B*). The siPORT used as a transfection reagent had no effect on the expression of PRLR-L or PRLR-S. Amplicon sequencing confirmed the results of qRT-PCR.

In the Ussing chamber experiments (Fig. 8), the PRLR-L knockdown monolayer (siPORT+, siRNA+) exhibited transcellular active calcium flux and electrical properties comparable to those of the control (siPORT−, siRNA−) or siPORT-treated (siPORT+, siRNA−) monolayers (Fig. 8 and Table 4). Similar to the effect of PRL on the normal Caco-2 monolayer in Fig. 1, rhPRL enhanced the transcellular active calcium flux of the siPORT-treated monolayer (siPORT+, siRNA−, rhPRL−) from 9.25 ± 1.08 ($n = 5$) to 17.05 ± 0.65 nmol·h^{-1}·cm^{-2} (siPORT+, siRNA−, rhPRL+) ($n = 5$, $P < 0.01$). The TER of the siPORT-treated monolayer was also decreased by PRL (Table 4). After incubation with PRLR-L siRNA, the PRL-enhanced calcium transport and the PRL-altered TER in Caco-2 monolayer were completely reverted to basal levels. These findings indicated that PRL exerted its stimulatory action on calcium transport in the Caco-2 monolayer via PRLR-L.

DISCUSSION

PRL has been shown to exert both genomic and nongenomic actions on duodenum and proximal jejunum (25, 50, 51). In the present study, the effect of PRL on transepithelial calcium transport in Caco-2 monolayer was nongenomic, since the responses to PRL could be observed within 60 min and were not diminished by 50 μmol/l DRB, which is an inhibitor of gene transcription (43). We also demonstrated that the nongenomic action of PRL was mediated by the PKC and ROCK pathways.

The Caco-2 monolayer is a suitable model for investigating PRL action on transcellular active calcium transport because Caco-2 cells possess functional PRLR and transcellular calcium transporters (19, 25). In the absence of transepithelial calcium gradient, electrogenic transcellular active calcium transport involves the functions of TRPV6, calbindin-D_{9K}, and PMCA (22). We previously showed (11) that PRL stimulated both apical calcium uptake and activity of the basolateral PMCA of purified duodenal membrane vesicles. The present results confirmed that transcellular calcium transport was increased by twofold after exposure to rhPRL, consistent with findings in the duodenal epithelium (25).

Interestingly, the TER of Caco-2 monolayer was decreased by PRL, similar to that observed after exposure to vitamin D, which is an important regulator of calcium absorption (14). Since the PD of the PRL-treated monolayer was not changed, it was conceivable that PRL did not interfere with the electrogenic transcellular sodium transport via Na^+-K^+-ATPases, which, in the absence of chemical gradient and diffusion

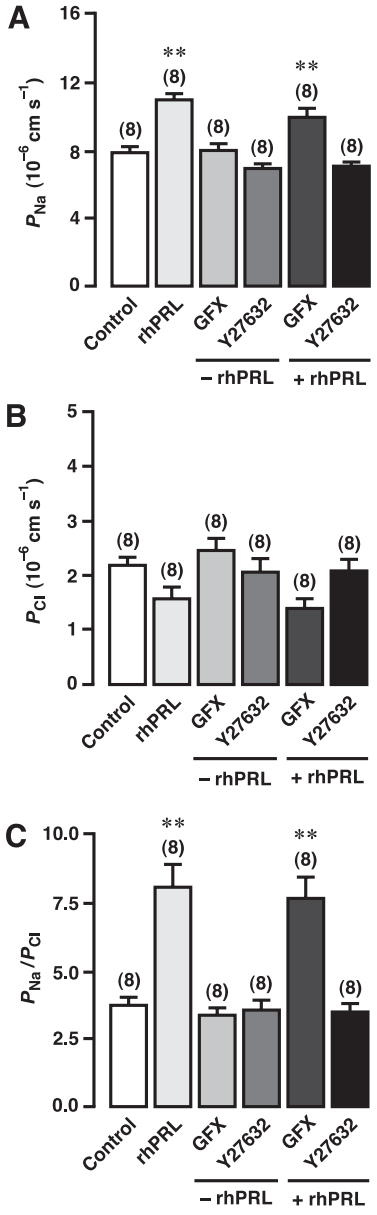

Fig. 4. Effects of rhPRL on sodium permeability (P_{Na}; *A*), chloride permeability (P_{Cl}; *B*), and P_{Na}/P_{Cl} (*C*), which indicate charge-selective property of Caco-2 monolayer. Cells were incubated with PKC inhibitor (1 μmol/l GFX) or ROCK inhibitor (1 μmol/l Y-27632) in the presence (+rhPRL) or absence (−rhPRL) of 600 ng/ml rhPRL. DMSO 0.3% (vol/vol) used as vehicle had no effect on these parameters (data not shown). $^{**}P < 0.01$ compared with control group. Numbers in parentheses represent the number of independent Snapwells.

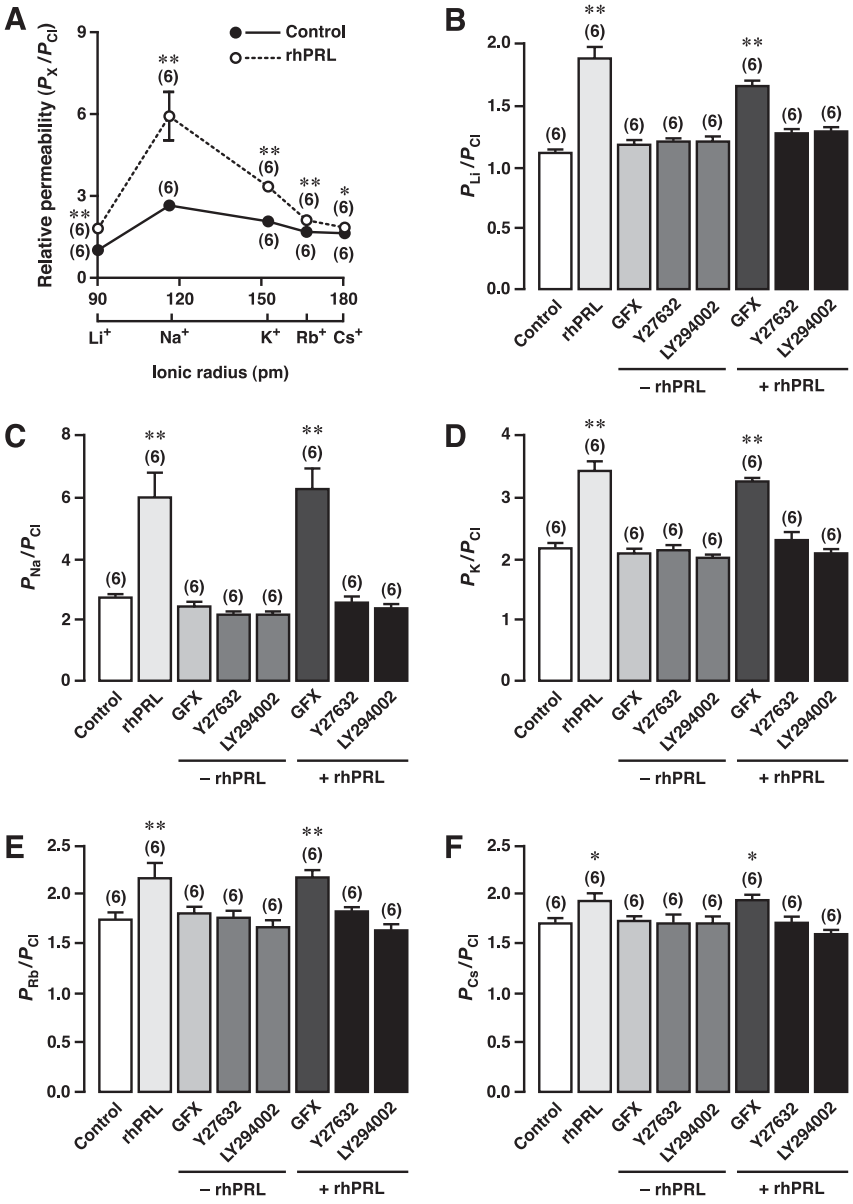

Fig. 5. *A*: effect of 600 ng/ml rhPRL on the relative paracellular permeability of the alkali metal ions over chloride (P_X/P_{Cl}; X = Li^+, Na^+, K^+, Rb^+, or Cs^+) plotted against their ionic radii. *B–F*: P_X/P_{Cl} of Caco-2 monolayer incubated with PKC inhibitor (1 μmol/l GFX), ROCK inhibitor (1 μmol/l Y-27632), or PI3K inhibitor (75 μmol/l LY-294002) in the presence (+rhPRL) or absence (−rhPRL) of 600 ng/ml rhPRL. DMSO 0.3% (vol/vol) used as vehicle had no effect on P_X/P_{Cl} (data not shown). $^*P < 0.05$, $^{**}P < 0.01$ compared with control group. Numbers in parentheses represent the number of independent Snapwells.

potential, contributed up to 95% of the PD (46). Although PRL increased the electrogenic transcellular calcium transport, changes in the PD should be very small and not detectable by the Ussing technique. The PD change ($V_{\Delta,Ca}$) due to the PRL-enhanced transcellular calcium transport, if present, could be estimated from the TER and the difference ($J_{\Delta,Ca}$) between the control (9.22 nmol·h^{-1}·cm^{-2}) and PRL-exposed (18.04 nmol·h^{-1}·cm^{-2}) fluxes, i.e., $V_{\Delta,Ca} = J_{\Delta,Ca}zF \times$ TER (z = +2, F = 96,485.34 C/mol, TER = 255.67 Ω·cm^2). Hence $V_{\Delta,Ca}$ was 120.88 μV, which could be considered negligible. When the monolayer was short-circuited, the external current (I_{sc}) moved across the monolayer via the low-resistance pathway, i.e., the paracellular pathway (20). Therefore, a decrease in TER that was calculated from PD and I_{sc} in the presence of PRL must have resulted from the PRL-induced increase in paracellular permeability, and thus enhanced paracellular calcium transport was anticipated.

Little is currently known regarding the paracellular calcium transport in Caco-2 monolayers. Generally, the paracellular passive calcium transport is more physiologically important since it is achieved at a small cost of energy and is nonsaturable (i.e., a graph of apical calcium vs. calcium flux shows linearity) (29). This transport mechanism, which occurs along the entire length of the small intestine, becomes significant when luminal calcium concentration exceeds 5 mmol/l, which is an average luminal calcium concentration in the rat duodenum (12, 55). When the apical calcium concentration was 20 mmol/l, the transcellular calcium flux contributed <10% of the total flux (Fig. 2). Nevertheless, transcellular calcium transport is still important during increased calcium demand, e.g., during pregnancy, lactation, and low calcium intake (8, 10). Here we found that PRL enhanced both transcellular and paracellular calcium transport as well as calcium permeability. The PRL-stimulated paracellular calcium flux at 5 mmol/l apical calcium was

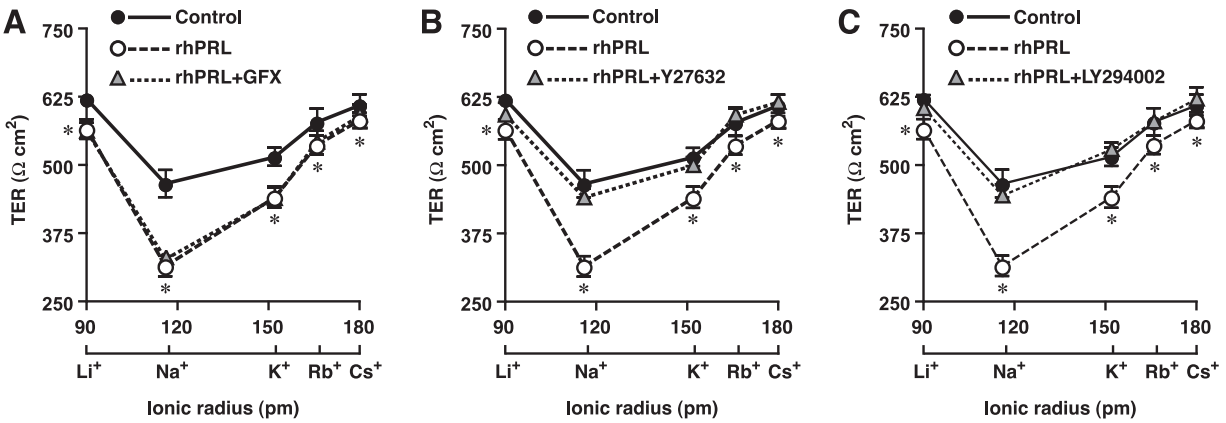

Fig. 6. Alterations of TER after apical Na^+ being substituted with other alkali metal ions. Caco-2 monolayers ($n = 6$ per studied ion) were directly incubated with 600 ng/ml rhPRL with or without PKC inhibitor (1 μmol/l GFX; *A*), ROCK inhibitor (1 μmol/l Y-27632; *B*), or PI3K inhibitor (75 μmol/l LY-294002; *C*). TER values of the monolayer exposed to inhibitors alone or vehicle (DMSO) are comparable to those of control (data not shown). Control and rhPRL data in *A* were reused in *B* and *C*. *$P < 0.01$, control vs. rhPRL.

~2.1-fold higher than that at 1.25 mmol/l calcium in the transcellular study, implicating the physiological significance of the paracellular transport. Moreover, as seen in Fig. 3, an increase in the apical calcium concentration also led to a divalent ion-induced conductance block, i.e., a linear increase in TER, as seen with many conventional ion channels (30, 40). Conductance block is probably caused by binding of calcium to the fixed negative charges of the paracellular proteins (49). A similar effect of high apical calcium has been reported in other epithelia, e.g., MDCK-II monolayer (49). After exposure to PRL, the increase in TER was attenuated, i.e., the paracellular conductance was increased, thus explaining increases in the paracellular calcium flux, calcium permeability, and slope of the apical calcium vs. paracellular calcium flux relationship.

Paracellular conductance and transport of ions can be regulated by changing the size- and/or charge-selective property of the paracellular pathway (32, 54). These properties are determined by different mechanisms (32). Paracellular size restriction, which is between 350 and 540 pm in the Caco-2 monolayer (9), is compromised by the myosin light chain kinase-mediated contraction of the perijunctional actomyosin ring complex and cytoskeletal arrangement (52). However, previous investigation using cytochalasin E, which widens the tight junction by disrupting actin polymerization, suggested that PRL-induced increase in duodenal calcium flux did not involve size selectivity of the paracellular pathway (50). This was confirmed by the present finding of no change in mannitol and PEG fluxes after exposure to PRL. Therefore, it appeared that

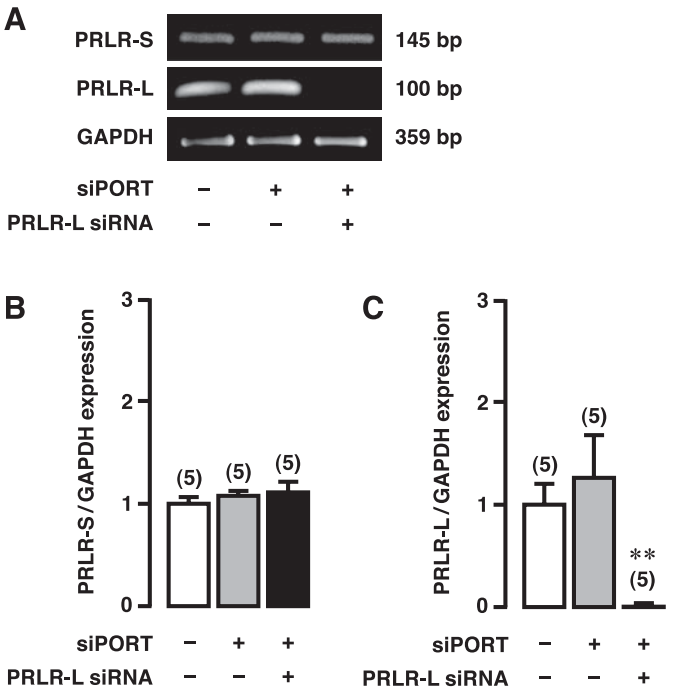

Fig. 7. Representative electrophoretic image (*A*) and quantitative real-time PCR (*B* and *C*) demonstrate expression of short (PRLR-S) and long (PRLR-L) forms of PRL receptor in Caco-2 monolayer incubated for 48 h with siPORT (transfection agent) or siPORT + 1 nmol/l PRLR-L short interference RNA (siRNA). The absence of PRLR-L expression confirms the success of PRLR-L knockdown. **$P < 0.01$ compared with control group (−siPORT/−siRNA). Numbers in parentheses represent the number of independent Snapwells.

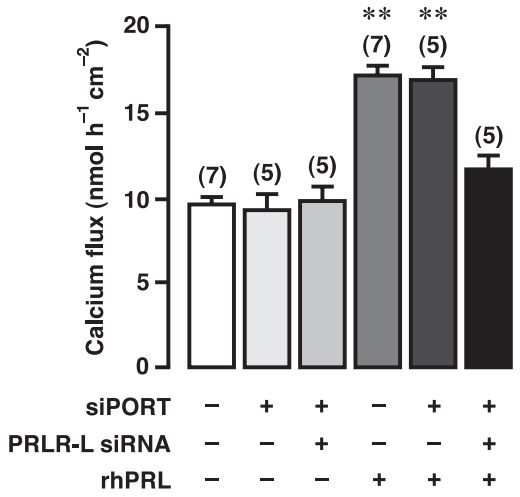

Fig. 8. Transcellular active calcium fluxes in Caco-2 monolayer exposed to 600 ng/ml rhPRL, siPORT (transfection agent), and/or 1 nmol/l siRNA targeting PRLR-L. **$P < 0.01$ compared with control group (−siPORT, −siRNA, −rhPRL). Numbers in parentheses represent the number of independent Snapwells.

Table 4. *Epithelial electrical parameters for PRLR-L knockdown experiment*

Condition	*n*	PD, mV	I_{sc}, μA/cm^2	TER, Ω·cm^2
Control	7	0.74±0.10	2.00±0.31	395.24±11.90
siPORT	5	0.64±0.12	2.00±0.32	390.00±29.15
siPORT+siRNA	5	0.80±0.13	2.00±0.32	400.00±15.81
rhPRL	7	0.83±0.06	3.14±0.26	258.10±12.12*
rhPRL+siPORT	5	0.72±0.19	3.40±0.68	206.67±22.11*
rhPRL+siPORT+siRNA	5	0.88±0.13	2.40±0.40	376.67±24.49

Values are means ± SE for transepithelial PD, I_{sc}, and TER in Caco-2 monolayer exposed to 600 ng/ml rhPRL, siPORT (transfection agent), and/or 1 nmol/l short interference RNA (siRNA) targeting PRLR-L. The monolayer was bathed on both sides with 1.25 mmol/l calcium-containing solution. The apical side was negative with respect to the basolateral side. *$P < 0.01$ vs. control group.

the epithelial charge selectivity, but not the size selectivity, regulated the intestinal paracellular calcium transport. Generally, charge selectivity is defined by fixed negative or positive charges on the extracellular loops of tight junction proteins of the claudin family, which provide a hindrance for the permeation of ions with the opposite charge (32). Expressions of some claudins are associated with increased calcium permeability. For example, claudin-16 is widely recognized to be important for paracellular calcium and magnesium reabsorption in the thick ascending limb of the loop of Henle (17). Expression of claudin-3 in the duodenum is under the regulation of vitamin D (34), a hormone that also stimulates paracellular calcium transport (14). However, it is not known whether PRL alters the functions or localization of claudins in the Caco-2 monolayer and intestinal epithelia.

To access the charge-selective property of the Caco-2 monolayer, we used P_{Na}/P_{Cl} as an indicator. Under control conditions, a P_{Na}/P_{Cl} of 3.73 is comparable to those previously reported in Caco-2 monolayer (9) and small intestine (12, 41), indicating that these epithelia are more permeable to cations than anions. In contrast, normal colonic epithelium is more permeable to anions (16). It is noteworthy that the paracellular selectivity causes sodium and chloride movement to deviate from the mobility ratio of ~0.6 in free solution (20, 41). In addition, permeabilities of other cations in the alkali metal series, i.e., Li^+, K^+, Rb^+, and Cs^+, are also greater than that of Cl^-, and comply with Eisenman sequence VII (i.e., $P_{Na} > P_K > P_{Rb} > P_{Cs} > P_{Li}$) (for review, see Ref. 18). Similar to that reported in other epithelia (49), the conductance (reciprocal of TER) of the paracellular pathway was greatest when NaCl was used as the primary conductor, as seen in the ionic radius vs. TER curve, which showed a V-shaped relationship (Fig. 6). Such patterns were not altered by PRL. Although the paracellular pathway of the Caco-2 monolayer manifests a selective property similar to that of typical ion channels, whereby an ion current is not simply determined by the ionic or hydrated size of the ion, PRL enhanced the paracellular permeability of both sodium and calcium, which are of comparable ionic sizes. Our findings that PRL increased P_{Na} and permeability to other alkali metal ions, but not P_{Cl}, suggested that PRL could increase the activity of the paracellular proteins with fixed negative charges by an unknown mechanism, thereby enhancing paracellular conductance, calcium permeability, and paracellular calcium transport.

PRL exerts its functions by binding to the membrane-bound PRLRs with a ratio of PRL to PRLRs of 1:2 (3). Two isoforms of PRLRs, i.e., PRLR-S and -L, have been identified in intestinal absorptive cells and Caco-2 cells (25). Investigations in mammary epithelia demonstrated that signal transduction of PRL was transferred by PRLR-L, whereas PRLR-S silenced PRL actions because it lacks the cytoplasmic tails required to activate downstream pathways (3, 6, 24, 42). On the other hand, PRLR-S may transmit PRL signals in the liver and endothelial cells (24, 44). In the PRLR-L knockdown Caco-2 monolayer, which expressed a normal level of PRLR-S, the effects of PRL on transcellular calcium transport and TER were totally abolished, indicating that actions of PRL are primarily mediated by PRLR-L.

Despite strong evidence pertaining to PRL-stimulated intestinal calcium absorption (10), little is known regarding PRL signal transduction in the intestinal epithelia and the Caco-2 monolayer. In mammary epithelia, PRL binding to PRLRs triggers dimerization of PRLRs, leading to activation of the putative JAK2 signaling (3). However, our recent investigation (25) elucidated that the PI3K pathway, but not the JAK2 pathway, is involved in the PRL-enhanced transcellular and paracellular calcium transport. The present data clearly showed that the PI3K pathway was involved in the rapid effects of PRL on the paracellular permeability to alkali metal ions and TER. Signal transduction of PRL via PI3K has also been reported in liver, pancreas, and T-lymphoma Nb2 cells (1, 7, 56). The PI3K pathway covers a large number of downstream targets, including PKC and ROCK (21). The Rho-related pathway was found to be associated with PRL signaling in endothelial cells (35), while the PKC pathway mediated PRL actions in cholangiocytes (48), adrenocortical cells (27), and the intestine, in which PKC enhanced intestinal calcium transport (4). Activation of the ROCK pathway increased paracellular permeability in several epithelia, such as brain endothelium and renal proximal tubule (28, 47). PKC-ROCK cross talk could also affect paracellular permeability in endothelial cells (47). Therefore, in the present study we focused on the PKC- and ROCK-mediated PRL actions in Caco-2 cells and were able to demonstrate that the ROCK pathway mediated PRL actions on transcellular and paracellular calcium transport, calcium permeability, charge selectivity, and TER. On the other hand, inhibition of the PKC pathway could only diminish transcellular calcium transport. Nevertheless, further investigations are required to demonstrate the detailed molecular mechanisms of PKC- and ROCK-mediated PRL actions in Caco-2 monolayer.

In conclusion, we provide evidence, for the first time, that PRL exerts its nongenomic stimulatory action on transcellular active calcium transport in the Caco-2 monolayer via the PKC and ROCK pathways. PRL also increased paracellular permeability and decreased TER via the ROCK pathway, thereby enhancing paracellular passive calcium transport. Moreover, PRL-induced increase in paracellular transport was by altering epithelial charge selectivity rather than size selectivity. The actions of PRL were mediated by the long isoform of PRLR. Our findings elaborate possible mechanisms of the PRL-stimulated intestinal calcium transport, which has long been reported in the rat (10).

GRANTS

This research was supported by grants from the Royal Golden Jubilee Program (PHD48K0063 to N. Thongon), the Mahidol University Postdoctoral Fellowship Program (to L-I. Nakkrasae), the Commission on Higher Education, and the Thailand Research Fund (RSA5180001 to N. Charoenphandhu and RTA5080008 to N. Krishnamra).

REFERENCES

1. **Amaral ME, Cunha DA, Anhê GF, Ueno M, Carneiro EM, Velloso LA, Bordin S, Boschero AC.** Participation of prolactin receptors and phosphatidylinositol 3-kinase and MAP kinase pathways in the increase in pancreatic islet mass and sensitivity to glucose during pregnancy. *J Endocrinol* 183: 469–476, 2004.
2. **Arbogast LA, Voogt JL.** Endogenous opioid peptides contribute to suckling-induced prolactin release by suppressing tyrosine hydroxylase activity and messenger ribonucleic acid levels in tuberoinfundibular dopaminergic neurons. *Endocrinology* 139: 2857–2862, 1998.
3. **Bachelot A, Binart N.** Reproductive role of prolactin. *Reproduction* 133: 361–369, 2007.
4. **Balogh G, de Boland AR, Boland R.** Influence of age on 1,25$(OH)_2$-vitamin D_3 activation of protein kinase C in rat duodenum. *Mol Cell Endocrinol* 129: 127–133, 1997.
5. **Banan A, Zhang LJ, Shaikh M, Fields JZ, Choudhary S, Forsyth CB, Farhadi A, Keshavarzian A.** θ Isoform of protein kinase C alters barrier function in intestinal epithelium through modulation of distinct claudin isotypes: a novel mechanism for regulation of permeability. *J Pharmacol Exp Ther* 313: 962–982, 2005.
6. **Berlanga JJ, Garcia-Ruiz JP, Perrot-Applanat M, Kelly PA, Edery M.** The short form of the prolactin (PRL) receptor silences PRL induction of the β-casein gene promoter. *Mol Endocrinol* 11: 1449–1457, 1997.
7. **Bishop JD, Nien WL, Dauphinee SM, Too CK.** Prolactin activates mammalian target-of-rapamycin through phosphatidylinositol 3-kinase and stimulates phosphorylation of p70S6K and 4E-binding protein-1 in lymphoma cells. *J Endocrinol* 190: 307–312, 2006.
8. **Boass A, Lovdal JA, Toverud SU.** Pregnancy- and lactation-induced changes in active intestinal calcium transport in rats. *Am J Physiol Gastrointest Liver Physiol* 263: G127–G134, 1992.
9. **Carr G, Haslam IS, Simmons NL.** Voltage dependence of transepithelial guanidine permeation across Caco-2 epithelia allows determination of the paracellular flux component. *Pharm Res* 23: 540–548, 2006.
10. **Charoenphandhu N, Krishnamra N.** Prolactin is an important regulator of intestinal calcium transport. *Can J Physiol Pharmacol* 85: 569–581, 2007.
11. **Charoenphandhu N, Limlomwongse L, Krishnamra N.** Prolactin directly enhanced Na^+/K^+- and Ca^{2+}-ATPase activities in the duodenum of female rats. *Can J Physiol Pharmacol* 84: 555–563, 2006.
12. **Charoenphandhu N, Tudpor K, Pulsook N, Krishnamra N.** Chronic metabolic acidosis stimulated transcellular and solvent drag-induced calcium transport in the duodenum of female rats. *Am J Physiol Gastrointest Liver Physiol* 291: G446–G455, 2006.
13. **Charoenphandhu N, Wongdee K, Tudpor K, Pandaranandaka J, Krishnamra N.** Chronic metabolic acidosis upregulated claudin mRNA expression in the duodenal enterocytes of female rats. *Life Sci* 80: 1729–1737, 2007.
14. **Chirayath MV, Gajdzik L, Hulla W, Graf J, Cross HS, Peterlik M.** Vitamin D increases tight-junction conductance and paracellular Ca^{2+} transport in Caco-2 cell cultures. *Am J Physiol Gastrointest Liver Physiol* 274: G389–G396, 1998.
15. **D'Souza T, Indig FE, Morin PJ.** Phosphorylation of claudin-4 by PKCε regulates tight junction barrier function in ovarian cancer cells. *Exp Cell Res* 313: 3364–3375, 2007.
16. **Davis GR, Santa Ana CA, Morawski SG, Fordtran JS.** Permeability characteristics of human jejunum, ileum, proximal colon and distal colon: results of potential difference measurements and unidirectional fluxes. *Gastroenterology* 83: 844–850, 1982.
17. **Efrati E, Arsentiev-Rozenfeld J, Zelikovic I.** The human paracellin-1 gene (*hPCLN-1*): renal epithelial cell-specific expression and regulation. *Am J Physiol Renal Physiol* 288: F272–F283, 2005.
18. **Eisenman G, Horn R.** Ionic selectivity revisited: the role of kinetic and equilibrium processes in ion permeation through channels. *J Membr Biol* 76: 197–225, 1983.
19. **Fleet JC, Eksir F, Hance KW, Wood RJ.** Vitamin D-inducible calcium transport and gene expression in three Caco-2 cell lines. *Am J Physiol Gastrointest Liver Physiol* 283: G618–G625, 2002.
20. **Greger R.** Epithelial transport. In: *Comprehensive Human Physiology: From Cellular Mechanisms to Integration*, edited by Greger R, Windhorst U. Berlin: Springer, 1996.
21. **Hirsch E, Costa C, Ciraolo E.** Phosphoinositide 3-kinases as a common platform for multi-hormone signaling. *J Endocrinol* 194: 243–256, 2007.
22. **Hoenderop JG, Nilius B, Bindels RJ.** Calcium absorption across epithelia. *Physiol Rev* 85: 373–422, 2005.
23. **Hou J, Paul DL, Goodenough DA.** Paracellin-1 and the modulation of ion selectivity of tight junctions. *J Cell Sci* 118: 5109–5118, 2005.
24. **Jahn GA, Daniel N, Jolivet G, Belair L, Bole-Feysot C, Kelly PA, Djiane J.** In vivo study of prolactin (PRL) intracellular signalling during lactogenesis in the rat: JAK/STAT pathway is activated by PRL in the mammary gland but not in the liver. *Biol Reprod* 57: 894–900, 1997.
25. **Jantarajit W, Thongon N, Pandaranandaka J, Teerapornpuntakit J, Krishnamra N, Charoenphandhu N.** Prolactin-stimulated transepithelial calcium transport in duodenum and Caco-2 monolayer are mediated by the phosphoinositide 3-kinase pathway. *Am J Physiol Endocrinol Metab* 293: E372–E384, 2007.
26. **Kahle KT, Macgregor GG, Wilson FH, Van Hoek AN, Brown D, Ardito T, Kashgarian M, Giebisch G, Hebert SC, Boulpaep EL, Lifton RP.** Paracellular Cl^- permeability is regulated by WNK4 kinase: insight into normal physiology and hypertension. *Proc Natl Acad Sci USA* 101: 14877–14882, 2004.
27. **Kaminska B, Ciereszko RE, Opalka M, Dusza L.** Prolactin signaling in porcine adrenocortical cells: involvement of protein kinases. *Domest Anim Endocrinol* 23: 475–491, 2002.
28. **Kapus A, Szászi K.** Coupling between apical and paracellular transport processes. *Biochem Cell Biol* 84: 870–880, 2006.
29. **Karbach U.** Paracellular calcium transport across the small intestine. *J Nutr* 122: 672–677, 1992.
30. **Kerschbaum HH, Cahalan MD.** Monovalent permeability, rectification, and ionic block of store-operated calcium channels in Jurkat T lymphocytes. *J Gen Physiol* 111: 521–537, 1998.
31. **Kimizuka H, Koketsu K.** Ion transport through cell membrane. *J Theor Biol* 6: 290–305, 1964.
32. **Krause G, Winkler L, Mueller SL, Haseloff RF, Piontek J, Blasig IE.** Structure and function of claudins. *Biochim Biophys Acta* 1778: 631–645, 2008.
33. **Krishnamra N, Wirunrattanakij Y, Limlomwongse L.** Acute effects of prolactin on passive calcium absorption in the small intestine by in vivo perfusion technique. *Can J Physiol Pharmacol* 76: 161–168, 1998.
34. **Kutuzova GD, DeLuca HF.** Gene expression profiles in rat intestine identify pathways for 1,25-dihydroxyvitamin D_3 stimulated calcium absorption and clarify its immunomodulatory properties. *Arch Biochem Biophys* 432: 152–166, 2004.
35. **Lee SH, Kunz J, Lin SH, Yu-Lee LY.** 16-kDa prolactin inhibits endothelial cell migration by down-regulating the Ras-Tiam1-Rac1-Pak1 signaling pathway. *Cancer Res* 67: 11045–11053, 2007.
36. **Little D, Dean RA, Young KM, McKane SA, Martin LD, Jones SL, Blikslager AT.** PI3K signaling is required for prostaglandin-induced mucosal recovery in ischemia-injured porcine ileum. *Am J Physiol Gastrointest Liver Physiol* 284: G46–G56, 2003.
37. **McLaughlin J, Padfield PJ, Burt JP, O'Neill CA.** Ochratoxin A increases permeability through tight junctions by removal of specific claudin isoforms. *Am J Physiol Cell Physiol* 287: C1412–C1417, 2004.
38. **Murphy EF, Hooiveld GJ, Muller M, Calogero RA, Cashman KD.** Conjugated linoleic acid alters global gene expression in human intestinal-like Caco-2 cells in an isomer-specific manner. *J Nutr* 137: 2359–2365, 2007.
39. **Nakane M, Ma J, Rose AE, Osinski MA, Wu-Wong JR.** Differential effects of vitamin D analogs on calcium transport. *J Steroid Biochem Mol Biol* 103: 84–89, 2007.
40. **Nasi E, del Pilar Gomez M.** Divalent cation interactions with light-dependent K channels. Kinetics of voltage-dependent block and requirement for an open pore. *J Gen Physiol* 114: 653–672, 1999.
41. **Powell DW.** Barrier function of epithelia. *Am J Physiol Gastrointest Liver Physiol* 241: G275–G288, 1981.
42. **Qazi AM, Tsai-Morris CH, Dufau ML.** Ligand-independent homo- and heterodimerization of human prolactin receptor variants: inhibitory action of the short forms by heterodimerization. *Mol Endocrinol* 20: 1912–1923, 2006.

43. **Rebsamen MC, Sun J, Norman AW, Liao JK.** 1α,25-Dihydroxyvitamin D_3 induces vascular smooth muscle cell migration via activation of phosphatidylinositol 3-kinase. *Circ Res* 91: 17–24, 2002.
44. **Ricken AM, Traenkner A, Merkwitz C, Hummitzsch K, Grosche J, Spanel-Borowski K.** The short prolactin receptor predominates in endothelial cells of micro- and macrovascular origin. *J Vasc Res* 44: 19–30, 2007.
45. **Salas PJ, López EM.** Validity of the Goldman-Hodgkin-Katz equation in paracellular ionic pathways of gallbladder epithelium. *Biochim Biophys Acta* 691: 178–182, 1982.
46. **Schultz SG, Zalusky R.** Ion transport in isolated rabbit ileum. I. Short-circuit current and Na fluxes. *J Gen Physiol* 47: 567–584, 1964.
47. **Stamatovic SM, Dimitrijevic OB, Keep RF, Andjelkovic AV.** Protein kinase Cα-RhoA cross-talk in CCL2-induced alterations in brain endothelial permeability. *J Biol Chem* 281: 8379–8388, 2006.
48. **Taffetani S, Glaser S, Francis H, DeMorrow S, Ueno Y, Alvaro D, Marucci L, Marzioni M, Fava G, Venter J, Vaculin S, Vaculin B, Lam IP, Lee VH, Gaudio E, Carpino G, Benedetti A, Alpini G.** Prolactin stimulates the proliferation of normal female cholangiocytes by differential regulation of Ca^{2+}-dependent PKC isoforms. *BMC Physiol* 7: 6, 2007.
49. **Tang VW, Goodenough DA.** Paracellular ion channel at the tight junction. *Biophys J* 84: 1660–1673, 2003.
50. **Tanrattana C, Charoenphandhu N, Limlomwongse L, Krishnamra N.** Prolactin directly stimulated the solvent drag-induced calcium transport in the duodenum of female rats. *Biochim Biophys Acta* 1665: 81–91, 2004.
51. **Tudpor K, Charoenphandhu N, Saengamnart W, Krishnamra N.** Long-term prolactin exposure differentially stimulated the transcellular and solvent drag-induced calcium transport in the duodenum of ovariectomized rats. *Exp Biol Med (Maywood)* 230: 836–844, 2005.
52. **Turner JR.** "Putting the squeeze" on the tight junction: understanding cytoskeletal regulation. *Semin Cell Dev Biol* 11: 301–308, 2000.
53. **Van Itallie CM, Anderson JM.** The role of claudins in determining paracellular charge selectivity. *Proc Am Thorac Soc* 1: 38–41, 2004.
54. **Van Itallie CM, Anderson JM.** Claudins and epithelial paracellular transport. *Annu Rev Physiol* 68: 403–429, 2006.
55. **Wasserman RH.** Vitamin D and the dual processes of intestinal calcium absorption. *J Nutr* 134: 3137–3139, 2004.
56. **Yamauchi T, Kaburagi Y, Ueki K, Tsuji Y, Stark GR, Kerr IM, Tsushima T, Akanuma Y, Komuro I, Tobe K, Yazaki Y, Kadowaki T.** Growth hormone and prolactin stimulate tyrosine phosphorylation of insulin receptor substrate-1, -2, and -3, their association with p85 phosphatidylinositol 3-kinase (PI3-kinase), and concomitantly PI3-kinase activation via JAK2 kinase. *J Biol Chem* 273: 15719–15726, 1998.
57. **Yee S.** In vitro permeability across Caco-2 cells (colonic) can predict in vivo (small intestinal) absorption in man—fact or myth. *Pharm Res* 14: 763–766, 1997.
58. **Zweibaum A, Triadou N, Kedinger M, Augeron C, Robine-Leon S, Pinto M, Rousset M, Haffen K.** Sucrase-isomaltase: a marker of foetal and malignant epithelial cells of the human colon. *Int J Cancer* 32: 407–412, 1983.

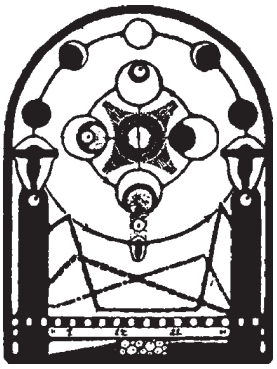

ELSEVIER

Cell Biology International 32 (2008) 1126–1135

Cell Biology International

www.elsevier.com/locate/cellbi

Prolactin decreases the expression ratio of receptor activator of nuclear factor κB ligand/osteoprotegerin in human fetal osteoblast cells

Dutmanee Seriwatanachai [a], Narattaphol Charoenphandhu [a,c,*], Tuangporn Suthiphongchai [b,c], Nateetip Krishnamra [a,c,*]

[a] *Department of Physiology, Faculty of Science, Mahidol University, Rama VI Road, Bangkok 10400, Thailand*
[b] *Department of Biochemistry, Faculty of Science, Mahidol University, Rama VI Road, Bangkok 10400, Thailand*
[c] *Consortium for Calcium and Bone Research, Faculty of Science, Mahidol University, Rama VI Road, Bangkok 10400, Thailand*

Received 18 December 2007; revised 28 March 2008; accepted 30 April 2008

Abstract

Prolactin (PRL) enhanced bone remodeling leading to net bone loss in adult and net bone gain in young animals. Studies in PRL-exposed osteoblasts derived from adult humans revealed an increase in the expression ratio of receptor activator of nuclear factor κB ligand (RANKL) and osteoprotegerin (OPG), thus supporting the previous finding of PRL-induced bone loss in adults. This study thus investigated the effects of PRL on the osteoblast functions and the RANKL/OPG ratio in human fetal osteoblast (hFOB) cells which strongly expressed PRL receptors. After 48 h incubation, PRL increased osteocalcin expression, but had no effect on cell proliferation. However, the alkaline phosphatase activity was decreased in a dose–response manner within 24 h. The effect of PRL on alkaline phosphatase was abolished by LY294002, a phosphoinositide 3-kinase (PI3K) inhibitor. PRL also decreased the RANKL/OPG ratio by downregulating RANKL and upregulating OPG expression, implicating a reduction in the osteoblast signal for osteoclastic bone resorption. It could be concluded that, unlike the osteoblasts derived from adult humans, PRL-exposed hFOB cells exhibited indices suggestive of bone gain, which could explain the in vivo findings in young rats. The signal transduction of PRL in osteoblasts involved the PI3K pathway.

Keywords: Alkaline phosphatase; hFOB; OPG; Osteocalcin; PI3K; Prolactin receptor; RANKL

1. Introduction

Pregnant and lactating mammals use prolactin (PRL) as a calcium-regulating hormone to stimulate intestinal calcium absorption and mobilize calcium from bone for fetal development and milk production (Charoenphandhu and Krishnamra, 2007; Lotinun et al., 1998; Thongon et al., 2008). However, PRL action on calcium metabolism was also reported in non-pregnant/lactating rats, in which PRL induced a positive calcium balance by directly stimulating the intestinal calcium absorption and renal calcium reabsorption (Jantarajit et al., 2007; Piyabhan et al., 2000). Interestingly, young rats were more responsive to PRL than adult and aging rats (Krishnamra et al., 1993; Krishnamra and Seemoung, 1996).

Studies of the in vivo effects of PRL on bone are generally complicated by chronic estrogen deficiency caused by PRL-induced hypogonadism (Wang and Chan, 1982; Wang et al., 1980). However, osteoblasts have been known to express PRL receptors (PRLR), which indicated that bone cells are direct targets of PRL (Coss et al., 2000). Our in vivo studies using bone histomorphometry in adult rats showed that PRL exerted an estrogen-independent action by enhancing bone turnover with a greater effect on bone resorption (Seriwatanachai et al., 2008). At the cellular level, PRL directly decreased osteocalcin expression and alkaline phosphatase activity in an osteoblast cell line (MG-63) derived from an adult human,

* Corresponding authors. Department of Physiology, Faculty of Science, Mahidol University, Rama VI Road, Bangkok 10400, Thailand. Tel./fax: +66 2354 7154.
E-mail addresses: naratt@narattsys.com (N. Charoenphandhu), scnks@mahidol.ac.th (N. Krishnamra).

1065-6995/$ - see front matter © 2008 International Federation for Cell Biology. Published by Elsevier Ltd. All rights reserved.
doi:10.1016/j.cellbi.2008.04.026

thus supporting the in vivo findings of PRL-induced bone loss (Seriwatanachai et al., 2008). Interestingly, the effects of PRL on bone varied with age. In contrast to adult rats (more than 8 weeks old), PRL stimulated calcium deposition and induced net bone gain in femur, tibia and sternum of 3-week-old young rats (Krishnamra and Seemoung, 1996). We therefore hypothesized that, unlike its action in MG-63 osteoblasts derived from adult humans, PRL may increase the cellular activities of osteoblasts derived from young humans leading to bone formation. Although the expression of PRLR in human fetal osteoblast (hFOB) cell lines had not been reported, we herein used differentiated hFOB cells, which had minimal chromosome aberration and exhibited the matrix-producing properties of normal differentiated osteoblasts (Harris et al., 1995; Subramaniam et al., 2002), in the investigation of PRL actions. In addition, undifferentiated hFOB cells have recently been shown to possess multilineage differentiation potential (Yen et al., 2007), suggesting that they retained the characteristics of fetal cells.

Bone turnover is a coupled process of the osteoblastic bone formation and osteoclastic bone resorption. Since osteoclasts did not express PRLR (Coss et al., 2000; Kelly et al., 2001), enhanced bone resorption in hyperprolactinemic rats could be due to changes in the osteoblast-expressed mediators, the receptor activator of nuclear factor κB ligand (RANKL) and osteoprotegerin (OPG). Binding of RANKL to its receptors on osteoclasts stimulated bone resorption, whereas binding to its decoy receptors, OPG, decreased bone resorption (Kostenuik, 2005). Thus, the RANKL/OPG ratio determined osteoclast activity, bone resorption as well as bone turnover (Abdallah et al., 2005; Grimaud et al., 2003; Kostenuik, 2005). Our recent findings of the PRL-induced increase in the RANKL/OPG ratio in MG-63 cells and decrease in the OPG expression in primary osteoblasts from adult rats supported the in vivo report of net bone loss in adult hyperprolactinemic rats (Seriwatanachai et al., 2008). Hence, it was possible that hFOB cells may respond to PRL by decreasing the RANKL/OPG expression ratio.

Nothing is known regarding PRL signaling in osteoblasts. The putative signaling pathway of PRL in mammary epithelia was the Janus kinase (JAK2) pathway (Bole-Feysot et al., 1998), whereas the phosphoinositide 3-kinase (PI3K) pathway was reported in non-mammary tissues, e.g., liver, duodenum, colon, pancreatic islets, and Nb2 lymphoma cells (Amaral et al., 2004; Bishop et al., 2006; Jantarajit et al., 2007; Puntheeranurak et al., 2007; Yamauchi et al., 1998). We recently demonstrated that the PRL-stimulated transepithelial calcium transport in the duodenum was via the PI3K, and not the JAK2 pathway (Jantarajit et al., 2007). Therefore, signal transduction of PRL in osteoblasts may also occur via the PI3K.

The objectives of the present study were (i) to demonstrate the expression of PRLR in hFOB cells; (ii) to study the effect of PRL on functions of hFOB cells, including cell proliferation, osteocalcin expression, and alkaline phosphatase activity; (iii) to show whether there was a change in the expression ratio of RANKL/OPG in PRL-exposed hFOB cells; and (iv) to investigate whether PRL signaling in hFOB cells involved the PI3K pathway.

2. Materials and methods

2.1. Cell culture

Human fetal osteoblast 1.19 (hFOB) cells (ATCC No. CRL-11372), an immortalized cell line, were propagated in DMEM/F-12 media, supplemented with 10% fetal bovine serum (FBS), 100 U/mL penicillin/streptomycin, and 0.25 μL/mL amphotericin B (Sigma, St. Louis, MO, USA). Cells were cultured in 75-cm^2 T-flasks at 37 °C in a 5% CO_2 in air humidified incubator. Culture medium was changed every 2 days, and the cultures were split 1:10 when cells had reached 80% confluence. Cells were counted using a hemocytometer and trypan blue dye exclusion.

Osteoblast-like MG-63 cells (ATCC No. CRL-1427; a kind gift from Dr Suttatip Kamolmatyakul, Prince of Songkla University, Thailand), derived from human osteosarcoma, were cultured in 75-cm^2 T-flasks with α-MEM supplemented with 10% FBS, 100 U/mL penicillin/streptomycin, and 0.25 μL/mL amphotericin B (Sigma). To induce maximal expression of PRLR, 1 μM dexamethasone and 0.1 μM 1,25-$(OH)_2D_3$ (Sigma) were also added to the medium, as previously described (Bataille-Simoneau et al., 1996). Cells were incubated at 37 °C with 5% CO_2, and subcultured according to the ATCC's protocol.

2.2. Immunofluorescent analysis

hFOB cells were cultured on a coverslip at 10^5 cells/coverslip in the presence of 0.2% FBS for 16 h. Cells were fixed for 10 min with 3% paraformaldehyde and 2% sucrose at 25 °C, washed 3 times with PBS, and permeabilized for 5 min with 0.5% Triton X-100 in PBS at 25 °C. Non-specific sites were blocked with 10% FBS for 30 min at room temperature. Samples were then incubated overnight at 4 °C with 1:300 rabbit polyclonal anti-PRLR primary antibody (Santa Cruz Biotechnology, Santa Cruz, CA, USA), and finally with 1:200 Alexa Fluor 488-conjugated goat anti-rabbit secondary antibody (Molecular Probes, Eugene, OR, USA). Images were captured with an inverted fluorescent microscope (model Eclipse TE2000-U; Nikon, Tokyo, Japan).

2.3. Cell proliferation assay

hFOB cells were inoculated in a 96-well culture plate (5000 cells/well). After 48 h incubation with 1, 10, 100, 1000 ng/mL PRL, the culture medium was replaced by a medium containing 10% 3-(4,5-dimethylthiazol-2-yl)-2,5-diphenyltetrazolium bromide (MTT) (Sigma). After 3 h incubation with MTT at 37 °C, the absorbance of each well was determined at 540 nm by a microplate reader (model Multiscan EX; Thermo Labsystems, Cergy-Pontoise, France), as described previously (Mosmann, 1983). The absorbance of control cells was considered to be 100%. The relative proliferation of PRL-exposed cells was presented as a percent of control. Each sample was an average of 6 replications, and the relative proliferation of each n was averaged from 3 independent samples (triplicate).

2.4. Alkaline phosphatase activity assay

MG-63 or hFOB cells were cultured in 6-well culture plates (10^5 cells/well). Alkaline phosphatase activity was determined by the conversion of *p*-nitrophenyl phosphate to *p*-nitrophenol, as previously described (Coss et al., 2000). In brief, cells were washed twice with PBS pH 7.4, and incubated for 1 h with 2 mL solution containing (in mM) 100 Na_2CO_3, 10 $MgCl_2$, 20 *p*-nitrophenyl phosphate (Sigma), pH 10.3. Thereafter, 1 mL of 5 M NaOH was added. Color development was quantified immediately at 410 nm.

2.5. Preparation of total RNA and RT-PCR

As previously described (Charoenphandhu et al., 2007; Seriwatanachai et al., 2008), the total RNA of hFOB cells was prepared by using the RNeasy mini kit (Qiagen, Valencia, CA, USA). Two micrograms of the total RNA were reverse-transcribed with the oligo-dT_{20} primer and SuperScript III kit (Invitrogen, Carlsbad, CA, USA) to cDNA by a thermal cycler (model Minicycler; MJ Research, Watertown, MA, USA). Sense and antisense primers for PRLR, osteocalcin, RANKL, OPG, and glyceraldehyde-3-phosphate dehydrogenase (GAPDH) are shown in Table 1. GAPDH served as a control gene to check the consistency of the reverse transcription and to normalize values between samples. After amplification with Taq polymerase (Qiagen), the PCR products were visualized on a 1% agarose gel stained with 1.0 μg/mL ethidium bromide under a trans-UV system (model Quantity One 2000; BioRad, Hercules, CA, USA). The cycle-band intensity curve was plotted for each gene to obtain an optimal PCR cycle which fell in the exponential phase. For a semi-quantitative analysis, the expression of a studied gene in the control group was considered to be 100%, while that in the experimental group was calculated as a percent change relative to the value of the control group.

2.6. Western blot analysis

hFOB cells were lysed in a lysis buffer (150 mM Tris–HCl pH 7.4, 150 mM NaCl, 0.1% SDS, 1% Triton X-100, 1% Nonidet P-40, protease inhibitor, 1 M NaF, 1 M β-glycerophosphate, 0.5 M Na_3VO_4, 1 M DTT, 1% sodium deoxycholate, and 5 mM EDTA) (Sigma). After 30 min incubation at 4 °C, lysates were sonicated and centrifuged at 12,000 × *g* for 10 min at 4 °C, and heated for 5 min at 95 °C before being loaded on a gel. Proteins (100 μg/well) were separated by sodium dodecylsulfate polyacrylamide gel electrophoresis (SDS-PAGE), and subsequently transferred to a nitrocellulose membrane (Amersham, Buckinghamshire, UK) by electroblotting. Non-specific binding sites on the membrane were blocked for 1 h at room temperature by 5% skim milk in TBS containing 0.1% Tween-20. Membranes were probed overnight at 4 °C with 1:2000 rabbit polyclonal anti-RANKL or anti-OPG primary antibodies (Santa Cruz), and re-probed with 1:5000 mouse anti-β-actin antibody (Santa Cruz). After 1 h incubation at 25 °C with 1:2000 goat anti-rabbit or anti-mouse secondary antibodies (Santa Cruz), blots were visualized using the enhanced chemiluminescence (ECL Plus) kit (Amersham). Expression of each protein in the control group was considered as 100%.

2.7. Experimental protocols

Protocol 1

The objective of this protocol was to determine the expression of PRLR in hFOB cells. Normally, osteoblasts constitutively express PRLR; however, some osteoblastic cell lines, e.g., MG-63 cells, require mediators such as vitamin D or dexamethasone for PRLR expression (Bataille-Simoneau et al., 1996). Therefore, hFOB cells were cultured in the presence of 0.2% and 10% fetal bovine serum (FBS; controls), 0.1 μM 1,25-$(OH)_2D_3$ (Vit D) (Sigma), 1 μM dexamethasone (DEX) (Sigma), or a combination of Vit D and DEX. Expression of PRLR transcripts was determined by RT-PCR, and expression of PRLR proteins was demonstrated by immunofluorescent imaging.

Protocol 2

To investigate the direct effects of PRL on osteoblast functions, hFOB cells were incubated in normal media (control) or medium containing 1, 10, 100 or 1000 ng/mL recombinant human PRL (rhPRL) (purity >97% as determined by SDS-PAGE; R&D Systems, Minneapolis, MN, USA) at 37 °C for

Table 1
Homo sapiens oligonucleotide sequences used in the PCR experiment

Gene	Reference or accession no.	Primer (forward/reverse)	Product length (bp)	Cycle
PRLR	[a]	5′-AAATGTGGCATCTGCAACCGTTTTCAC-3′ 5′-GCACTTGCTTGATGTTGCAGTGAAGTT-3′	1790	30
OC	[a]	5′-GGCCAGGCAGGTGCGAAGC-3′ 5′-GCCAGGCCAGCAGAGCGACAC-3′	271	30
RANKL	[a]	5′-GCCAGTGGGAGATGTTAG-3′ 5′-TTAGCTGCAAGTTTTCCC-3′	486	33
OPG	[a]	5′-GCTAACCTCACCTTCGAG-3′ 5′-TGATTGGACCTGGTTACC-3′	324	22
GAPDH[b]	NM_002046	5′-CACCCACTCCTCCACCTTTG-3′ 5′-CCACCACCCTGTTGCTGTAG-3′	110	20

PRLR, prolactin receptor; OC, osteocalcin; RANKL, receptor activator of nuclear factor κB ligand; OPG, osteoprotegerin; GAPDH, glyceraldehyde-3-phosphate dehydrogenase.

[a] Seriwatanachai et al., 2008.

[b] Custom-design primer.

0, 0.5, 3, 6, 12, 24 and 48 h prior to determination of alkaline phosphatase activity. The maximal suppression of alkaline phosphatase activity by PRL was seen at 48 h similar to that reported previously by Seriwatanachai et al. (2008). Therefore, the 48 h incubation period was used to demonstrate the effects of PRL on osteoblast proliferation and functions, including osteocalcin mRNA expression and RANKL/OPG mRNA and protein expression. Expression of mRNAs and proteins was determined in triplicate by RT-PCR and Western blot analysis, respectively.

Protocol 3

Since one of the signaling pathways of PRL was the PI3K pathway (Jantarajit et al., 2007; Puntheeranurak et al., 2007), this protocol aimed to demonstrate whether PRL affected osteoblast activity via this pathway. hFOB or MG-63 cells were incubated at 37 °C for 48 h with normal media (control) or media containing 0.3% dimethyl sulfoxide (DMSO; vehicle; Sigma), 100 nM LY294002 (PI3K inhibitor; Sigma), 100 ng/mL rhPRL, or 100 ng/mL rhPRL plus 100 nM LY294002. Finally, the alkaline phosphatase activity was determined.

2.8. Statistical analysis

Results are expressed as mean ± SEM. Multiple comparisons were performed by one-way analysis of variance (ANOVA) with Newman–Keuls post-test. The level of significance for all statistical tests was $P < 0.05$. Data were analyzed by GraphPad Prism 4.0 for Mac OS X (GraphPad Software, San Diego, CA, USA).

3. Results

3.1. hFOB cells expressed mRNAs and proteins of PRLR

Our RT-PCR study revealed a constitutive expression of PRLR in hFOB cells under the control condition (Fig. 1A). In contrast to the previous report on MG-63 cells (Seriwatanachai et al., 2008), the expression of PRLR in hFOB cells was not altered by 1,25-$(OH)_2D_3$, dexamethasone or the combination of both. Both agents were known to upregulate PRLR in other osteoblast cell lines, e.g., MG-63 and Saos-2 cells (Bataille-Simoneau et al., 1996). Immunofluorescent analysis confirmed that hFOB cells strongly expressed PRLR proteins (Fig. 1B). These findings indicated that this fetal osteoblast cell line served as a target of PRL.

3.2. PRL upregulated osteocalcin expression in hFOB cells

Since PRL stimulates bone growth and bone calcium deposition in young animals, we studied osteoblast functions that were associated with bone formation. We found that PRL had no effect on hFOB cell proliferation (Fig. 2A). However, 100 and 1000 ng/mL rhPRL increased the expression of osteocalcin mRNA from the control level (100.00 ± 5.74%) to 155.27 ± 13.02% ($n = 5$, $P < 0.05$) and 174.73 ± 12.08 ($n = 5$, $P < 0.01$), respectively. The results implied the stimulatory effect of PRL on osteoblastic functions in fetal osteoblasts.

3.3. PRL decreased alkaline phosphatase activity in hFOB cells

In contrast to the osteocalcin expression, the activity of alkaline phosphatase was decreased by 100 and 1000 ng/mL rhPRL to 83.31 ± 2.97% ($n = 5$, $P < 0.05$) and 77.70 ± 5.07% ($n = 5$, $P < 0.01$), respectively (Fig. 3A). A time-dependent study showed a significant decrease in alkaline phosphatase activity at 24 h after exposure to 1000 ng/mL rhPRL (Fig. 3B).

3.4. PRL decreased the expression ratio of RANKL/OPG in hFOB cells

Effects of rhPRL exposure on the markers of osteoblast-mediated activation of bone resorption are presented in Fig. 4. The expression ratio of RANKL and OPG, both of which were

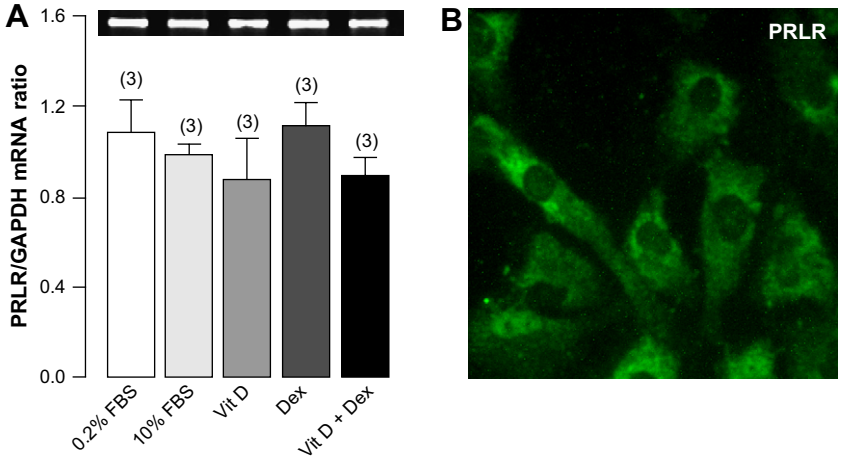

Fig. 1. (A) Expression of PRLR transcripts in hFOB cells exposed for 48 h to 0.2% and 10% fetal bovine serum (FBS, control), 0.1 μM 1,25-$(OH)_2D_3$ (Vit D), 1 μM dexamethasone (DEX), or a combination of Vit D and DEX (Vit D + DEX). A representative electrophoretic image of PRLR is also demonstrated. Numbers in parentheses are numbers of independent flasks. (B) A representative immunofluorescent image showing PRLR protein expression in hFOB cells ($n = 5$), magnification ×400.

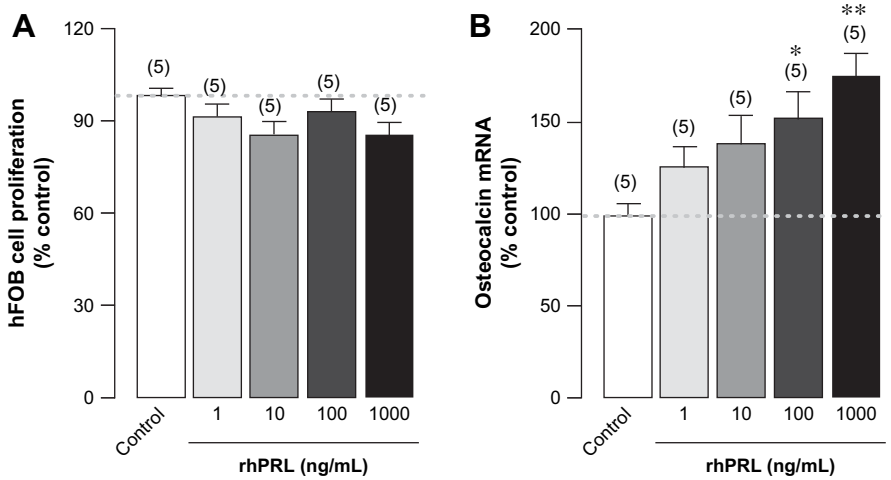

Fig. 2. Dose-dependent changes in (A) cell proliferation and (B) osteocalcin mRNA expression in hFOB cells incubated for 48 h with 1, 10, 100 or 1000 ng/mL rhPRL. Values of the control groups were normalized to 100%. *$P < 0.05$, **$P < 0.01$ compared with the control group. Numbers in parentheses are numbers of independent flasks. Experiments were performed in triplicate.

synthesized by osteoblasts, represented bone resorption (Kostenuik, 2005). Expression of RANKL transcripts were decreased by 10, 100 and 1000 ng/mL rhPRL to 76.56 ± 4.97% ($n = 3, P < 0.05$), 76.81 ± 3.96% ($n = 3, P < 0.05$) and 57.58 ± 7.73% ($n = 3, P < 0.01$) of the control level, respectively, while RANKL protein was decreased by 100 and 1000 ng/mL rhPRL to 71.53 ± 2.79% ($n = 7, P < 0.01$) and 64.78 ± 6.46% ($n = 7, P < 0.01$). Although PRL did not change the expression of OPG transcripts, 100 and 1000 ng/mL rhPRL upregulated expression of OPG protein to 122.96 ± 5.42% ($n = 5, P < 0.05$) and 140.12 ± 7.53% ($n = 5, P < 0.001$), respectively. Therefore, the ratios of RANKL/OPG mRNAs in hFOB cells were significantly decreased by 24, 21 and 43% after 48 h exposure to 10, 100 and 1000 ng/mL rhPRL, respectively, while the ratios of RANKL/OPG proteins were decreased by 41% and 56% after 100 and 1000 ng/mL rhPRL exposure. The decreased RANKL/OPG ratio implicated a suppression of the osteoclast-mediated bone resorption by PRL.

3.5. PRL-mediated decreases in alkaline phosphatase activity in hFOB and MG-63 cells were completely blocked by a PI3K inhibitor

Because the PI3K pathway was one of the signaling pathways of PRL, we investigated whether PRL used this pathway in osteoblasts (i.e., hFOB and MG-63 cells). We found that LY294002, a specific PI3K inhibitor, at concentrations ranging from 10 nM to 1 μM did not affect the viability or the proliferation rate of hFOB and MG-63 cells (Fig. 5A,B). Exposure to 100 ng/mL rhPRL decreased alkaline phosphatase activity in both hFOB and MG-63 cells; however, this PRL action was completely abolished by 100 nM LY294002 (Fig. 5C,D). DMSO, a vehicle for LY294002 preparation, and 100 nM LY294002 alone had no effect on the alkaline phosphatase activity in both cell lines. The results suggested that PRL decreased the osteoblastic alkaline phosphatase activity via the PI3K pathway.

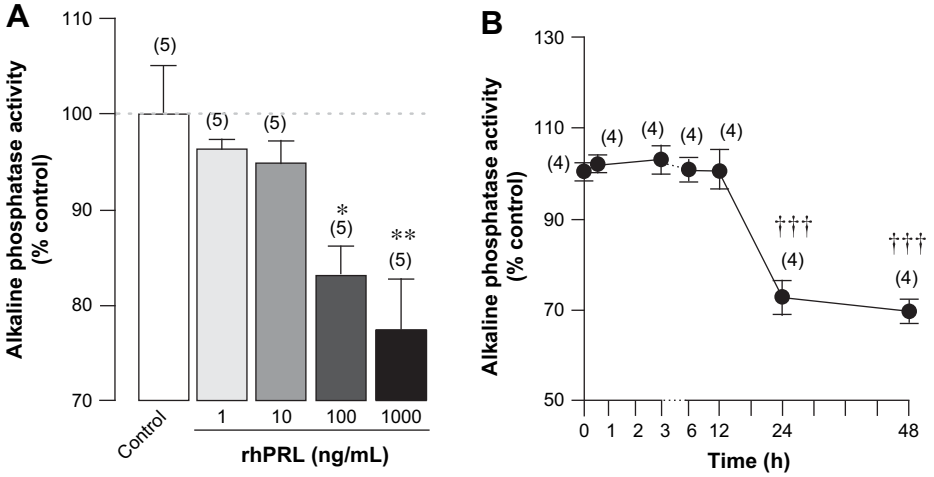

Fig. 3. Dose-dependent changes in alkaline phosphatase activity (A) in hFOB cells incubated for 48 h with 1, 10, 100 or 1000 ng/mL rhPRL. Values of the control groups were normalized to 100%. *$P < 0.05$, **$P < 0.01$ compared with the control group. (B) Time-dependent changes in alkaline phosphatase activity in hFOB cells exposed to 1000 ng/mL rhPRL. The value at 0 h was normalized to 100%. $^{\dagger\dagger\dagger}P < 0.001$ compared with the values at 0 h. Numbers in parentheses are numbers of independent flasks. Experiments were performed in triplicate.

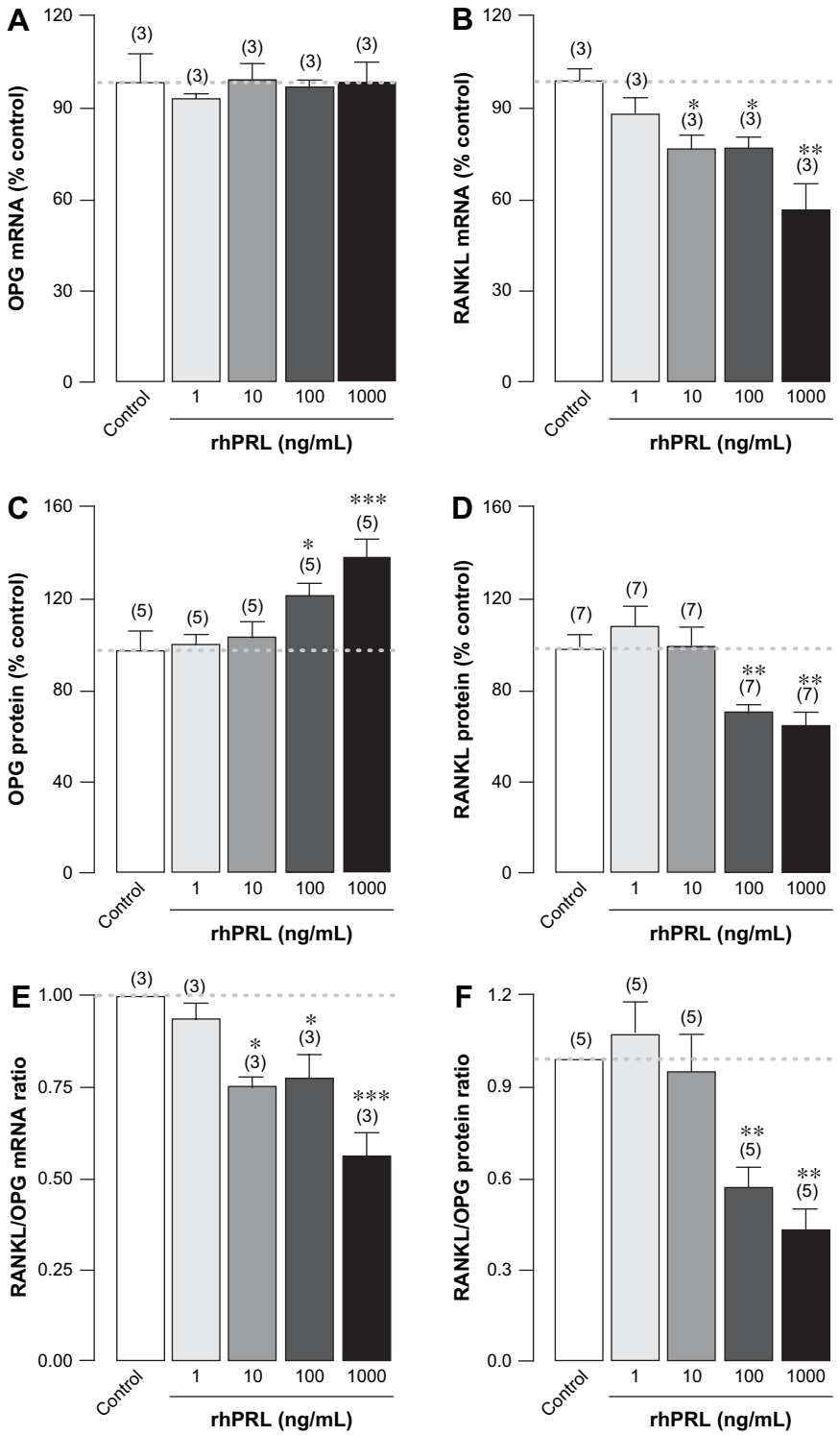

Fig. 4. Dose-dependent changes in the mRNA expressions of OPG (A) and RANKL (B), protein expressions of OPG (C) and RANKL (D), and the ratios of RANKL/OPG mRNA (E) and protein (F) expressions in hFOB cells incubated for 48 h with 1, 10, 100 or 1000 ng/mL rhPRL. Values of the control groups were normalized to 100%. $^{*}P < 0.05$, $^{**}P < 0.01$, $^{***}P < 0.001$ compared with the control group. Numbers in parentheses are numbers of independent flasks. Experiments were performed in triplicate.

4. Discussion

In adult animals, high bone turnover is a characteristic of both physiological and pathological hyperprolactinemia (Krishnamra et al., 1997; Lotinun et al., 2003; Meaney et al., 2004). Generally, high bone turnover accelerates bone loss, especially when the resorption cavities are incompletely replaced. However, under certain conditions, such as during growth hormone administration, the increased bone turnover shifts the balance between bone formation and resorption

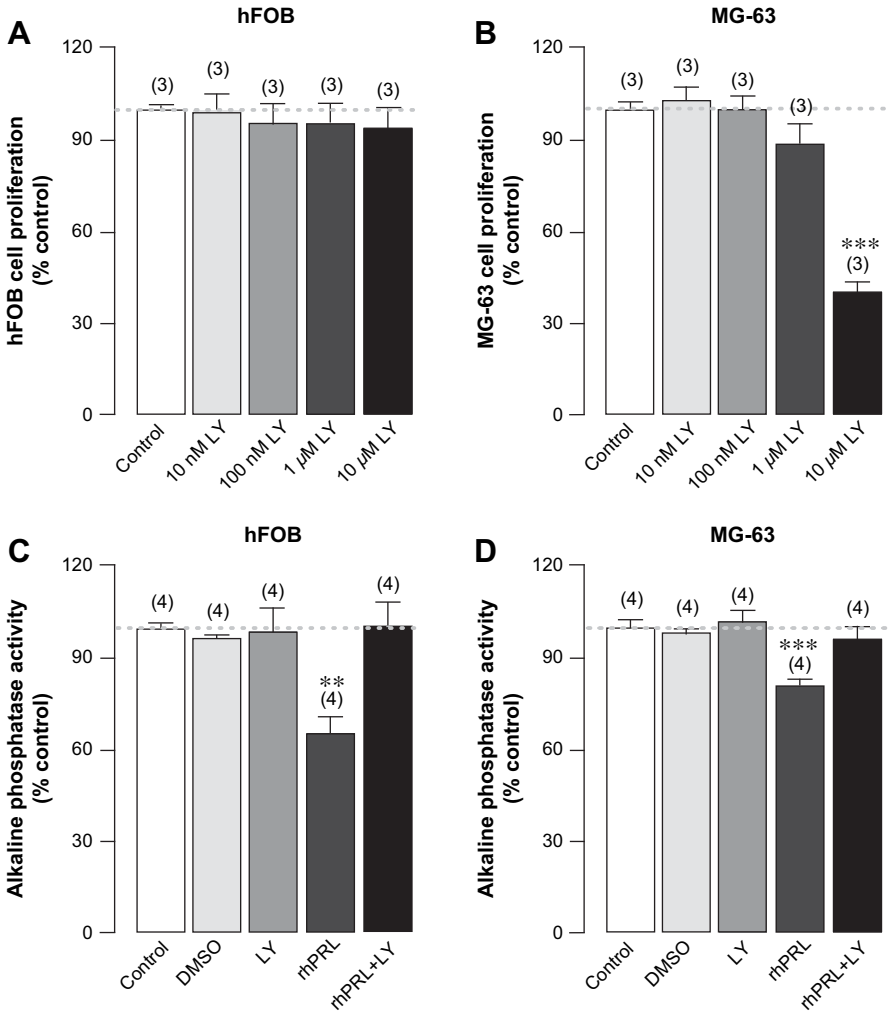

Fig. 5. (A,B) Proliferation of hFOB and MG-63 cells after incubation for 48 h with 10 nM, 100 nM, 1 μM or 10 μM LY294002 (LY, PI3K inhibitor). (C,D) Alkaline phosphatase activity in hFOB and MG-63 cells incubated for 48 h in normal culture media (control) or media containing 0.3% DMSO (vehicle), 100 nM LY294002, 100 ng/mL rhPRL, or 100 ng/mL rhPRL plus 100 nM LY294002. Values of the control groups were normalized to 100%. $^{**}P < 0.01$, $^{***}P < 0.001$ compared with the control group. Numbers in parentheses are numbers of independent flasks. Experiments were performed in triplicate.

toward net bone calcium deposition (Parfitt, 1991). Although high physiological PRL of ∼75−100 ng/mL during pregnancy did not produce a significant bone loss, transient osteopenia was reported after 3 months of lactation when plasma PRL ranged between 200 and 350 ng/mL (Prentice, 2000; Ritchie et al., 1998). Furthermore, high PRL levels (up to ∼1000 ng/mL) found in several pathological conditions, e.g., prolactinomas or prolonged antipsychotic drug use, induced massive bone loss and overt osteopenia (Biller et al., 1992; Crosignani, 2006; Meaney et al., 2004). Thus, PRL exposure in adult animals and humans, depending on the PRL concentrations, could lead to bone loss. On the other hand, by using the in vivo ^{45}Ca kinetic study, Krishnamra and Seemoung (1996) reported that young rats responded differently to PRL, i.e., by enhancing bone gain instead of bone loss despite the presence of high bone turnover. Moreover, PRL administration in 3-week-old weaned rats resulted in a dose-dependent increase in the calcium content of femur, tibia and vertebrae (Krishnamra and Seemoung, 1996). The present investigation showed an increase in osteocalcin expression and a decrease in the RANKL/OPG ratio in hFOB cells which indicated that PRL-exposed osteoblasts derived from immature animals could potentially induce bone gain.

Indeed, the in vivo osteopenic action of PRL had long been explained by estrogen deficiency due to PRL-induced hypogonadism (Meaney et al., 2004; Wang et al., 1980). However, the PRLR knockout mice manifested a 60% decrease in the rate of bone formation (Clément-Lacroix et al., 1999), and PRL-exposed rats exhibited high bone turnover with different histomorphometric patterns from those seen in ovariectomized (Ovx) rats, i.e., higher mineral apposition rate and bone formation rate (Seriwatanachai et al., 2008). It is possible that PRL could also exert a direct estrogen-independent action on bone cells. The finding of PRLR in osteoblasts also supported this hypothesis. Although the levels of PRLR transcript in MG-63 cells were significantly elevated in the presence of 1,25-$(OH)_2D_3$ and dexamethasone (Bataille-Simoneau et al., 1996), the expression of PRLR mRNAs and proteins in hFOB cells similar to that in the primary rat osteoblasts (Seriwatanachai et al., 2008) was constitutive and independent of both hormones.

We further investigated the effect of PRL on hFOB cell functions and found that PRL stimulated osteocalcin expression in hFOB cells without affecting cell proliferation. This effect of PRL agreed with the recent report on neonatal osteoblasts (Seriwatanachai et al., 2008), and was also consistent with the action of other hormones, such as leptin which enhanced osteoblast differentiation but not proliferation (Thomas et al., 1999). On the other hand, MG-63 cells derived from adult humans showed a decrease in osteocalcin expression after a 48-h PRL exposure (Seriwatanachai et al., 2008). The PRL-induced increase in the activity of hFOB cells supported our hypothesis that PRL could increase bone formation in osteoblasts derived from young animals.

Similar to the primary neonatal rat osteoblasts (Coss et al., 2000) and MG-63 cells (Seriwatanachai et al., 2008), PRL-exposed hFOB cells manifested a decrease in alkaline phosphatase activity. Although alkaline phosphatase is a classical marker of bone formation (Stein et al., 1996), its expression depends on the developmental stage of osteoblasts (Owen et al., 1990). Normally, osteoblasts have roles in all 3 steps of bone formation, i.e., cell proliferation, extracellular matrix maturation, and mineralization (Owen et al., 1990). Responses of osteoblast proliferation, gene expression and enzyme activities to various humoral factors depend on the stage of development of the cells. For example, transforming growth factor β and its downstream protein Smad3 inhibited osteoblast proliferation, but enhanced alkaline phosphatase activity, mineralization, and expression of bone matrix proteins (Sowa et al., 2002). Generally, alkaline phosphatase expression is increased immediately after cessation of cell proliferation, while the expression of osteocalcin, which is important for the formation of hydroxyapatite crystal lattices (Hoang et al., 2003), is increased later during matrix maturation near the onset of mineralization (Owen et al., 1990). Therefore, a disparate relationship between osteocalcin expression and alkaline phosphatase activity could be observed during the development of osteoblasts.

Since PRL enhanced osteocalcin expression in the matrix maturation step (Fig. 2B) without affecting the in vitro mineralization of primary rat osteoblasts (Charoenphandhu et al., 2008), it appeared that PRL increased bone calcium deposition in young rats by downregulating RANKL and upregulating OPG, thereby decreasing the RANKL/OPG ratio. Similar to PRL, growth hormone which increases bone turnover and bone gain (Brixen et al., 2000; Landin-Wilhelmsen et al., 2003; Schlemmer et al., 1991) also stimulates OPG synthesis in hFOB cells (Mrak et al., 2007). In contrast, MG-63 cells responded to 48-h PRL exposure by increasing the RAN KL/OPG ratio (Seriwatanachai et al., 2008). An increase in this ratio has been associated with osteopenic conditions, such as hyperparathyroidism and aging (Cao et al., 2003; Stilgren et al., 2004). In the transgenic mice, overexpression of RANKL increased the cortical porosity, whereas overexpression of OPG prevented bone loss and improved cortical bone strength (Kostenuik, 2005; Mizuno et al., 2002). The ~50% decrease in RANKL/OPG ratio in the present study implied that PRL could potentially suppress bone resorption, thus supporting the earlier report of greater calcium deposition in bones of PRL-treated young rats (Krishnamra and Seemoung, 1996).

Although the direct actions of PRL in osteoblasts have been demonstrated, nothing was known regarding its signaling pathway. PRL binding to PRLRs triggers dimerization of PRLRs and activation of the downstream signals (Bole-Feysot et al., 1998). In the mammary epithelia, PRL-PRLR complex used the JAK2 signaling pathway in the stimulation of milk production (Bole-Feysot et al., 1998). However, in other tissues, such as liver and calcium-transporting epithelia, e.g., duodenum and colon, mitogen-activated protein kinase (MAPK) and PI3K pathways have been reported (Amaral et al., 2004; Yamauchi et al., 1998). We recently showed that PRL directly stimulated duodenal calcium absorption (Jantarajit et al., 2007), and inhibited colonic Ca^{2+}-dependent Cl^- and K^+ secretion via the PI3K pathway (Puntheeranurak et al., 2007). By using a potent inhibitor of PI3K (LY294002), the present study showed that the suppressive effect of PRL on alkaline phosphatase activity in hFOB cells was completely abolished. Therefore, the PI3K pathway could be one of the signaling pathways of PRL in osteoblasts. The detailed signaling cascade, however, remains to be investigated.

It can be concluded that hFOB cells strongly and constitutively express PRLR. PRL directly increases osteocalcin mRNA expression, and decreases the RANKL/OPG ratio in these cells, indicating the stimulation of bone formation and suppression of bone resorption, respectively. PRL also decreases alkaline phosphatase activity, in part, via the PI3K signaling pathway. Our in vitro study supported the previous in vivo findings that, unlike mature rats, PRL enhances bone calcium deposition and bone gain in young rats.

Acknowledgements

We thank Dr Sinee Disthabanchong from the Faculty of Medicine, Ramathibodi Hospital, Mahidol University, for her technical guidance and helpful comments. We thank Dr Suttatip Kamolmatyakul from the Prince of Songkla University, Thailand, for a kind gift of MG-63 cells. This research was supported by grants from the Royal Golden Jubilee Program (to DS), the Thailand Research Fund (TRF) and the National Center for Genetic Engineering and Biotechnology (BIOTEC).

References

Abdallah BM, Stilgren LS, Nissen N, Kassem M, Jorgensen HR, Abrahamsen B. Increased RANKL/OPG mRNA ratio in iliac bone biopsies from women with hip fractures. Calcif Tissue Int 2005;76:90–7.

Amaral ME, Cunha DA, Anhê GF, Ueno M, Carneiro EM, Velloso LA, et al. Participation of prolactin receptors and phosphatidylinositol 3-kinase and MAP kinase pathways in the increase in pancreatic islet mass and sensitivity to glucose during pregnancy. J Endocrinol 2004;183:469–76.

Bataille-Simoneau N, Gerland K, Chappard D, Basle MF, Mercier L. Expression of prolactin receptors in human osteosarcoma cells. Biochem Biophys Res Commun 1996;229:323–8.

Biller BM, Baum HB, Rosenthal DI, Saxe VC, Charpie PM, Klibanski A. Progressive trabecular osteopenia in women with hyperprolactinemic amenorrhea. J Clin Endocrinol Metab 1992;75:692–7.

Bishop JD, Nien WL, Dauphinee SM, Too CK. Prolactin activates mammalian target-of-rapamycin through phosphatidylinositol 3-kinase and stimulates phosphorylation of p70S6K and 4E-binding protein-1 in lymphoma cells. J Endocrinol 2006;190:307–12.

Bole-Feysot C, Goffin V, Edery M, Binart N, Kelly PA. Prolactin (PRL) and its receptor: actions, signal transduction pathways and phenotypes observed in PRL receptor knockout mice. Endocr Rev 1998;19:225–68.

Brixen K, Hansen TB, Hauge E, Vahl N, Jorgensen JO, Christiansen JS, et al. Growth hormone treatment in adults with adult-onset growth hormone deficiency increases iliac crest trabecular bone turnover: a 1-year, double-blind, randomized, placebo-controlled study. J Bone Miner Res 2000;15:293–300.

Cao J, Venton L, Sakata T, Halloran BP. Expression of RANKL and OPG correlates with age-related bone loss in male C57BL/6 mice. J Bone Miner Res 2003;18:270–7.

Charoenphandhu N, Krishnamra N. Prolactin is an important regulator of intestinal calcium transport. Can J Physiol Pharmacol 2007;85: 569–81.

Charoenphandhu N, Teerapornpuntakit J, Methawasin M, Wongdee K, Thongchote K, Krishnamra N. Prolactin decreases expression of Runx2, osteoprotegerin and RANKL in primary osteoblasts derived from tibiae of adult female rats. Can J Physiol Pharmacol 2008;86:240–8.

Charoenphandhu N, Wongdee K, Tudpor K, Pandaranandaka J, Krishnamra N. Chronic metabolic acidosis upregulated claudin mRNA expression in the duodenal enterocytes of female rats. Life Sci 2007;80:1729–37.

Clément-Lacroix P, Ormandy C, Lepescheux L, Ammann P, Damotte D, Goffin V, et al. Osteoblasts are a new target for prolactin: analysis of bone formation in prolactin receptor knockout mice. Endocrinology 1999;140: 96–105.

Coss D, Yang L, Kuo CB, Xu X, Luben RA, Walker AM. Effects of prolactin on osteoblast alkaline phosphatase and bone formation in the developing rat. Am J Physiol Endocrinol Metab 2000;279:E1216–25.

Crosignani PG. Current treatment issues in female hyperprolactinaemia. Eur J Obstet Gynecol Reprod Biol 2006;125:152–64.

Grimaud E, Soubigou L, Couillaud S, Coipeau P, Moreau A, Passuti N, et al. Receptor activator of nuclear factor κB ligand (RANKL)/osteoprotegerin (OPG) ratio is increased in severe osteolysis. Am J Pathol 2003;163: 2021–31.

Harris SA, Enger RJ, Riggs BL, Spelsberg TC. Development and characterization of a conditionally immortalized human fetal osteoblastic cell line. J Bone Miner Res 1995;10:178–86.

Hoang QQ, Sicheri F, Howard AJ, Yang DS. Bone recognition mechanism of porcine osteocalcin from crystal structure. Nature 2003;425:977–80.

Jantarajit W, Thongon N, Pandaranandaka J, Teerapornpuntakit J, Krishnamra N, Charoenphandhu N. Prolactin-stimulated transepithelial calcium transport in duodenum and Caco-2 monolayer are mediated by the phosphoinositide 3-kinase pathway. Am J Physiol Endocrinol Metab 2007;293:E372–84.

Kelly PA, Binart N, Freemark M, Lucas B, Goffin V, Bouchard B. Prolactin receptor signal transduction pathways and actions determined in prolactin receptor knockout mice. Biochem Soc Trans 2001;29:48–52.

Kostenuik PJ. Osteoprotegerin and RANKL regulate bone resorption, density, geometry and strength. Curr Opin Pharmacol 2005;5:618–25.

Krishnamra N, Lotinun S, Limlomwongse L. Acute effect and mechanism of action of prolactin on the in situ passive calcium absorption in rat. Bone Miner 1993;23:253–66.

Krishnamra N, Seemoung J. Effects of acute and long-term administration of prolactin on bone ^{45}Ca uptake, calcium deposit, and calcium resorption in weaned, young, and mature rats. Can J Physiol Pharmacol 1996;74: 1157–65.

Krishnamra N, Seemoung J, Limlomwongse L. Acute effect of prolactin on bone ^{45}Ca accumulation in rats. Endocr J 1997;44:257–64.

Landin-Wilhelmsen K, Nilsson A, Bosaeus I, Bengtsson BA. Growth hormone increases bone mineral content in postmenopausal osteoporosis: a randomized placebo-controlled trial. J Bone Miner Res 2003;18:393–405.

Lotinun S, Limlomwongse L, Krishnamra N. The study of a physiological significance of prolactin in the regulation of calcium metabolism during pregnancy and lactation in rats. Can J Physiol Pharmacol 1998;76:218–28.

Lotinun S, Limlomwongse L, Sirikulchayanonta V, Krishnamra N. Bone calcium turnover, formation, and resorption in bromocriptine- and prolactin-treated lactating rats. Endocrine 2003;20:163–70.

Meaney AM, Smith S, Howes OD, O'Brien M, Murray RM, O'Keane V. Effects of long-term prolactin-raising antipsychotic medication on bone mineral density in patients with schizophrenia. Br J Psychiatry 2004; 184:503–8.

Mizuno A, Kanno T, Hoshi M, Shibata O, Yano K, Fujise N, et al. Transgenic mice overexpressing soluble osteoclast differentiation factor (sODF) exhibit severe osteoporosis. J Bone Miner Metab 2002;20:337–44.

Mosmann T. Rapid colorimetric assay for cellular growth and survival: application to proliferation and cytotoxicity assays. J Immunol Methods 1983;65:55–63.

Mrak E, Villa I, Lanzi R, Losa M, Guidobono F, Rubinacci A. Growth hormone stimulates osteoprotegerin expression and secretion in human osteoblast-like cells. J Endocrinol 2007;192:639–45.

Owen TA, Aronow M, Shalhoub V, Barone LM, Wilming L, Tassinari MS, et al. Progressive development of the rat osteoblast phenotype in vitro: reciprocal relationships in expression of genes associated with osteoblast proliferation and differentiation during formation of the bone extracellular matrix. J Cell Physiol 1990;143:420–30.

Parfitt AM. Growth hormone and adult bone remodelling. Clin Endocrinol (Oxf) 1991;35:467–70.

Piyabhan P, Krishnamra N, Limlomwongse L. Changes in the regulation of calcium metabolism and bone calcium content during growth in the absence of endogenous prolactin and during hyperprolactinemia: a longitudinal study in male and female Wistar rats. Can J Physiol Pharmacol 2000; 78:757–65.

Prentice A. Calcium in pregnancy and lactation. Annu Rev Nutr 2000;20: 249–72.

Puntheeranurak S, Schreiber R, Spitzner M, Ousingsawat J, Krishnamra N, Kunzelmann K. Control of ion transport in mouse proximal and distal colon by prolactin. Cell Physiol Biochem 2007;19:77–88.

Ritchie LD, Fung EB, Halloran BP, Turnlund JR, Van Loan MD, Cann CE, et al. A longitudinal study of calcium homeostasis during human pregnancy and lactation and after resumption of menses. Am J Clin Nutr 1998;67:693–701.

Schlemmer A, Johansen JS, Pedersen SA, Jorgensen JO, Hassager C, Christiansen C. The effect of growth hormone (GH) therapy on urinary pyridinoline cross-links in GH-deficient adults. Clin Endocrinol (Oxf) 1991;35:471–6.

Seriwatanachai D, Thongchote K, Charoenphandhu N, Pandaranandaka J, Tudpor K, Teerapornpuntakit J, et al. Prolactin directly enhances bone turnover by raising osteoblast-expressed receptor activator of nuclear factor κB ligand/osteoprotegerin ratio. Bone 2008;42:535–46.

Sowa H, Kaji H, Yamaguchi T, Sugimoto T, Chihara K. Smad3 promotes alkaline phosphatase activity and mineralization of osteoblastic MC3T3-E1 cells. J Bone Miner Res 2002;17:1190–9.

Stein GS, Lian JB, Stein JL, Van Wijnen AJ, Montecino M. Transcriptional control of osteoblast growth and differentiation. Physiol Rev 1996;76: 593–629.

Stilgren LS, Rettmer E, Eriksen EF, Hegedus L, Beck-Nielsen H, Abrahamsen B. Skeletal changes in osteoprotegerin and receptor activator of nuclear factor-κB ligand mRNA levels in primary hyperparathyroidism: effect of parathyroidectomy and association with bone metabolism. Bone 2004;35:256–65.

Subramaniam M, Jalal SM, Rickard DJ, Harris SA, Bolander ME, Spelsberg TC. Further characterization of human fetal osteoblastic hFOB 1.19 and hFOB/ERα cells: bone formation in vivo and karyotype analysis using multicolor fluorescent in situ hybridization. J Cell Biochem 2002;87: 9–15.

Thomas T, Gori F, Khosla S, Jensen MD, Burguera B, Riggs BL. Leptin acts on human marrow stromal cells to enhance differentiation to osteoblasts and to inhibit differentiation to adipocytes. Endocrinology 1999;140: 1630–8.

Thongon N, Nakkrasae LI, Thongbunchoo J, Krishnamra N, Charoenphandhu N. Prolactin stimulates transepithelial calcium transport and modulates paracellular permselectivity in Caco-2 monolayer: Mediation by PKC and ROCK pathways. Am J Physiol Cell Physiol 2008;294:C1158–68.

Wang C, Chan V. Divergent effects of prolactin on estrogen and progesterone production by granulosa cells of rat Graafian follicles. Endocrinology 1982;110:1085–93.

Wang C, Hsueh AJ, Erickson GF. Prolactin inhibition of estrogen production by cultured rat granulosa cells. Mol Cell Endocrinol 1980;20:135–44.

Yamauchi T, Kaburagi Y, Ueki K, Tsuji Y, Stark GR, Kerr IM, et al. Growth hormone and prolactin stimulate tyrosine phosphorylation of insulin receptor substrate-1, -2, and -3, their association with p85 phosphatidylinositol 3-kinase (PI3-kinase), and concomitantly PI3-kinase activation via JAK2 kinase. J Biol Chem 1998;273:15719–26.

Yen ML, Chien CC, Chiu IM, Huang HI, Chen YC, Hu HI, et al. Multilineage differentiation and characterization of the human fetal osteoblastic 1.19 cell line: a possible in vitro model of human mesenchymal progenitors. Stem Cells 2007;25:125–31.